The Chemistry and Physics of

STRATOSPHERIC
OZONE

Andrew Dessler

The Chemistry and Physics of Stratospheric Ozone

The Chemistry and Physics of Stratospheric Ozone

Andrew E. Dessler
UNIVERSITY OF MARYLAND
EARTH SYSTEM SCIENCE
INTERDISCIPLINARY CENTER
COLLEGE PARK
MD 20742
USA

ACADEMIC PRESS

Contents

v

vi   **Contents**

Preface

Over the past decade or so, stratospheric ozone has been a subject of intense research that has vastly improved our understanding of the subject. And although it cannot be said that a scientific subject is ever completely "solved", there is little argument that our understanding of stratospheric ozone is far better now than it was even 5 years ago. Further, as our knowledge and understanding have matured, there has been a natural slowing in the rate of discoveries and in the development of new theoretical insights. The field has progressed to the stage that the theories are adequate not only to explain past experiments but also of accounting for most new experimental findings. As a result, I feel that it is now possible to write a textbook detailing our knowledge of stratospheric ozone that will (hopefully) remain relevant for some years.

In this book I present an account of what I have learned in the past 11 years about the physical processes that regulate stratospheric ozone. The presentations assume knowledge of the atmosphere at the level of an advanced undergraduate in atmospheric sciences, but it requires no specialized knowledge of chemistry or the stratosphere. To help those not familiar with stratospheric chemistry, a glossary is provided at the end of the book that defines commonly used terms in the field.

Deciding what material to include and exclude was a difficult task, and I regret that there are several subject areas that receive only fleeting coverage. In particular, I would have liked to include more about stratospheric dynamics, radiative transfer, and kinetics. I take some solace, however, in the knowledge that no book is ever truly complete—any attempt on my part at writing a book that included everything about a subject would have meant the book would never have been written.

This Page Intentionally Left Blank

Acknowledgments

This Page Intentionally Left Blank

Chapter 1 | The Ozone Problem

The atmosphere is traditionally divided into layers on the basis of temperature (Figure 1.1). The lowest layer of the atmosphere, the troposphere, is characterized by decreasing temperature with increasing altitude. It contains ~90% of the mass of the atmosphere, as well as most of the Earth's clouds and weather. The temperature minimum located between 10 and 15 km altitude (~100 and 200 hPa pressure) is called the tropopause, and it demarcates the boundary between the troposphere and the layer above it, the stratosphere. In the stratosphere, the temperature increases with altitude, primarily because of heating from the absorption of ultraviolet radiation by ozone. The stratosphere contains ~9.9% of the mass of the atmosphere. The temperature maximum near 50 km (~1 hPa) is called the stratopause, and marks the boundary between the stratosphere and the layer above it, the mesosphere. In the mesosphere, the temperature again decreases with altitude, primarily because of radiative cooling by carbon dioxide (CO_2). The top of the mesosphere is bounded by a temperature minimum called the mesopause. Above the mesopause sits the thermosphere. In this book, we are concerned almost exclusively with the stratosphere.

Molecular nitrogen (N_2) and molecular oxygen (O_2) make up ~99% of the mass of the atmosphere. Because N_2 is about four times more abundant than O_2, the average molecular weight of the atmosphere is ~29 g mol^{-1}. Of the remaining ~1%, there are several gases whose abundance in the atmosphere is small but whose impact on the atmosphere is not. Many of these gases absorb photons with wavelengths in the thermal infrared (between a few and ~20 μm), where O_2 and N_2 are essentially transparent. As a result, these trace gases, which include CO_2, water vapor (H_2O), and ozone (O_3), exert an important influence on the Earth's climate.

The atmosphere also filters the solar radiation reaching the surface. Most solar radiation incident on the top of the atmosphere is in the wavelength range between ~100 nm and a few micrometers. Wavelengths less than 200 nm are absorbed fairly high in the atmosphere (50–150 km altitude) by O_2, N_2, and O (see Chamberlain and Hunten [1], Section 1.5.1), while wavelengths greater than ~300 nm can penetrate to the Earth's surface. For wavelengths between 200 and 300 nm, ozone (O_3) is the primary absorber, and without O_3 much of this
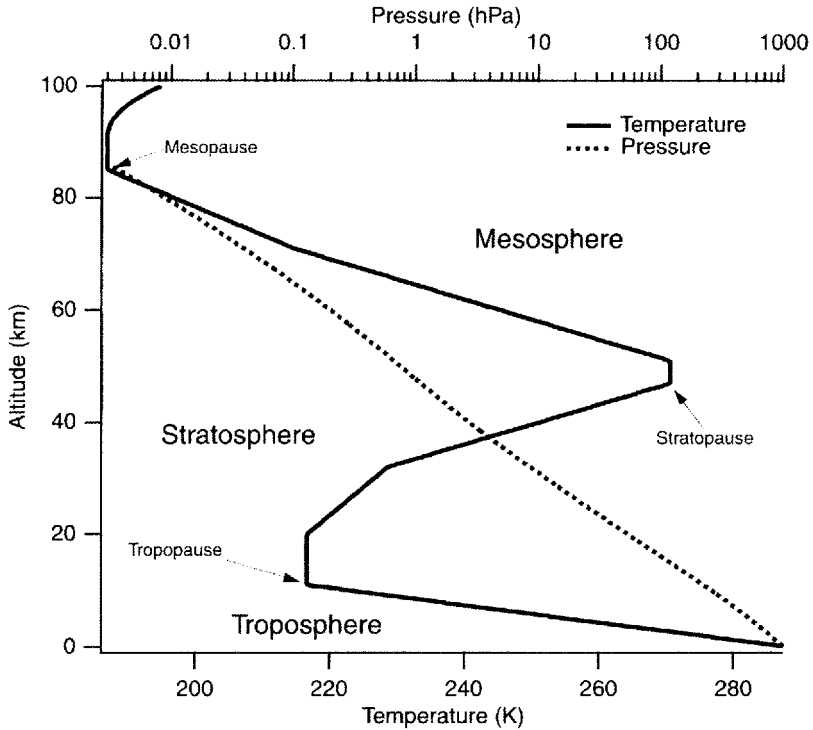
Figure 1.1 Typical temperature and pressure profiles. Based on the 1976 US Standard Atmosphere.

radiation would reach the ground. The role O_x plays in absorbing these photons is crucial because a photon of 250 nm wavelength has an energy of ~5 eV, enough to break chemical bonds in DNA or interfere in other ways with biological processes [2–4].

Luckily for the Earth's various life forms, O_3 has a prodigious ability to absorb radiation with wavelengths between 200 and 300 nm. At its maximum at 250 nm, the absorption cross-section of O_3 is 1.15×10^{-17} cm^2, dropping to 3.4×10^{-19} cm^2 at 300 nm (see DeMore *et al.* [5], Table 7). To get an idea of how effective O_3 is as an absorber, we can estimate the transmission of radiation through a typical atmospheric column using the Lambert–Beer exponential absorption law:

$$Tr = \exp(-\sigma C) \tag{1.1}$$

where Tr is the fraction of the incident beam that is transmitted, σ is the cross-section of O_3 at that wavelength (cm^2), and C is the total column abundance of O_3, which is typically around 10^{19} molecules cm^{-2}. At 250 nm, the transmission is $\sim 10^{-50}$. This is a phenomenally small number, and indicates that essentially none of the 250 nm radiation incident on the top of the atmosphere makes it through the O_3 to the surface. At 300 nm, where the O_3 cross-section is considerably smaller, about 3% of the incident beam makes it to the surface.

The study of O_3 has become a subject of public interest since it was noted that the effluents of our society might lead to a gradual lowering of the amount of O_3 in the atmosphere. This reduction, in turn, would lead to enhanced ultraviolet radiation at the surface of the Earth, which would be detrimental to various life forms at the surface. Much of the research detailed in this book was performed with the goal of better understanding the processes by which mankind affects the abundance of O_3. For a history of the early research into O_3, see Dobson [6] and Nicolet [7].

O_3 is also an important component of the atmosphere for other, less politically charged reasons. One of these is the role O_3 plays in the energy balance of the stratosphere. As discussed above, O_3 is a prodigious absorber of ultraviolet photons. In addition, O_3 also absorbs strongly in the infrared, especially near 9.6 µm [8]. This absorption of solar and infrared radiation heats the stratosphere, and is one of the main reasons the temperature of the stratosphere increases with height.

On an annual and global mean, the stratosphere is approximately in radiative equilibrium. The absorption of solar and infrared radiation by O_3 exceeds the emission of infrared radiation by O_3 by about 15 W m^{-2}. Thus, O_3 is a net heat source for the stratosphere. This net heating of the stratosphere is balanced by the net infrared cooling of CO_2 and H_2O [9].

Stratospheric O_3 also causes a net heating of the troposphere–surface system. Solar absorption by stratospheric O_3 reduces the input of solar energy to the troposphere–surface system by 7 W m^{-2}. Downward infrared emission by stratospheric O_3, on the other hand, warms the troposphere–surface system by 2 W m^{-2}. Enhanced infrared emission from stratospheric CO_2 and H_2O owing to the higher stratospheric temperatures warms the troposphere–surface system by 7 W m^{-2}. The net effect is a warming of the troposphere–surface system by about 2 W m^{-2} [9]. Depletion of stratospheric O_3 will therefore tend to cool the surface [10], although the exact magnitude and sign of the effect is dependent on the altitude of O_3 changes [11].

O_3 is indeed an important molecule in the stratosphere. Because it plays a role in so many aspects of the stratosphere, an understanding of O_3 requires the development of an integrated view of the dynamical, chemical, and radiative processes of the stratosphere. Such a view bridges traditional disciplines of chemistry and physics, and is emblematic of the necessity of thinking broadly in order to understand the problems confronting Earth.

1.1 The Ideal Gas Law

Before talking about O_3, let us first discuss the ideal gas law, which relates pressure, density, and temperature:

$$\text{pressure} = \text{constant} \times \text{density} \times \text{temperature} \qquad (1.2)$$

In stratospheric research, pressure is usually expressed in hectopascals (hPa) or millibars (mb), which are equivalent units, e.g. 1 hPa = 1 mb. Pressure is also occasionally expressed in torr (1 torr = 1.3332 hPa). When using the ideal gas law, however, pressure must generally be converted to the MKS unit pascal (Pa; 1 Pa = 0.01 hPa = 1 kg m^{-1} s^{-2}). Temperature is always expressed in degrees kelvin (K). The constant used determines the form of density. If the constant is the universal gas constant ($R = 8.31$ J mol^{-1} K^{-1}) then the density is in moles per cubic meter (mol^{-1} m^{-3}). If the constant is the gas constant for dry air ($R = 287$ J kg^{-1} K^{-1}) then the density is in kilograms per cubic meter (kg m^{-3}). Finally, if the constant is Boltzmann's constant ($k = 1.38 \times 10^{-23}$ J molecule^{-1} K^{-1}), then the density is in molecules per cubic meter—also known as the number density. It should be obvious that it is crucial to make sure that the units in the equation are consistent. Failure to do so can result in errors of several orders of magnitude and cause you to look foolish in front of your colleagues. Trust me.

The most common form of density used in stratospheric research is number density, almost always with units of molecules per cubic centimeter. If the pressure used in the ideal gas law is the partial pressure of a gas, then the density determined will be the density of that particular gas. The number density of constituent X (X = O_2, N_2, O_3, H_2O, etc.) is generally denoted [X]. If the total pressure is used in the ideal gas law, then the total number density, denoted [M], is determined. We will also use the symbol M in chemical equations to refer to "any molecule", without regard to its elemental make-up. In practice, this means that M refers to N_2 and O_2. A useful shortcut to calculating number density is

$$[X] \ (\text{in molecules cm}^{-3}) = 7.25 \times 10^{18} P/T \qquad (1.3)$$

where pressure P is the partial pressure of X in hectopascals and temperature T is in Kelvin. If P is the total pressure, then the total number density [M] is calculated. Note that the sum of the number densities of the individual components of the atmosphere must sum to the total number density—just as the sum of the partial pressures must sum to the total pressure.

Another useful way of expressing the abundance of a constituent is the volume mixing ratio (VMR). Conceptually, the VMR of constituent X is the fraction of molecules in a given volume that are X. Mathematically, the VMR is the ratio of the number density of X to the total number density: [X]/[M]. VMRs are dimensionless

and never exceed 1. Because the VMR is typically small, it is usually multiplied by 10^6, 10^9, or 10^{12} to obtain parts per million by volume (ppmv), parts per billion by volume (ppbv), or parts per trillion by volume (pptv), respectively. For example, a VMR of 5×10^{-6} or 5 ppmv of O_3 means that 5 out of every 1×10^6 (or 1 out of every 200,000) molecules in a sample is an O_3 molecule. Finally, the sum of the VMRs of all of the constituents in an air mass must equal 1.

Why is the VMR useful? Assume that the number density of X in an air parcel at pressure P_0 and temperature T_0 is $[X]_0$. Now assume that the air parcel moves to a new location in the atmosphere and the temperature and pressure change to P_{new} and T_{new}. According to Boyle's law and Charles' law, the number density of X changes to

$$[X]_{new} = [X]_0 \frac{P_{new}}{P_0} \frac{T_0}{T_{new}} \tag{1.4}$$

Now consider the VMR. The initial mixing ratio of X is $[X]_0/[M]_0$, where $[M]_0$ is the initial total number density. The VMR at the new temperature and pressure is $[X]_{new}/[M]_{new}$, where $[X]_{new}$ is given in Equation 1.4 and

$$[M]_{new} = [M]_0 \frac{P_{new}}{P_0} \frac{T_0}{T_{new}} \tag{1.5}$$

Combining Equations (1.4) and (1.5), the VMR at the new location is

$$\frac{[X]_{new}}{[M]_{new}} = \frac{[X]_0}{[M]_0} \tag{1.6}$$

Thus, while the number density of a constituent changes when temperature or pressure in an air mass change, the VMR does not. In other words, the VMR is *conserved* for changes in the pressure or temperature of a parcel. This property makes VMR useful. It should be noted that one can also define a mass mixing ratio (see problem 4 at the end of the chapter), but this is rarely used in stratospheric research.

1.2 Ozone Morphology

Figure 1.2 shows contours of both the number density and VMR of O_3 in the latitude–height plane. O_3 reaches maximum values of both number density (4.6×10^{12} molecules cm^{-3} at ~25 km) and VMR (10 ppmv at ~32 km) over the equator. As one moves away from the equator, the number density peak moves to lower altitudes, but
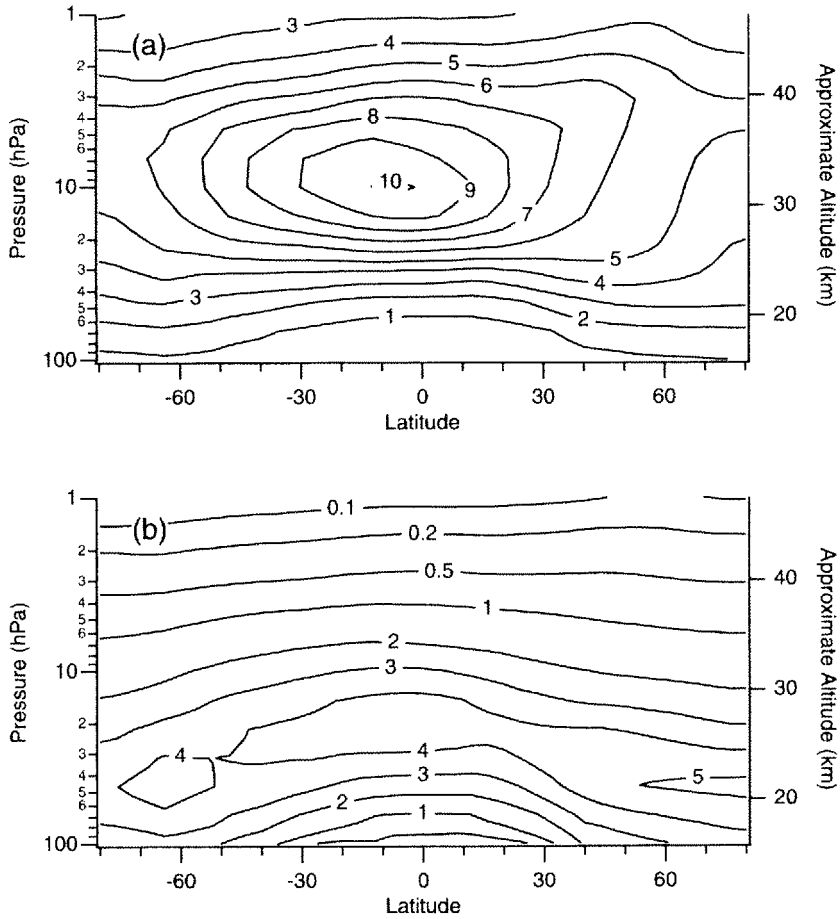
Figure 1.2 Contours of (a) O_3 volume mixing ratio (ppmv) and (b) contours of O_3 number density (10^{12} molecules cm^{-3}) in December 1992. Data are from the UARS Reference Atmosphere Project (W. J. Randel, personal communication, 1998).

remains approximately constant at around $4 \times 10^{12} - 5 \times 10^{12}$ molecules cm^{-3}. The peak in the VMR rises to higher altitudes as one moves away from the equator, and the magnitude of the peak decreases.

Another quantity widely used in stratospheric science is "column O_3". This quantity is the total number of molecules of O_3 in a column of unit cross-sectional area (usually a square centimeter) running from the Earth's surface to the top of the atmosphere. Typical values of column O_3 range from 10^{18} to 10^{19} molecules of

O_3 cm^{-2}. For simplicity, column O_3 is almost always expressed in Dobson Units (DU). The Dobson Unit is the height of the O_3 in the column (in millicentimeters) if compressed to standard temperature (273 K) and pressure (1 atm = 1013 hPa). For example, 1×10^{19} molecules of O_3 cm^{-2} would, if compressed to STP, form a volume 1 cm by 1 cm in cross-sectional area and 0.37 cm in height—which is 370 DU. From Figure 1.2b, one can see that most of the O_3 in the stratosphere is located between 100 and 10 hPa. Because of this, this region has come to be known as the "ozone layer". Only a small fraction of the O_3 column lies above about 35 km, and about 10% of the O_3 column resides in the troposphere.

There are two reasons why column O_3 is of interest to researchers. First, it is relatively easy to measure from the ground and from space. As a result, there is an extensive record of column O_3 measurements, some of it extending back to the 1930s. Second, as mentioned earlier, the O_3 in the atmosphere screens the biologically dangerous short-wavelength portion of sunlight before it reaches the surface of the Earth. It is the total column of O_3 that is the most important determinant of how much of the harmful radiation is screened by the atmosphere—with how the O_3 is distributed in the column being of less importance. Thus, column O_3 is a crucial quantity in determining how changes in the atmosphere affect the biosphere [4,3].

Figure 1.3 shows contours of northern hemisphere column O_3 on March 21, 1992. The plot shows that, in general, column O_3 increases as one moves from the equator toward the pole. In addition, there is significant longitudinal variability. At 60°N, for
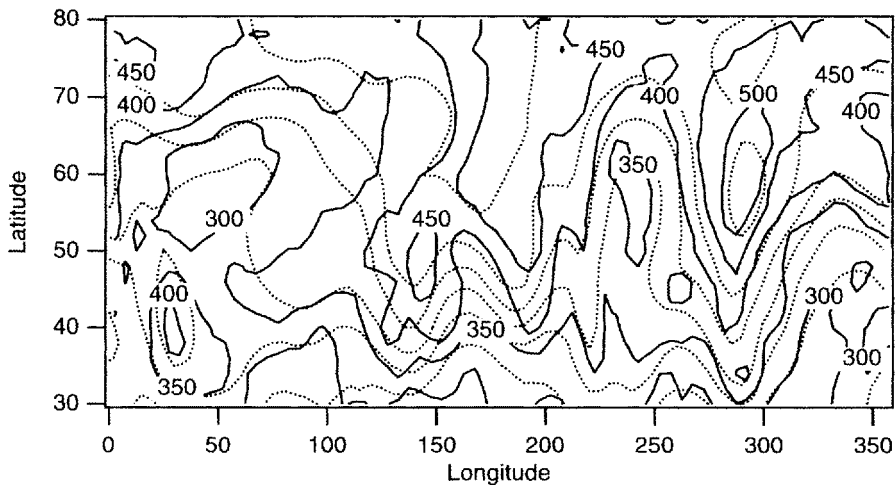
Figure 1.3 Northern hemisphere mid-latitude column O_3 distribution on March 21, 1992 (black lines). Also shown are geopotential height contours on the 300 hPa surface (dotted lines, no labels) from the UKMO analysis. Column O_3 values are version 7 TOMS data.

example, column O_3 ranges from about 275 DU at 50° longitude to about 525 DU at 290° longitude.

Also shown on the plot are contours of geopotential height on the 300 hPa surface. Much of the longitudinal variability in column O_3 is associated with the lifting or lowering of the upper troposphere by tropospheric weather systems. The reasonably close correspondence between the column O_3 and the passage of weather systems was first noted by Dobson [6], and will be discussed further in Chapter 5.

Figure 1.4a shows the annual cycle in column O_3 in 1979. Minimum column O_3 values are found over the equator (~275 DU), with column O_3 increasing as one moves away from the equator. At mid- and high latitudes there is a strong seasonal cycle in column O_3. At 60°S, average column O_3 varies from 315 DU in March, the southern hemisphere late summer/early fall, to 425 DU in October, the southern hemisphere early spring. A larger cycle occurs at 60°N, with average column O_3 ranging from 320 DU in September, the northern hemisphere late summer/early fall, to over 500 DU in March, the northern hemisphere late winter/early spring. Also note that the high-latitude column O_3 maximum is larger in the northern hemisphere (500 versus 425 DU), and appears near the pole in the northern hemisphere but considerably off the pole in the southern hemisphere. These hemispheric differences in
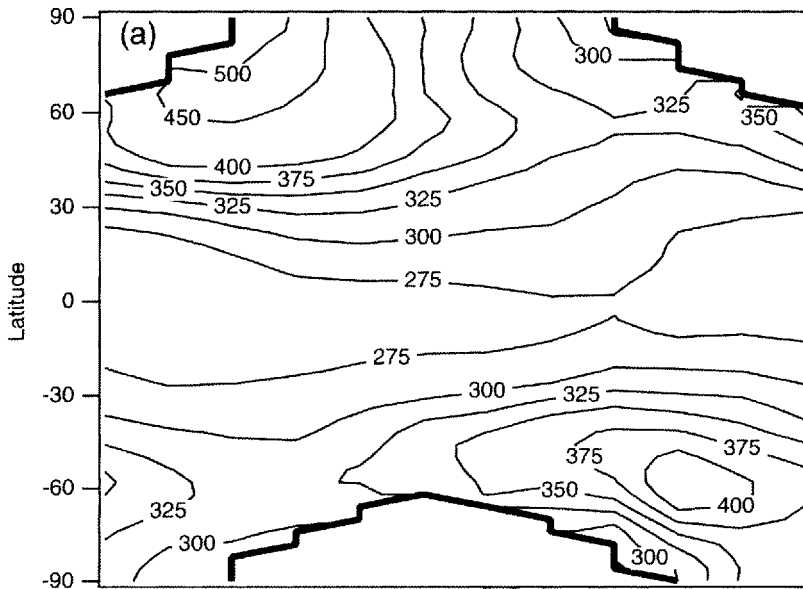
column O_3 distribution are caused by differences in the stratospheric circulation in the two hemispheres.

There are several aspects of these plots that might strike the reader as puzzling. First, as we will discuss in Chapter 3, O_3 is produced by sunlight. Because the equatorial region receives considerably more sunlight than the poles, one might expect to find higher column O_3 over the equator. This is not the case—instead, the regions of high O_3 abundance do not correlate with the regions of high O_3 production. The region with the highest production rate (the tropics) actually contains the lowest column O_3 abundances. Second, the high-latitude column O_3 maximum occurs in the late winter and early spring, after these regions have experienced several months of total or near-total darkness. Again, this seems inconsistent with the fact that O_3 is formed by sunlight.

These peculiarities in the column O_3 distribution underscore the importance of the transport of O_3 for understanding the O_3 distribution. O_3 is indeed predominantly
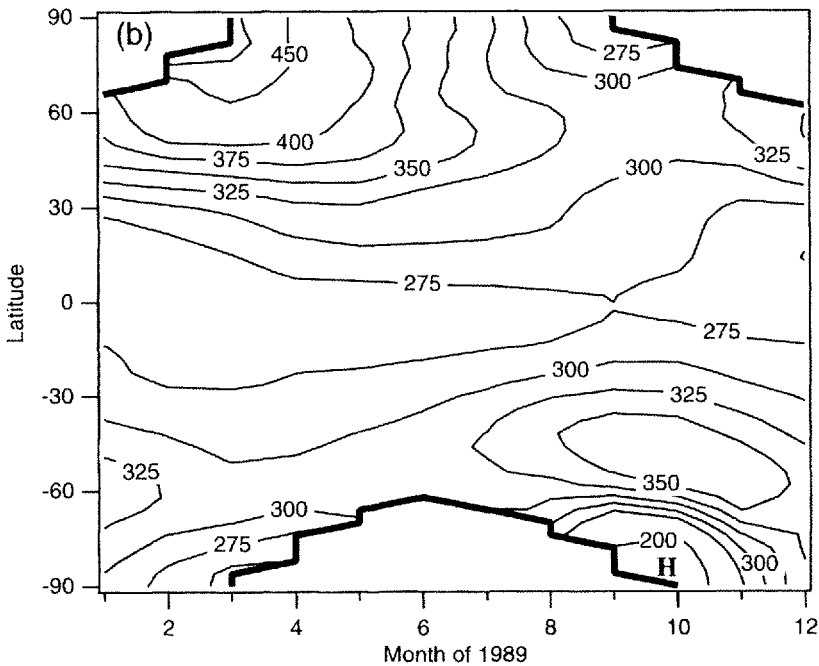
**Figure 1.4** Contours of zonally and monthly averaged column O_3 (DU) in (a) 1979 and (b) 1989. Tick marks represent the middle of the month. The "H" symbol located in October at high southern latitude in 1989 marks the location of the ozone hole. Column O_3 values are version 7 TOMS data. TOMS requires sunlight for its measurements; the heavy solid line marks the region where total darkness prevents data from being obtained.

produced near the equator. However, poleward transport moves this O_3 to higher latitudes. The magnitude of the transport has a seasonal cycle which is a primary contributor to the seasonal cycle in mid- and high-latitude column O_3. The rate of transport is largest in the winter, and this leads to the build-up of O_3 during the darkness of high-latitude winter. We discuss stratospheric transport of O_3 in Chapter 5.

An aside: can you breath in the stratosphere?

Imagine that you are designing a high-speed supersonic passenger aircraft to fly in the stratosphere at, say, 25 km. You might think that, to save weight, you would not carry oxygen for the passengers to breath, but will instead compress stratospheric air up to 1000 hPa and fill the cabin with that. Is this a good idea?

Probably not. First, air compressed adiabatically to 1000 hPa would have a temperature equal to its potential temperature. Air at 25 km has a potential temperature of about 600 K, so you would need to cool this air after compression but before it was sent into the cabin—otherwise, the passengers would cook.

Second, it is generally believed that breathing high levels of O_3 can be harmful to human health. Values of O_3 of over 100–150 ppbv are generally considered unhealthy and to be avoided. In the stratosphere, O_3 abundances of ~4–7 ppmv, or about 50 times greater than the unhealthy level, are typical. Obviously, you would need to scrub this O_3 out of the air before it is sent into the cabin—otherwise you would poison the passengers. And O_3 is not the only toxic constituent in the stratosphere: there are several others that would have to be removed prior to breathing the air.

From this it is clear that the stratosphere is a surprisingly toxic place, and you would not want to breath it without treating the air to make it more hospitable.

1.3 The Decline of Ozone

Over the past few decades, the abundance of stratospheric O_3 has been declining. Depending on the timing, magnitude, and location of the O_3 decline, the decrease of stratospheric O_3 is traditionally divided into several different scientific problems. We will discuss these now.

1.3.1 The Antarctic "ozone hole"

One of the most important events in atmospheric science was the publication by Farman *et al.* [12] of measurements of column O_3 taken over Antarctica between the late 1950s and mid-1980s. Their data showed that the spring values of column O_3 in

the mid-1980s were 50% lower than column O_3 measurements taken in the 1960s. Further research showed the dramatic evolution of what has come to be known as the Antarctic "ozone hole". The Antarctic O_3 profile in late August 1993 looks normal (Figure 1.5), with a column abundance of 287 DU. By mid-October, however, virtually all of the O_3 between 14 and 19 km altitude has been destroyed, reducing the column to below 100 DU. The area of the ozone hole (as defined by the 220 DU contour) in 1992 and 1993 was about 25×10^6 km^2 (see WMO [13], Figure 1.28), or about 10% of the southern hemisphere. The ozone hole can also be seen in Figure 1.4b in October.

Farman *et al.* [12] correctly postulated that this depletion of O_3 was related to the build-up of man-made chlorofluorocarbons (CFCs), although it took several years for the exact mechanisms to be deduced. Both scientifically and politically, this observation of significant lower stratospheric O_3 loss was a shock. Prior to the Farman *et al.* observation, state-of-the-art models had predicted that the continued release of CFCs would result in decreases of O_3 in the upper stratosphere near 40 km (see WMO [15], Chapter 13), with little effect lower in the atmosphere. Because
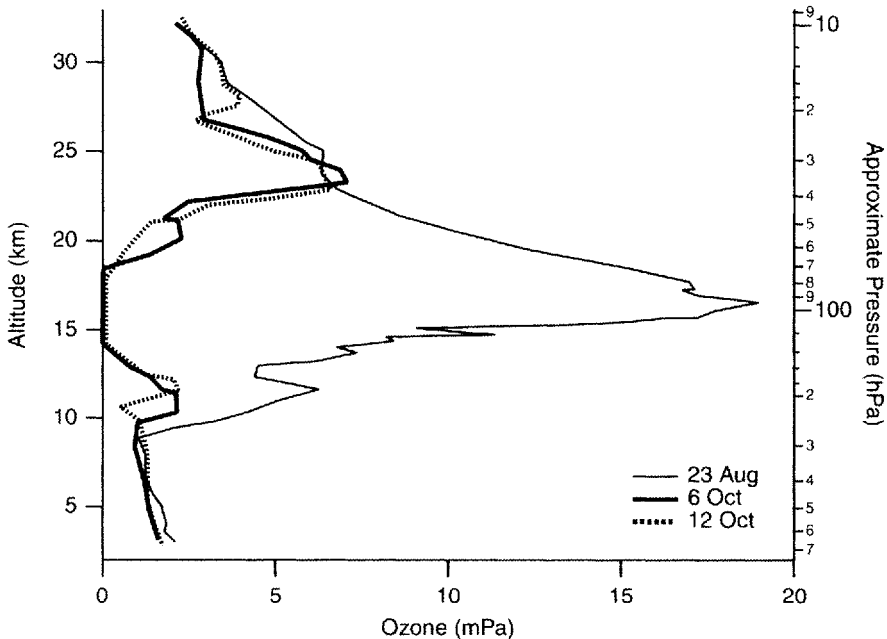

Figure 1.5 O_3 profiles measured in the Antarctic vortex by balloon sondes in 1993 [14]. O_3 abundance is expressed in partial pressure (mPa); dividing by the pressure yields the VMR (e.g. 20 mPa at 100 hPa is 2 ppmv).

little of the column's O_3 is located in the upper stratosphere, trends in column O_3 would only become observable sometime in the twenty-first century.

The unexpected observation of significant loss of O_3 in the lower stratosphere, where the majority of the O_3 column resides, meant that something scientifically interesting as well as potentially disastrous was occurring. The Antarctic ozone hole is now one of the most thoroughly studied and well-understood phenomena in the atmosphere. It turns out that the unique meteorological properties of the southern hemisphere polar region, in particular the low temperatures, combined with part per billion concentrations of anthropogenic chlorine lead to unique polar chemistry that results in rapid destruction of O_3. It should be noted that this polar chemistry also occurs in the Arctic, but, owing to differences in the meteorology of the hemispheres, less O_3 loss occurs in the Arctic. This topic is discussed in detail in Chapter 7.

1.3.2 Mid-latitude trends

The Antarctic ozone hole is a dramatic and disturbing event, but its remote location renders it effectively irrelevant to much of the world's population, most of whom live at northern mid-latitudes. Of great concern to this majority, however, is the realization that O_3 is also decreasing at mid-latitudes in both hemispheres. Figure 1.4a shows the annual cycle of column O_3 in 1979. A comparison with Figure 1.4b, the annual cycle of column O_3 in 1989, shows definite differences. In general, the mid- and high-latitude column O_3 is about 5% lower in 1989 than it is in 1979. At low latitudes, there is little or no difference in column O_3.

It is important to not infer too much from the comparison between Figures 1.4a and 1.4b. First, when comparing atmospheric measurements, one must take care not to interpret random variability as a trend. We have not provided any evidence to show that the differences in these column O_3 maps could not result from year-to-year variability. Second, one must consider other factors, such as the solar cycle or periodic meteorological phenomenon such as the quasi-biennial oscillation (QBO). The observed differences between 1979 and 1989 column O_3 abundances might not be a trend but part of a repeating cycle.

To identify trends in the data, researchers process the time series of column O_3 data using statistical models that remove all of the known sources of cyclical variability (e.g. solar cycle, annual cycle, quasibiennial oscillation) as well as random variability [16,17]. Changes in O_3 that remain are attributed to chemical destruction by anthropogenic trace gases. Figure 1.6 shows the latitudinal distribution of the column O_3 trend determined from such a model. It shows, in agreement with our eyeball estimate, that column O_3 has decreased by 3–9% per decade at mid- and high latitudes, with little change at low latitudes. The large erosion of column O_3 at high southern latitudes is attributed to the growth of the ozone hole during this period.
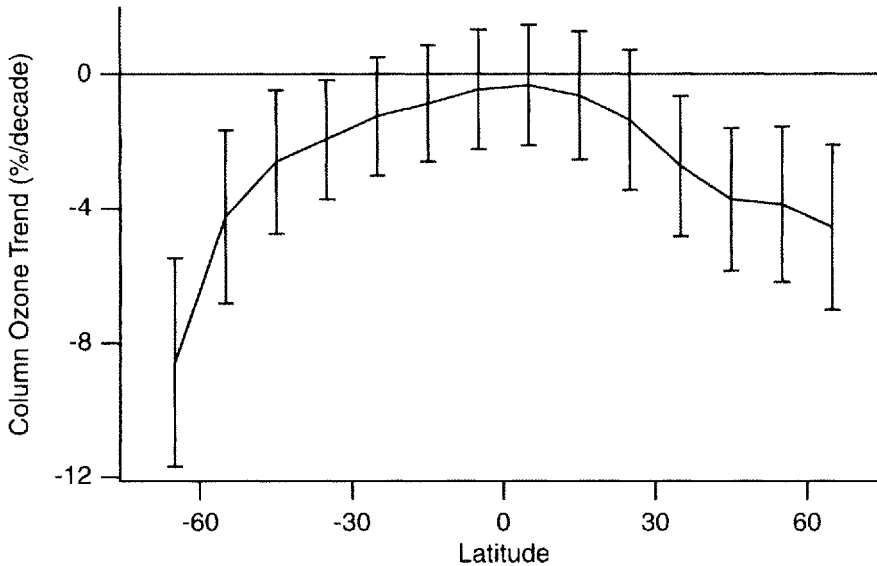
Figure 1.6 Annually averaged column O_3 trend versus latitude. The trend was determined from TOMS data (version 7) covering the time period between 11/78 and 10/94. (After McPeters *et al.* [18], Figure 4a.)

Figure 1.7 shows the altitude dependence of the O_3 trend. In agreement with Figure 1.6, there is little change in O_3 over the equator. The O_3 trends increase as one moves away from the equator in both hemispheres. The large O_3 trend in the high-latitude southern hemisphere near 100 hPa is again due to the growth of the Antarctic ozone hole over the time period of the study.

As predicted in the mid-1980s (see WMO [15], Chapter 13), there is indeed significant loss of O_3 in the upper stratosphere (~2–1 hPa, ~45–50 km). As previously discussed, however, only a few percent of the O_3 column is found in the upper stratosphere, so significant reductions in O_3 in this region cause relatively small changes in column O_3. Instead, most of the column O_3 resides in the mid- and lower stratosphere, so it is the changes in this region that primarily determine changes in the column.

Figure 1.8 shows the average northern mid-latitude trend between 1980 and 1996. Over most of the stratosphere during this time, a statistically significant decline in O_3 occurred. The greatest loss of O_3 (7% decade^{-1}) occurred in the upper and lower stratosphere, with the least loss occurring in the mid-stratosphere. (See also Randel *et al.* [20].)
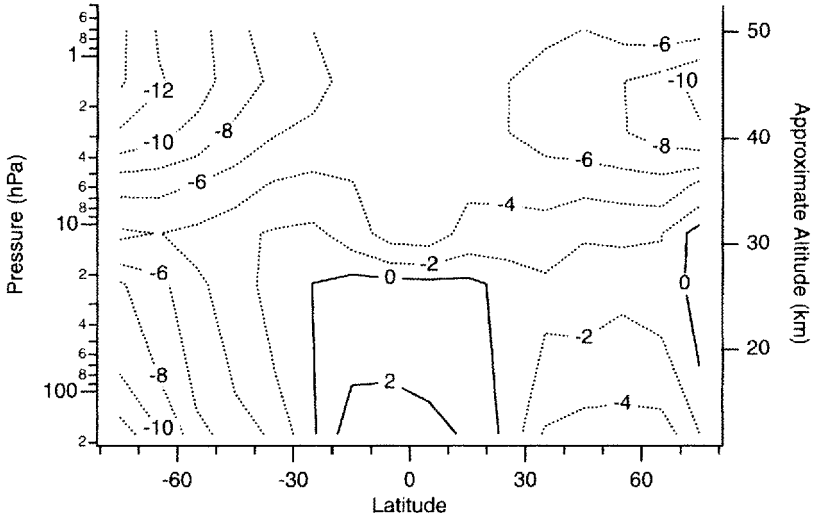
Figure 1.7 Contours of annually averaged O_3 trend (% decade^{-1}) measured by the Nimbus-7/SBUV instrument. The trend is calculated using data measured between 11/78 and 6/90 (see Hood *et al.* [19] for details on the statistical model used).
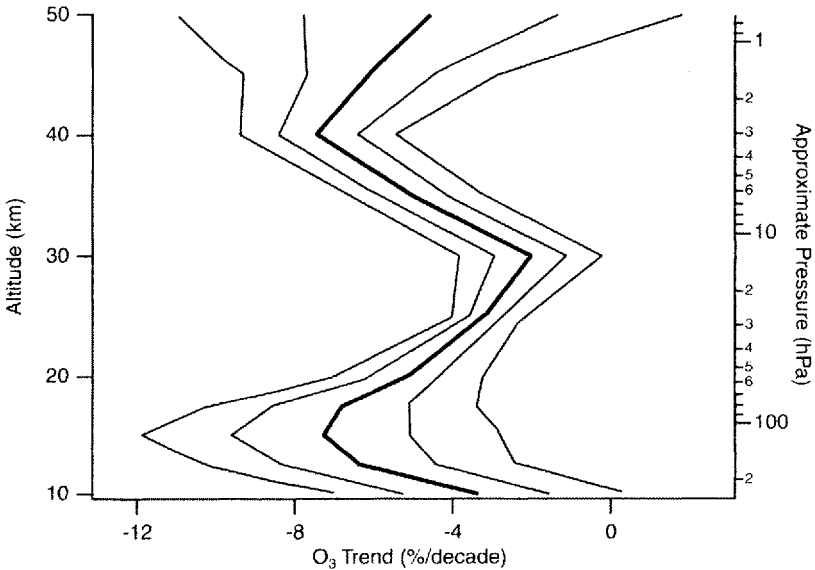
Figure 1.8 Estimate of the mean trend (1980–96) using four instrument systems (SAGE, Umkehr, SBUV, and sondes) at northern mid-latitudes (thick line). The thin lines are the combined 1- and 2-σ uncertainties. (After SPARC [21], Figure 3.54.)

1.3.3 The eruption of Mount Pinatubo

The eruption of Mount Pinatubo, a volcano in the Philippines (15°N, 120°E), on June 15, 1991 injected ~20 × 10^{12} g (20 Mt) of SO_2 into the stratosphere [22,23]. This SO_2 is oxidized to sulfate, and this in turn leads to the formation and growth of small liquid droplets comprised primarily of H_2O and H_2SO_4. These droplets, which are known as stratospheric sulfate aerosols, can perturb the chemical composition of the stratosphere two ways. First, they provide surfaces on which chemical reactions can take place. Second, they intercept and scatter solar and infrared radiation, which changes the heating of the stratosphere and the rates of photolytic reactions. The net result of the increase in aerosols after the eruption of Mount Pinatubo was a decline in column O_3 over most of the globe.

Figure 1.9 shows globally averaged column O_3 measurements between 1991 and 1993, the period 6 months before to about 2½ years after the eruption. Also shown are average, maximum, and minimum monthly averages for the period 1979–90. Column O_3 was very close to the average in 1991. Starting in early 1992, about 6 months after the eruption, column O_3 begins a noticeable decline. By late 1992, column O_3 was about 3% lower than pre-Pinatubo average column O_3, a difference
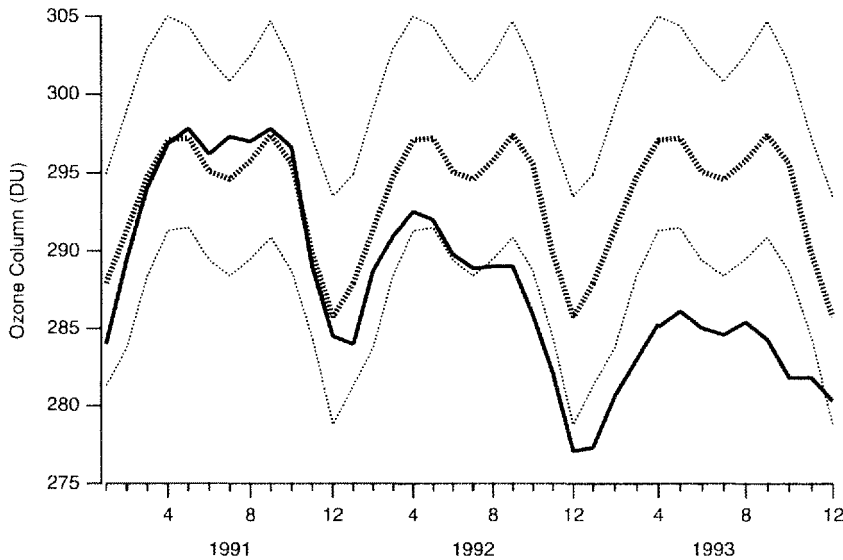
Figure 1.9 Column O_3 (DU) averaged between 65°N and 65°S versus month of year. Monthly averaged data for 1991, 1992, and 1993 are shown as the heavy solid line. The heavy dashed line is the monthly average for 1979–1990. The light dashed lines are the maximum and minimum monthly averages between 1979 and 1990. Data are a combination of version 7 Nimbus 7/TOMS and Meteor/TOMS.

that falls below the 1979–90 variability. By 1994 (not shown), column O_3 began recovering to its pre-eruption values. See also [24–26].

There is now a consensus that the low values of column O_3 in 1992–93 are causally related to the injection of SO_2 into the stratosphere by the 1991 eruption of Mount Pinatubo. We will discuss this further in Chapter 6.

1.4 In this book . . .

We hope that this brief introduction has sparked an interest in stratospheric O_3. In the rest of this book, our goal is to describe the chemical and physical processes that determine the distribution and abundance of O_3 in the stratosphere, as well as the chemical and physical processes that cause the Antarctic ozone hole, the mid-latitude trends, and the decline of O_3 after the eruption of Mount Pinatubo. In so doing, we hope to give the reader a sense of the beauty and elegance of stratospheric O_3.

Problems

1. Show how the constant 7.25×10^{18} in Equation (1.3) is derived. What would the constant be if one expressed pressure in torr and wanted the density in mol cm^{-3}? And in g cm^{-3}?

2. Unit-mania. Determine the density in the form requested, given the pressure and temperature:

Form of density	Temperature	Pressure
molecules cm^{-3}	–80°C	75 torr
kg m^{-3}	230 K	30 mb
mol cm^{-3}	250 K	2 hPa

3. Mixing ratio.
(a) The VMR of O_3 in the upper stratosphere (3 hPa, 240 K) is 2 ppmv. What is the number density of O_3?
(b) If a parcel of this air is moved to the lower stratosphere (50 hPa, 210 K), what is the VMR and number density of O_3 at the new location of the parcel? Assume that there are no chemical changes in the parcel.

4. VMR and MMR. There are really two types of mixing ratio: volume mixing ratio (VMR) and mass mixing ratio (MMR). As described above, the VMR of constituent X is the ratio of number density of X to the ambient number density: [X]/[M]. MMR

is, analogously, the ratio of the mass density of X to the ambient mass density: ρ_X/ρ_M. Write an expression to convert from VMR to MMR for H_2O.

5. Pass the sunscreen! Assume column O_3 decreases by 50%. How does the number of 250 and 300 nm photons reaching the surface change? If you were a sunscreen manufacturer, would you be more concerned with changes in surface radiation at 250 or 300 nm? Assume that the absorption cross-section of O_3 is 1.15×10^{-17} cm^2 and 3.4×10^{-19} cm^2 at 250 and 300 nm, respectively, and column O_3 is 350 DU before it is halved.

Chapter 2 | Fundamentals of Stratospheric Chemistry

Before we discuss the stratosphere in detail, we first review some of the fundamental concepts of atmospheric chemistry and stratospheric science.

2.1 Kinetics

Thermodynamics reveals whether a process will occur spontaneously or not. For example, at a pressure of 1 atm, ice is stable below 273.15 K. At higher temperatures, thermodynamics reveals that ice will spontaneously convert to water. Common experience tells us that the time for an ice cube to melt at room temperature is a few minutes. Surprisingly, thermodynamics also tells us that the diamond form of carbon is unstable under typical atmospheric conditions and will spontaneously convert to graphite. Whoever said that "diamonds are forever" apparently did not look up the free energy of the various forms of carbon. In defense of the advertising executive who came up with the slogan, however, our daily experience tells us that the conversion from diamond into graphite is slow, occurring over time-scales much longer than advertising executives' careers. In other words, thermodynamics provides information about the eventual outcome of a process. But it provides no information about the *rate* of the process. For studies of the chemistry of the atmosphere, however, a knowledge of the rate of a process is crucial. In this section, we discuss what determines the rates of chemical reactions, a field referred to as chemical kinetics.

2.1.1 First-order reactions

A first-order reaction is one in which a reactant spontaneously transforms itself into one or more products. Examples of this include radioactive decay and isomerization. The rate of a first-order reaction is equal to the product of a rate constant and the abundance of the reactant X:

$$\text{rate} = k[X] \tag{2.1}$$

where k is the first-order rate constant for the reaction, and it has units of inverse seconds (s^{-1}). [X], the abundance of X, can be expressed in either number density or VMR units. If [X] is expressed in number density (molecules cm^{-3}), then the rate has units of molecules per cubic centimeter per second (molecules cm^{-3} s^{-1}). If [X] is expressed in volume mixing ratios (VMRs), then the rate is in VMR per second (VMR s^{-1}).

If there are no other sources or sinks of X, then the time derivative of [X] is equal to the instantaneous rate of the reaction:

$$\frac{d[X]}{dt} = -\text{rate} = -k[X] \tag{2.2}$$

The rate of a reaction is always a positive number, so the minus sign indicates that X is being consumed.

Rearranging and integrating Equation (2.2) with the initial condition that the concentration of X at $t = 0$ is $[X]_0$ yields an expression for [X] as a function of time t:

$$[X](t) = [X]_0 e^{-kt} \tag{2.3}$$

Note that over any time interval $1/k$, |X| is reduced by a factor of $1/e$ ($1/2.72 \approx 0.368$). As a result, $1/k$ is often referred to as the e-folding time or lifetime of X. The concept of lifetime will be discussed at length later in this chapter.

Photolysis Sunlight is composed of ultraviolet, visible, and near-infrared radiation similar to that emitted by a black body at ~5700 K (see Goody and Yung [8], Appendix 9). These solar photons carry energies of 1 to a few electronvolts, enough to break bonds in many molecules. As a result, the absorption of solar photons by molecules in the atmosphere often results in the molecules being split into fragments. This process, known as photolysis, is an important process in the stratosphere. A typical photolytic reaction is the photolysis of nitric acid (HNO_3):

$$HNO_3 + h\nu \longrightarrow OH + NO_2 \tag{2.4}$$
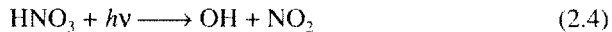
where $h\nu$ represents the energy of a photon.

Photolysis is usually treated as a first-order process, so that the rate at which a molecule is split into fragments is the product of a photolysis frequency (typically designated J) and the concentration of the molecule. The rate of Equation (2.4) is:

$$\text{rate} = J[HNO_3] \tag{2.5}$$

J, of course, has units of inverse seconds.

The photolysis frequency J at a given point in space and time is the integral of the product of the photon flux $q(\lambda)$, the absorption cross-section $\sigma(\lambda)$, and the quantum

yield $\varepsilon(\lambda)$. The integral extends over the portion of the solar spectrum whose photons have sufficient energy to dissociate the molecule:

$$J = \int_{\lambda_1}^{\lambda_2} q(\lambda)\sigma(\lambda)\varepsilon(\lambda)d\lambda \qquad (2.6)$$

As indicated, all of the terms in the integral are generally functions of wavelength. The photon flux $q(\lambda)$ is also a function of many other variables, including the total amount of ozone located above the point, the albedo (reflectivity) of the surface, and solar zenith angle (SZA). The absorption cross-section $\sigma(\lambda)$ will often vary with temperature. The quantum yield $\varepsilon(\lambda)$, the fraction of photons absorbed that leads to fragmentation of the molecule, can also be a function of temperature. In most cases the quantum yield is nearly 1, but it is often less at wavelengths near the energetic cut-off for dissociation of the molecule. For more discussion of photolysis, see Brasseur and Solomon [27], Chapter 4.

As mentioned above, the photolysis frequency is generally a strong function of the SZA. The SZA is the angle between the Sun and the point located directly over the observer's head (the zenith). Thus, an SZA of 0° means that the Sun is directly overhead, while an SZA of 90° means that the Sun is near the horizon. SZAs greater than ~90° mean that the Sun is below the horizon, i.e. it's night-time. At night, photolysis does not occur. It should be noted that for an observer in the stratosphere the sun does not set exactly at 90° owing to the observer's great height above the surface. Instead, the Sun can still be seen several degrees past 90°, with the exact SZA of sunset depending on the observer's altitude.

Figure 2.1 shows altitude profiles of the daytime-averaged photolysis frequencies of several important trace constituents in the stratosphere. The change in the photolysis frequency with altitude provides information about the wavelength dependence of the absorption cross-section of the molecule. For example, NO_2 absorbs visible radiation (wavelengths between 400 and 900 nm) strongly. Because the atmosphere is essentially transparent to visible radiation, the radiation field is fairly constant with height, and the photolysis frequency for this constituent shows little altitude dependence. For species that absorb shorter-wavelength ultraviolet radiation, on the other hand, the photolysis frequency shows significant dependence on altitude. This arises because O_3 efficiently absorbs ultraviolet radiation, so there is more ultraviolet radiation above the ozone layer, leading to higher photolysis rates there than at lower altitudes. The photolysis frequency for HNO_3, for example, decreases by more than 2 orders of magnitude as one descends from the upper to the lower stratosphere.

Note that the Earth, clouds, and atmosphere radiate similar to a black body at ~200–300 K. These photons of terrestrial origin have wavelengths greater than ~4 μm and generally do not have enough energy to break bonds in molecules. The absorption of these photons can, however, excite rotational and vibrational modes in a molecule, and the interaction of these photons with the atmosphere has important consequences for the Earth's climate.
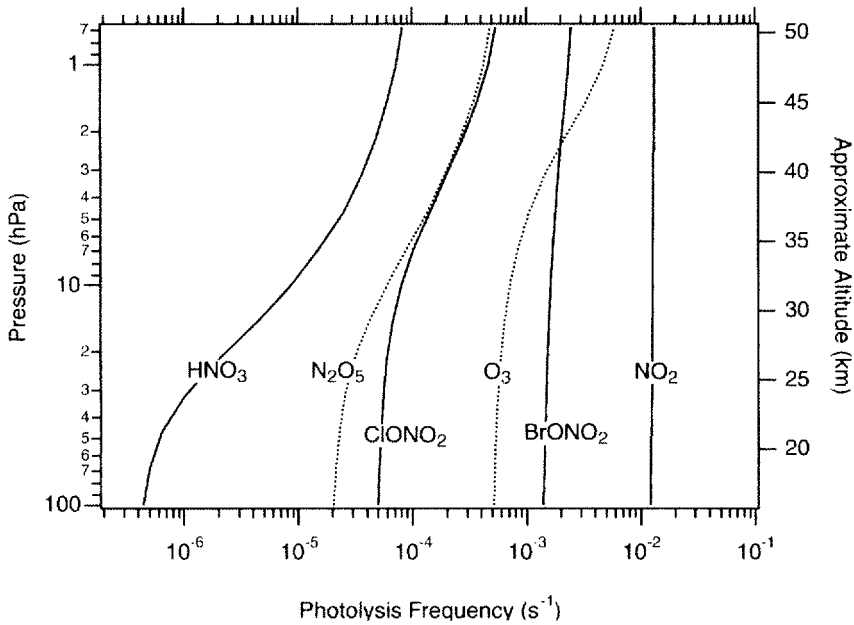
Figure 2.1 Daytime average photolysis frequencies versus pressure for selected species. The rates are for typical mid-latitude conditions. The O_3 photolysis rate is the sum of the rates of the $O(^3P)$ and $O(^1D)$ product channels. The rates are calculated by the photolysis routine from the Goddard three-dimensional Chemical Transport Model [28].

2.1.2 Second-order reactions

A second-order reaction is one with two reactants, such as the reaction between chlorine monoxide (ClO) and atomic oxygen (O):

$$ClO + O \longrightarrow Cl + O_2 \tag{2.7}$$

and whose rate is the product of a rate constant and the concentrations of the reactants:

$$rate = k[ClO][O] \tag{2.8}$$

Second-order reaction rate constants have units of cubic centimeters per molecule per second (cm^3 molecule^{-1} s^{-1}), and are generally functions of temperature. Unlike

first-order reactions, the abundances of the reactants in Equation (2.8) must be expressed in number density units. If there are no other sources or sinks of the reactants or products, then by the conservation of mass,

$$\text{rate} = -\frac{d[\text{ClO}]}{dt} = -\frac{d[\text{O}]}{dt} = \frac{d[\text{Cl}]}{dt} = \frac{d[\text{O}_2]}{dt} \qquad (2.9)$$

Temperature dependence of reactions   Svante Arrhenius first suggested in 1887 that second-order rate constants vary exponentially with inverse temperature. The functional form of a second-order rate constant is often written

$$k = A \exp\left(-\frac{E_a}{RT}\right) \qquad (2.10)$$

The pre-exponential factor A, which has the same units as the rate constant, is related to the fraction of collisions between the reactants that results in a successful reaction. Reactions in which essentially every collision results in a reaction have A factors of $\sim 10^{-10}$ cm^3 molecule^{-1} s^{-1}. Reactions in which the reactants must have very specific orientations only occur for a small fraction of the collisions, and can have A factors as small as 10^{-17} cm^3 molecule^{-1} s^{-1}.

In addition to this constraint on orientation, there is also in general a repulsive force between the reactants that must be overcome for a reaction to take place. This is expressed in Equation (2.10) as E_a, the "activation energy" of the reaction. The term $\exp(-E_a/(RT))$, where R is the gas constant and T is the temperature (K), is proportional to the number of molecules whose average translational kinetic energy exceeds the threshold E_a. It is these molecules that are able to surmount the repulsive force and react.

E_a can be as large as 20 kJ mol^{-1}. For these reactions, the rate constant will increase by ~50–70% for a 10 K increase in stratospheric temperature. Other reactions, especially those involving a molecule with an unpaired electron (known as a radical), have an E_a of zero. Some second-order reactions even have negative activation energies or show a dependence on pressure in addition to temperature. These reactions are more complicated than simple two-body bimolecular reactions, and involve the formation of reaction intermediates prior to formation of the products.

The NASA Panel for Data Evaluation [5] publishes tables of A factors and E_a/R for virtually every second-order reaction of stratospheric interest. This indispensable resource is widely used by stratospheric modelers.

2.1.3 Association reactions

An association or three-body reaction is one in which two reactants combine to form a single product molecule. An example of such a reaction is the formation of chlorine nitrate ($CIONO_2$)

$$CIO + NO_2 \xrightarrow{M} CIONO_2 \qquad (2.11)$$
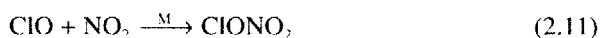
These reactions typically take place in two steps. First, the reactants collide to form an excited intermediate molecule:

$$CIO + NO_2 \longrightarrow CIONO_2* \qquad (2.12)$$

where the asterisk signifies an excited state. The $CIONO_2*$ molecule contains too much internal energy for it to exist for more than a few vibrational periods, and two things can subsequently happen to it. First, the $CIONO_2*$ molecule can collide with a third body, denoted M, but generally N_2 or O_2, which carries away some of the internal energy of the excited molecule, thereby stabilizing it:

$$CIONO_2* + M \longrightarrow CIONO_2 + M \qquad (2.13)$$

Alternatively, it can decompose back into CIO and NO_2, in which case there is no net reaction:

$$CIONO_2* \longrightarrow CIO + NO_2 \qquad (2.14)$$
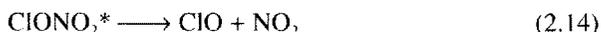
If the pressure is sufficiently high, in other words [M] is large, then every excited intermediate that is formed will collide with a third-body M, and form the stable molecule. In this case, the formation rate of $CIONO_2$ is equal to the rate of formation of the excited intermediate $CIONO_2*$. This is known as the "high-pressure limit" of the reaction. At low pressures, [M] is small and the excited intermediate $CIONO_2*$ usually decomposes back to CIO and NO_2. In this case, the formation rate of $CIONO_2$ is set by the collision rate between $CIONO_2*$ and M. This is known as the "low-pressure limit". At pressures between these limits the rate of the reaction is set by a combination of the two processes.

The rate of an association reaction is often written as

$$\text{rate} = k*[X][Y] \qquad (2.15)$$

where $k*$ is the effective second-order rate constant (with units of cm^3 molecule^{-1} s^{-1}) for the three-body reaction, and [X] and [Y] are the abundances of the reactants in molecules per cubic centimeter. It must be remembered that for these reactions, $k*$

depends not only on temperature but also on pressure. The NASA Panel for Data Evaluation publishes tables of kinetic data and a formula for calculating the effective second-order rate constant k* of a reaction given the temperature and pressure (see DeMore *et al.* [5], pp. 8–11).

2.1.4 Other types of reactions

Thermal decomposition   Thermal decomposition occurs when a molecule splits into fragments following nonreactive collisions with other molecules—usually N_2 or O_2. An example is the thermal decomposition of the chlorine monoxide dimer (ClOOCl):

$$ClOOCl \xrightarrow{M} ClO + ClO \tag{2.16}$$

This reaction is the opposite of a three-body association reaction. First, collisions between ClOOCl and M transfer energy to ClOOCl and create the excited intermediate ClOOCl*. This excited intermediate can either collide with another M and have some internal energy taken out, leading to the restabilization of the intermediate, or the excited intermediate can fall apart into fragments:

$$ClOOCl^* \longrightarrow ClO + ClO \tag{2.17}$$

At stratospheric temperatures, this type of reaction breaks bonds in only the most weakly bound molecules (such as ClOOCl).

The rate of reaction (2.16) is generally written as a first-order process:

$$\text{rate} = k^T[ClOOCl] \tag{2.18}$$

where k^T is the thermal decomposition rate constant with units of inverse seconds. In practice, k^T must be calculated from the rate of the association reaction and the equilibrium constant between the reactant and products (see DeMore *et al.* [5], Table 3).

Heterogeneous reactions   Reactions can also occur on the surfaces of liquid and solid particles. For example, an important heterogeneous reaction in the stratosphere is

$$ClONO_2 + HCl \xrightarrow{\text{particle}} Cl_2 + HNO_3 \tag{2.19}$$

Much like association reactions, this simple-looking reaction actually represents a far more complicated process [29–32]. Typically, one of the reactants is first

absorbed onto/into the particle (in this case, HCl). Then, reactions occur as the other reactant (in this case, $ClONO_2$) collides with the particle. Because of this, heterogeneous reactions are usually written as a first-order loss process for the constituent that reacts on collision:

$$\text{rate} = k^{\text{II}}[ClONO_2] \tag{2.20}$$

where k^{II} is a first-order rate constant with units of inverse seconds. Using simple collision theory, we can write k^{II} as

$$k^{\text{II}} = \frac{VA\gamma}{4} \tag{2.21}$$

V is the thermal velocity of the molecule, in this case $ClONO_2$. For a typical molecule at stratospheric temperatures, V is several hundred meters per second. A is the particle surface area per unit volume, also known as the surface area density (abbreviated SAD). γ, called the reactive uptake coefficient, is the fraction of collisions between the reactant and the particle that result in a reaction. γ is therefore dimensionless and always between 0 and 1. In general, γ is a function of temperature, pressure, particle radius, water vapor abundance, and the gas phase abundance of the absorbed constituent (in this example, HCl) [29,33].

There are two general types of particles in the stratosphere: sulfate aerosol and polar stratospheric clouds (PSCs). Sulfate aerosol particles are the more common. First characterized by Junge et al. [34], these particles are liquid, and their composition varies with temperature (Figure 2.2). Above ~215 K, H_2SO_4 makes up 70–80% of the mass of the aerosol, with water making up virtually all of the remainder. As the particles cool, they absorb water vapor, decreasing the relative abundance of H_2SO_4. At temperatures below ~200 K, the particles absorb significant amounts of HNO_3 [35,36]. The majority of the aerosol particles in the stratosphere are found in the lower stratosphere in the so-called "Junge layer".

Aerosol particles are initially formed ("nucleated") in rising tropical air masses [38]. This produces large numbers (~10^5 particles cm^{-3}) of extremely small (a few angstroms in radius) H_2SO_4/H_2O particles [39]. Then, on a time-scale of a day or so, these particles coagulate, resulting in the formation of fewer (10^2–10^3 particles cm^{-3}), larger particles. A binary phase droplet, such as these H_2SO_4/H_2O particles, can, in general, achieve equilibrium with the vapor phase of one of its components, but not both. Because of the much greater abundance of H_2O compared to H_2SO_4 in the stratosphere, these H_2SO_4/H_2O particles are in equilibrium with respect to water, but are subsaturated with respect to H_2SO_4. H_2SO_4 produced in the stratosphere from the oxidation of sulfur-bearing species is therefore rapidly absorbed by the particles. This causes the composition of the aerosol particles to change, and to regain equilibrium the particle absorbs water. Through this process, and coagulation, the
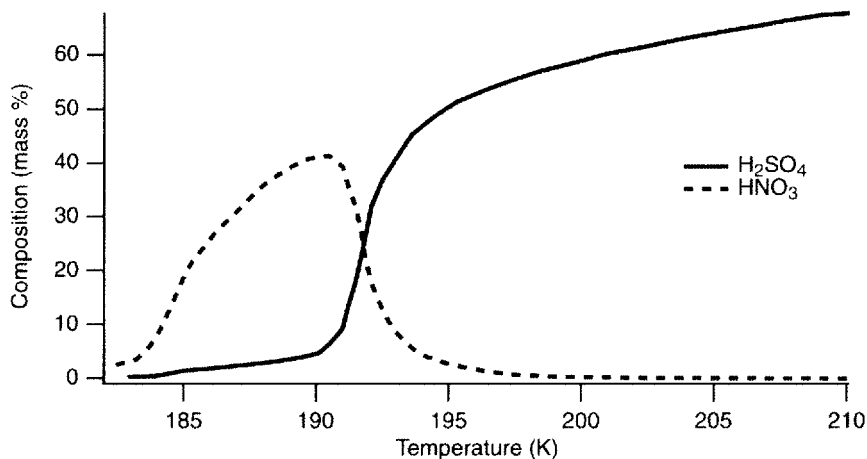
Figure 2.2 Composition of stratospheric aerosols versus temperature. The remainder of the aerosol mass is made up by water. (After Carslaw *et al.* [37], Figure 7d.)

particles grow. Aerosol particles are lost when they are transported back into the troposphere as part of the mean stratospheric circulation (see Chapter 5), which occurs on a time-scale of 1 or 2 years [40]. For a more detailed discussion of the life cycle of nonvolcanic stratospheric aerosols, see [39].

One source of the H_2SO_4 in aerosols is SO_2 and OCS produced at the surface from biogenic and anthropogenic activities. These species are transported into the stratosphere as part of the overall general circulation (see Chapter 5) and are oxidized there to H_2SO_4 [41,42]. This source of sulfur can produce an aerosol SAD of about 0.8 μm^2 cm^3 at around 20 km (see Yue *et al.* [43], Figure 7a), decreasing rapidly with altitude. We refer to these nonvolcanic sources as "background" sources of aerosols.

Volcanic eruptions are capable of episodically injecting huge amounts of sulfur, usually in the form of SO_2 or H_2S, directly into the stratosphere. The SO_2 is subsequently oxidized to H_2SO_4 [42] on a time-scale of about 1 month [22,44]. This H_2SO_4 is rapidly absorbed by aerosol particles, allowing the aerosol particles to absorb water and grow. Because aerosol particles are flushed out of the stratosphere in 1–2 years, most of the aerosol surface area due to a volcano will have been flushed out of the stratosphere after a few years.

The eruption of Mount Pinatubo in June of 1991, for example, injected ~20×10^{12} g of SO_2 into the stratosphere in just a few days [22,23]. This increased the lower-stratospheric SAD by a factor of 30 or more over background [45]. Figure 2.3 shows northern hemisphere profiles of aerosol SAD for background
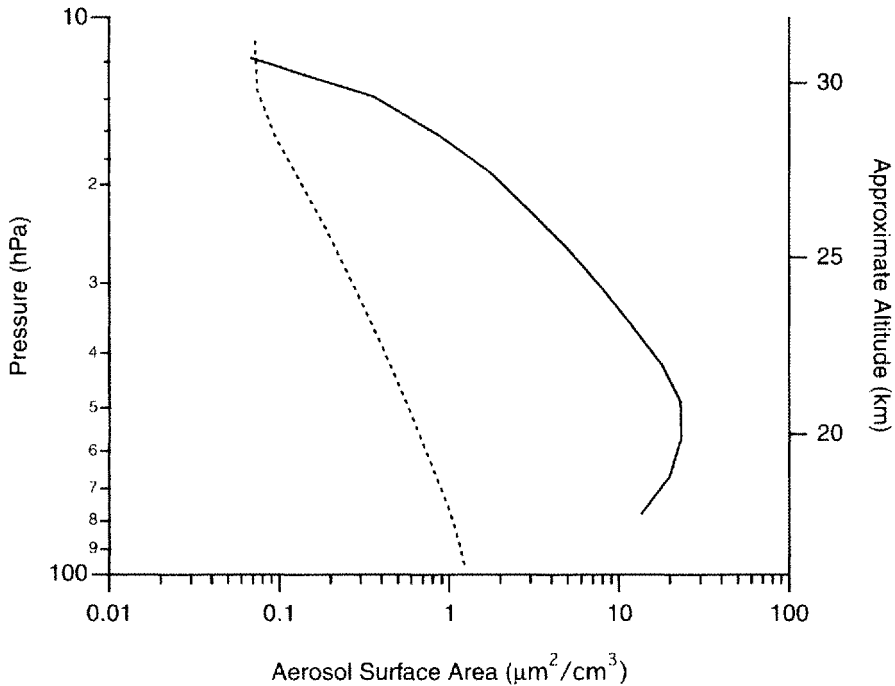
Figure 2.3 Sulfate aerosol surface area density versus pressure. The dashed line is an estimate of the background aerosol amount. The solid line is a high-latitude northern hemisphere profile obtained in March 1992, and shows enhanced aerosol amounts resulting from the eruption of Mount Pinatubo. (After Dessler *et al.* [46], Figure 1c.)

conditions and after the eruption of Mount Pinatubo. Most of the impact on SAD was in the lower stratosphere, with the volcanic enhancement rapidly decreasing with altitude. We will discuss the implications of this on the chemistry of the stratosphere in Chapter 6.

There are ~10 aerosol particles cm^{-3} in the lower stratosphere [47]. Under background conditions these aerosol particles have typical radii of 0.1–0.2 mm [39,45,48]. After the eruption of Mount Pinatubo the typical radii of the particles increased to ~0.5 μm [45,48]. The distribution of particle sizes around these typical sizes is usually described by unimodal or bimodal lognormal distributions [49,50]. These are simple analytic functions of the total number of aerosol particles and one or two "effective radii". The effective radius is the third moment of the size distribution divided by the second moment, and can be thought of as a typical value for the distribution.

PSCs are found in the polar regions during the winter and early spring. The cold

temperatures there (less than ~196 K) permit the condensation of water vapor and nitric acid into various liquid and solid forms. These clouds serve as sites for heterogeneous reactions that are necessary for polar O_3 destruction and the formation of the Antarctic ozone hole. We will discuss PSCs in detail in Chapter 7.

2.2 The Continuity Equation

In order to understand the chemistry of the stratosphere, one must understand the continuity equation. At a given point in the stratosphere, the continuity equation for a constituent X is

$$\frac{\partial [X]}{\partial t} = P - L[X] - \nabla \cdot (V[X]) \tag{2.22}$$

P is the photochemical production term—the amount of X produced per unit volume per second. Photochemical loss is written as the product of a loss frequency L, typically with units of inverse seconds, and the abundance of X. This convention is adopted because the rate of destruction of X is generally proportional to its abundance (there are exceptions to this, however). Production, on the other hand, is generally independent of the abundance of X. The far-right term on the right-hand side of Equation (2.22) is the divergence of the flux of X. This term represents net transport of X in or out of the unit volume by the wind. Typically, each term in Equation (2.22) (P, $L[X]$, etc.) will have units of molecules per cubic centimeter per second or VMR per second.

The continuity equation is the atmospheric equivalent of balancing a checkbook. The terms on the right-hand side of the equation represent the sources and sinks of X in the unit volume. If the sources and sinks balance, then there is no net change in the abundance of X, and $\partial [X]/\partial t$ is zero. If, on the other hand, the sources and sinks of X do not balance, then the abundance of X must be changing in response. Note that photochemical production (P) always leads to a positive time rate of change, while loss ($L[X]$) always leads to a negative time rate of change. The transport term, however, can be either positive or negative.

Depending on the location, time of year, and species in question, the right-hand side of the continuity equation might be dominated by one or two of the terms—and the remaining term(s) can be neglected. A common situation in stratospheric chemistry is the case where the photochemistry terms (P and $L[X]$) are much larger than the transport term ($\nabla \cdot (V[X])$). In this case, the transport of X can be neglected, and Equation (2.22) can be written as

$$\frac{\partial [X]}{\partial t} \approx P - L[X] \tag{2.23}$$

Let us further assume that $P = P_0(1+\sin(\omega t))$, where P_0 (molecules cm^{-3} s^{-1}) is a constant, and L (s^{-1}) is a constant. In other words, the production varies over the time period $1/\omega$, while the loss frequency L is constant. In the real atmosphere, production and loss will often vary over periods of 24 h (although in this example only production is varying), so a typical value of ω is $2\pi/(24$ h). The general solution to Equation (2.23) is then

$$[X](t) = \frac{P_0\omega^2 + L^2P_0 - LP_0\omega \cos(\omega t) + L^2P_0 \sin(\omega t)}{L(L^2 + \omega^2)} + C_1e^{-Lt} \qquad (2.24)$$

The right-hand side of Equation (2.24) has two terms: a perturbation term (C_1e^{-Lt}) and a "steady-state" term (($P_0\omega^2 + \ldots)/(L(L^2 + \omega^2)$)). The steady-state term represents the abundance of X that is consistent with the photochemical production and loss rates—it is important to realize that this term is not necessarily constant with time. The perturbation term accounts for departures of [X] from its steady-state abundance. Note that the value of the perturbation, initially C_1, is reduced by a factor of $1/e$ every $1/L$ units of time, i.e. $1/L$ is the "e-folding time" of the perturbation. As $t \to \infty$, the perturbation term goes to zero, and X achieves its steady-state abundance.

The e-folding time $1/L$ turns out to be a crucial parameter for understanding the behavior of [X] as a function of time. The perturbation term does not change significantly over time periods much shorter than $1/L$; we will show later in this section that the steady-state term will also not change significantly over time periods much less than $1/L$. As a result—and this is an important point—the abundance of X does not change significantly over lengths of time much shorter than $1/L$. For these time-scales, we say that constituent X is "conserved". On the other hand, over lengths of time much longer than $1/L$, the concentration of [X] can change significantly.

The implications of this are important. For example, $1/L$ for ClONO$_2$ in the lower stratosphere is a few hours. If two measurements of [ClONO$_2$] are made in the same air parcel a few minutes apart, the abundance of ClONO$_2$ will be about the same, regardless of what happens to the air parcel between the measurements—the chemistry is simply not fast enough to change [ClONO$_2$]. However, if the time between measurements is a few days, then we cannot expect [ClONO$_2$] to be unchanged. We define $\tau = 1/L$ to be the "lifetime" of the constituent. As we will discuss in the next section, this quantity is widely used in stratospheric chemistry. Note that this lifetime is the same as that derived for first-order reactions (Equation (2.3)).

There are two limiting cases for the steady-state term of Equation (2.24). If $L \gg \omega$, then the lifetime of X is much shorter than the time scale for production to vary. From Equation (2.24), $[X]_{ss}$, the steady-state abundance of X, is

$$[X]_{ss}(t) \cong \frac{L^2P_0 + L^2P_0 \sin(\omega t)}{LL^2} = \frac{P_0(1 + \sin(\omega t))}{L} = \frac{P}{L} \qquad (2.25)$$

Remember that P is a function of time ($P = P_0(1 + \sin(\omega t))$), while L is constant. In this case, $[X]_{ss}$ is set by the instantaneous production rate and loss frequency, and will vary throughout the day as the production rate varies. In other words, the chemistry is so fast that the abundance of X reacts essentially instantly to the variation of P with time, and $[X]_{ss}$ is determined by the instantaneous values of P and L. This is often referred to as "photochemical steady state".

If $L << \omega$, then the lifetime of X is much longer than the time-scale for production to vary, and

$$[X]_{SS}(t) \cong \frac{P_0\omega^2 - LP_0\omega\cos(\omega t)}{L\omega^2} = \frac{P_0}{L} \qquad (2.26)$$

where we have used the fact that $P_0\omega^2 >> LP_0\omega\cos(\omega t)$ in the simplification. In this case, the chemistry is slow compared to the rate of variation of production. As a result, the abundance of X is determined by the average value of P and L. In other words, the production rate equals the loss rate when averaged over $1/\omega$. The instantaneous production rate will not, in general, equal instantaneous loss rate. We refer to this condition as "diurnal steady state".

As stated earlier, production and loss rates both tend to vary strongly during the day as photolysis rates change. This means that if the loss lifetime $1/L$ is much shorter than this, then the system will be in photochemical steady state, and $[X]$ can vary during the day—i.e. $[X]$ will display a diurnal cycle. If the loss lifetime $1/L$ is comparable to or longer than 24 h, then the system will be in diurnal steady state, and $[X]$ will not vary significantly during the day—i.e. $[X]$ will display little diurnal variations. Note that in no case can $[X]$ change significantly over periods of time much shorter than $1/L$.

Finally, this example was based on the assumption that the transport term of the continuity equation was small compared to the production and loss terms, a situation that arises frequently in the stratosphere. However, it is worth emphasizing that this assumption does not mean that transport is, in general, unimportant. Even for species for which transport of that species is unimportant, transport can be important for other constituents that determine the production rate and loss frequency for X.

2.3 Lifetimes, Time-scales, and Time Constants

In the last section we introduced the term "lifetime". In this section we discuss this further and introduce the related quantities "time-scale" and "time constant". These three quantities, which have units of time and are often used interchangeably, are important and used frequently in the literature and in colloquial contexts.

Previously, we saw how the abundance of a constituent cannot change over lengths of time much shorter than the lifetime $1/L$ of a constituent. This leads us to a general definition of the terms "lifetime", "time-scale", and "time constant": the length of time over which a quantity can change or a process operates. For example, if one puts a pot of cold water on the stove and wants to know when it starts to boil, how often does one check the pot (remembering, of course, that a watched pot never boils)? One could check the pot every 5 s, or one could check the pot every 5 days. But we know from experience that it takes a few minutes to boil water on a stove, and so you would likely check the pot about that often. In this example, we would say that the time-scale for water to boil is a few minutes. As another example, the time-scale for paint to dry is several hours. So if you are asked to determine when a painted surface has dried, you would not check every few minutes or every few weeks, but every hour or so. In both of these cases, the time-scale gives you an idea of about how long the processes under investigation take.

It turns out that a knowledge of the time constants of a problem is invaluable for isolating its important aspects. For example, we discussed in Chapter 1 that column O_3 declined over much of the Earth during the 1980s. It is also well known that the arrangement of the Earth's continents affects the circulation of the stratosphere and thereby helps determine the distribution and amount of stratospheric O_3. We also know that the arrangements of continents can change. Could the decline in column O_3 during the 1980s be caused by changes in the arrangement of the continents? Of course not, and the reason is based on time-scales. The topography of the Earth does change, and this might indeed change the distribution of stratospheric O_3, but significant change takes tens of millions of years. Thus, over the time period of the O_3 changes under investigation (a decade), we know that there were no significant changes to the topography of the Earth. We can therefore neglect continental drift and mountain building as a cause of O_3 loss over the last decade or so. Instead, we search for those processes that can affect O_3 and were changing on a time-scale of decades. This method—identifying relevant time-scales and ignoring processes whose time-scales are too long or too short—is a useful approach that is used throughout science.

In the previous section, the lifetime $1/L$ of a constituent was derived from the solution of a simplified continuity equation (Equation (2.23)). However, there is a simpler way to define the lifetime of a chemical constituent: the "replacement lifetime". The replacement lifetime is equal to the total abundance of the constituent divided by the rate at which the constituent is produced or destroyed. One can therefore define a replacement lifetime with respect to loss, τ_L,

$$\tau_L = \frac{[X]}{(\text{total loss rate})} = \frac{[X]}{L[X]} = \frac{1}{L} \tag{2.27}$$

or with respect to production, τ_P,

$$\tau_P = \frac{[X]}{(\text{total production rate})} = \frac{[X]}{P} \qquad (2.28)$$

Note that the replacement lifetime with respect to loss in Equation (2.27) gives the same $1/L$ lifetime as was derived earlier in this chapter. At photochemical steady state the lifetimes of X with respect to production and loss are equal. It is also possible to define a replacement lifetime with respect to transport τ_T, but it is rarely used. Throughout this book and most of the literature, the lifetime of a constituent generally refers to the reciprocal of the loss frequency, $1/L$.

2.3.1 Multiple-loss processes

If a constituent X has several loss pathways, then the total loss frequency is the sum of the loss frequencies of the individual pathways: $L_{tot} = L_1 + L_2 + \ldots + L_n$. For each individual loss process, we can define a loss lifetime for that process $\tau_n = 1/L_n$. The lifetime with respect to the combined loss pathways is

$$\tau = \frac{1}{L_1 + L_2 + \ldots + L_n} = \frac{1}{\dfrac{1}{\tau_1} + \dfrac{1}{\tau_2} + \ldots + \dfrac{1}{\tau_n}} \qquad (2.29)$$

Note that lifetimes add in the same way that resistors in parallel add.

It should be clear from Equation (2.29) that one can ignore loss pathways whose loss frequency is much smaller than other loss frequencies for the constituent. Stated another way, one can ignore any loss process if the loss lifetime for that process is much longer than the loss lifetimes of other loss processes.

2.3.2 Global lifetimes

The $1/L$ lifetime that we have discussed up to this point is a "local" lifetime: it is the length of time that a molecule will survive at a given point in space before being chemically destroyed. For long-lived species, meaning species whose local lifetime in the lower stratosphere is years or longer ($1/L > 10^8$ s), transport of the species is an important determinant of its stratospheric distribution. For these species the "global lifetime" is often of interest. The global lifetime can be thought of as the average length of time between the emission or formation of a molecule and its

destruction. It is equal to the total atmospheric burden divided by the total atmospheric loss rate:

$$\tau_{global} = \frac{\text{total atmospheric burden}}{\text{total loss rate}} = \frac{\int [X] dV}{\int L[X] dV} \tag{2.30}$$

where the integral extends over the entire atmosphere. Note that this is analogous to the simple "replacement lifetime" discussed in the previous section (see Equation (2.27)).

One can also calculate a "stratospheric lifetime" where the integral in the denominator of Equation (2.30) extends only over the stratosphere. Many species, such as the chlorofluorocarbons (CFCs), are destroyed only in the stratosphere and above. Their global and stratospheric lifetimes will therefore be the same. Species with significant tropospheric sinks, such as CH_4, have global lifetimes shorter than their stratospheric lifetimes. Table 2.1 shows the stratospheric lifetimes of several gases of importance in stratospheric chemistry.

Table 2.1 Stratospheric lifetimes.

Gas	Lifetime (years)
N_2O	122 ± 24
CH_4	93 ± 18
CFC-12 (CCl_2F_2)	87 ± 17
CFC-113 (CCl_3CF_3)	100 ± 32
CCl_4	32 ± 6
CH_3CCl_3	34 ± 7
H-1211 ($CBrClF_2$)	24 ± 6

Based on the CFC-11 lifetime of 45 ± 7 years.
From Volk *et al.* [51], Table 5.

2.4 Coordinate Systems

In order to analyze and interpret a set of atmospheric measurements, one must first put those measurements into a coordinate system. For example, if one is studying polar O_3 loss, then the measurements of most interest are those in the lower stratosphere and at high latitudes—and one must be able to select those measurements out of any data set of interest. In this case, pressure and latitude might be the coordinates of choice.

2.4.1 Vertical coordinates

The most obvious vertical coordinate is geometric altitude, e.g. how many meters above some reference level (such as mean sea level) an air parcel is. Altitude,

however, turns out to be difficult to measure from balloon or aircraft platforms, and as a consequence is rarely used. Pressure, however, is easily measured by *in situ* instruments, making it the most common vertical coordinate. The pressure at the tropopause ranges from ~300 hPa at high latitudes to 100 hPa over the equator. Pressure decreases monotonically with altitude, and at the stratopause its value is ~1 hPa.

A quantity that is related to pressure is pressure altitude Z^*. The pressure altitude of a given pressure p is calculated using the equation

$$Z^* = -H \ln \left(\frac{p}{p_0} \right) \tag{2.31}$$

where H is the scale height, a constant with a typical value of ~7 km. p_0 is a reference pressure (often 1000 hPa, and in the same units as p).

Another commonly used vertical coordinate is potential temperature. The concept of potential temperature is based on an adiabatic process, one in which no heat flows into or out of the air parcel. If an air parcel moves adiabatically to a lower pressure, then the parcel will expand. Because no heat flows into the parcel, the work done to expand the parcel is provided by the internal energy of the parcel, and the temperature of the parcel decreases. Conversely, if an air parcel moves adiabatically to a higher pressure, the parcel is compressed. The work done on the parcel by the atmosphere during the compression increases the internal energy of the parcel, leading to a temperature increase.

The potential temperature of an air parcel is the temperature that the parcel would have if it were moved adiabatically to a reference pressure, usually the surface pressure (1000 hPa). It can be shown (for example, see Houghton [52], p. 22) that

$$\theta = T \left(\frac{p}{p_0} \right)^{-\kappa} \tag{2.32}$$

where θ is the potential temperature (often referred to simply as "theta"), which has units of kelvin. T and p are the temperature (K) and pressure of the parcel, respectively. p_0 is the reference pressure. Note that the units on p and p_0 can be anything as long as they are the same. κ, which is numerically equal to 2/7, is the ratio $(c_p - c_v)/c_p$, where c_p and c_v are the heat capacities of air at constant pressure and volume, respectively. The potential temperature of the tropopause ranges from 320 K at high latitudes to 380 K over the equator. Potential temperature increases monotonically with altitude, and at the stratopause its value is ~2000 K.

The advantage of potential temperature over pressure can be seen in Figure 2.4, which shows a 15 day time series of pressure, temperature, and potential temperature for a typical mid-latitude air parcel. While flow in the stratosphere is approximately horizontal, individual parcels can experience significant changes in
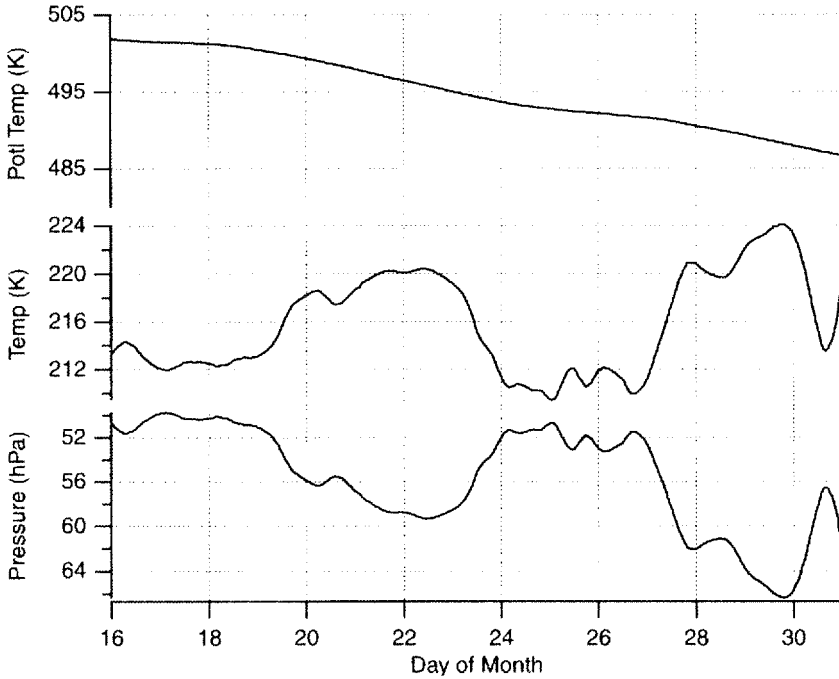
Figure 2.4 Time series of potential temperature, temperature, and pressure for a typical mid-latitude air mass at the equinox, as determined from a trajectory model [53].

pressure on time-scales of 1 day. These short-term fluctuations are, however, adiabatic. Thus, when the pressure of the parcel is increasing (decreasing), the temperature of the air parcel is increasing (decreasing) in such a way that the potential temperature remains constant. The result is that the potential temperature changes by only a few percent over the 15 day time series, despite large changes in pressure. In the parlance of stratospheric science, potential temperature is better conserved than pressure. It is this quality that makes potential temperature a useful vertical coordinate.

This leads to an important question: over what time-scales are the potential temperature of an air parcel conserved? The assumption underlying the concept of potential temperature is that the air parcel is adiabatic: heat flow into or out of the air parcel is zero. As we will show in Chapter 5, however, air in the tropical stratosphere is being heated (i.e. the potential temperature of parcels increase with time), while the mid- and high-latitude stratosphere is being cooled (i.e. the potential temperature of parcels decreases with time) [54]. The time series in Figure 2.4, for example, shows that potential temperature of the mid-latitude parcel is indeed

decreasing with time, albeit slowly ($\partial\theta/\partial t \approx 1$ K day^{-1}). Figure 2.5 plots the zonally and annually averaged radiative damping time-scale, which is the time-scale over which a temperature perturbation is damped. This damping time can be considered the lifetime of potential temperature (much as the damping time for a chemical perturbation can be thought of as the lifetime). Over periods shorter than this damping time, potential temperature is conserved. Potential temperature is conserved for ~30 and ~5 days in the lower and upper stratosphere, respectively.

This discussion brings up an interesting point. It is often said that flow in the stratosphere is generally horizontal. From the previous discussion, however, it should be clear that flow in the stratosphere actually occurs close to surfaces of constant potential temperature, also known as isentropic (constant entropy) surfaces. However, because the surfaces of constant potential temperature on average lie close to surfaces of constant geometric altitude, flow in the stratosphere is indeed approximately horizontal.

2.4.2 Horizontal coordinates

Winds in the stratosphere are predominantly horizontal and zonal (east–west). Components of the wind velocity in the meridional (north–south) and vertical
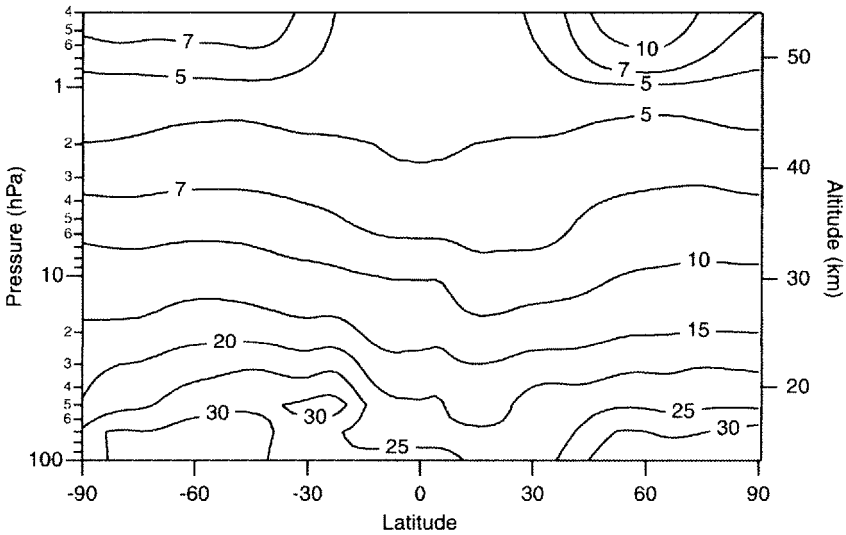
Figure 2.5 Contours of zonally and annually averaged radiative damping time-scale (days). (After Newman and Rosenfield [55].)

directions, while critically important to the distribution of trace gases in the stratosphere, are smaller than the zonal component of the wind velocity. The dominance of zonal flow means that the air tends to be well mixed in the zonal direction. In other words, air at different longitudes but the same latitude and altitude is more similar than air at different latitudes or different altitudes. For this reason, data from the same latitude and altitude but different longitudes are often averaged together to obtain a "zonal average". Many of the plots in this book are zonal averages (e.g. see Figure 2.5).

While flow in the stratosphere is predominantly zonal, individual air parcels can experience significant changes in their latitude on a time-scale of a day. Such displacements are caused by planetary-scale waves, and are often reversible, so that the air parcel will return to its original latitude after one to a few days. At a given latitude, one therefore often finds that some of the air parcels have a chemical composition characteristic of other latitudes. This means that latitude is often not the best choice of horizontal coordinate.

We have, however, a horizontal coordinate that is conserved during reversible meridional transport by planetary-scale waves. It is known as potential vorticity (PV) [56]. Thus, while the latitude of a parcel might change during transport by planetary-scale waves, its PV remains constant. Mathematically, PV is related to the curl of the wind field, the rotation of the Earth, and the local thermal gradient, and may be thought of conceptually as a fluid dynamical analog of angular momentum. PV is normally positive in the northern hemisphere and negative in the southern hemisphere, consistent with the sense of the Earth's rotation, and increases in absolute magnitude with latitude on surfaces of constant potential temperature. PV is conserved on time-scales similar to the time-scale over which potential temperature is conserved (Figure 2.5).

As a result, air at the same altitude and PV tends to be more similar than air at the same latitude, making PV a superior horizontal coordinate [57,58]. For simplicity, PV is often expressed in units of equivalent latitude. The equivalent latitude of a PV value is the latitude circle that encloses the same area as the PV contour. Because of its convenience, equivalent latitude will be used frequently in this book—often in the context of a zonally averaged equivalent-latitude plot. In this type of plot, data at the same equivalent latitude and altitude are averaged together, regardless of longitude, to obtain a two-dimensional view of the atmosphere. Because equivalent latitude more accurately separates different air masses, this type of plot will better capture strong meridional gradients in the data—such as those found around the polar vortex (discussed in Chapter 7). Finally, it should be noted that equivalent latitude can be calculated from geophysical parameters other than PV [59,60].

2.4.3 Tracers of atmospheric motion

A long-lived tracer is a constituent that has a stratospheric lifetime of years or longer. The sources of most long-lived tracers are in the troposphere, while their sinks are

primarily in the stratosphere. A good example is nitrous oxide (N_2O), which is produced near the surface through both natural and anthropogenic activities. It enters the stratosphere with a VMR of ~310 ppbv, and it is destroyed in the middle and upper stratosphere. The local lifetime of N_2O is ~100 years at 20 km, ~10 years at 25 km, ~1 year at 30 km, and a few months at 40 km.

The distribution of N_2O is in general determined by a combination of chemistry and dynamics. Figure 2.6 shows a zonal average distribution of the N_2O VMR. Note the strong gradients in N_2O VMR in both the horizontal and vertical. The vertical gradient results primarily from the rapidly increasing loss rate of N_2O with altitude combined with relatively slow vertical transport in the stratosphere. The horizontal gradients occur in regions of slow horizontal mixing. This will be discussed further in Chapter 5.

Because of these gradients, we can use the abundance of N_2O to help determine the recent history of air masses [61,62]. The tropical lower stratosphere, for example, contains N_2O VMRs greater than ~250 ppbv, a higher value than found at higher latitudes or altitudes. Thus, a measurement of N_2O VMR of greater than 250 ppbv in the mid-latitudes suggests that this air is of tropical origin and has recently been transported to mid-latitudes. Similarly, an observation of lower stratospheric air with less than 100 ppbv of N_2O suggests that this air was likely recently transported from higher altitudes.
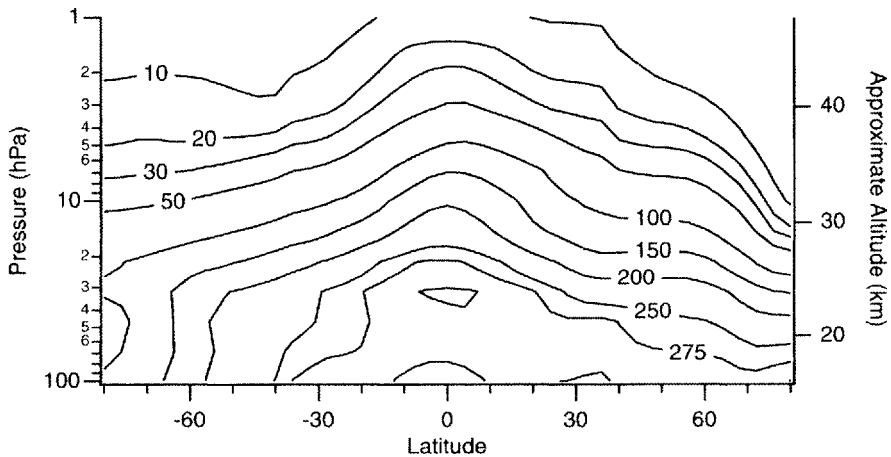

Figure 2.6 Zonal-average contours of N_2O VMR (ppbv) for December 1992. Data are from the UARS Reference Atmosphere Project (W. J. Randel, personal communication, 1998).

Problems

1. Equation (2.24) was derived based on production rate $P = P_0(\sin(\omega t)+1)$ and loss rate $L = L_0[X]$, where P_0 (molecules cm^{-3} s^{-1}) and L_0 (s^{-1}) are constants. The first term on the right-hand side is the "steady-state" part of the solution. The second term $(C_1 \exp(-L_0 t))$ is the perturbation term that damps with a lifetime of $1/L_0$. For the rest of this problem, we will assume that C_1 is 0.

(a) What is the time-scale for the production of X to vary? (In other words, the average production is P_0, but instantaneous production varies about this average value. What is the characteristic time-scale for P to vary about P_0?)

(b) What is the time-scale of the loss chemistry of X? (In other words, what is the lifetime of X with respect to loss processes?)

From the form of Equation (2.24) it should be obvious that [X] is a sinusoid that shows no long-term trends. Thus, it must be in some form of steady state.

(c) To satisfy yourself of this, calculate $\partial[X](t)/\partial t$ and show that the long-time average of this quantity is zero (by long time, I mean that the time over which we average $\gg 1/\omega$). Also, calculate the long-time average production and loss rates of X. Are they equal?

The next thing you're probably asking yourself is: is the system in "photochemical steady state" in the strictest sense? In other words, does the production equal loss at all points in time, or just in the average?

Let's look at two cases: first, assume that $L_0 \gg \omega$.

(d) In words, what does this condition mean?

(e) Calculate the loss rate for this condition. Is it equal to production? Does this make sense?

Now, let's assume that $L_0 \ll \omega$.

(f) In words, what does this condition mean?

(g) Calculate the loss rate for this condition. Is it equal to production? Does this make sense?

(h) Explain, in a few sentences, under what conditions a system is in the strict photochemical steady state—i.e. instantaneous production equals loss at all points in time.

2. Under certain conditions, the reactive uptake coefficient γ for loss of $ClONO_2$ on an aerosol is 0.05. What is the lifetime of lower-stratospheric $ClONO_2$ for background and volcanically perturbed conditions with respect to reaction on an aerosol? How do these lifetimes compare with the lifetime of $ClONO_2$ with respect to photolysis?

3. Which constituents in Figure 2.1 are primarily photolyzed by visible radiation? Which are primarily photolyzed by ultraviolet radiation?

4. Assume there is some constituent X which is produced at a constant rate of $P = 10^6$ molecules cm^{-3} s^{-1}. Constituent X is lost through photolysis, and the photolysis rate constant J_x is 0.1 s^{-1}.

(a) What is the steady-state concentration (neglecting transport)?

(b) What are the replacement lifetimes with respect to production and loss at the steady state?

(c) Suppose that the J value for loss of X suddenly doubles to 0.2 s^{-1} (for example, if the air parcel goes over a reflective cloud). What is the new steady-state concentration of X?

(d) The concentration of X cannot instantaneously achieve this new steady-state value. Instead, after the J value changes the concentration of X will tend toward its new steady-state value. Write the equation that describes how the abundance of X achieves its new steady-state value. How long does it take for X to achieve its new steady-state value?

5. The atmospheric lifetime of a constituent was defined in Equation (2.30). The stratospheric lifetime is defined (by analogy) to be

$$\tau_{strat} = \frac{\text{total atmospheric burden}}{\text{total stratospheric loss rate}} = \frac{\int_{atm}[X]dV}{\int_{strat} L[X]dV}$$

where the integral in the numerator is over the entire atmosphere, and the integral in the denominator is over the stratosphere.

(a) The atmospheric lifetime of CH_4 is ~10 years, while the stratospheric lifetime is ~100 years. What does this tell you about where in the atmosphere CH_4 is destroyed?

(b) The main loss process of CH_4 is through reaction with OH radicals. This reaction has a large temperature dependence. How does this explain the answer to (a)? Assume [OH] is approximately constant throughout the atmosphere.

Chapter 3 | Ozone Production and Loss

3.1 Chapman Chemistry

The first successful attempt to quantitatively understand the photochemistry of ozone (O_3) was made by Chapman in 1930 [63]. He proposed that O_3 is created by the dissociation of O_2 to form O atoms, followed by the reaction between O and O_2:

$$O_2 + h\upsilon \longrightarrow O + O \tag{3.1}$$

$$\underline{2 \times (O_2 + O \xrightarrow{\ M\ } O_3)} \tag{3.2}$$

$$\text{net: } 3O_2 + h\upsilon \longrightarrow 2O_3 \tag{3.3}$$
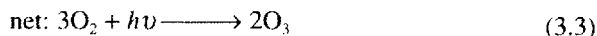
Most of the photolysis of O_2 in the stratosphere occurs at wavelengths in the Schumann–Runge bands (175–200 nm) and the Hertzberg continuum (extending to 242 nm) [64].

O_3 is destroyed by ultraviolet photons:

$$O_3 + h\upsilon \longrightarrow O_2 + O \tag{3.4}$$

O produced in reaction (3.4) can be in one of two electronic states: ^3P ("triplet P") or ^1D ("singlet D"). $O(^1D)$ is an excited electronic state, and is produced when the incident photon has a wavelength of less than ~300 nm. For wavelengths longer than ~325 nm, the O atom is produced in the ground state $O(^3P)$. For incident photons with wavelengths between 300 and 325 nm, both $O(^1D)$ and $O(^3P)$ are produced [65] (see also DeMore et al. [5], Table 8). Because of their higher internal energy, $O(^1D)$ atoms are more reactive than $O(^3P)$.

$O(^1D)$ is rapidly converted to $O(^3P)$ through collisions with molecules such as O_2 and CO_2. As a result, the abundance of $O(^1D)$ is between 10^{-6} and 10^{-7} of the abundance of $O(^3P)$ in the stratosphere. We will hereafter refer to $O(^3P)$ atoms simply as O atoms; reactions specifically requiring $O(^1D)$ atoms will be so designated.

The last important Chapman reaction is the direct reaction between O_3 and O:

$$O_3 + O \longrightarrow O_2 + O_2 \tag{3.5}$$

In addition to these, Chapman discussed several other reactions now known to be unimportant. This set of reactions, known as the Chapman reactions, form the cornerstone of stratospheric O_3 chemistry.

3.2 The Odd-oxygen Family

Considering just the Chapman reactions, the lifetimes $1/L$ of O_3 and O for typical mid-latitude lower-stratospheric conditions are

$$\tau_{O_3} = \frac{1}{L} = \frac{1}{J_{O_3} + k_{O+O_3}[O]} \approx 1000 \text{ s} \qquad (3.6)$$

$$\tau_O = \frac{1}{L} = \frac{1}{k_{O+O_2}[O_2] + k_{O+O_3}[O_3]} \approx 0.002 \text{ s} \qquad (3.7)$$

It turns out that $J_{O_3} \gg k_{O+O_3}[O]$, so the loss of O_3 is dominated by photolysis, while $k_{O+O_2}[O_2] \gg k_{O+O_3}[O_3]$, so the loss of O atoms is dominated by reaction with O_2 to form O_3.

The lifetime of O_3 is 10^3–10^6 times greater than the lifetime of O in the stratosphere. Other constituents have lifetimes of days, weeks, months, or longer—many orders of magnitude longer than the lifetime for O_3. In addition, many phenomena of interest, such as the Antarctic ozone hole, mid-latitude trends, and perturbations from volcanoes, occur on time-scales of months to decades. As a result, the "ozone" problem involves time-scales ranging over 15 orders of magnitude. This leads to both conceptual and computational difficulties.

Let us define a new constituent, odd oxygen (O_x), to be the sum of O_3 and O (each of these has an odd number of oxygen atoms, hence the name). The number density of odd oxygen, $[O_x]$, is defined to be the sum of the number densities of $[O_3]$ and [O]. Similarly, the volume mixing ratio (VMR) of O_x is defined to be the sum of the VMRs of O_3 and O.

To understand why this is useful, let us write the continuity equation for O_3 and O:

$$\frac{\partial[O_3]}{\partial t} = k_{O+O_2}[O][O_2] - J_{O_3}[O_3] - k_{O+O_3}[O][O_3]$$

$$\frac{\partial[O]}{\partial t} = -k_{O+O_2}[O][O_2] - k_{O+O_3}[O][O_3] + J_{O_3}[O_3] + 2J_{O_2}[O_2] \qquad (3.8)$$

Note that we have neglected transport in this example. Summing these equations, we obtain a continuity equation for O_x:

$$\frac{\partial[O_3]}{\partial t} + \frac{\partial[O]}{\partial t} = \frac{\partial([O_3] + [O])}{\partial t}$$

$$= \frac{\partial[O_x]}{\partial t} = 2J_{O_2}[O_2] - 2k_{O+O_3}[O][O_3] \tag{3.9}$$

The right-hand side of Equation (3.9) has two terms. The first term, $2J_{O_2}[O_2]$, is equal to twice the rate at which O_2 is photolyzed to form O (reaction (3.1)). This is the rate at which O_x is being produced. The second term, $2k_{O+O_3}[O][O_3]$, is twice the rate at which O_3 and O react to form O_2. This is the rate at which O_x is being destroyed. The factor of 2 in front of these terms accounts for the fact that each of these reactions creates or destroys two members of O_x. The net rate of change of O_x is the difference between these terms.

Notable by their absence in Equation (3.9) are the terms representing the reaction between O and O_2 to form O_3 (reaction (3.2)) and the photolysis of O_3 to form O_2 and O (reaction (3.4)). These reactions destroy one member of O_x, but create another. Reaction (3.2), for example, results in the loss of an O atom but the creation of an O_3 molecule. Because the abundance of O_x is the sum of the abundances of O and O_3, these two reactions produce no *net* change in the abundance of O_x.

Let us now calculate the lifetime of O_x in the lower stratosphere. When calculating the lifetime of a chemical family, one cannot generally calculate it as $1/L$ because the loss rate of the family is generally not proportional to the abundance of the family. For O_x, the loss rate is $2k_{O+O_3}[O_3][O]$. Instead, we calculate the lifetime as the abundance of O_x divided by the total loss rate:

$$\tau_{O_x} = \frac{[O_x]}{2k_{O+O_3}[O_3][O]} \approx \frac{1}{2k_{O+O_3}[O]} \approx 5 \text{ years} \tag{3.10}$$

We have used the approximation $[O_x] \approx [O_3]$ to go from the first expression for τ_{O_x} to the second; we will show this approximation is accurate in the next section. It turns out that this estimate of the lifetime of O_x is too large by a factor of about 10–20 because we have neglected several reactions that destroy O_x—these will also be discussed in the next section. A more accurate calculation would reveal that the lifetime of O_x in the lower stratosphere is several months, decreasing to days in the upper stratosphere.

To review: O_x is created by the photolysis of O_2 (reaction (3.1)) and destroyed by the reaction of O_3 and O (reaction (3.5)) on time-scales of months in the lower stratosphere, decreasing to less than a day in the upper stratosphere. On time-scales that are short compared with this, the sum of the abundances of O_3 and O is constant. While their sum is constant, however, O_3 and O are interconverting on a time-scale of tens of minutes or less. Figure 3.1 shows a schematic of this.
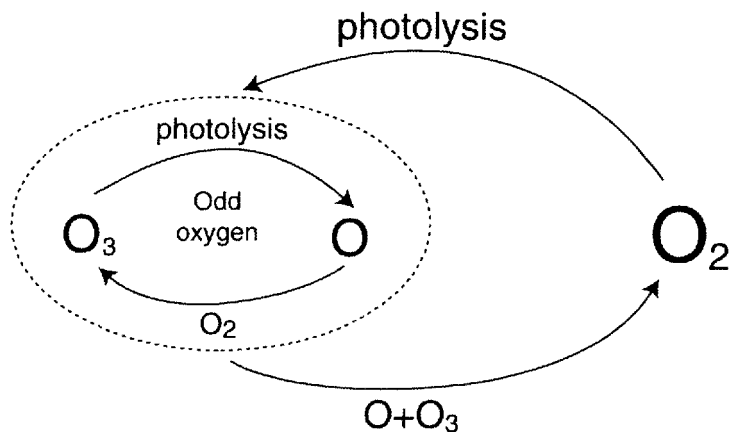
Figure 3.1 Schematic of the Chapman odd-oxygen system.

3.2.1 Partitioning of odd oxygen

An important question still remains: what fraction of O_x is in the form of O_3 and how much is in the form of O? In other words, how is O_x partitioned among its constituents? Considering just the reactions that interconvert O_x (reactions (3.2) and (3.4)), and assuming photochemical steady state, then production of O_3 equals its loss:

$$J_{O_3}[O_3] = k_{O+O_2}[O_2][O] \qquad (3.11)$$

where the left-hand side is the loss rate of O_3 and the right-hand side is the production rate of O_3 (alternatively, production of O equals its loss; the left-hand side is the production rate of O atoms and the right-hand side is the loss rate of O atoms). Rearranging Equation (3.11), we get:

$$\frac{[O]}{[O_3]} = \frac{J_{O_3}}{k_{O+O_2}[O_2]} \qquad (3.12)$$

Figure 3.2 shows that this ratio ranges from 10^{-7} in the lower stratosphere to 10^{-2} in the upper stratosphere. Thus, nearly all O_x in the stratosphere is in the form of O_3. This justifies our assumption (used in Equation (3.10)) that $[O_x] \approx [O_3]$. Note that, at night, photolysis ceases ($J_{O_3} = 0$) and all of the O atoms are converted to O_3 via reaction (3.2). Thus, all of O_x is in the form of O_3 at night.
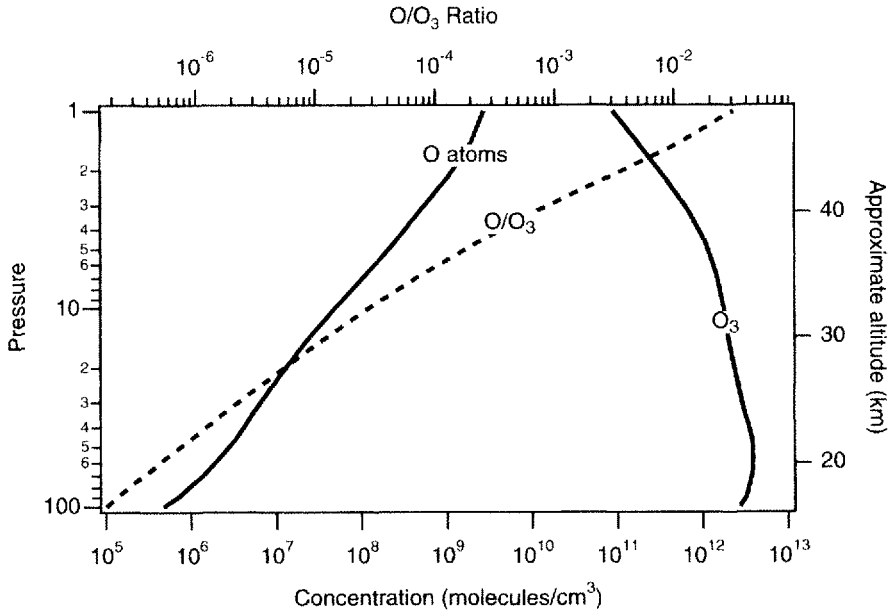
Figure 3.2 Calculated profiles of the O_3 and O number density (solid lines, bottom axis), and the ratio $[O]/[O_3]$ (dashed line, top axis). Calculation is for 45°N equinoctial conditions based on daytime-average constituent abundances and photolysis rates.

In the previous calculation, we assumed photochemical steady-state conditions for the members of O_x. How good an assumption is this? To study this question, let us revisit the continuity equations for O_3 and O atoms (Equation (3.8)). Assuming that the reactions that interconvert O_x (reactions (3.2) and (3.4)) are much faster than the reactions that produce and destroy O_x, we can rewrite Equation (3.8), neglecting the O_x production and loss terms:

$$\frac{\partial[O_3]}{\partial t} = k_{O+O_2}[O][O_2] - J_{O_3}[O_3]$$

$$\frac{\partial[O]}{\partial t} = -k_{O+O_2}[O][O_2] + J_{O_3}[O_3]$$

(3.13)

These differential equations are appropriate for time periods short compared to the lifetime of O_x. Over longer time periods, the terms representing production and loss of O_x (as well as transport) can have a significant cumulative effect.

The differential equations in Equation (3.13) can be solved analytically to obtain:

$$[O_3](t) = \frac{1}{1 + \frac{k_{O+O_2}[O_2]}{J_{O_3}}} \left(\exp\left(-\left(J_{O_3} + k_{O+O_2}[O_2]\right)t\right) + \frac{k_{O+O_2}[O_2]}{J_{O_3}} \right) C$$

$$\tag{3.14}$$

$$[O](t) = \frac{1}{1 + \frac{k_{O+O_2}[O_2]}{J_{O_3}}} \left(1 - \exp\left(-\left(J_{O_3} + k_{O+O_2}[O_2]\right)t\right) \right) C$$

where we have assumed that $[O] = 0$ at $t = 0$ and C is a constant of integration that is determined by the concentration of O_x. Deviations from the steady state are represented by the exponential terms in Equation (3.14). The system approaches its steady-state value with an e-folding time of $1/(J_{O_3} + k_{O+O_2}[O_2])$, which is the reciprocal of the sum of the loss frequencies of O_3 and O. Because the lifetime of O is much shorter than the lifetime of O_3, $k_{O+O_2}[O_2] \gg J_{O3}$, and $1/(J_{O_3} + k_{O+O_2}[O_2]) \approx 1/(k_{O+O_2}[O_2])$. Thus, the perturbation term is damped on a time-scale equal to the lifetime of O atoms, which is much less than a second in the stratosphere. Conditions in the atmosphere do not change significantly on such short time-scales, so it is reasonable to assume that O_3 and O are always in the photochemical steady state.

Taking the limit of Equation (3.14) as time goes to infinity, the perturbation terms in Equation (3.14) are zero. In this case, the $[O]/[O_3]$ ratio becomes $J_{O_3}/(k_{O+O_2}[O_2])$, which is the same result as was obtained when considering the solution to Equation (3.14).

Why have we spent time and effort in this chapter defining O_x? The reason is that O_x offers conceptual advantages versus thinking about the species O_3 and O as separate entities. The lifetime of O_3 is minutes or less in the stratosphere. Thus, one would expect that on time-scales much longer than this, the abundance of O_3 can change significantly. In this chapter, however, we have shown that (1) the lifetime of O_x is much longer than the lifetime of O_3, and (2) virtually all of O_x is in the form of O_3. As a result, the abundance of O_3 can in reality only change on time-scales comparable to or longer than the lifetime of O_x. This is true because photolysis of O_3 creates an O atom that almost all of the time reacts with O_2 to reform O_3. Therefore, photolysis of O_3 does not represent a *net* sink of O_3.

It is, in fact, quite common in both formal and colloquial situations for people to use "ozone" where they really mean "odd oxygen". For example, the literature is filled with statements such as: "the lifetime of ozone in the lower stratosphere is months." Strictly speaking, this is incorrect. Photolysis destroys O_3 rapidly, with a typical lifetime $1/L$ of minutes or less throughout the stratosphere. However, the lifetime of O_x is months, and virtually all of O_x is in the form of ozone. Thus, if you follow an air parcel in the lower stratosphere, you will see that its O_3 abundance is constant on time-scales shorter than the lifetime of O_x. This does not mean that O_3 is not being destroyed

in the parcel. On the contrary, all of the O_3 in the parcel is destroyed many times every day that the parcel is in sunlight. However, O_3 is reformed in the parcel at almost exactly the same rate. Only on time-scales of the lifetime of O_x are the effects of the imbalance between production and loss of O_3 large enough for its concentration to change noticeably. Thus, the statement that the lifetime of O_3 in the lower stratosphere is months, while technically incorrect, is true in a practical sense.

In addition, there is a computational advantage to using O_x for numerically modeling the stratosphere. To predict the abundance of constituent X at a given point in time and space, models of the stratosphere integrate the differential equation

$$[X]_t = \int_0^t \frac{\partial[X]}{\partial t}\, dt + [X]_0 = \int_0^t \left(P - L[X] - \nabla \cdot (V[X]) \right) dt + [X]_0 \quad (3.15)$$

To numerically solve Equation (3.15), the integral is broken into short time segments of length Δt and converted into a summation—a process often referred to as "discretization" (the literature on numerically solving differential equations is extensive, e.g. see Press *et al.* [66], Chapter 15). The difference in lifetimes of the stratospheric constituents means that there are several very different time-scales over which the dependent variables (O_3, O, and other constituents) are changing (this is known as a "stiff" set of differential equations). In order to maintain stability of the integration, one is required to follow the variation in the solution on the shortest time-scale, in this case the lifetime of O. Thus, a model of the lower stratosphere that considered O_3 and O as separate and independent species would have to have a time step Δt of less than τ_O (less than a millisecond in the lower stratosphere). With such a small time step, it is impractical for a model to integrate Equation (3.15) for seasonal or yearly time periods, and therefore it would be impossible to simulate many of the phenomena that are of interest. By modeling O_x instead of both O_3 and O, however, one can take advantage of the much longer lifetime of O_x, and use a bigger time step in the model.

3.3 Catalytic Loss Cycles

Calculations of O_3 abundance based on just the Chapman reactions yield estimates of O_x that are considerably larger than measurements. The reason for this is that we have neglected an important O_3 loss pathway: radical catalysis [67].

A catalyst is defined as a substance, often used in small amounts relative to the reactants, that increases the rate of a reaction without being consumed in the process. With this definition in mind, consider the chemical reaction sequence first suggested by Stolarski and Cicerone [68]:

$$Cl + O_3 \rightarrow ClO + O_2$$
$$\underline{ClO + O \rightarrow Cl + O_2} \qquad\qquad (3.16)$$
$$O_3 + O \rightarrow O_2 + O_2$$
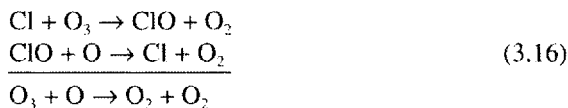
In this reaction set, Cl acts as a catalyst by facilitating the conversion of O_x to O_2 without being consumed. For this catalytic cycle to be important, it has to destroy O_x at a rate comparable to or faster than the rate at which O and O_3 directly react. Otherwise the catalytic cycle will have little impact on the overall rate of O_x destruction. Thus, we have to evaluate how fast the catalytic cycle (3.16) destroys O_x.

3.3.1 Rate-limiting step

What determines the rate that a catalytic cycle destroys O_x? To figure this out, let us look more closely at the cycling between Cl and ClO (Figure 3.3). ClO is formed only through reaction of Cl with O_3. Cl is reformed when ClO reacts with either O or with NO.

When the cycle is completed by ClO + O, then two O_x are destroyed, as shown in reaction (3.16). When ClO reacts with NO, however, the following cycle results:

$$Cl + O_3 \rightarrow ClO + O_2$$
$$ClO + NO \rightarrow Cl + NO_2$$
$$\underline{NO_2 + h\nu \rightarrow NO + O} \qquad\qquad (3.17)$$
$$O_3 + h\nu \rightarrow O_2 + O$$
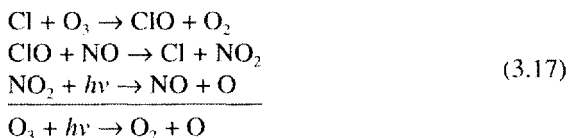
Note that this reaction scheme *does not* destroy O_x; instead it merely converts O_3 to O.

In other words, every reaction between ClO and O leads to the loss of two O_x. But not every reaction between Cl and O_3 leads to O_x loss; if the resulting ClO reacts with NO, then a null cycle (reaction (3.17)) results. Therefore, the rate of O_x loss in reaction (3.16) is set by the rate of the reaction between ClO and O, and not by the rate of reaction between Cl and O_3. In general, the rate at which a catalytic cycle destroys O_x is determined by the slowest reaction in the cycle, which is known as the rate-limiting step. We can therefore write the rate of O_x loss through reaction (3.16) as $2k_{ClO+O}[ClO][O]$. The factor of 2 accounts for the fact that every trip through the catalytic cycle destroys two O_x members (one O_3 and one O).

Figure 3.4 shows the ratio of the rate of O_x loss through the ClO–Cl catalytic cycle ($2k_{ClO+O}[ClO][O]$) to the rate of O_x loss through the O_3+O reaction ($2k_{O_3+O}[O_3][O]$) as a function of ClO abundance. If this ratio is much less than 1, then loss through the ClO–Cl catalytic cycle is insignificant compared with loss through the direct O_3+O reaction. If the ratio is much greater than 1, then the catalytic loss dominates the
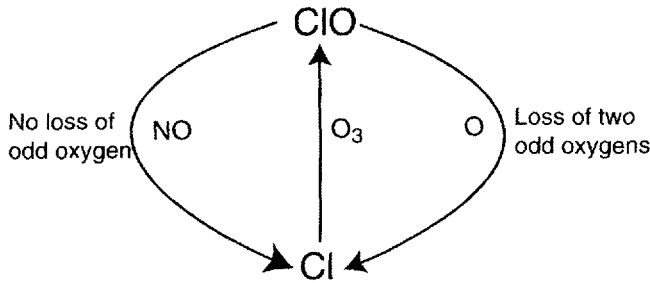
Figure 3.3 Schematic of the Cl–ClO system. Arrows denote pathways for conversion between Cl and ClO. Each arrow is labeled by the reactant that accomplishes the conversion (e.g. the arrow going from Cl to ClO labeled with O_3 means that Cl is converted to ClO through reaction with O_3).

direct reaction. Figure 3.4 shows that these two loss pathways are equal for a ClO mixing ratio of ~20 parts per trillion by volume. Typical stratospheric abundances of ClO are tens to hundreds of parts per trillion by volume [46,69–71], indicating that destruction of O_x through this catalytic cycle is important. The importance of this conclusion cannot be overstated: the ClO radical, even in abundances as small as a
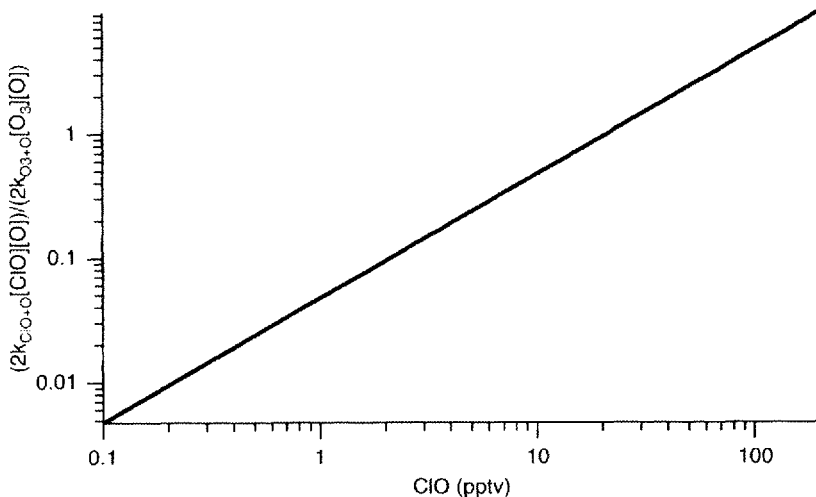
Figure 3.4 Ratio of $2k_{ClO+O}[ClO][O]$ to $2k_{O_3+O}[O_3][O]$ versus the abundance of ClO. Computed for lower stratospheric conditions: temperature of 210 K, $[O_3]$ = 2 ppmv, and rate constants from DeMore *et al.* [5].

few tens of parts per trillion by volume, is capable of destroying significant amounts of O_x, despite O_x abundances of several parts per million by volume.

3.3.2 Other catalytic cycles

The Cl–ClO cycle is just one of several catalytic cycles that destroy odd oxygen in the stratosphere. There is an NO–NO_2 cycle [72] that is quite similar to the Cl–ClO cycle:

$$\begin{aligned} NO + O_3 &\rightarrow NO_2 + O_2 \\ \underline{NO_2 + O \rightarrow NO + O_2} \\ O_3 + O &\rightarrow O_2 + O_2 \end{aligned} \qquad (3.18)$$

The rate-limiting step of this cycle is the reaction between NO_2 and O. There is also an analogous OH–HO_2 cycle:

$$\begin{aligned} OH + O_3 &\rightarrow HO_2 + O_2 \\ \underline{HO_2 + O \rightarrow OH + O_2} \\ O_3 + O &\rightarrow O_2 + O_2 \end{aligned} \qquad (3.19)$$
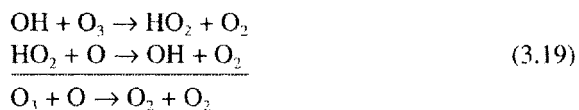
The rate-limiting step of this cycle is the reaction between HO_2 and O.

Note that these three cycles (reactions (3.16)–(3.19)) are rate limited by reactions involving O atoms. Other cycles, rate limited by reactions involving other species, tend to be (relatively) more important in regions where O atoms are rare (such as the lower stratosphere). The cycle

$$\begin{aligned} OH + O_3 &\rightarrow HO_2 + O_2 \\ \underline{HO_2 + O_3 \rightarrow OH + O_2 + O_2} \\ O_3 + O_3 &\rightarrow O_2 + O_2 + O_2 \end{aligned} \qquad (3.20)$$
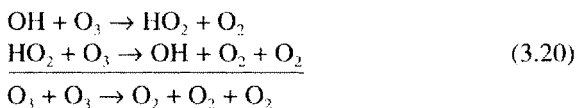
is rate limited by the reaction between HO_2 and O_3. Another important cycle in the lower stratosphere is

$$\begin{aligned} HO_2 + ZO &\rightarrow HOZ + O_2 \\ HOZ + h\nu &\rightarrow OH + Z \\ Z + O_3 &\rightarrow ZO + O_2 \\ \underline{OH + O_3 \rightarrow HO_2 + O_2} \\ O_3 + O_3 &\rightarrow O_2 + O_2 + O_2 \end{aligned} \qquad (3.21)$$
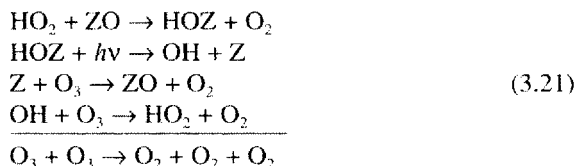
where Z is either Cl or Br. The rate-limiting step is the reaction between HO_2 and ZO.

The reaction between ClO and BrO has three product channels:

$$ClO + BrO \longrightarrow BrCl + O_2 \tag{3.22a}$$

$$ClO + BrO \longrightarrow ClOO + Br \tag{3.22b}$$

$$ClO + BrO \longrightarrow OClO + Br \tag{3.22c}$$
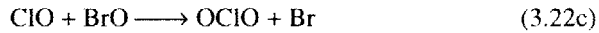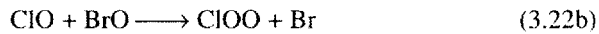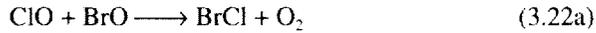
If the reaction follows either reactions (3.22a) or (3.22b), then net loss of O_x occurs:

$$
\begin{array}{l}
Cl + O_3 \rightarrow ClO + O_2 \\
Br + O_3 \rightarrow BrO + O_2 \\
ClO + BrO \rightarrow BrCl + O_2 \\
\underline{BrCl + h\nu \rightarrow Br + Cl} \\
O_3 + O_3 \rightarrow O_2 + O_2 + O_2
\end{array}
\tag{3.23}
$$

$$
\begin{array}{l}
Cl + O_3 \rightarrow ClO + O_2 \\
Br + O_3 \rightarrow BrO + O_2 \\
ClO + BrO \rightarrow ClOO + Br \\
\underline{ClOO + M \rightarrow Cl + O_2 + M} \\
O_3 + O_3 \rightarrow O_2 + O_2 + O_2
\end{array}
\tag{3.24}
$$
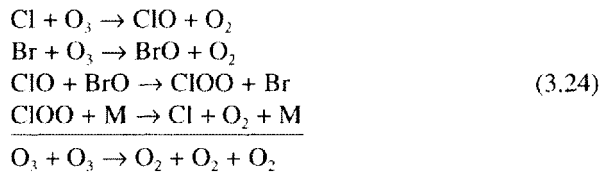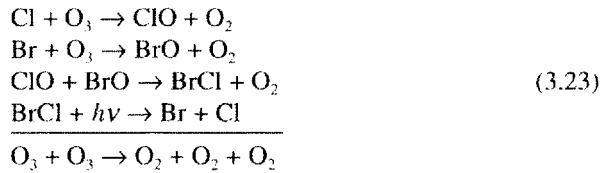
These BrO–ClO cycles are both rate limited by the reaction between BrO and ClO. Cycles (3.23) and (3.24) are important in the formation of the Antarctic ozone hole, which we will discuss in detail in Chapter 7.

If the reaction between BrO and ClO follows reaction (3.22c), then there is no net loss of O_x:

$$
\begin{array}{l}
Cl + O_3 \rightarrow ClO + O_2 \\
Br + O_3 \rightarrow BrO + O_2 \\
ClO + BrO \rightarrow OClO + Br \\
\underline{OClO + h\nu \rightarrow ClO + O} \\
O_3 + h\nu \rightarrow O_2 + O
\end{array}
\tag{3.25}
$$
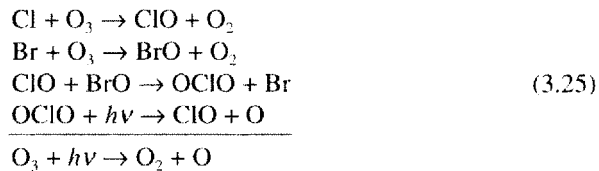
There are two more O_x-destroying reaction sequences that rely on the production of NO and O_2 from the photolysis of NO_3:

$$
\begin{array}{l}
NO + O_3 \rightarrow NO_2 + O_2 \\
NO_2 + O_3 \rightarrow NO_3 + O_2 \\
\underline{NO_3 + h\nu \rightarrow NO + O_2} \\
O_3 + O_3 \rightarrow O_2 + O_2 + O_2
\end{array}
\tag{3.26}
$$

$$ClONO_2 + h\nu \rightarrow Cl + NO_3$$
$$NO_3 + h\nu \rightarrow NO + O_2$$
$$NO + O_3 \rightarrow NO_2 + O_2$$
$$Cl + O_3 \rightarrow ClO + O_2 \tag{3.27}$$
$$\underline{ClO + NO_2 \xrightarrow{M} ClONO_2}$$
$$O_3 + O_3 \rightarrow O_2 + O_2 + O_2$$
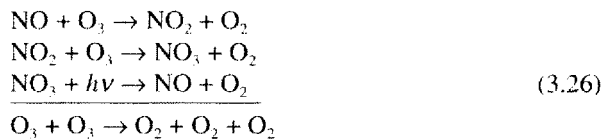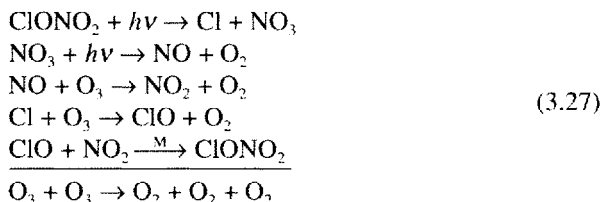
The rate-limiting step of both of these reactions is the rate of photolysis of NO_3 to NO. Note that if NO_3 is photolyzed to NO_2 and O, then these cycles lead to no net loss of O_x—because the O atom produced will react with O_2 to reform O_3. These last two cycles are of limited importance in regulating O_x.

3.4 Odd-oxygen Production and Loss Rates

The continuity equation for O_x can be written

$$\frac{\partial[O_x]}{\partial t} = P_{O_x} - L[O_x] - \nabla \cdot (V[O_x]) \tag{3.28}$$

Production of O_x is almost entirely due to photolysis of O_2, so $P \approx 2J_{O_2}[O_2]$. The factor of two accounts for the fact that each O_2 molecule photolyzed produces two O_x. Figure 3.5a shows the annually averaged P_{O_x}. Production increases with altitude over most of the stratosphere, reaching a maximum over the equator at about 2 hPa. The increase with altitude of P_{O_x} occurs because the photolysis rate J_{O_2} increases with altitude faster than $[O_2]$ decreases, so their product increases with altitude. Above 2 hPa, J_{O_2} ceases to increase rapidly with height, so the decrease in $[O_2]$ causes their product to decrease with altitude. Also note that P_{O_x} at a given pressure is greatest over the equator. This is consistent with the fact that the lower latitudes receive, on average, more sunlight. Figure 3.5b shows the lifetime of O_x with respect to production ($\tau_p = [O_x]/P$).

The total loss rate of O_x is the sum of two times the rates of the rate limiting step of each catalytic cycle plus two times the rate of the reaction between $O_3 + O$: $L[O_x]$ = $2k_{ClO+O}[ClO][O] + 2k_{NO_2+O}[NO_2][O] + 2k_{HO_2+O}[HO_2][O] + \ldots + 2k_{O_3+O}[O_3][O]$. Again, the factor of 2 accounts for the fact that each O_x destruction pathway destroys two O_x. Figure 3.6a shows the annually averaged loss rate of O_x; Figure 3.6b shows the lifetime of O_x with respect to loss ($[O_x]/(L[O_x]) = 1/L$). The hemispheric asymmetry in the lower stratosphere of Figure 3.6 is due to the rapid loss of O_3 associated with the Antarctic ozone hole.

As with production, Figure 3.6a shows that the loss rate of O_x increases rapidly with altitude throughout most of the stratosphere, reflecting the increase with altitude of the abundances of O and the O_x-destroying reactive radicals. Below about
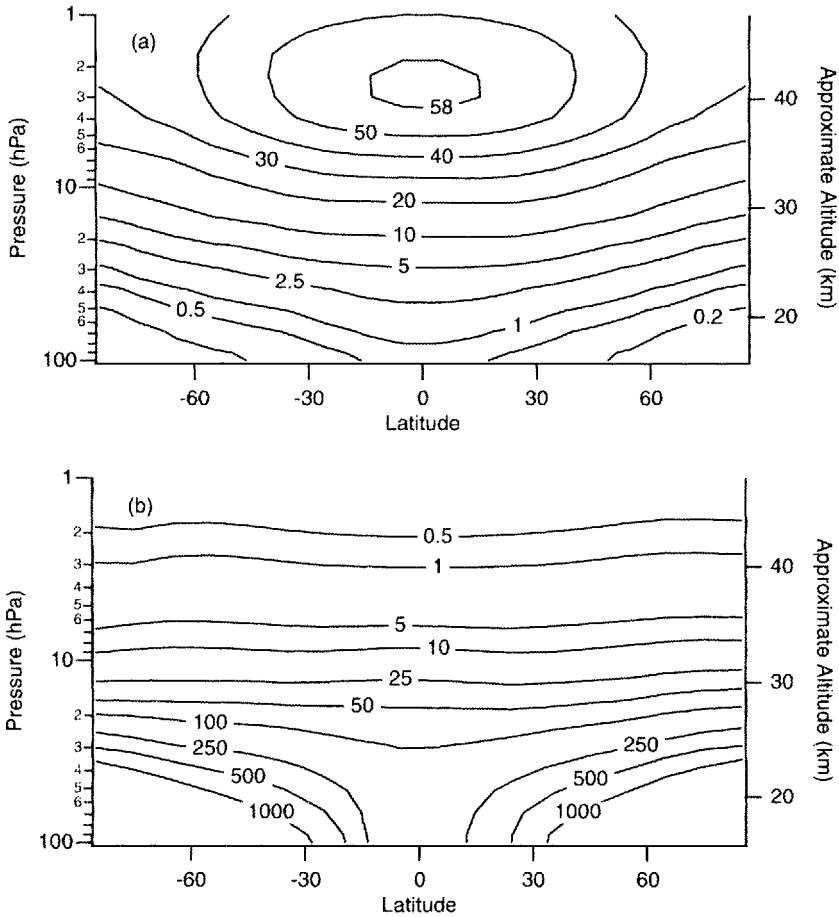
Figure 3.5 Contours of annually averaged (a) O_x production rate (in 10^5 molecules cm^{-3} s^{-1}) and (b) O_x lifetime with respect to production ($[O_x]/P$), in days. These calculations are from the Goddard two-dimensional climatological circulation model [73].

30 km, Figures 3.5a and 3.6a show that the annually averaged production and loss rates are generally not equal. Production exceeds loss in the tropics, while loss exceeds production in the extratropics. Transport of O_x from the tropics to higher latitudes closes the budget, and ensures that the annually averaged change of lower-stratospheric O_x is close to zero. This will be discussed in detail in Chapter 5.

Above 30 km, the rates of production and loss are approximately equal. In this region, chemistry is much faster than transport of O_x, so we can assume that O_x is in steady state. Between about 10 and 2 hPa, the lifetime of O_x is greater than a day, so
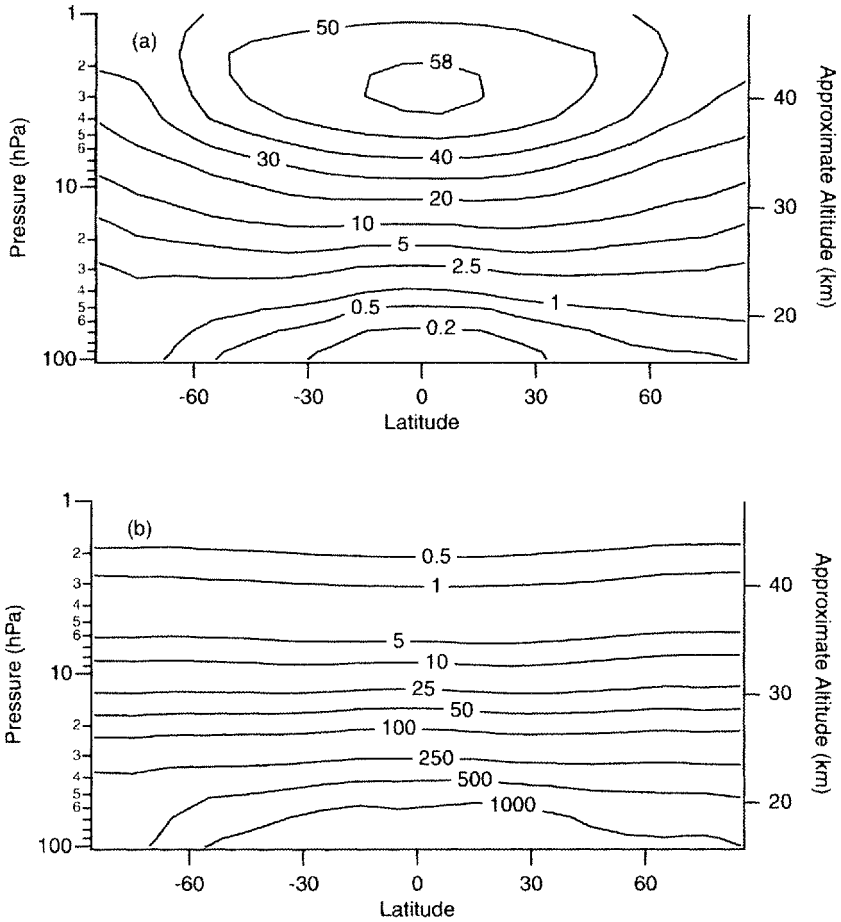
Figure 3.6 Contours of annually averaged (a) O_x loss rate (in 10^5 molecules cm^{-3} s^{-1}) and (b) O_x lifetime with respect to loss ($1/L$) (in days). These calculations are from the Goddard two-dimensional climatological circulation model [73].

P_{O_x} and $L[O_x]$ are equal when averaged over 24 h; the system is therefore in the diurnal steady state. Above ~2 hPa, the lifetime of O_x is much less than a day, and instantaneous production and loss of O_x can be considered equal throughout the day; the system is therefore in photochemical steady state.

Figures 3.7 and 3.8 show the contributions of the various catalytic cycles to the
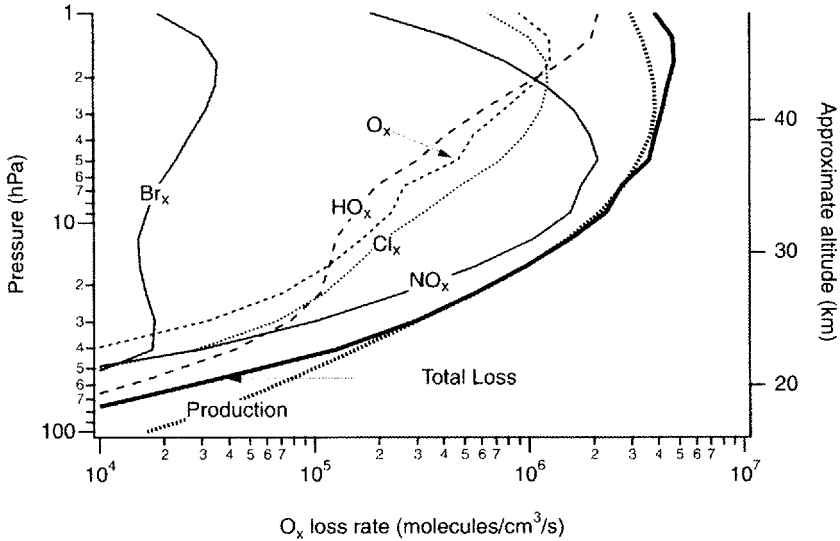
Figure 3.7 Twenty-four hour average O_x production and loss rates for the various catalytic cycles. Calculated for 35°N, September conditions. (After Osterman *et al.* [75], Figure 2.)
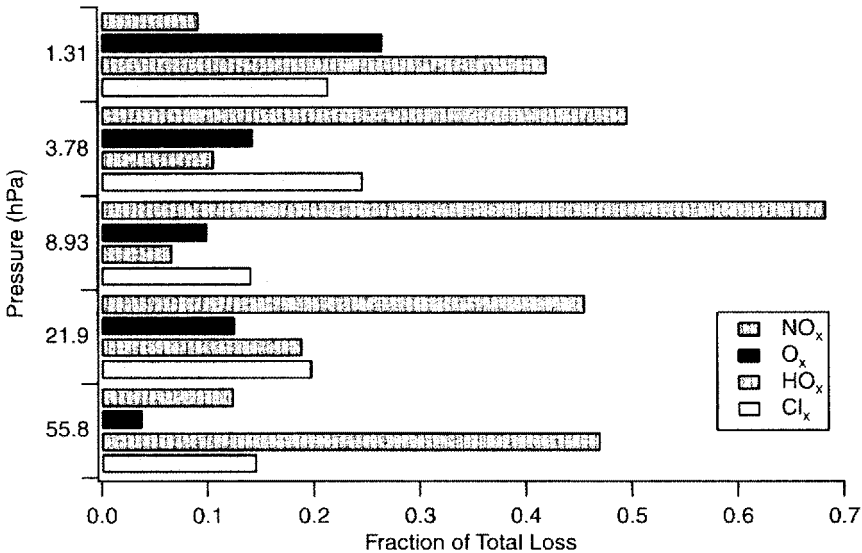
Figure 3.8 Fraction of total O_x loss contributed by the various chemical families. Calculated for 35°N, September conditions. (Adapted from Osterman *et al.* [75], Figure 2.)

total loss rate of O_x. The O_x line represents the contribution from the direct reaction between O_3 and O (reaction (3.5)). This reaction is responsible for a few percent of total loss in the lower stratosphere, increasing to a maximum of ~30% of the total loss in the upper stratosphere. Note that this explains why our estimate of lower stratospheric O_x lifetime earlier in this chapter was too large. By considering only the O_3–O reaction in our calculation of the O_x loss rate, we underestimated the lower stratospheric loss rate by a factor of ~20, leading to an estimate of O_x lifetime that was a factor of ~20 too large.

Virtually all of the O_x loss attributed to NO_x chemistry occurs through the NO_2–NO catalytic cycle (reaction (3.18)). NO_x-catalyzed loss is most important in the mid-stratosphere near 10 hPa (~30 km), where it causes two-thirds of the O_x loss. The HO_x line represents the sum of the two OH–HO_2 cycles (reactions (3.19) and (3.20)). The cycle rate limited by HO_2+O_3 is more important in the lower stratosphere [74], while the cycle rate limited by HO_2+O is more important in the upper stratosphere. Together, these two cycles dominate O_x loss in both the lower and upper stratosphere, where they are responsible for about half of the O_x loss.

The Cl_x line represents the sum of the catalytic cycles that are rate limited by ClO+O, ClO+HO_2, and ClO+BrO (reactions (3.16), (3.21), and (3.23), respectively). Together, these Cl_x cycles are responsible for about 15–25% of O_x loss throughout the stratosphere. It should be noted that mankind is responsible for approximately 80% of the chlorine in the stratosphere in the late 1990s, and is therefore responsible for the vast majority of the loss due to the Cl_x cycles. In this way, human society has significantly increased the total loss rate of O_x in the stratosphere.

Finally, the Br_x line (not shown in Figure 3.8) represents the sum of the bromine catalytic cycles, which are rate limited by BrO+HO_2 (reaction (3.21)) and BrO+O. The cycle limited by BrO+O was not discussed previously; it is the bromine analog to the ClO–Cl cycles. The Br_x cycles are responsible for ~20% of odd-oxygen loss around 50 hPa (~20 km), declining rapidly with increasing altitude.

These relative rates should be considered a general guide. The importance of the various catalytic cycles to O_x loss rate as well as the total O_x loss rate varies with latitude, season, aerosol surface area density, and other geophysical parameters.

Also plotted in Figure 3.7 are the 24 h average total O_x production and loss rates. In the lower stratosphere, production exceeds loss. This is not troubling because the lifetime of O_x is weeks to months (e.g. see Figure 3.6), so the system is not in the photochemical steady state, and we do not expect production and loss to be equal.

As one goes to higher altitudes, the O_x lifetime decreases. Above ~10 hPa (~30 km), the system is in a steady state, and one expects average production and loss to be equal. Between about 30 and 40 km, this is indeed the case. Above ~40 km, however, predicted loss significantly exceeds predicted production. This is a long-standing problem with our understanding of upper stratospheric photochemistry and is known as the model "ozone deficit" [64,71,75,76]. Simply stated,

models of the upper stratosphere tend to predict lower O_3 abundances than measurements indicate. The reasons for this remain a topic of active research.

Problems

1. It has been suggested that one way to combat the decrease in stratospheric O_3 is to manufacture O_3 and transport it to the stratosphere. Let's look further at this idea.

(a) Estimate the total number of molecules of O_3 in the atmosphere. Given this many O_3 molecules, how many molecules of O_x are there in the atmosphere?

(b) Estimate how much energy (in joules) it took to produce this number of molecules of O_x. (Hint: two O_x molecules are produced when an O_2 molecule is dissociated by a photon.)

(c) Given a lifetime of O_x of 3 months, what is the power required to maintain the atmosphere's O_x.

(d) The total energy consumed by society during 1987 was $\sim 80 \times 10^{18}$ J. How does this rate of power consumption compare with the power necessary to maintain the ozone layer. Would it be feasible (just from an energy point of view) for mankind to maintain the ozone layer?

2. The rate-limiting step. Assume a simple system composed of the following constituents: ClO, Cl, O_3, O, and NO, and the following reactions:

$$ClO + NO \rightarrow Cl + NO_2$$
$$ClO + O \rightarrow Cl + O_2$$
$$Cl + O_3 \rightarrow ClO + O_2$$
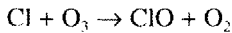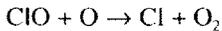
Assume that $[O_3]$, $[O]$, $[NO]$, and $[Cl_x]$ are fixed. Values typical of the mid-latitude upper stratosphere are:

Constituent	Value (daytime average)
$[Cl_x] = [ClO] + [Cl]$	9×10^7 molecules cm^{-3}
$[O_3]$	6.5×10^{11} molecules cm^{-3}
$[O]/[O_3]$	0.0008
$[NO]$	7×10^8 molecules cm^{-3}
k_{ClO+NO}	2×10^{-11} cm^3 molecule^{-1} s^{-1}
k_{ClO+O}	4×10^{-11} cm^3 molecule^{-1} s^{-1}
k_{Cl+O_3}	10^{-11} cm^3 molecule^{-1} s^{-1}

(a) Calculate [Cl] and [ClO], assuming the photochemical steady state.

(b) The "rate-limiting step" of the ClO–Cl catalytic cycle is the reaction between ClO and O. Calculate the rate of this reaction using the value of [ClO] calculated in (a).

(c) Assume k_{Cl+O_3} is doubled (to 2×10^{-11} cm^3 molecule^{-1} s^{-1}), with all other rates as given above. Recalculate [Cl], [ClO], and the rate of ClO + O. How much of an impact on the rate of odd-oxygen loss does this reaction rate have?

(d) Assume k_{ClO+O} is doubled (to 8×10^{-11} cm^3 molecule^{-1} s^{-1}), with all other rates as given above. Recalculate [Cl], [ClO], and the rate of ClO + O. How much of an impact on the rate of odd-oxygen loss does this reaction rate have?

(e) In words, explain why this result is consistent with the concept of a "rate-limiting step".

3. Let us estimate the abundance of upper stratospheric ozone. In this problem, we start by making the assumption of photochemical steady-state conditions between O_3 and O.

(a) Using just the Chapman reactions, write an equation in terms of the relevant ks, Js, and $[O_3]$, $[O]$, and $[O_2]$ that equate production and loss of odd oxygen.

(b) The equation in (a) contains the concentrations of both $[O_3]$ and $[O]$. Using the steady-state relation between them, eliminate $[O]$ from the equation.

(c) Solve this equation for $[O_3]$ using typical values for the upper stratosphere (at 35°N; 3.1 hPa; equinox conditions, 3×10^{-10} s^{-1} for J_{O_2} (daytime averaged), 2×10^{-3} s^{-1} for J_{O_3} (daytime averaged), 2×10^{-15} cm^3 molecule^{-1} s^{-1} for k_{O+O_3}, 8×10^{-17} cm^3 molecule^{-1} s^{-1} for k_{O+O_2} (effective bimolecular rate), and 1.8×10^{16} molecule cm^{-3} for $[O_2]$).

(d) From this, calculate $[O_x]$.

Measurements of ozone from the UARS MLS instrument reveal O_3 concentrations of ~6.5×10^{11} molecules cm^{-3} at 3.1 hPa.

(e) How does this compare with what you calculated? Why are these not the same?

(f) Recalculate $[O_3]$ after including another loss process: ClO + O. Assume that $[ClO] = 5 \times 10^7$ molecule cm^{-3}, and $k_{ClO+O} = 3.8 \times 10^{-11}$ cm^3 molecule^{-1} s^{-1}.

4. Estimate J_{O_2} in the lower stratosphere given that the lifetime of O_x is 3 months. Assume the photochemical steady state (and neglect transport). Based on this estimate, what is the lifetime of O_2 with respect to photolysis in this region?

5. Around 40 km (where all of the major O_x loss pathways involve O atoms), the lifetime of O_x is a day, and the lifetime of O_3 is a minute. Based on this, what fraction of O atoms that are formed from O_3 photolysis react with O_2 to reform O_3?

Chapter 4 | Chemical Families and Partitioning

In the previous chapter we saw how O_x production and loss rates are determined by the concentrations of O_3 and O, a few key radicals such as HO_2, OH, NO_2, ClO, and BrO, and several rate constants and photolysis rates. The transport term is determined from the wind velocity and O_x fields. Substituting estimates of these values into the continuity equation and then integrating,

$$[O_x] = \int_0^{t'} \frac{\partial[O_x]}{\partial t}\ dt + [O_x]_0 = \int_0^{t'} \left(P_{O_x} - L[O_x] - \nabla \cdot (V[O_x])\right) dt + [O_x]_0 \qquad (4.1)$$

produces an estimate of $[O_x]$. By integrating Equation (4.1) over a sufficiently long time (usually several years), an estimate that is insensitive to the initial guess of O_x (represented by $[O_x]_0$) is obtained. Note that Equation (4.1) determines $[O_x]$ at one point in space—models of the stratosphere simultaneously integrate Equation (4.1) at many points throughout the stratosphere in order to determine the $[O_x]$ field for the entire stratosphere.

Many of the important questions in atmospheric sciences today revolve around estimating how man is changing the atmosphere. For example, the release of chlorofluorocarbons (CFCs) at the ground leads to an increase in the abundance of ClO in the stratosphere (we will discuss this in detail later in this chapter). If one knows by how much the abundance of ClO increased due to the release of CFCs, then Equation (4.1) can be integrated two times: once using the natural level of ClO (the abundance of ClO without the influence of CFCs) and a second time using the perturbed level of ClO (taking into account the influence of CFCs). Comparison of the $[O_x]$ determined using these different scenarios shows how the release of CFCs affects O_x.

This simple sounding recipe, however, proves far more difficult to perform in practice. Determining the abundances of radicals such as ClO and how the abundances of these radicals change in response to atmospheric perturbations is a complicated and nontrivial task, and one which is the primary focus of this chapter. Only with an understanding of the mechanisms that regulate the abundances of radicals, however, is one able to predict the response of the O_x abundance to various perturbations, both man-made (like the addition of CFCs to the stratosphere) and natural

(like the addition of sulfur compounds to the stratosphere from the eruption of Mount Pinatubo, or the 11 year cycle in ultraviolet radiation from the Sun).

4.1 Chemical Families

In the previous chapter we defined the odd-oxygen family (O_x), whose members are O_3 and O. In a manner analogous to O_x, we will define several new families in this chapter whose members include the radicals that are involved in O_x loss: inorganic chlorine, Cl_y; odd nitrogen, NO_y; odd hydrogen, HO_x; and inorganic bromine, Br_y.

Before continuing, we will summarize some important characteristics of chemical families.

4.1.1 Source

For every chemical family, there is a source gas whose destruction by photolysis or oxidation leads to the formation of a member of the chemical family. The source gas for O_x, for example, is O_2 (reaction (3.1)):

$$O_2 + h\nu \longrightarrow O + O$$

4.1.2 Cycling

Members of a chemical family interconvert rapidly, compared to the rate at which the family is created or destroyed. For O_x, for example, the reactions

$$O_2 + O \xrightarrow{\ M\ } O_3$$
$$O_3 + h\nu \longrightarrow O_2 + O$$
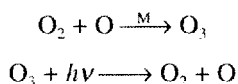
convert one form of O_x into another, without changing in the total abundance of O_x, at a rate much faster than O_x is created and lost. An equivalent way of saying this is that the lifetimes of the members of a chemical family are much shorter than the lifetime of the family.

Normally, the lifetime of a constituent is defined to be $[X]/(L[X]) = 1/L$, where L is the loss frequency for the constituent and $[X]$ is its abundance. Note that this is true because the loss rate for an individual constituent is almost always proportional to the abundance of the constituent. For a chemical family, however, the loss rate is proportional to the abundance of one or more members of the family, and as a result the lifetime is $[X_y]/(L[Z])$, where $[X_y]$ is the abundance of the chemical family and

$L[Z]$ is the loss rate of the family, written as the product of a loss frequency L and the abundance of Z, a member of family X_y. The lifetime of O_x, for example, is

$$\tau_{O_x} = \frac{[O_x]}{2k[O_3][O] + 2k[ClO][O] + 2(\text{other RLS})} \tag{4.2}$$

where "other RLS" represents the sum of the rates of the rate-limiting steps of the other catalytic cycles. Note that we have included in the denominator of Equation (4.2) only those reactions that are net losses for O_x. Thus, the reactions $O_2 + O$ and O_3 photolysis are not included.

The members of a chemical family can also be generally divided into two groups: reservoirs and active species. Active species are reactive—they are often radicals—and are the members of a family involved in the catalytic cycles that destroy O_x (e.g. Cl, ClO, NO, NO$_2$). Reservoir species, on the other hand, are more stable molecules (e.g. HCl, HNO$_3$) that do not react with O_x and therefore do not catalyze loss of O_x. How a chemical family is partitioned between these active and reservoir species is crucial for determining how effective it is in destroying O_x.

4.1.3 Loss

A chemical family is destroyed through chemical reactions that destroy members of a chemical family without creating other members of the family. Again using O_x as an example, reaction (3.5),

$$O_3 + O \longrightarrow O_2 + O_2$$

destroys two O_x constituents and reforms the source gas O_2. Not all chemical families have loss reactions. If a family does not have any chemical loss processes, then its concentration continues to build up until the source gas has been depleted.

4.2 Odd chlorine—Cl$_y$

4.2.1 Source

In the early 1970s, measurements of CFCs [77] in the troposphere showed that CFCs were present in abundances corresponding to their total integrated production. CFCs, it was inferred, were not being destroyed, but were simply accumulating in the troposphere. Based on this observation, Molina and Rowland [78] postulated that CFCs could be transported into the stratosphere where they would be destroyed by high-energy ultraviolet photons. This would result in chlorine atoms being released from the CFCs in the stratosphere, and these Cl atoms could participate in the

catalytic cycles that destroy O_3. Based on the work of Molina and Rowland [78], as well as the discovery of the Antarctic ozone hole, the United Nations Environmental Program (UNEP) organized the Vienna Convention on the Protection of the Ozone Layer. This resulted in the signing of the Montreal Protocol in 1987 and the Copenhagen Amendment in 1992, which committed the signatories to cease production of many of the CFCs implicated in O_3 loss by the end of 1995. For their contributions to stratospheric research, Mario Molina, F. Sherwood Rowland, and Paul Crutzen were awarded the 1995 Nobel Prize for chemistry.

It is now known that the scenario suggested by Molina and Rowland [78] is essentially correct. Halogenated organic molecules, most of which are man-made, are released at the ground. These molecules all have long tropospheric lifetimes, and therefore survive long enough to be transported into the stratosphere. It should be noted that much of the chlorine in the troposphere, such as that in sea salt or volcanic ejecta, is water-soluble [79] and therefore rapidly washed out by rain. As a result, chlorine from these sources does not reach the stratosphere.

Figure 4.1 shows a time series of the abundance of organic chlorine in the troposphere. The amount of tropospheric chlorine increased nearly exponentially between 1960 and the mid-1990s, reflecting the rapidly increasing use of these
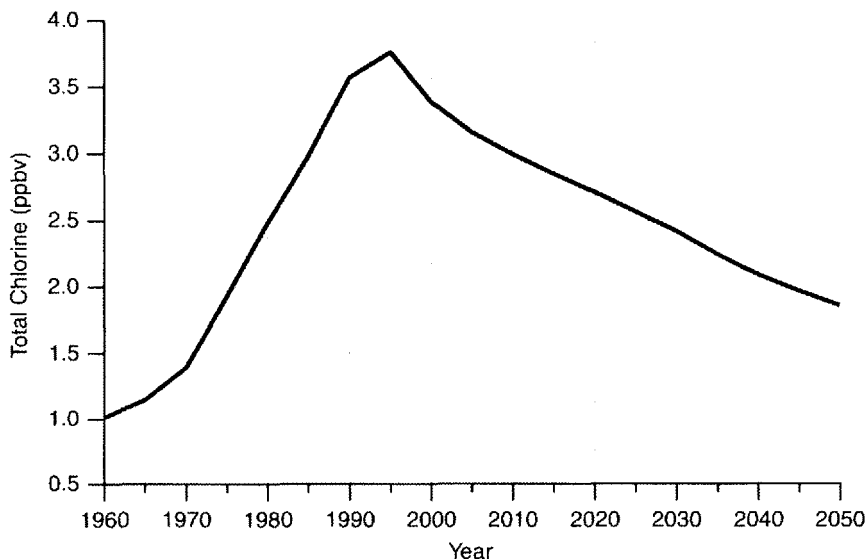
Figure 4.1 Total tropospheric chlorine. From Table 6.3 of WMO [13], and assuming CH_3Cl to be 0.6 ppbv. Chlorine amounts prior to the mid-1990s are based on measurements. Chlorine amounts after this time are estimates based on adherence to the Montreal Protocol and its amendments.

useful molecules. Tropospheric chlorine peaked near the beginning of 1994 [80], and is presently decreasing, owing primarily to the reduction in CFC production stipulated by the Montreal Protocol.

Because transport time between the troposphere and stratosphere is slow, the concentration of total chlorine in the stratosphere corresponds well to the tropospheric concentration of 3–5 years earlier [81–83]. This suggests that the amount of chlorine in the stratosphere is expected to peak between 1997 and 1999 and decline thereafter.

Measurements indicate the abundance of organic chlorine in the troposphere peaked in early 1994 at ~3700 pptv [80]. Of this, about 3 ppbv of chlorine was contained in the major CFCs, chlorinated hydrocarbons, hydrochlorofluorocarbons (HCFCs), and halons. Virtually all of these molecules result from human activities. Most of the rest was attributable to CH$_3$Cl (methyl chloride), the main natural source of chlorine in the stratosphere, which is produced from algal growth in the marine/aquatic environments (see WMO [13], Section 2.2.3). Satellite data have also confirmed that the dominant sources of chlorine in the stratosphere are man-made organic chlorine molecules [84]. Table 4.1 lists the major organic chlorine molecules and their tropospheric abundances.

Table 4.1 Tropospheric abundances of chlorine source gases for the stratosphere in the mid 1990s.

Species	Industrial name	Tropospheric abundance (pptv)	Cl atom abundance (pptv)[a]	Fraction of total Cl (%)
CCl$_3$F	CFC11, R11	272	816	22.1
CCl$_2$F$_2$	CFC12, R12	532	1064	28.8
CCl$_4$	CFC10, R10	103	412	11.1
CF$_3$CCl$_3$	CFC113, R113	84	252	6.8
CH$_3$CCl$_3$	—	109	327	8.8
CHF$_2$Cl	HCFC22, R22	117	117	3.2
CH$_3$Cl	—	600	600	16.2
Others			~100	3.0
Total			~3700	

From Table 1 of Montzka *et al.* [80], except for CH$_3$Cl, which is from Table 2.1 of WMO [13].
[a] Cl atom abundance = the tropospheric abundance of the molecule times the number of Cl atoms in the molecule.

We will define the total abundance of Cl atoms tied up in long-lived organic molecules to be CCl$_y$:

$$[CCl_y] \approx 2 \times [CCl_2F_2] + 3 \times [CCl_3F] + [CH_3Cl] + 4 \times [CCl_4] \atop + 3 \times [CH_3CCl_3] + 3 \times [C_2Cl_3F_3] + [CHClF_2] \qquad (4.3)$$

Note that we have multiplied the abundance of each molecule by the number of chlorine atoms in the molecule to determine the concentration of chlorine atoms. Species not listed in Equation (4.3) make up only a few percent of CCl$_y$. Hereinafter, we will refer to the chlorine-bearing organic molecules as CCl$_y$.

Once in the stratosphere, CCl$_y$ is destroyed primarily through photolysis by ultraviolet photons, with a minor fraction of loss occurring through oxidation. The local lifetime 1/L for several CCl$_y$ species, as well as N$_2$O and CH$_4$, is plotted in Figure 4.2. In general, the local lifetime decreases from decades in the lower stratosphere to weeks or months in the upper stratosphere because the abundance of ultraviolet photons and oxidizing radicals both increase rapidly with altitude. Note that lifetimes of species that are destroyed primarily by oxidation (e.g. CH$_4$) decrease more slowly with increasing altitude than the species that are destroyed primarily by photolysis (e.g. N$_2$O, F12, F11).

An aside: do CFCs really make it into the stratosphere? Or, when I jump out a window, I hit the ground

Some people object to the idea that CFCs, emitted near the surface, are transported into the stratosphere. They point out that CFCs generally have molecular
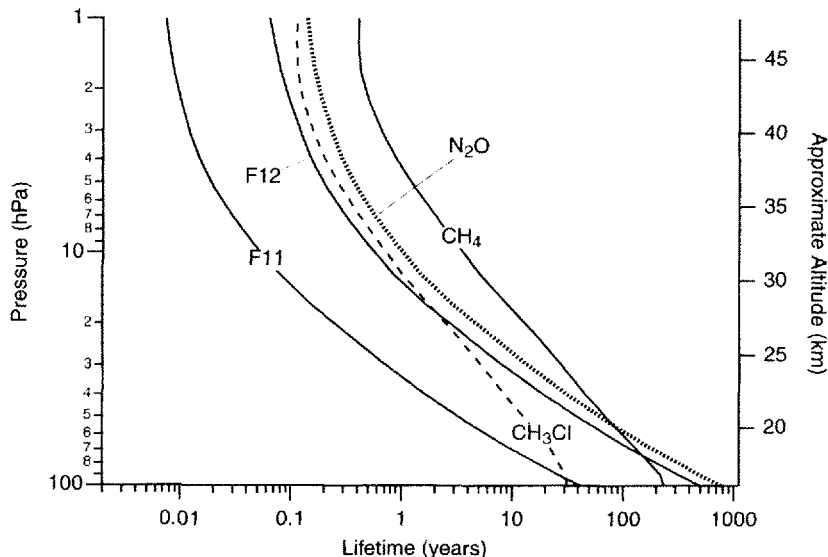
Figure 4.2 Daytime-average local photochemical loss lifetime 1/L versus pressure for several long-lived species. Values are an annual and global average (from the Goddard two-dimensional climatological circulation model [73]).

weights of 100 or more, while the average molecular weight of air is 29. Thus, CFCs are heavier than air and, the argument goes, such molecules should stay near the ground.

Fortunately, this line of reasoning is false. It is true that heavier molecules do sink toward the ground while lighter molecules rise towards the top of the atmosphere. Opposing this separation, however, are mass-independent mixing processes that tend to homogenize the atmospheric column. Whether the atmosphere separates into layers on the basis of mass is determined by the relative time-scales for these processes.

For the atmosphere to separate into layers based on mass, molecular diffusion must be the dominant process. It turns out that this process is extremely slow. The kinematic viscosity of air at the surface is $v \approx 0.2$ cm^2 s^{-1}. We can estimate the time-scale for air to diffuse through a scale height ($H \approx 7$ km), which is approximately the height of the troposphere, as $H^2/v = 8 \times 10^4$ years. Thus, if undisturbed by other processes, the atmosphere would diffusively separate into layers by mass on a time-scale of tens to hundreds of thousands of years.

Opposing molecular diffusion are mass-independent mixing processes such as convection in the troposphere and gravity-wave breaking in the stratosphere. In the troposphere, bulk mixing processes are rapid, homogenizing the troposphere on a time-scale of a month or so. Transport into the stratosphere occurs on a time-scale of years. Thus, these processes mix the atmosphere much faster than it can diffusively separate. The net result is that CFCs do not stay near the ground but are transported into the stratosphere, where they are destroyed.

It should be noted that the kinematic viscosity is inversely proportional to density. Thus, at 120 km, where the density is about 10^{-7} of the surface, the time-scale for molecular diffusion through a scale height of 7 km is about $H^2/v = 8 \times 10^{-3}$ years ≈ 3 days. Under these conditions, molecular diffusion can become important, and the atmosphere does indeed begin to separate into layers based on mass at these altitudes.

A few paragraphs earlier we wrote "Fortunately, this line of reasoning is false." Why is it fortunate that the atmosphere does not separate by mass? Argon (atomic weight 40), for example, makes up about 1% of the atmosphere. If the atmosphere did separate by layers, Ar would make up a layer several tens of meters thick near the ground. Since we cannot breathe Ar, it is indeed fortunate that the line of reasoning presented at the beginning of this section is false.

4.2.2 Partitioning

When a CCl$_y$ molecule is destroyed in the stratosphere the chlorine atoms that are bound up in it are released. They are subsequently converted into one of several inorganic chlorine-bearing species. The sum of these species is defined to be odd chlorine or Cl$_y$:

$$[Cl_y] = [HCl] + [ClONO_2] + [ClO] + [HOCl] + [Cl] + 2 \times [ClOOCl] \quad (4.4)$$

Loss of CCl_y through photolysis and oxidation is exactly compensated for by an increase in the abundance of Cl_y. Thus, the sum of $[Cl_y]$ and $[CCl_y]$ in an air mass remains constant over time. ClOOCl is only important in the polar wintertime lower stratosphere, and we will therefore ignore it until our discussion about polar O_3 loss in Chapter 7. Additionally, the destruction of CCl_y also releases fluorine atoms. The chemistry of fluorine will be discussed later in this chapter.

Figure 4.3 shows the local lifetimes $1/L$ of the members of the Cl_y family. It is immediately obvious that Cl and ClO have lifetimes that are much shorter than the other members of Cl_y. Such short lifetimes arise because ClO and Cl interconvert with each other rapidly—much like O and O_3. In analogy to O_x, we define a new constituent Cl_x:

$$[Cl_x] = [ClO] + [Cl] \quad (4.5)$$

Lifetime (hours)
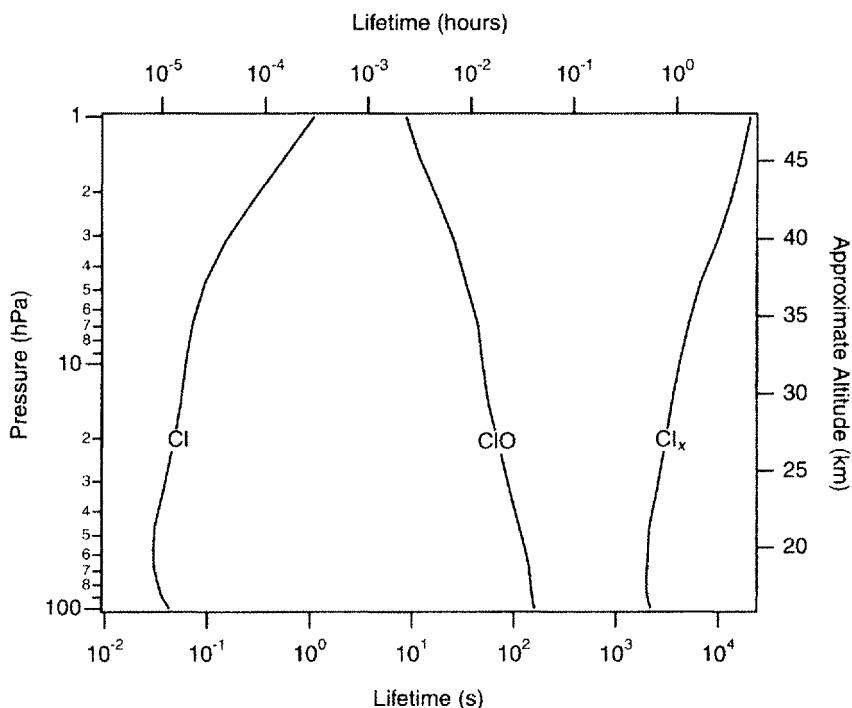
Cl$_x$ can be thought of as a "family within a family". The lifetime of Cl$_x$ is much longer than the lifetimes of ClO and Cl for the same reason that the lifetime of O$_x$ is much longer than the lifetime of O$_3$ and O. Therefore, on time-scales that are short compared to the lifetime of Cl$_x$, the abundance of Cl$_x$ remains constant, while the ClO and Cl molecules are rapidly interconverting. On time-scales that are long compared to the lifetime of Cl$_x$, Cl$_x$ will be interconverting with the other members of Cl$_y$.

Cl$_x$ comprises the active components of Cl$_y$—i.e. those members of Cl$_y$ involved in the catalytic cycles that destroy O$_x$—and is generally referred to as "reactive" or "active" chlorine. Cl$_x$ is also referred to as ClO$_x$ or Cl*. The remaining members of Cl$_y$ (mainly HCl and ClONO$_2$) are reservoir species.
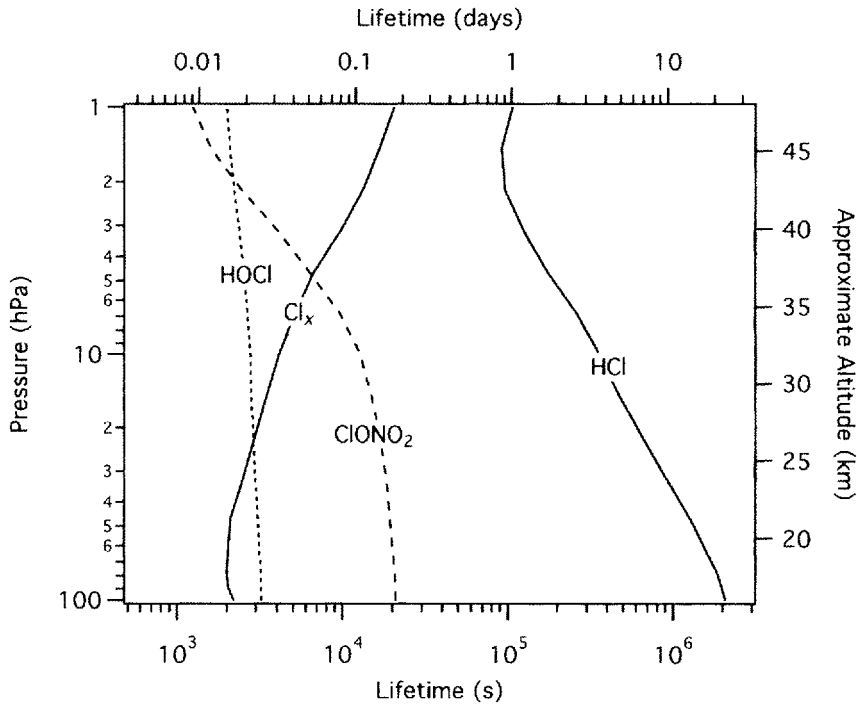
Figure 4.3 Lifetime of the components of Cl$_y$. Calculated for 45°N equinoctial conditions based on daytime-average constituent abundances and photolysis rates: $\tau_{ClO} \sim 1/(k_{ClO+NO}[NO] + k_{ClO+O}[O])$, $\tau_{Cl} \sim 1/(k_{Cl+O_3}[O_3])$, $\tau_{ClONO_2} \sim 1/(J_{ClONO_2} + k_{O+ClONO_2}[O] + k_{OH+ClONO_2}[OH])$, $\tau_{HCl} \sim 1/(k_{HCl+OH}[OH])$, $\tau_{HOCl} \sim 1/(J_{HOCl})$, $\tau_{Cl_x} \sim 1/(k^*_{ClO+NO_2}[NO_2] + k_{Cl+CH_4}[CH_4]([Cl]/[ClO]) + k_{ClO+HO_2}[HO_2])$.

Figure 4.4 shows in more detail the chemistry between these species. ClO is converted to Cl in the reactions

$$ClO + NO \longrightarrow Cl + NO_2 \tag{4.6}$$
$$ClO + O \longrightarrow Cl + O_2 \tag{4.7}$$
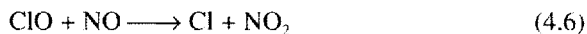
while Cl is converted to ClO in the reaction

$$Cl + O_3 \longrightarrow ClO + O_2 \tag{4.8}$$

Because the lifetimes of both ClO and Cl are short, the ClO–Cl system reaches equilibrium rapidly compared to the rate that conditions in the atmosphere change. It is therefore a standard assumption that ClO and Cl are always in the photochemical steady state.

Using the assumption that ClO and Cl are in the photochemical steady state, we can calculate the ratio

$$\frac{[Cl]}{[ClO]} = \frac{k_{ClO+NO}[NO] + k_{ClO+O}[O]}{k_{Cl+O_3}[O_3]} \tag{4.9}$$

During the day, this ratio is $\sim 10^{-1}$ in the lower stratosphere, rising to ~ 0.1 in the upper stratosphere. In other words, $[ClO] \gg [Cl]$, so that to a good approximation $[Cl_x] \approx [ClO]$ in the stratosphere. In the lower stratosphere, the term $k_{ClO+NO}[NO] \gg k_{ClO+O}[O]$. Above ~ 35 km, the atomic O term becomes important.

At night, the abundances of NO and O are very small. Thus, after sunset, Cl is converted to ClO through reaction with O_3, but there is no competing reaction to reform Cl. As a result, at night Cl_x is composed entirely of ClO. This is predicted by Equation (4.9), which predicts a $[Cl]/[ClO]$ ratio of 0 when $[NO]$ and $[O]$ are 0.

NO, O

ClO   Cl

O3
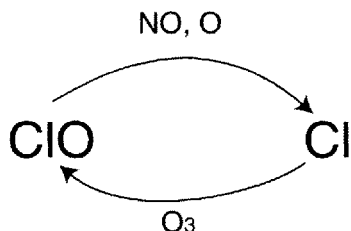
Figure 4.4 Schematic of the partitioning between the constituent components of Cl_x: ClO and Cl. Each arrow is marked with the reactants that facilitate the conversion indicated by the arrow.

The reactions that interconvert ClO and Cl (reactions (4.6)–(4.8)) have no effect on the abundance of Cl$_y$ because they are converting one form of Cl$_y$ to another. Instead, Cl$_x$ is only lost when ClO or Cl are converted to the Cl$_y$ reservoir species HCl, ClONO$_2$, or HOCl. Figure 4.5 shows a schematic of the partitioning among the Cl$_y$ reservoir species. Note that, in general, the reservoir species only interconvert with Cl$_x$. Only under rare circumstances will the reservoir species react with each other; these circumstances will be discussed in Chapters 6 and 7.

Formation of reservoirs from Cl$_x$ ClONO$_2$ is formed from Cl$_x$ in the three-body reaction

$$ClO + NO_2 \xrightarrow{\text{M}} ClONO_2 \tag{4.10}$$
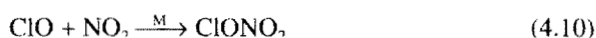
HCl is formed from Cl$_x$ primarily in the reaction

$$Cl + CH_4 \longrightarrow HCl + CH_3 \tag{4.11}$$

with a few percent of the production from

$$Cl + H_2 \longrightarrow HCl + H \tag{4.12}$$
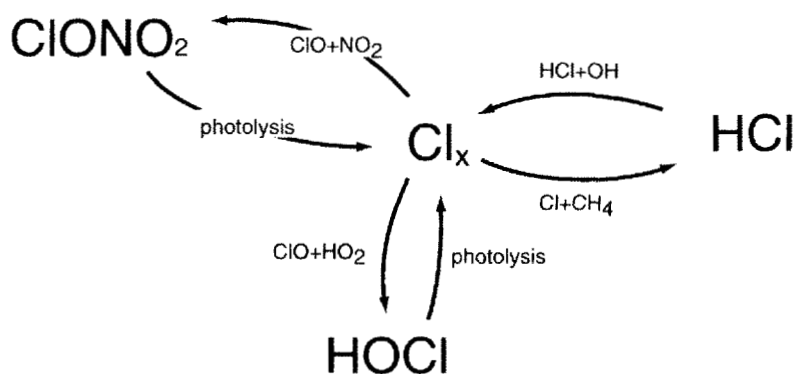
Figure 4.5 Schematic of the conversion pathways between species of the Cl$_y$ family.

The reaction between ClO and OH generally forms Cl and HO_2 as products. However, a small fraction (~7%) of the reactions between ClO and OH also form HCl [85]:

$$ClO + OH \longrightarrow HCl + O_2 \qquad (4.13)$$
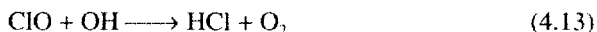
While this reaction occurs throughout the stratosphere, it is primarily important in the upper stratosphere [64,86,87].

HOCl is formed from Cl_x primarily in the reaction

$$ClO + HO_2 \longrightarrow HOCl + O_2 \qquad (4.14)$$

In rare circumstances, formation of HOCl in heterogeneous reactions can be important. This will be discussed further in Chapters 6 and 7.

Formation of Cl_x from reservoirs $ClONO_2$ is converted to Cl_x through the photolysis reaction

$$\begin{aligned} ClONO_2 + h\nu &\longrightarrow Cl + NO_3 \\ &\longrightarrow ClO + NO_2 \end{aligned} \qquad (4.15)$$
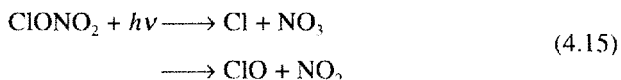
The majority of $ClONO_2$ molecules photolyze to produce Cl and NO_3, with the remainder producing ClO and NO_2 (see DeMore *et al.* [5], Table 40). Oxidation of $ClONO_2$ by the stratospheric radicals such as OH, O, and Cl becomes important above about 35 km, and is the dominant loss process of $ClONO_2$ near the stratopause.

HCl is converted to Cl_x in the reaction

$$HCl + OH \longrightarrow Cl + H_2O \qquad (4.16)$$

The pathway for conversion of HOCl to Cl_x is photolysis,

$$HOCl + h\nu \longrightarrow OH + Cl \qquad (4.17)$$

with a minor contribution (less than 1%) from oxidation,

$$HOCl + OH \longrightarrow H_2O + ClO \qquad (4.18)$$

In addition to the gas phase reactions discussed above, there are several heterogeneous reactions occurring on the surfaces of sulfate aerosols that involve members of Cl_x. The sticking coefficients of these reactions are strong functions of temperature,

and in general these reactions are important only for an enhanced sulfate aerosol surface area density (SAD), such as that found immediately after a volcanic eruption, or at temperatures below ~200 K. These conditions are rarely found in the stratosphere, and therefore these heterogeneous reactions can be generally ignored. There are, however, certain circumstances where these reactions can have an impact [88]. We will discuss the role of these heterogeneous reactions in Chapters 6 and 7.

Figure 4.6 shows vertical profiles of the various members of Cl$_y$. The figure shows CCl$_y$ decreasing rapidly with altitude, consistent with its destruction through photolysis. At the same time, Cl$_y$ increases with altitude. It should be noted that the total chlorine content (the sum of CCl$_y$ and Cl$_y$) is approximately constant throughout the stratosphere. This is true because the rate of change of CFCs in the troposphere is small compared to the rate at which air is transported through the stratosphere (a few years, see Chapter 5).
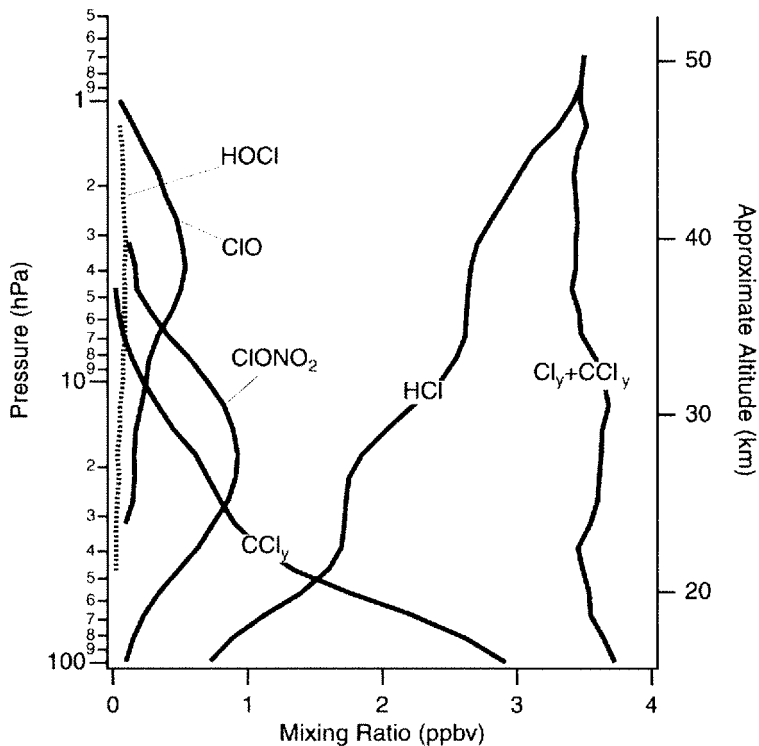
Figure 4.6 Measurements of the major components of stratospheric chlorine versus pressure. Data were measured in November 1994 and between 20°N and 49°N [89].

Over the entire stratosphere, HCl is the dominant form of Cl_y. In the lower and mid-stratosphere, $ClONO_2$ makes up most of the remainder of Cl_y. In the upper stratosphere, ClO is the second most abundant form of Cl_y. HOCl makes up at most a few percent of Cl_y, while the abundance of Cl atoms makes up a negligible fraction of Cl_y.

Figures 4.7 through 4.10 show meridional cross-sections of Cl_y, ClO, $ClONO_2$, and HCl. The abundance of Cl_y increases with both altitude and latitude, consistent with the mean overturning circulation (discussed in Chapter 5) combined with the rapid destruction of CCl_y in the mid- and upper-stratosphere.

The HCl distribution (Figure 4.8) has a shape similar to the distribution of Cl_y, with the abundance of HCl increasing with both altitude and latitude. The abundance of $ClONO_2$ (Figure 4.9) increases with altitude in the lower stratosphere, reaches a maximum in the mid-stratosphere, and decreases at higher altitudes. Further, the abundance of lower-stratospheric $ClONO_2$ as a fraction of Cl_y is greater in the winter hemisphere than in the summer hemisphere [90]. And as one might expect, lower-stratospheric HCl shows the opposite seasonal cycle (Figure 4.8).
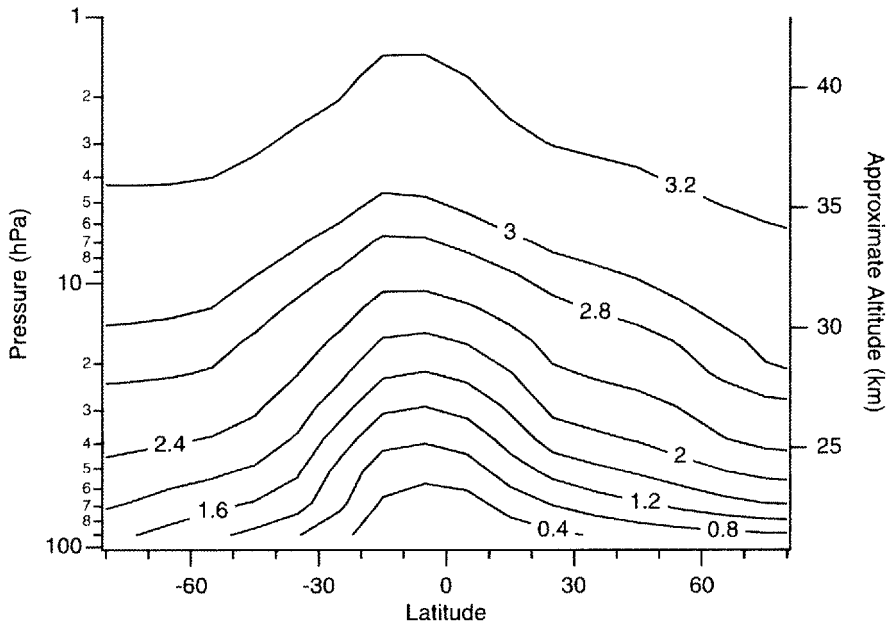
Figure 4.7 Contours of Cl_y abundance (ppbv) for December. Values are from the Goddard two-dimensional climatological circulation model [73]. Based on a model run to the steady state using CFC emission levels for 1990.
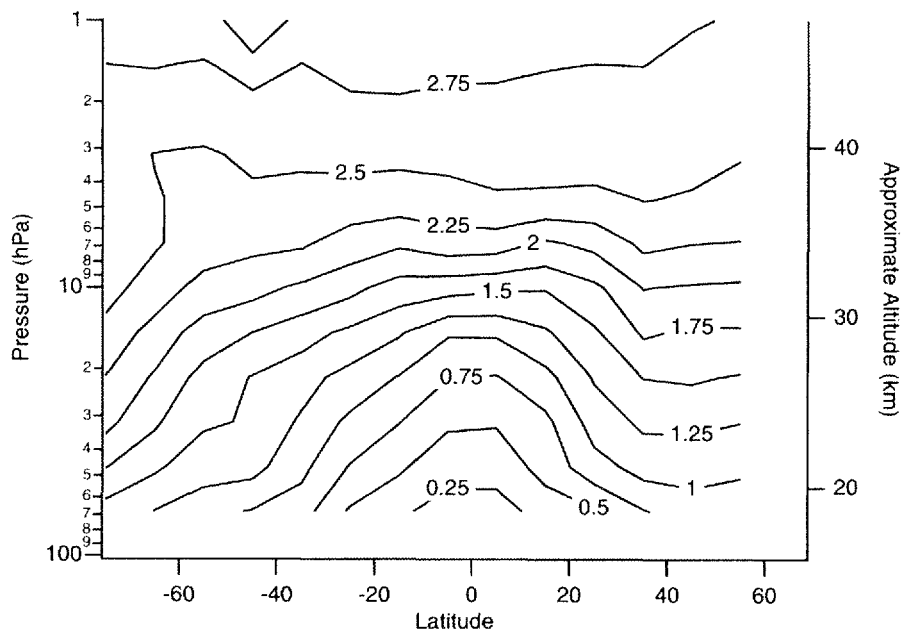
Figure 4.8 Contours of zonally averaged HCl abundance (ppbv). Plot made from both sunset and sunrise measurements (version 18) by the Halogen Occultation Experiment (HALOE) on the UARS between February 4 and March 16, 1994.

The abundance of ClO is plotted in Figure 4.10. Because $[Cl_x] \approx [ClO]$, this quantity can also be considered the abundance of Cl$_x$. The figure shows ClO abundance increasing with altitude throughout the stratosphere. In the lower stratosphere this increase is due to increasing Cl$_y$ abundances. In the mid- and upper stratosphere, it is due to increasing loss rates of ClONO$_2$ and HCl compared to the loss rate of ClO. During winter, the polar region experiences 24 h of darkness every day—this is known as polar night. In this situation, all photolysis reactions cease, and loss of ClO through reaction with NO$_x$ to reform ClONO$_2$, or through reaction with other ClO radicals to form ClOOCl, continues unabated. As a result, the abundance of ClO during polar night is approximately zero. The chemistry of the polar night region will be discussed at length in Chapter 7.

Based on our discussions up to this point, we present the following general picture of the partitioning between the major components of Cl$_y$: Cl$_x$, ClONO$_2$, and HCl. During the day, the members of Cl$_x$, Cl and ClO cycle rapidly with each other. On time-scales that are long compared to the lifetimes of Cl$_x$ and ClONO$_2$, but short compared to the lifetime of HCl, Cl$_x$ is consumed to produce ClONO$_2$, and
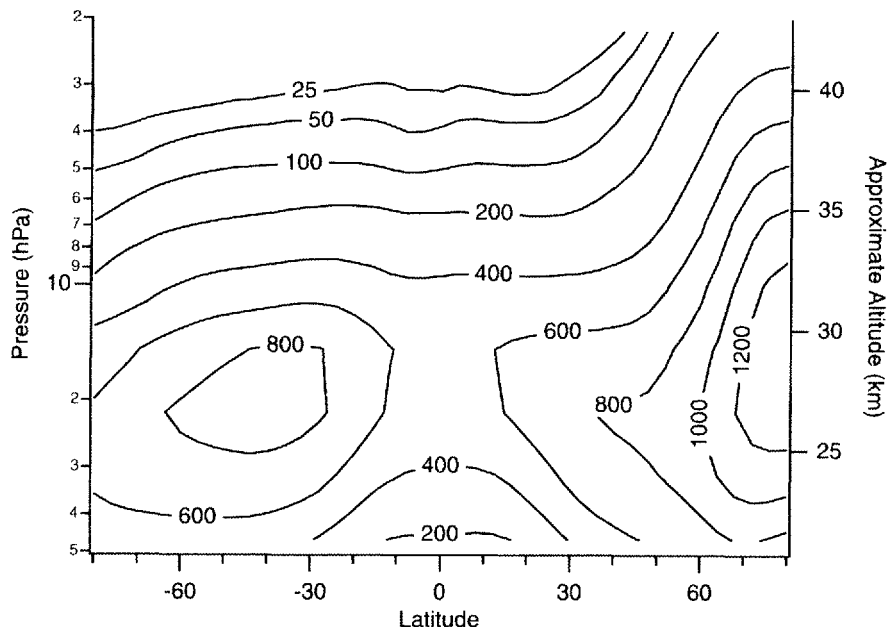
Figure 4.9 Contours of zonally averaged daytime $ClONO_2$ abundance (pptv) for December 1992, derived from UARS CLAES data (version 8).

photolysis of $ClONO_2$ reforms Cl_x. On time-scales that are long compared to the life-times of HCl, Cl_x is converted to HCl, and HCl is destroyed to reform Cl_x.

Because of the different time-scales, we can divide the problem of Cl_y partitioning into three separate parts: the partitioning between Cl and ClO, the partitioning between Cl_x and $ClONO_2$, and the partitioning between HCl and the sum of Cl_x and $ClONO_2$ (Figure 4.11).

The partitioning of Cl_x was discussed at length earlier in this section, and we will not repeat it here. The partitioning between Cl_x and $ClONO_2$ can be seen in Figure 4.12. The abundance of Cl_x rises just after sunrise due to the initiation of $ClONO_2$ photolysis (reaction (4.15)) and, in the upper stratosphere, $ClONO_2$ oxidation. The abundance of Cl_x increases until the rate of formation of $ClONO_2$ (reaction (4.10)) balances the rate of destruction of $ClONO_2$. At this point, the Cl_x–$ClONO_2$ system is in photochemical steady state [69], and the relative abundance of $ClONO_2$ and Cl_x can be written as

$$\frac{[Cl_x]}{[ClONO_2]} \approx \frac{[ClO]}{[ClONO_2]} = \frac{J_{ClONO_2}}{k^*_{ClO+NO_2}[NO_2]} \qquad (4.19)$$
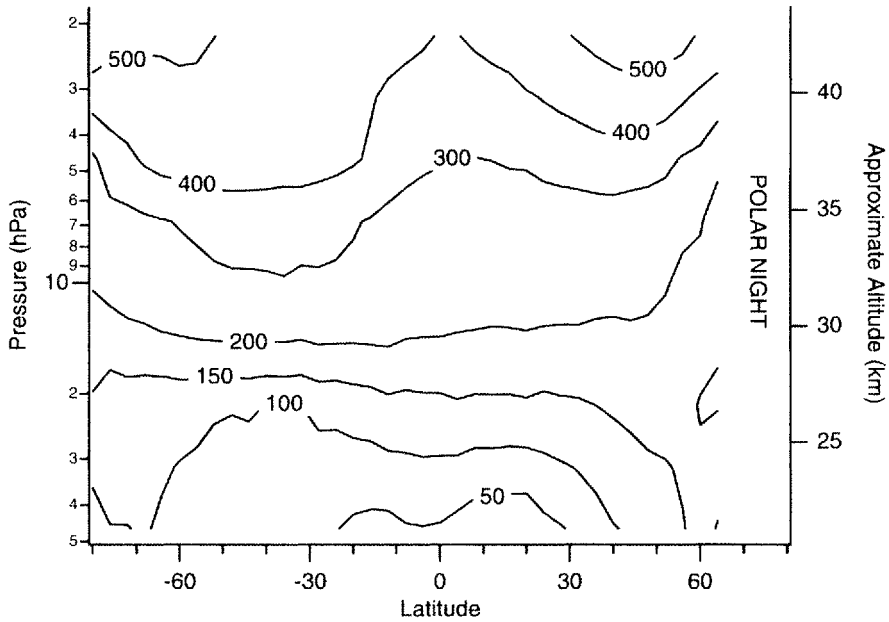
Figure 4.10 Contours of zonally averaged daytime ClO abundance (pptv) for December 1992, derived from UARS MLS data (version 4).

During the daytime, this ratio is ~0.1–0.2 during the day in the lower stratosphere, rising to 20–100 in the upper stratosphere. After sunset, the Cl$_x$ abundance decreases as ClO reacts NO$_2$ to reform ClONO$_2$. In the lower and mid-stratosphere, this process rapidly depletes Cl$_y$, and throughout most of the night the abundance of Cl$_x$ is essentially zero. In the upper stratosphere, the recombination reaction (4.10) is slow due to
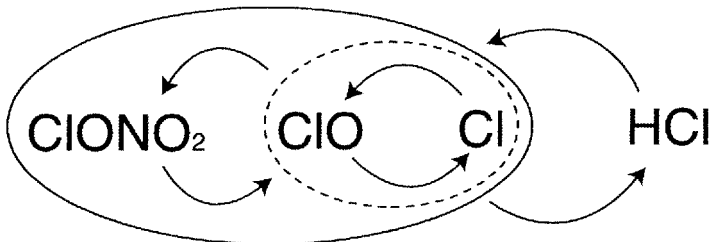
Figure 4.11 Schematic of Cl$_y$ partitioning among its major members. The cycles are grouped by time constant.

the low pressure found there. As a result, Cl_x decays slowly throughout the night, and can still maintain an appreciable concentration at sunrise of the next day.

We next consider the partitioning between [HCl] and the sum of $[ClONO_2]$ and $[Cl_x]$. In the lower and mid-stratosphere, $[ClONO_2] \gg [Cl_x]$, and the ratio $([ClONO_2] + [Cl_x])/[HCl] \approx [ClONO_2]/[HCl]$. We next expand this ratio in terms of the ratios of constituents that are directly related by chemical reactions [90]:

$$\frac{[ClONO_2]}{[HCl]} = \frac{[ClONO_2]}{[ClO]} \frac{[ClO]}{[Cl]} \frac{[Cl]}{[HCl]} \tag{4.20}$$
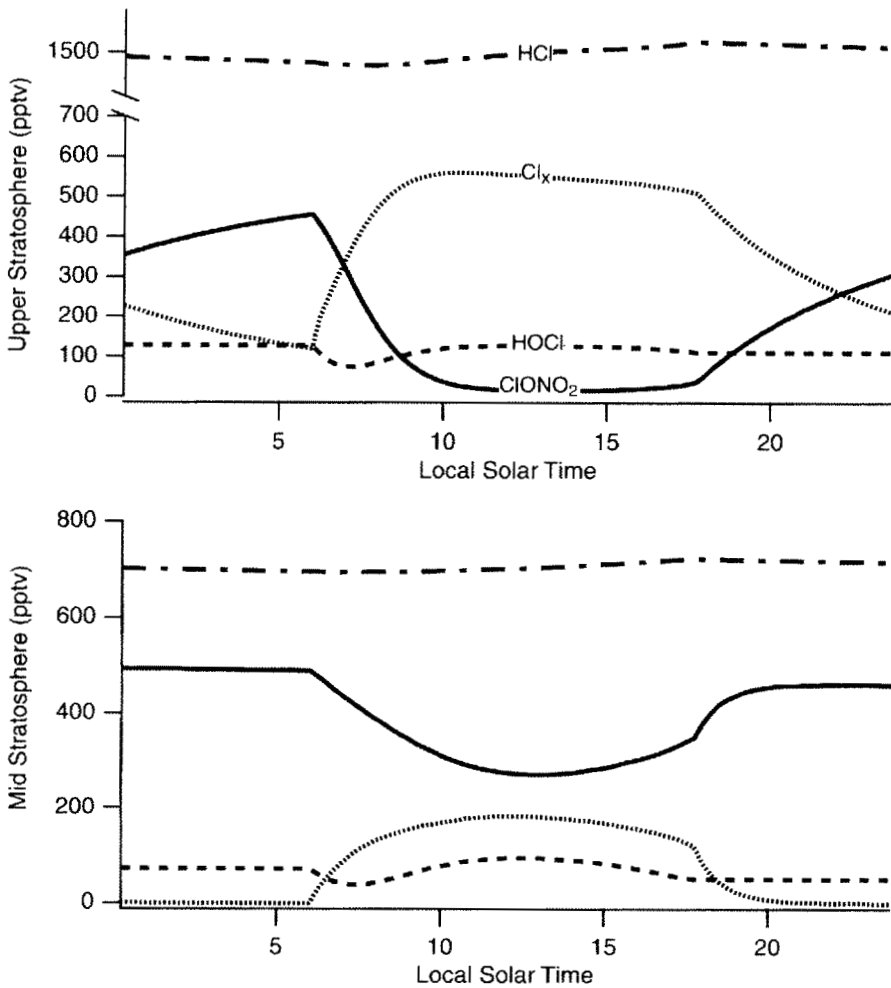
Assuming steady-state conditions, Equation (4.20) can be rewritten as

$$\frac{[ClONO_2]}{[HCl]} \approx \frac{k_{ClO+NO_2}[NO_2]}{J_{ClONO_2}} \times \frac{k_{CHO_3}[O_3]}{(k_{ClO+O}[O] + k_{ClO+NO}[NO])} \frac{k_{HCl+OH}[OH]}{k_{CH_4+Cl}[CH_4]} \quad (4.21)$$

In the lower and mid-stratosphere, $k_{ClO+NO}[NO] \gg k_{ClO+O}[O]$. And substituting the steady-state relation $(k_{NO+O_3}[O_3] + k_{NO+ClO}[ClO])/J_{NO_2}$ for $[NO_2]/[NO]$, we obtain the expression

$$\frac{[ClONO_2]}{[HCl]} \approx \frac{k_{ClO+NO_2}}{J_{ClONO_2}} \times \frac{(k_{CHO_3}k_{NO+O_3}[O_3]^2 + k_{CHO_3}k_{NO+ClO}[ClO][O_3])}{k_{ClO+NO} J_{NO_2}}$$

$$\times \frac{k_{HCl+OH}[OH]}{k_{CH_4+Cl}[CH_4]} \quad (4.22)$$

In the lower stratosphere, $k_{CHO_3}k_{NO+O_3}[O_3]^2$ is several orders of magnitude larger than $k_{CHO_3}k_{NO+ClO}[ClO][O_3]$, decreasing to about five times larger in the mid-stratosphere. Thus, the ratio in Equation (4.22) is approximately quadratically dependent on $[O_3]$, linearly dependent on $[OH]$ and $[CH_4]$, and less sensitive to changes in $[ClO]$. Note that we have neglected chlorine-activating heterogeneous reactions, which are generally unimportant.
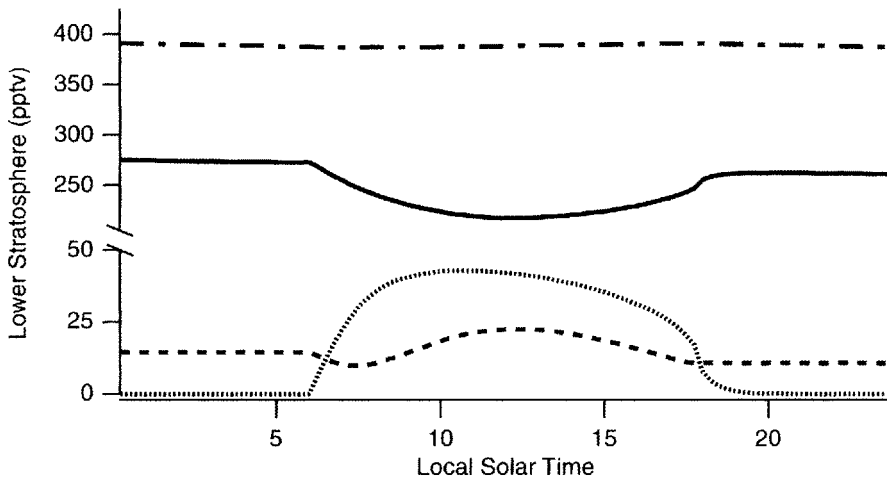
Figure 4.12 Diurnal cycle of the components of Cl$_y$ derived from a model incorporating the reaction set of JPL 94 [91]. The model run is at 45°N on March 21, 1996 and using background aerosol abundances. "Upper stratosphere" is the 3.16 hPa level of the model, "mid-stratosphere" is the 14.7 hPa level, and "lower stratosphere" is the 57.0 hPa level.

Note that the lifetime of HCl is sufficiently long that we do not expect Equation (4.22) to be satisfied at any particular instant in time but only when the abundances and other parameters are averaged over the lifetime of HCl.

In the upper stratosphere, during the day $[Cl_x] \gg [ClONO_2]$, and the ratio $[Cl_x]/[HCl]$ is the important partitioning parameter. Following the logic used for $[ClONO_2]/[HCl]$, we rewrite the ratio $[Cl_x]/[HCl]$ in terms of the ratios of constituents that are directly related by chemical reactions:

$$\frac{[Cl_x]}{[HCl]} \approx \frac{[ClO]}{[HCl]} = \frac{[ClO]}{[Cl]} \frac{[Cl]}{[HCl]} \tag{4.23}$$

Using a photochemical steady-state relation between Cl and HCl and Equation (4.9), the photochemical steady-state relation between Cl and ClO, we get

$$\frac{[Cl_x]}{[HCl]} \approx \frac{k_{Cl+O_3}[O_3]}{k_{ClO+NO}[NO] + k_{ClO+O}[O]} \frac{k_{HCl+OH}[OH]}{k_{CH_4+Cl}[CH_4]} \tag{4.24}$$

Owing to the reasonably short lifetime of HOCl, over most of the day HOCl is in the photochemical steady state with Cl_x. The relative abundance of HOCl and Cl_x can be written [92] as

$$\frac{[Cl_x]}{[HOCl]} \approx \frac{[ClO]}{[HOCl]} = \frac{J_{HOCl} + k_{HOCl+OH}[OH]}{k_{ClO+HO_2}[HO_2]} \tag{4.25}$$

where we utilize the approximation $[Cl_x] \approx [ClO]$. The ratio is near unity in the lower stratosphere, rising to 10–20 at 1 hPa. Both production and loss cease at sunset, leaving the concentration of HOCl to hold steady throughout the night. Despite its relatively short lifetime throughout the stratosphere, HOCl shows little diurnal cycle.

Finally, it should be noted that the behavior of the abundance of a species during the day is constrained by its lifetime. If the species has a lifetime longer than a day—HCl, for example—then its abundance can exhibit only small changes during a day. Species with lifetimes shorter than a day can exhibit significant diurnal variations (Figure 4.12). The abundance of ClO, for example, rises rapidly in the morning, remains elevated throughout the day, and then decreases significantly after sunset. It should be noted, however, that short-lived species are not guaranteed to exhibit large diurnal variations. HOCl, which has a lifetime comparable to or shorter than Cl_x, for example, shows little diurnal change. In this case, the production rate and loss frequency of HOCl vary diurnally so that the ratio P/L remains approximately constant throughout the day, leading to an approximately constant abundance of HOCl.

Another aside: how do we know that CFCs are responsible for stratospheric chlorine?

In the last aside, we explained CFCs are expected to reach the stratosphere despite being heavier than air. In this brief aside, we present evidence that CFCs actually make it and are responsible for most of the chlorine found there:

(1) CFCs have been detected in the stratosphere [93]. And since they have no sources other than the surface, this proves they must be transported there from the troposphere.

(2) HF has been detected in the stratosphere [84]. The only source of stratospheric HF is the breakdown of CFCs, so its presence in the stratosphere is positive proof that CFCs are being destroyed in the stratosphere, and their chlorine and fluorine are being released.

(3) The abundance of total chlorine in the stratosphere (~3.6 ppbv in the mid-1990s) corresponds well to the tropospheric abundance of CFCs and other long-lived halogenated organic molecules.

Combining these lines of reasoning, it is indisputable that CFCs are the main source of stratospheric chlorine.

4.2.3 Loss of Cl$_y$

There are no chemical loss processes for the Cl$_y$ family in the stratosphere. Instead, the concentration of Cl$_y$ in an air parcel increases until all of the CCl$_y$ has been destroyed.

4.3 Odd Nitrogen—NO$_y$

4.3.1 Source

Much like CFCs, nitrous oxide (N$_2$O) is a stable molecule with a tropospheric source, which, because of its stability, is transported into the stratosphere. Once in the stratosphere, destruction of N$_2$O creates NO$_y$.

N$_2$O is thought to be primarily of natural origin, although significant anthropogenic sources do exist (see WMO [13], Section 2.5) [94]. In the mid-1990s, the tropospheric concentration of N$_2$O was 310 ppbv (see WMO [13], Section 2.5), and had been growing at 0.5–1.2 ppbv/year [94], about 0.16–0.39% per year.

The major stratospheric loss process for N$_2$O is photolysis:

$$N_2O + h\nu \longrightarrow N_2 + O \qquad (4.26)$$

which accounts for ~90% of the loss (see WMO [13], Section 2.5). Because of its strong triple bond, N$_2$ is essentially inert in the lower and middle atmosphere; as a

result, N_2 is not included in NO_y. Therefore, reaction (4.26) does not produce NO_y. Other loss processes include [95]

$$N_2O + O(^1D) \longrightarrow N_2 + O_2 \tag{4.27}$$

$$N_2O + O(^1D) \longrightarrow NO + NO \tag{4.28}$$

$$N_2O + h\nu \longrightarrow NO + N(^4S) \tag{4.29}$$
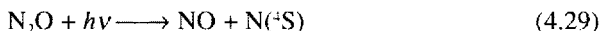
Reaction (4.27) does not produce NO_y. Reaction (4.28), while a minor loss process for N_2O, is the major source of NO_y in the stratosphere. Reaction (4.29) is also a source of NO_y, but it is much less important than reaction (4.28).

NO_y is also formed in the stratosphere from dissociation of N_2 caused by collisions with solar protons, galactic cosmic rays, and associated electrons [96]. In addition, NO_y produced in the mesosphere and thermosphere from photolysis of N_2 and precipitating electrons dissociating N_2 can be transported into the stratosphere [97]. These NO_y sources, however, are minor compared to the oxidation of N_2O.

4.3.2 Partitioning

Odd nitrogen, NO_y, is defined to be

$$\begin{aligned}[NO_y] &= [N] + [NO] + [NO_2] + [NO_3] + 2 \times [N_2O_5] \\ &+ [ClONO_2] + [BrONO_2] + [HNO_3] + [HO_2NO_2]\end{aligned} \tag{4.30}$$

Thus, NO_y represents the abundance of N atoms that are not bound up in either N_2 or N_2O. This is analogous to the definition for Cl_y, which contained all of the Cl atoms that were not in a CFC or other organic molecule.

There are three other points of note. First, the concentration of N_2O_5 in Equation (4.30) is multiplied by 2 to account for the fact that each N_2O_5 molecule contains two N atoms. Second, $ClONO_2$, which is a member of the Cl_y family, is also a member of the NO_y family. This shows that the various chemical families are coupled—i.e. changes in the partitioning of one family can affect the partitioning of another. Third, in the stratosphere, N and HO_2NO_2 make up a small fraction of NO_y species, and play a limited role in stratospheric chemistry.

Figure 4.13 shows typical lifetimes for the NO_y species. Following the pattern set in our discussion of the Cl_y family, we group the short-lived species NO, NO_2, and NO_3 together and define their sum to be NO_x:

$$[NO_x] = [NO] + [NO_2] + [NO_3] \tag{4.31}$$

NO_x includes the members of the NO_y family that participate in catalytic cycles that destroy ozone—in other words the "active" components of NO_y.
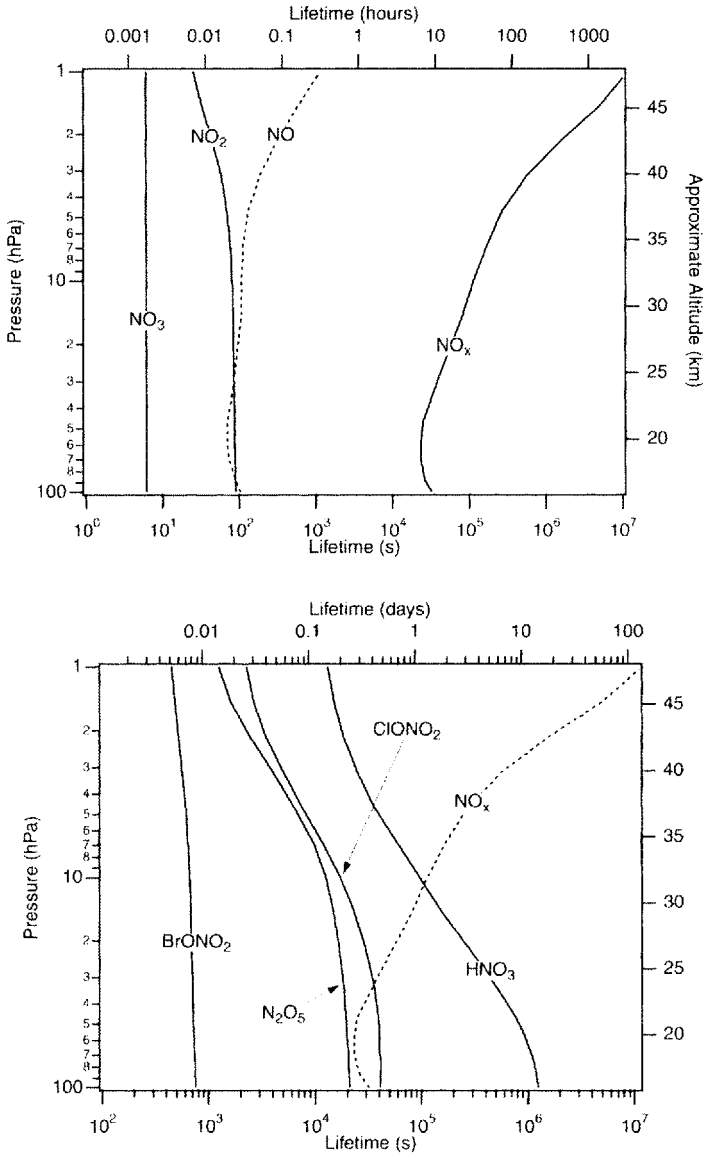
Figure 4.13 Lifetime of NO$_y$ and its components, calculated for 45°N equinoctial conditions based on daytime-average constituent abundances and photolysis rates: $\tau_{NO} \sim 1/(k_{ClO+NO}[ClO] + k_{NO+O_3}[O_3]$ $+ k_{NO+HO_2}[HO_2])$, $\tau_{NO_2} \sim 1/(J_{NO_2} + k_{NO_2+O}[O])$, $\tau_{NO_3} \sim 1/J_{NO_3}$, $\tau_{NO_x} \sim [NO_x]/(k^*_{NO_2+OH}[OH][NO_2] +$ $k^*_{BrO+NO_2}[BrO][NO_2] + k^*_{ClO+NO_2}[ClO][NO_2] + 2k^*_{NO_2+NO_3}[NO_2][NO_3])$, $\tau_{ClONO_2} \sim 1/(J_{ClONO_2} +$ $k_{O+ClONO_2}[O] + k_{OH+ClONO_2}[OH])$, $\tau_{BrONO_2} \sim 1/(J_{BrONO_2} + k_{aerosol})$, $\tau_{HNO_3} \sim 1/(J_{HNO_3} + k_{HNO_3+OH}[OH])$.

Figure 4.14 shows the major interconversion pathways of NO_x. NO is converted to NO_2 in the reactions

$$NO + O_3 \longrightarrow NO_2 + O_2$$
$$ClO + NO \longrightarrow Cl + NO_2 \tag{4.32}$$

Note that the second reaction (reaction (4.6)) is also an important reaction for partitioning Cl_x. In the upper stratosphere, the reaction with HO_2 becomes important:

$$NO + HO_2 \longrightarrow NO_2 + OH \tag{4.33}$$
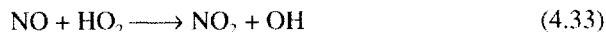
NO_2 is converted back to NO through the reactions

$$NO_2 + h\nu \longrightarrow NO + O \tag{4.34}$$
$$NO_2 + O \longrightarrow NO + O_2 \tag{4.35}$$

NO_3 is formed from NO_2 in the reaction

$$NO_2 + O_3 \longrightarrow NO_3 + O_2 \tag{4.36}$$

NO_3 is converted to NO and NO_2 through photolysis:

$$NO_3 + h\nu \longrightarrow NO_2 + O \tag{4.37}$$
$$NO_3 + h\nu \longrightarrow NO + O_2 \tag{4.38}$$

About eight times as many NO_3 molecules photolyze to form NO_2 and O as form NO and O_2 (see DeMore et al. [5], p. 158).
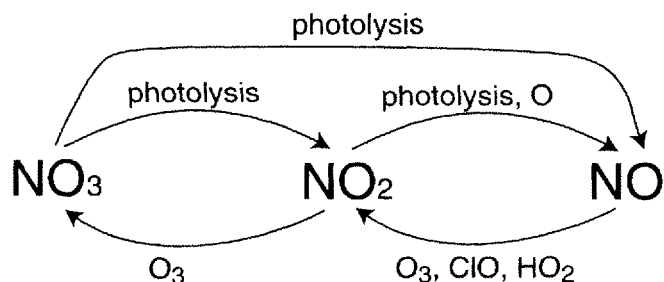
Figure 4.14 Schematic of the partitioning between NO, NO_2, and NO_3 (the sum of which is NO_x). Each arrow is marked with the reactants that facilitate the conversion.

As with any chemical family, the reactions that interconvert NO, NO$_2$, and NO$_3$ (reactions (4.32)–(4.38) and (4.6)) have no effect on the abundance of NO$_x$. NO$_x$ is only lost when NO, NO$_2$, or NO$_3$ is converted to HNO$_3$, ClONO$_2$, BrONO$_2$, or N$_2$O$_5$.

Figure 4.15 shows how the composition of NO$_x$ changes throughout the day. During daytime, NO$_x$ is almost entirely composed of NO and NO$_2$, with the abundance of NO$_3$ practically zero. Because of the short lifetimes of both NO and NO$_2$, these species are generally assumed to be in photochemical steady state during daylight. The daytime ratio of the abundance of NO to NO$_2$ can be approximated:

$$\frac{[\text{NO}]}{[\text{NO}_2]} = \frac{J_{\text{NO}_2} + k_{\text{NO}_2+\text{O}}[\text{O}]}{k_{\text{NO}+\text{O}_3}[\text{O}_3] + k_{\text{NO}-\text{ClO}}[\text{ClO}]} \tag{4.39}$$

This has been well verified by atmospheric observations [98–100].

At sunset, the reactions that convert NO$_2$ to NO cease, allowing the reaction between NO and O$_3$ to convert virtually all NO to NO$_2$. As a result, at night, the vast majority of NO$_x$ is in the form of NO$_2$.

During the day, the abundance of NO$_3$ is set by a steady-state balance between loss of NO$_3$ through photolysis (reactions (4.37) and (4.38)) and formation of NO$_3$ through NO$_2$+O$_3$ (reaction (4.36)). Because of the extremely fast photolysis of NO$_3$, this turns out to be small: typical stratospheric daytime abundances of NO$_3$ are tens to hundreds of parts per quadrillion by volume (parts in 10^{15}). After sunset, the abundance of NO$_3$ rises as production of NO$_3$ from NO$_2$+O$_3$ (reaction (4.36)) is unopposed by photolysis. In the lower and mid-stratosphere, the abundance of NO$_3$ builds up until a steady-state balance is achieved between production of NO$_3$ through NO$_2$+O$_3$ (reaction (4.36)) and loss of NO$_3$ through reaction with NO$_2$ to form N$_2$O$_5$ (reaction (4.40)):

$$[\text{NO}_3]_{\text{night}} = \frac{k_{\text{NO}_2+\text{O}_3}[\text{O}_3]}{k^*_{\text{NO}_2+\text{NO}_3}} \tag{4.40}$$

Note that Figure 4.15 shows NO$_3$ rising as a fraction of NO$_x$ throughout the night. This occurs despite a constant abundance of NO$_3$ because the abundance of NO$_x$ decreases throughout the night as it is converted to N$_2$O$_5$.

In the upper stratosphere, the rate of reaction between NO$_3$ and NO$_2$ to form N$_2$O$_5$ (reaction (4.40)) is slow enough that the system never reaches steady state; instead, NO$_3$ builds up throughout the night. Typical night-time values of NO$_3$ are a few parts per trillion by volume in the lower stratosphere, rising to a few tenths of a part per billion by volume in the upper stratosphere.

Upper Stratosphere

NO₂ ....
NO ——
NO₃ - - -

Mid Stratosphere

Lower Stratosphere
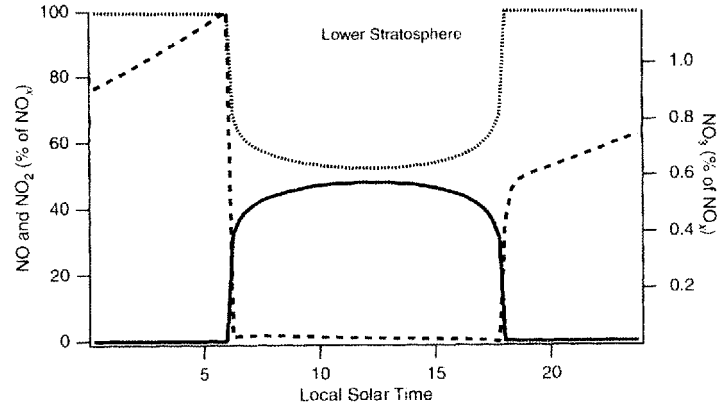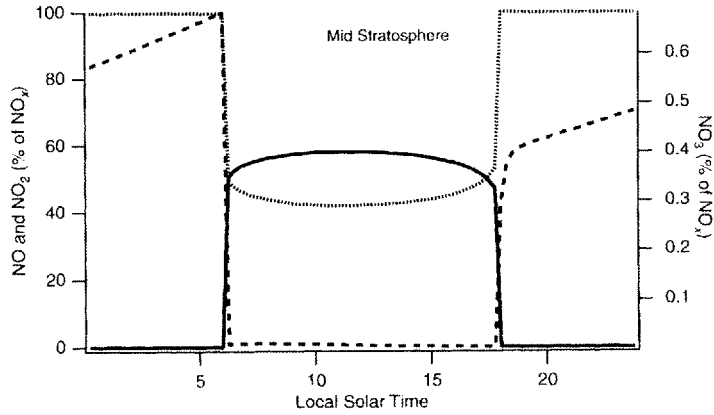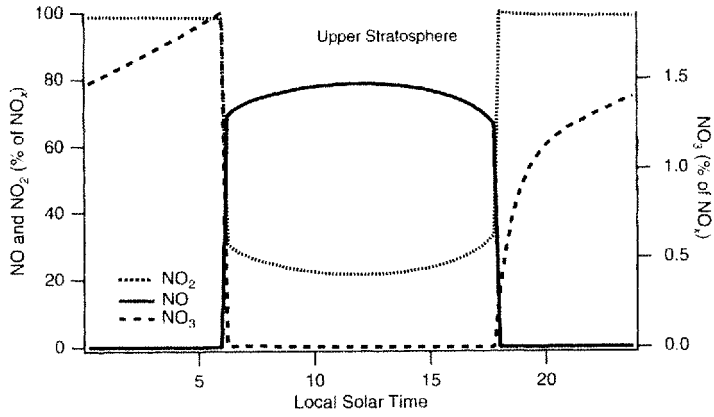
Figure 4.16 shows a schematic of the interconversion pathways for the major members of NO$_y$. NO$_x$ species interconvert rapidly compared to the time-scale with which NO$_y$ is produced or destroyed, but slowly compared to the time-scale with which the members of NO$_x$ interconverts.

Formation of reservoirs from NO$_x$ NO$_x$ is converted to the various reservoir species primarily in three-body reactions. N$_2$O$_5$ is produced by the reaction

$$NO_2 + NO_3 \xrightarrow{M} N_2O_5 \tag{4.41}$$

Because of the extremely low abundances of NO$_3$ during the day, this process is important only at night. This reaction consumes two NO$_x$ molecules for each N$_2$O$_5$ created. HNO$_3$ is produced from NO$_x$ by the reaction

$$OH + NO_2 \xrightarrow{M} HNO_3 \tag{4.42}$$

ClONO$_2$ is formed from NO$_x$ in the reaction (4.10):

$$ClO + NO_2 \xrightarrow{M} ClONO_2$$
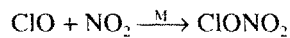
BrONO$_2$ is formed in an analogous reaction:

$$BrO + NO_2 \xrightarrow{M} BrONO_2 \tag{4.43}$$
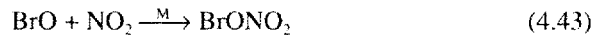
Formation of NO$_x$ from reservoirs   The destruction of these NO$_y$ reservoirs reforms NO$_x$. N$_2$O$_5$ is destroyed by photolysis and thermal decomposition to reform NO$_x$:

$$N_2O_5 + h\nu \longrightarrow NO_2 + NO_3 \tag{4.44}$$

$$N_2O_5 + M \longrightarrow NO_2 + NO_3 + M \tag{4.45}$$
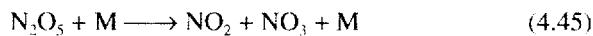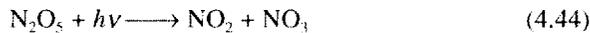
Thermal decomposition (reaction (4.45)) makes up ~1% of the loss of N$_2$O$_5$ in the lower and mid-stratosphere, and as much as 10% in the upper stratosphere, owing to the warmer temperatures and lower pressure found there.

Figure 4.15 Fraction of NO$_y$ in the form of NO, NO$_2$, and NO$_3$ derived from a model incorporating the JPL 94 reaction set [91]. Note that the NO$_3$ scale is on the right. "Upper stratosphere" is from the 3.16 hPa level of the model, "mid stratosphere" is 14.7 hPa, and "lower stratosphere" is 57.0 hPa. The model run is at 45°N on March 21, 1996 and using background aerosol abundances.
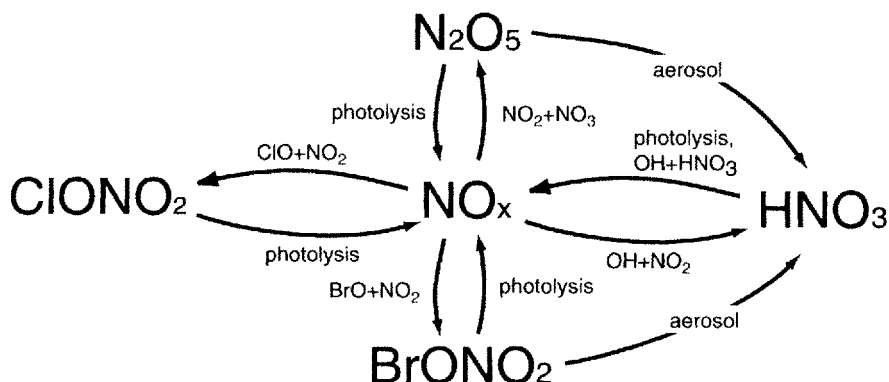
Figure 4.16 Schematic of the NO_y family. Arrows indicate conversion pathways between species.

HNO_3 is destroyed by photolysis and oxidation by OH:

$$HNO_3 + h\nu \longrightarrow OH + NO_2 \tag{4.46}$$

$$HNO_3 + OH \longrightarrow NO_3 + H_2O \tag{4.47}$$
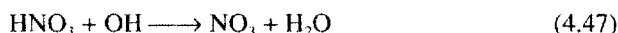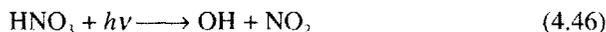
These two processes make comparable contributions to HNO_3 loss in the lower stratosphere. As the altitude increases, photolysis becomes progressively more important, until, in the upper stratosphere, it dominates.

$ClONO_2$ and $BrONO_2$ are converted back to NO_x via photolysis and, at high altitudes for $ClONO_2$, oxidation. (See the discussions of the odd chlorine (Cl_y) and odd bromine (Br_y) families for more about these processes.)

Interconversion among NO_y reservoirs   An important feature of the NO_y family is the existence of reaction pathways that directly convert the reservoir species N_2O_5, $BrONO_2$, and $ClONO_2$ into HNO_3. These reactions all take place on sulfate aerosol surfaces. As a result, these reactions will be most important in the lower stratosphere, with diminishing importance in the mid-stratosphere and essentially no importance in the upper stratosphere, and the efficacy of these reactions will depend on the sulfate aerosol SAD available for reaction. The SAD is highly variable in both time and space, and thus the effect of these reactions will also be variable.

The most important heterogeneous reaction in the stratosphere is the hydrolysis of N_2O_5 on aerosol surfaces to form HNO_3 [101]:

$$N_2O_5 + H_2O \xrightarrow{\text{aerosol}} 2HNO_3 \tag{4.48}$$

The sticking coefficient γ for this reaction is ~0.1, with a very small dependence on temperature (see DeMore *et al.* [5], note 17 of Table 64).

The hydrolysis of ClONO$_2$ and BrONO$_2$ are generally less important. The sticking coefficient of the hydrolysis of ClONO$_2$ is a strong function of temperature, and in general these reactions are important only for enhanced SAD, such as that found immediately after a volcanic eruption, or at temperatures below ~200 K. These conditions are rarely found in the stratosphere, and therefore these heterogeneous reactions can be generally ignored. There are, however, certain circumstances where these reactions can have an impact [88]. The sticking coefficient for the hydrolysis of BrONO$_2$ is quite large (~0.8, independent of temperature [102]), but due to the small abundance of Br in stratosphere this reaction has little impact on NO$_y$ partitioning. Again, the exception is during times of high SAD, such as that found after a volcanic eruption (this will be discussed further in Chapter 6).

Figure 4.17 shows vertical profiles of total NO$_y$ and its major stratospheric components. In the lower and mid-stratosphere, HNO$_3$ makes up most of NO$_y$. In the upper stratosphere, NO$_x$ is the dominant component. The plot also shows that the N$_2$O$_5$ abundance is higher at sunrise than at sunset. This is consistent with N$_2$O$_5$ being formed at night and destroyed during the day.

Figures 4.18–4.21 show zonal mean cross-sections of NO$_y$, NO$_x$, HNO$_3$, and N$_2$O$_5$. Cross-sections of the other important NO$_y$ species, ClONO$_2$ and BrONO$_2$, are shown in Figures 4.9 and 4.35. Much like Cl$_y$, the abundance of NO$_y$ increases with both altitude and latitude over most of the stratosphere, consistent with the mean
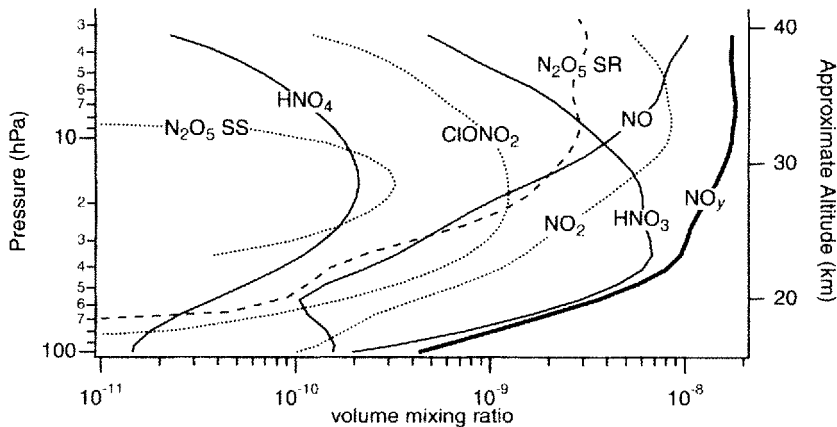
Figure 4.17 Measurements of the major stratospheric components of odd nitrogen versus pressure. Data were measured at sunset, except for N$_2$O$_5$, for which both sunset (SS) and sunrise (SR) data are shown. Data were measured on September 25, 1993 over Fort Sumner, New Mexico (35°N). (After Sen *et al.* [103].)
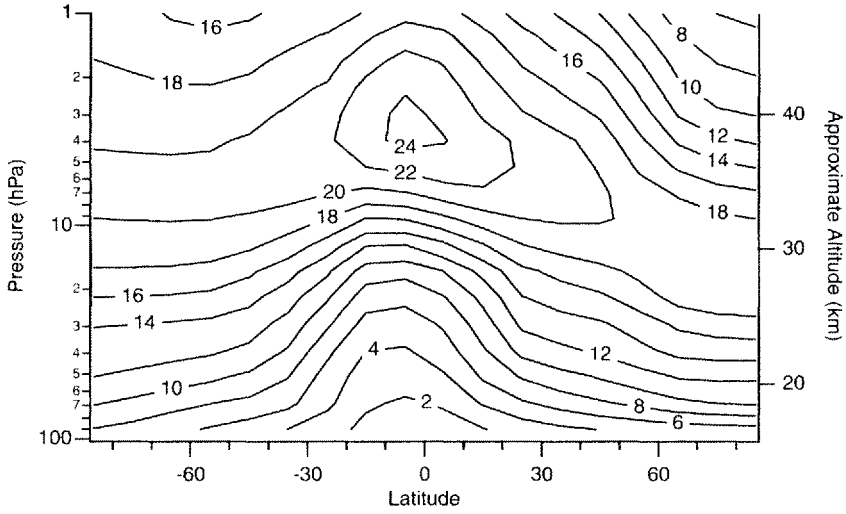
Figure 4.18 Contours of NO$_y$ abundance (ppbv) for December. Values are from the Goddard two-dimensional climatological circulation model [73]. Based on a model run to steady state using N$_2$O emission levels for 1990. The model likely overestimates upper-stratospheric NO$_y$ by a few parts per billion by volume [104].
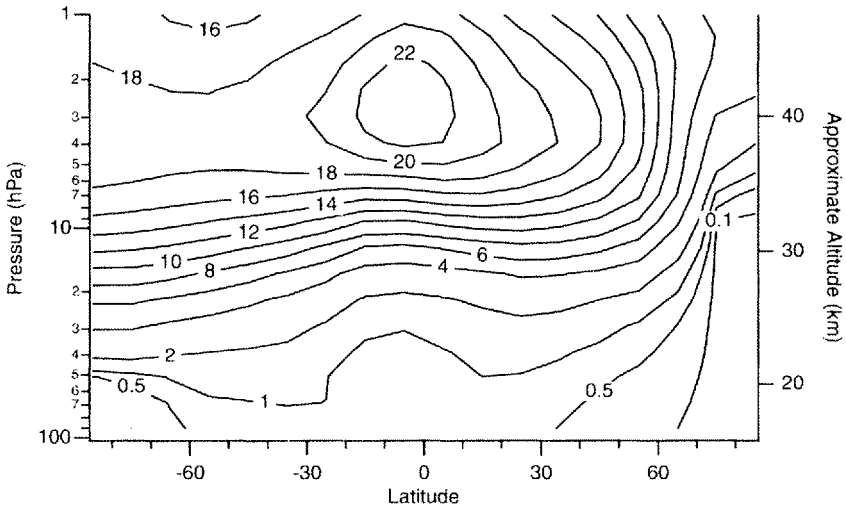

Figure 4.19 Contours of NO$_x$ abundance (ppbv) for December. Values are from the Goddard two-dimensional climatological circulation model [73]. Based on a model run to steady state using N$_2$O emission levels for 1990.
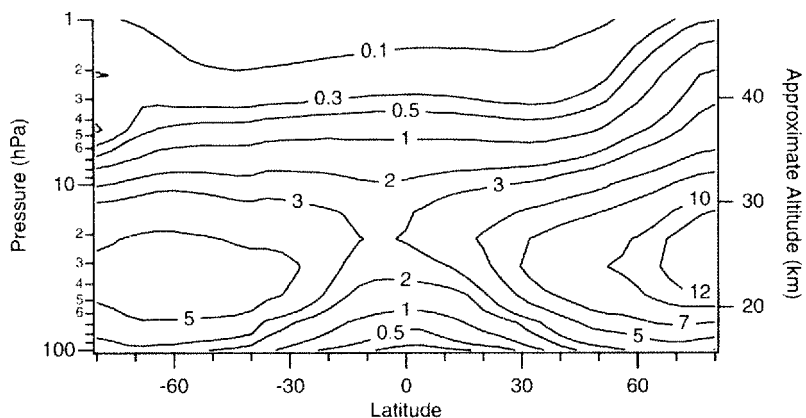
Figure 4.20 Contours of zonally averaged daytime HNO$_3$ abundance (ppbv) for December 1992. Data are from the UARS Reference Atmosphere Project (W. J. Randel, personal communication, 1998).
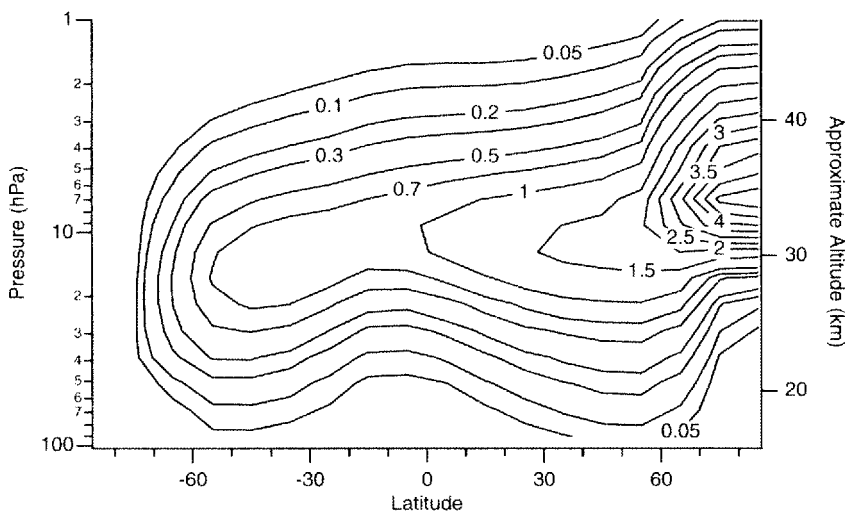
Figure 4.21 Contours of daytime-average N$_2$O$_5$ abundance (ppbv) for December. Values are from the Goddard two-dimensional climatological circulation model [73]. Based on a model run to steady state using N$_2$O emission levels for 1990.

overturning circulation (discussed in Chapter 5) combined with the rapid destruction of N_2O in the mid- and upper stratosphere. Unlike the distribution of Cl_y, however, the abundance of NO_y reaches a maximum in the upper stratosphere and decreases at higher altitudes. This decrease is due to the reaction

$$N + NO \longrightarrow N_2 + O \qquad (4.49)$$

which is a significant loss pathway for NO_y in the upper stratosphere [104]. The Cl_y distribution, in contrast, does not show a similar decrease because there is no comparable loss pathway for Cl_y.

The abundance of NO_x (Figure 4.19) increases with altitude throughout most of the stratosphere due to increases in both the abundance of NO_y and the ratio of $[NO_x]/[NO_y]$ with altitude. The increase of the ratio of $[NO_x]/[NO_y]$ with altitude results from an increase in the formation rate of NO_x from NO_y reservoir species (typically from photolysis reactions) relative to the loss rate of NO_x to form NO_x reservoir species (typically through three-body reactions). In the upper stratosphere, NO_y is composed almost entirely of NO_x, so the decrease in NO_y in the upper stratosphere is mirrored by a similar decrease in NO_x. Note that in the polar night region the abundance of NO_x is low because, in the absence of photolysis, the reaction between NO_2 and NO_3 to form N_2O_5 depletes NO_x.

The abundances of HNO_3 (Figure 4.20) and N_2O_5 (Figure 4.21) both increase with altitude in the lower stratosphere, reach a maximum in the mid-stratosphere, and decrease at higher altitudes. This pattern occurs because of the competition between two factors. First, the ratios $[HNO_3]/[NO_y]$ and $[N_2O_5]/[NO_y]$ both decrease with altitude over most of the stratosphere—for the same reason that the ratio $[NO_x]/[NO_y]$
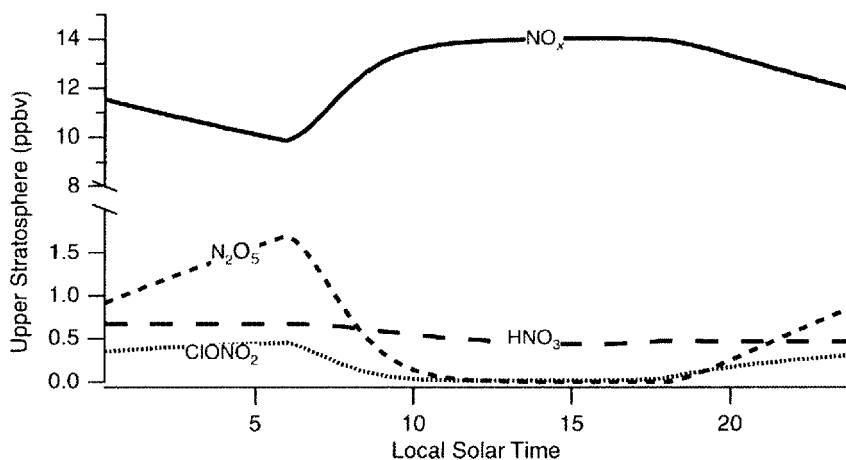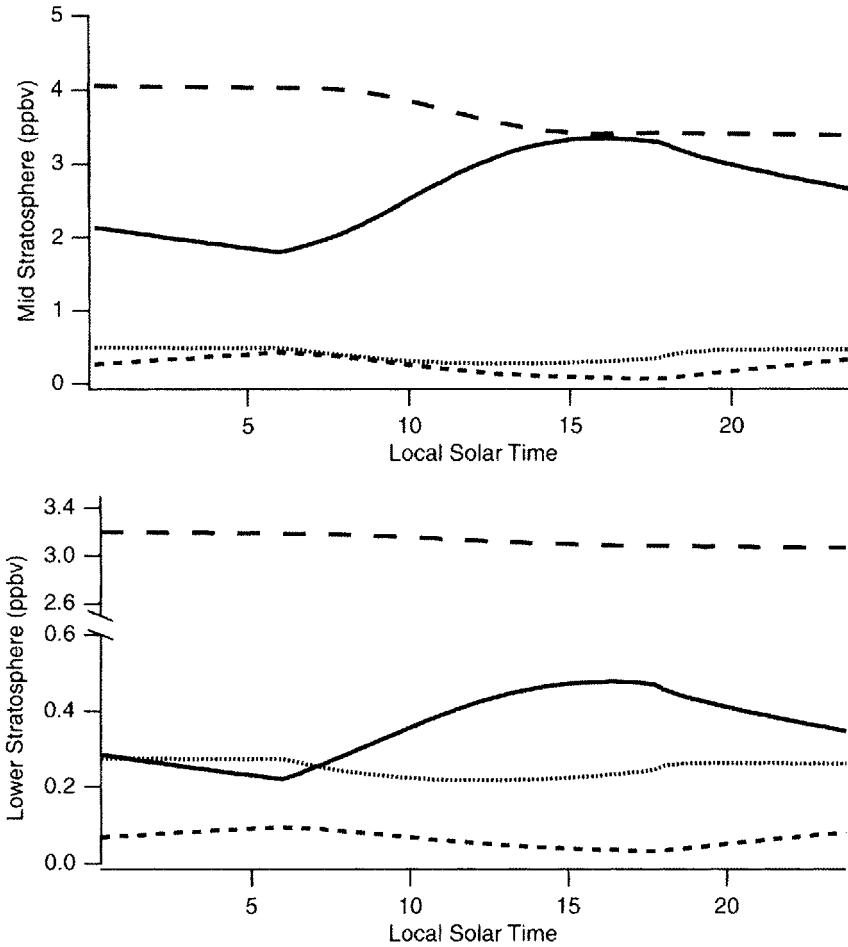
Figure 4.22 Diurnal cycle of the major components of NO$_y$ derived from a model incorporating the reaction set of JPL 94 [91]. The model run is at 45°N on March 21, 1996 and using background aerosol abundances; "upper stratosphere" is from the 3.16 hPa level of the model, "mid stratosphere" is 14.7 hPa, and "lower stratosphere" is 57.0 hPa.

increases with altitude. Second, the abundance of NO$_y$ increases with altitude in the stratosphere. In the lower stratosphere, the abundance of NO$_x$ increases faster than the ratios [HNO$_3$]/[NO$_y$] and [N$_2$O$_5$]/[NO$_y$] decrease. As a result, the abundances of HNO$_3$ and N$_2$O$_5$ increase with altitude in the lower stratosphere. In the mid- and upper stratosphere, the decrease in the ratios [HNO$_3$]/[NO$_y$] and [N$_2$O$_5$]/[NO$_y$] dominates the changes in NO$_y$ with altitude, leading to an overall decrease in the abundances of HNO$_3$ and N$_2$O$_5$.

Both HNO_3 and N_2O_5 also display strong latitudinal gradients, with their abundances increasing as one moves from the summer pole to the winter pole. As discussed previously, N_2O_5 is formed at night and destroyed during the day. In the summer polar region, which experiences 24 h of sunlight every day, the N_2O_5 formation rate is approximately zero, so the steady-state abundance of N_2O_5 is close to zero. In the winter polar region, which experiences 24 h of darkness every day, the photolysis of N_2O_5 ceases, and the abundance of N_2O_5 can build up to several parts per billion by volume. In between these two extremes, the average abundance of N_2O_5 is a function of the length of night.

HNO_3 is formed both during the day (reaction (4.42)) and at night (reaction (4.48)). In the winter hemisphere, photolysis rates are low and the lifetime of HNO_3 is long. Continued production of HNO_3 in this region from N_2O_5 hydrolysis therefore leads to a build-up of HNO_3 in the winter hemisphere.

Typical diurnal cycles of the components of NO_x are shown in Figure 4.22. Because the lifetime of NO_y is comparable to or longer than a day throughout the stratosphere (see Figure 4.13), instantaneous production and loss of NO_x will, in general, not balance. Instead, during the day, there is a net production of NO_x and a net loss of NO_y reservoirs. At night, the reverse occurs: there is a net loss of NO_x and a net production of NO_y reservoir. But the system is in diurnal steady state, so that over 24 h, production and loss of the constituents of NO_y will approximately balance [105]. $BrONO_2$ is not shown because its abundance is so small (a few parts per trillion by volume).

During the day, photolysis and oxidation of $ClONO_2$ produces NO_x. At the same time, NO_x is consumed as the reaction between ClO and NO_2 reforms $ClONO_2$. The net production of NO_x during the day from the net loss of $ClONO_2$ is

$$\int_{daytime} (J_{ClONO_2}[ClONO_2] - k^*_{ClO+NO_2}[ClO][NO_2])dt \qquad (4.50)$$

This net increase in NO_x is accompanied by an equal net production of Cl_x between sunrise and sunset. At sunset, the abundance of Cl_x is nonzero, and the reaction between ClO and NO_2 to reform $ClONO_2$ is a net night-time sink of NO_x. The magnitude of this night-time sink of NO_x is approximately equal to the daytime source of NO_x from $ClONO_2$ destruction. As a result, the net decrease in $ClONO_2$ during the day is balanced by production at night, so over 24 h the net change in $ClONO_2$ abundance is approximately zero. Figure 4.23 plots the contributions of $ClONO_2$ chemistry to NO_x production during the day and NO_x loss during the night. At all altitudes, the source and sink due to $ClONO_2$ are a few percent of the total source and sink of NO_x.

During the day, photolysis and oxidation of HNO_3 (reactions (4.46) and (4.47)) produce NO_x. At the same time, NO_x is consumed in the reaction between OH and NO_2 (reaction (4.42)), which reforms HNO_3. The net production of NO_x from HNO_3 during the day is the difference between these processes:

$$\int_{daytime} (J_{HNO_3}[HNO_3] + k_{HNO_3+OH}[HNO_3][OH] - k^*_{OH+NO_2}[OH][NO_2])dt \qquad (4.51)$$
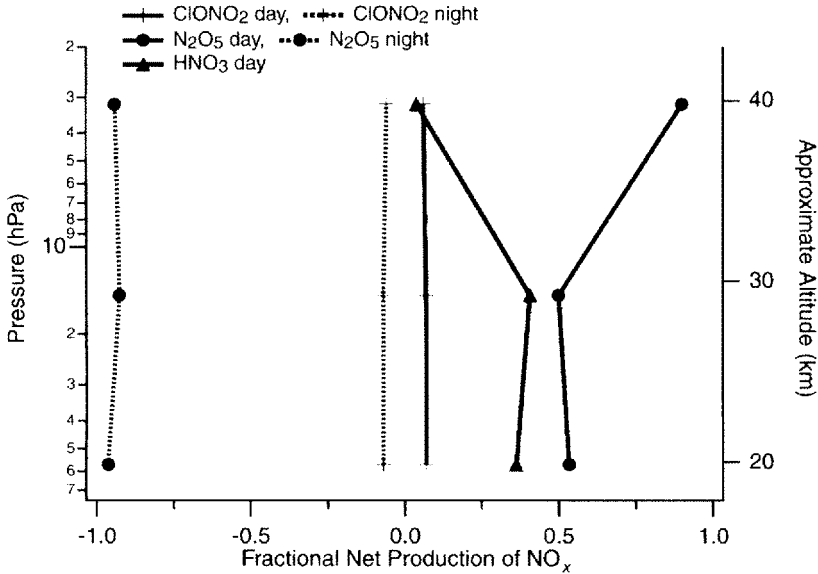
Figure 4.23 Contributions of reactions involving N$_2$O$_5$, ClONO$_2$, and HNO$_3$ to net production of NO$_x$. The net contributions are divided into daytime and night-time contributions. Over 24 h, net production is approximately zero. Calculated for 45°N on March 21, using the background aerosol SAD.

As shown in Figure 4.23, these HNO$_3$ reactions contribute 40–50% to the total NO$_x$ production in the lower and mid-stratosphere and smaller amounts in the upper stratosphere. Production of HNO$_3$ through reaction (4.42) and loss of HNO$_3$ through photolysis and oxidation all cease at sundown, so HNO$_3$ is neither a source nor a sink of NO$_x$ at night.

During the day, photolysis and thermal decomposition of N$_2$O$_5$ (reactions (4.44) and (4.45)) produces NO$_x$. Due to the extremely low values of NO$_3$ during the day, there is essentially no formation of N$_2$O$_5$ from NO$_x$ (reaction (4.41)). Thus, the net production of NO$_x$ from N$_2$O$_5$ during the day is:

$$2 \int_{\text{daytime}} (J_{N_2O_5}[N_2O_5] + k_{N_2O_5+M}[N_2O_5][M])dt \qquad (4.52)$$

where the factor of 2 accounts for the fact that two NO$_x$ molecules are produced for each N$_2$O$_5$ destroyed. As shown in Figure 4.23, N$_2$O$_5$ contributes about 50% to the total NO$_x$ production in the lower and mid-stratosphere and a few percent in the upper stratosphere.

At night, when NO$_3$ photolysis ceases, the concentration of NO$_3$ increases, and the

reaction between NO_2 and NO_3 (reaction (4.41)) converts NO_x to N_2O_5 at night. As shown in Figure 4.23, this reaction is responsible for the vast majority of the loss of NO_x at night.

Note that in the lower and mid-stratosphere, ~90% of the NO_x lost at night goes into N_2O_5, while only half of the NO_x produced during the day comes from N_2O_5, with most of the rest coming from HNO_3. This apparent mass imbalance is accounted for by the hydrolysis of N_2O_5 on the surface of stratospheric aerosols (reaction (4.48)). This reaction converts enough N_2O_5 into HNO_3 to ensure that there is, in general, no net production or loss of NO_x, HNO_3 or N_2O_5 over 24 h [106].

Because of the relatively small amount of bromine in the stratosphere compared to NO_x, bromine reactions generally produce and consume a negligible amount of NO_x. Bromine reactions can, however, have an important impact during periods of both extended sunlight and high aerosol loading, such as that found in high-latitude summer after volcanic eruptions [107].

4.3.3 Loss of NO_y

NO_y is lost in reaction (4.49):

$$N + NO \longrightarrow N_2 + O$$

This reaction is important only in the upper stratosphere and mesosphere owing to the low abundance of N atoms at lower altitudes [104]. As discussed previously, this loss process in the upper stratosphere and mesosphere causes the abundance of NO_y to peak in the upper stratosphere (Figure 4.18).

Considering the stratosphere as a whole, the abundance of NO_y is determined by a balance between stratosphere production from N_2O oxidation, chemical loss of NO_y in the upper stratosphere, and transport of NO_y-rich air out of the stratosphere and into the troposphere, with transport into the stratosphere being generally minor.

4.4 Odd Hydrogen—HO_x

4.4.1 Production

Odd hydrogen, HO_x, is defined to be

$$[HO_x] = [HO_2] + [OH] + [H] \tag{4.53}$$

This family contains only active species, i.e. radicals that are involved in catalytic cycles that destroy O_x, and no reservoir species. This is consistent with the Cl_x and NO_x subfamilies, which also contain O_x-destroying species.

HO$_x$ is derived primarily from the oxidation of H$_2$O. There are three ways that H$_2$O can be oxidized to produce HO$_x$. The most important is the gas phase oxidation of an H$_2$O molecule to form two HO$_x$ molecules:

$$H_2O + O(^1D) \longrightarrow OH + OH \tag{4.54}$$

O(^{1}D) is a product of O$_3$ photolysis, which implies that the flux of ultraviolet radiation is an important factor in determining the production rate of HO$_x$. As we show later, the abundance of stratospheric HO$_x$ is strongly dependent on the solar zenith angle (SZA).

Hydrolysis of N$_2$O$_5$ on sulfate aerosols followed by photolysis of the HNO$_3$ product also leads to the net production of HO$_x$ in the lower stratosphere:

$$
\begin{aligned}
&NO_2 + NO_3 \xrightarrow{M} N_2O_5 \\
&N_2O_5 + H_2O \xrightarrow{aerosol} 2HNO_3 \\
&2 \times (HNO_3 + h\nu \longrightarrow OH + NO_2) \\
&NO_2 + O_3 \longrightarrow NO_3 + O_2 \\
\hline
&net: H_2O + O_3 \longrightarrow OH + OH + O_2
\end{aligned}
\tag{4.55}
$$
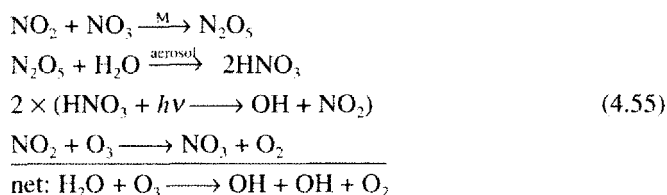
Note that formation of N$_2$O$_5$ occurs only at night, while photolysis of HNO$_3$ requires sunlight. Therefore, this cycle requires alternating periods of day and night.

Hydrolysis of BrONO$_2$ followed by photolysis of HOBr and HNO$_3$ also leads to net production of HO$_x$:

$$
\begin{aligned}
&BrO + NO_2 \xrightarrow{M} BrONO_2 \\
&BrONO_2 + H_2O \xrightarrow{aerosol} HOBr + HNO_3 \\
&HOBr + h\nu \longrightarrow OH + Br \\
&HNO_3 + h\nu \longrightarrow OH + NO_2 \\
&Br + O_3 \longrightarrow BrO + O_2 \\
\hline
&net: H_2O + O_3 \longrightarrow OH + OH + O_2
\end{aligned}
\tag{4.56}
$$
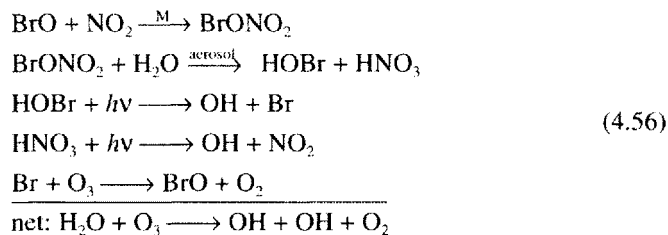
Unlike the N$_2$O$_5$ cycle, the BrONO$_2$ cycle runs during the day because the formation of BrONO$_2$, unlike N$_2$O$_5$, occurs during the daytime. At night, photolysis stops, and so therefore does this cycle. Hydrolysis of ClONO$_2$ can also lead to production of HO$_x$ through a series of reactions analogous to the BrONO$_2$ cycle. This pathway is, however, negligible due to the generally slow rate of ClONO$_2$ hydrolysis, and will not be discussed further.

HO$_x$ can also be formed during the gas phase oxidation of CH$_4$:

$$CH_4 + O(^1D) \longrightarrow CH_3 + OH \tag{4.57}$$

Subsequent oxidation of the CH_3 radical yields another OH molecule, so reaction (4.57) can be considered to produce two HO_x molecules. Oxidation of CH_3 also leads to the production of carbon monoxide (CO) [108–110]. In the lower stratosphere, transport from the troposphere is also an important source of CO. The primary sink of CO in the stratosphere is oxidation by OH [111]:

$$OH + CO \longrightarrow CO_2 + H \qquad (4.58)$$
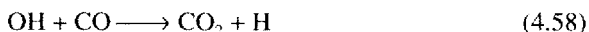
Oxidation of H_2 by $O(^1D)$ will also lead to the production of two HO_x molecules [112–114]. Finally, at high SZAs, such as at sunset or sunrise, photolysis of HO_2NO_2 is a potentially important source of HO_x [115].

In the mid- and upper stratosphere, the gas phase oxidation of H_2O (reaction (4.54)) is the dominant source of HO_x. Oxidation of CH_4 and H_2 combine to contribute ~10–15% to HO_x production, with the exact amount varying with latitude and altitude. Due to the low aerosol SAD in this region, HO_x production through the N_2O_5 and $BrONO_2$ cycles is negligible in this region.

In the lower stratosphere, the fraction of HO_x production attributable to each of these HO_x production mechanisms is a function of, among other things, altitude, SZA, length of day, and the aerosol SAD. As in the upper stratosphere, gas phase oxidation of water vapor (reaction (4.54)) is the dominant source of HO_x. The N_2O_5 cycle (cycle (4.55)) is responsible for around 10% of HO_x production in the lower stratosphere for background amounts of aerosol SAD. The production of HO_x from this cycle initially increases as the aerosol SAD increases. Above an aerosol SAD of ~5 $\mu m\ cm^{-3}$ (about five times the background SAD), however, the hydrolysis of N_2O_5 "saturates" [116], meaning that increases in the aerosol SAD beyond this point have little effect on the rate of N_2O_5 hydrolysis and therefore little effect on the rate of HO_x production.

The $BrONO_2$ cycle (cycle (4.56)) is responsible for a percent or less of HO_x production in the lower stratosphere for background amounts of the aerosol SAD. Unlike the N_2O_5 cycle (reaction (4.55)), however, this cycle does not "saturate" [102]; instead, the rate of HO_x production from this cycle increases linearly with increasing SAD, even at extremely high aerosol SADs. As a consequence, this cycle can become important for large surface area abundances, such as those found after large volcanic eruptions. And as discussed previously, the $BrONO_2$ cycle runs when exposed to sunlight, and is therefore more important for regions of the atmosphere that are exposed to long periods of daylight, such as the high-latitude summer stratosphere [107]. N_2O_5 and $BrONO_2$ hydrolysis reactions are discussed in detail in Chapter 6.

Oxidation of CH_4 and H_2 combine to contribute about 20% to HO_x production in the lower stratosphere, with the exact amount dependent on latitude and altitude.

Finally, HO_x is also produced throughout the stratosphere from the destruction of relatively short-lived species such as HOCl, HOBr, and H_2O_2. Usually, destruction

of these species is not counted as *net* HO$_x$ production because their formation consumes HO$_x$. In other words, it is only those reactions or cycles that break an O–H bond in water, a C–H bond in methane, or a H–H bond in H$_2$ that are considered net HO$_x$ production. It should be noted that this definition of HO$_x$ production, while widely made in the field, is somewhat arbitrary. Depending on the situation, other definitions of HO$_x$ production might be appropriate.

4.4.2 Partitioning

In Equation (4.53), we defined HO$_x$ to be the sum of HO$_2$, OH, and H. In the stratosphere, however, H atoms are a negligible component of HO$_x$ owing to the rapid conversion of H atoms to HO$_2$ in the three-body reaction

$$H + O_2 \xrightarrow{\text{M}} HO_2 \tag{4.59}$$

The lifetime of a H atom with respect to this reaction is about 10^{-5} s in the lower stratosphere, rising to about 0.1 s in the upper stratosphere. This short lifetime for H atoms translates into small abundances: the ratio [H]/[HO$_x$] ranges from 10^{-8} in the lower stratosphere to 0.01 in the upper stratosphere.

As a result of this, one can ignore H in the stratosphere, and HO$_x$ can be approximated by the sum of HO$_2$ and OH. Further, one can assume that the production of a H atom in a reaction is equivalent to the production of an HO$_2$ molecule.

Figure 4.24 shows the conversion pathways between OH and HO$_2$. OH is converted to HO$_2$ primarily through the reactions

$$OH + O_3 \longrightarrow HO_2 + O_2 \tag{4.60}$$

$$OH + O \longrightarrow H + O_2 \xrightarrow{\text{M}} HO_2 \tag{4.61}$$

$$OH + CO \longrightarrow H + CO_2$$
$$H + O_2 \xrightarrow{\text{M}} HO_2 \tag{4.62}$$
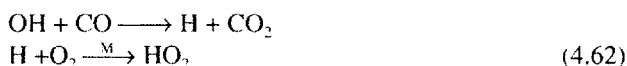
Reaction (4.60) dominates the conversion from OH to HO$_2$ in the lower and mid-stratosphere. In the upper stratosphere, where O atoms are abundant, reaction (4.61) dominates. Reaction (4.62) is generally minor, except near the tropopause, where it can make a significant contribution.

HO$_2$ is converted to OH primarily through the reactions

$$HO_2 + O_3 \longrightarrow OH + O_2 + O_2 \tag{4.63}$$

$$HO_2 + NO \longrightarrow OH + NO_2 \tag{4.64}$$

$$HO_2 + O \longrightarrow OH + O_2 \tag{4.65}$$
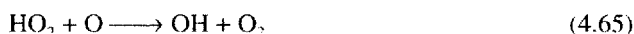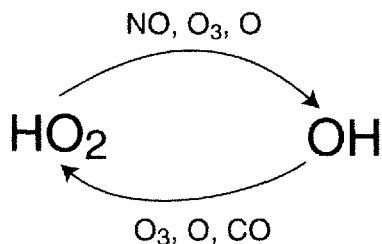
Figure 4.24 Schematic of the partitioning between OH and HO_2 (the sum of which is HO_x). Each arrow is marked with the reactants that facilitate the conversion indicated by the arrow.

In the lower stratosphere, reactions (4.63) and (4.64) contribute approximately equally to the conversion of HO_2 to OH, with virtually no contribution from reaction (4.65). In the mid-stratosphere, reaction (4.64) dominates, with smaller contributions from the other reactions. In the upper stratosphere, reaction (4.65) dominates. The lifetimes of HO_2 and OH with respect to these reactions are shown in Figure 4.25.
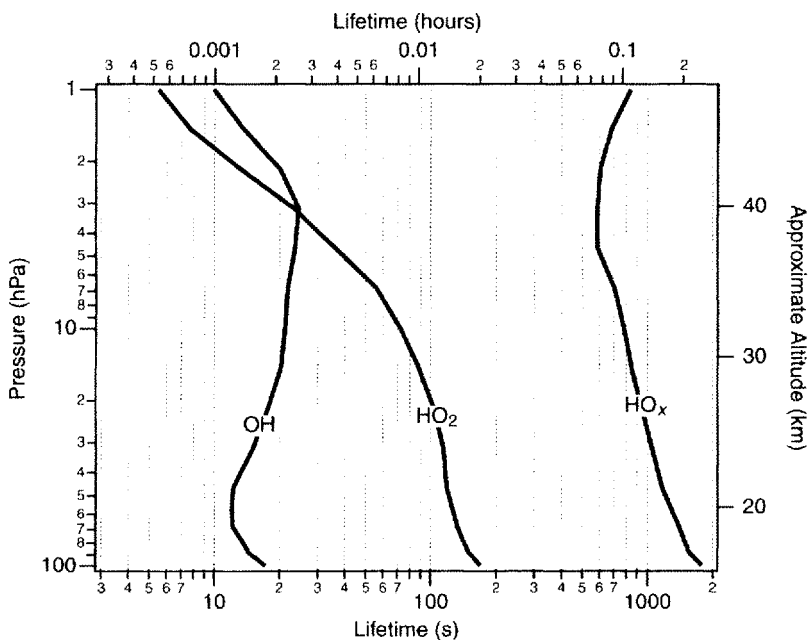
Figure 4.25 Lifetime of the components of HO_x. Calculated for 45°N equinoctial conditions based on daytime-average constituent abundances and photolysis rates: $\tau_{OH} \sim 1/(k_{OH+O_3}[O_3] + k_{OH+O}[O] + k_{OH+CO}[CO])$, $\tau_{HO_2} \sim 1/(k_{HO_2+O_3}[O_3] + k_{HO_2+NO}[NO] + k_{HO_2+O}[O])$, $\tau_{HO_x} \sim [HO_x]/(2k_{OH+HO_2}[OH][HO_2] + 2k_{HNO_3+OH}[HNO_3][OH])$.

Assuming photochemical steady state, the ratio [OH]/[HO$_2$] can be approximated by the expression

$$\frac{[OH]}{[HO_2]} = \frac{k_{HO_2+O_3}[O_3] + k_{HO_2+NO}[NO] + k_{HO_2+O}[O]}{k_{OH+O_3}[O_3] + k_{OH+O}[O] + k_{OH+CO}[CO]} \qquad (4.66)$$

This simple equation for HO$_x$ partitioning agrees well with measurements in the lower stratosphere [74,117]. Figure 4.26 shows a model estimate of the [OH]/[HO$_2$] ratio.

OH and HO$_2$ also react to form the short-lived species HOCl, HOBr, and H$_2$O$_2$. HOCl and HOBr are formed in the gas phase reactions

$$ClO + HO_2 \longrightarrow HOCl + O_2 \qquad (reaction\ (4.14))$$

$$BrO + HO_2 \longrightarrow HOBr + O_2 \qquad (4.67)$$
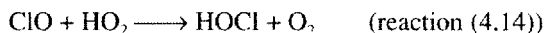
and are destroyed by photolysis and oxidation to form OH (reactions (4.17), (4.85), and (4.86)). Due to their reasonably short lifetimes (see Figures 4.3 and 4.29), HOCl and HOBr are in the photochemical steady state during the day (e.g. see Equation (4.25) and the accompanying discussion). As a result, over most of the day the loss of HO$_x$ from formation of HOCl and HOBr is balanced by production of HO$_x$ from destruction of HOCl and HOBr. These species do not, therefore, usually represent net sources or sinks of HO$_x$.
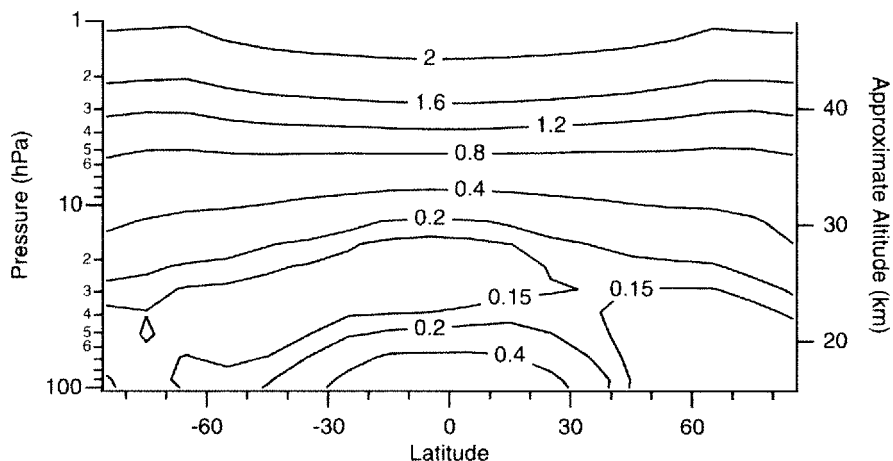
Figure 4.26 Annually averaged daytime-average [OH]/[HO$_2$] ratio. Values are from the Goddard two-dimensional climatological circulation model [73].

The formation of HOCl and HOBr consumes HO_2, while destruction of HOCl and HOBr produces OH. Thus, while there is no net change in HO_x when these species are in photochemical steady state, there *is* a net change in the partitioning of HO_x. In other words, measurements of OH and HO_2 reveal slightly more OH relative to HO_2 than is predicted by the simple partitioning model in Equation (4.66). A more exact calculation of the $[OH]/[HO_2]$ ratio must include terms to account for this [117].

H_2O_2 is formed primarily in the reaction

$$HO_2 + HO_2 \xrightarrow{M} H_2O_2 + O_2 \qquad (4.68)$$

Photolysis (to produce two OH radicals) is the dominant loss mechanism throughout the stratosphere. H_2O_2 is also destroyed by reaction with OH:

$$H_2O_2 + OH \longrightarrow H_2O + HO_2 \qquad (4.69)$$
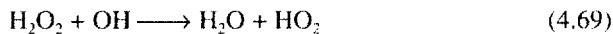
The lifetime of H_2O_2 is about a few days in the lower stratosphere, decreasing to a few hours in the upper stratosphere. As with HOCl and HOBr, production of H_2O_2 consumes HO_2 while destruction of H_2O_2 produces OH. However, HO_x cycles slowly enough through H_2O_2 that its production/destruction has little effect on the partitioning of HO_x.

Model estimates of the OH and HO_2 abundance are plotted in Figure 4.27. Global measurements of HO_x species in the middle and upper stratosphere have not yet been made, but profiles can be found in the literature [92,118–123]. In the lower stratosphere, there is a large database of HO_x measurements. Measurements of lower-stratospheric OH obtained at a range of altitudes, latitudes, and NO_x, O_3, and H_2O abundances are shown in Figure 4.28 plotted against the SZA. Surprisingly, the measurements show a strong correlation with the SZA, implying that variations of the other geophysical parameters have little affect on the OH abundance [74]. In general, current photochemical models of HO_x reproduce the stratospheric HO_x measurements reasonably well [74,123–125].

4.4.3 Loss of HO_x

To be consistent with our definition of HO_x production, we define HO_x loss to be those HO_x reactions that reform an H_2O molecule. The primary loss reaction for HO_x is the reaction between OH and HO_2, which destroys two HO_x molecules:

$$OH + HO_2 \longrightarrow H_2O + O_2 \qquad (4.70)$$
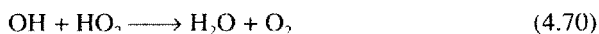
The rate that this cycle destroys HO_x is $2k_{OH+HO_2}[OH][HO_2]$. In the mid- and upper stratosphere, virtually all of the HO_x loss is from this reaction.
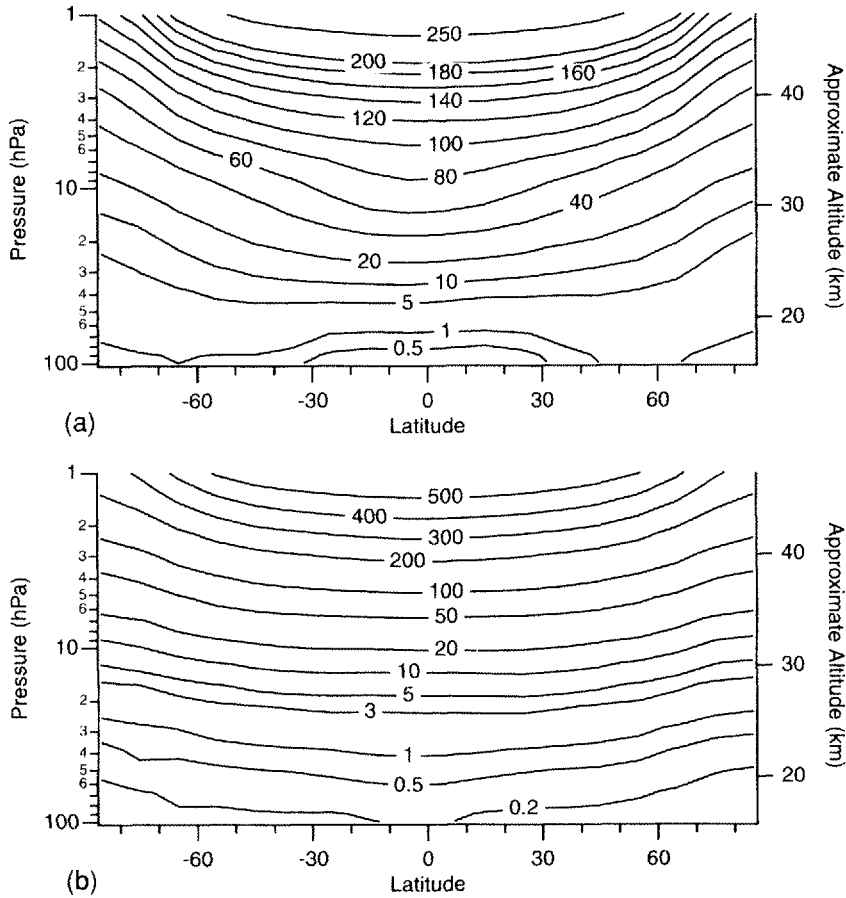
Figure 4.27 (a) Annually averaged daytime-average HO$_2$ abundance (pptv). (b) OH abundance (pptv). Values are from the Goddard two-dimensional climatological circulation model [73].

In the lower stratosphere, HO$_x$ is also destroyed catalytically by NO$_x$:

$$OH + NO_2 \xrightarrow{\text{M}} HNO_3 \qquad \text{(reaction (4.42))}$$

$$\underline{HNO_3 + OH \longrightarrow NO_3 + H_2O \qquad \text{(reaction (4.46))}}$$

$$OH + OH + NO_2 \longrightarrow NO_3 + H_2O \qquad\qquad (4.71)$$
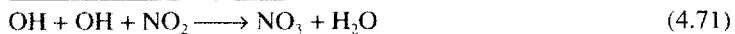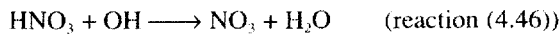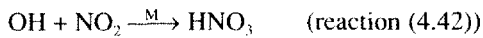
As with all catalytic cycles, the catalyst (in this case NO$_x$) is not consumed in the reaction. The rate-limiting step of this catalytic cycle is reaction (4.46), the reaction between HNO$_3$ and OH. Each trip through this cycle destroys two HO$_x$ molecules,
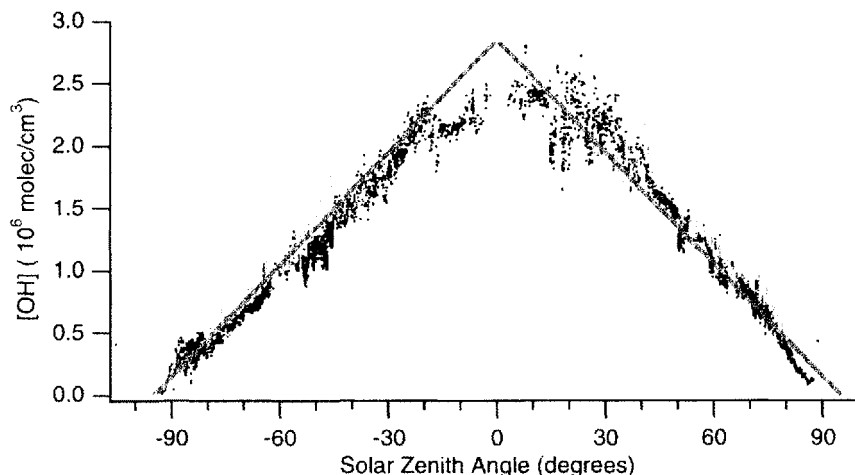
Figure 4.28 Lower stratospheric OH number density measured by the Harvard HO_x instrument [126] during the 1994 ASHOE-MAESA (black) and 1997 POLARIS (gray) missions (T. F. Hanisco, personal communication, 1998). The solid line is $3 \times 10^4 (95 - |SZA|)$. Negative SZAs correspond to times before local noon.

so the rate that this cycle destroys HO_x is $2k_{HNO_3+OH}[HNO_3][OH]$. The reaction between OH and HNO_4 can also be an important HO_x loss pathway. Finally, the reaction of OH with HCl (reaction (4.16)) is a non-negligible HO_x loss pathway. In the lower stratosphere the importance of these various HO_x loss terms are variable. No single term dominates at all times, and all have their moment in the Sun (so to speak).

Finally, it should be noted that at sunset the formation of HO_x ceases. Net loss of HO_x as well as the formation of short-lived HO_x reservoirs such as HOCl, HOBr, and H_2O_2 continue, however. The result is that HO_x is rapidly removed after sunset, and the abundance of HO_x can be considered zero during the night.

4.5 Odd Bromine—Br_y

4.5.1 Source

Odd bromine, Br_y, shares many similarities with the odd-chlorine family. Like chlorine, bromine atoms enter the stratosphere as components of long-lived organic molecules. The three main bromine-containing source gases for the stratosphere are CH_3Br (methyl bromide), $CBrClF_2$ (halon 1211), and $CBrF_3$ (halon 1301). The tropospheric abundances of these species in the mid-1990s was 10–15 pptv for

CH$_3$Br (see WMO [13], Table 6.3) [127], 3.5 pptv for CBrClF$_2$ [128], and 2.3 pptv for CBrF$_3$ [128]. Including small contributions from other species, total organic bromine entering the stratosphere at that time was ~15–20 pptv [129,130]. All of the halons and about half of the CH$_3$Br are anthropogenic in origin. Thus, about two-thirds of bromine in the stratosphere originated from human activities.

4.5.2 Partitioning

Once in the stratosphere, these organic bromine molecules are destroyed by oxidation and photolysis. As bromine atoms are released from the molecules, reactions convert them into one of several inorganic molecules, the sum of which we define to be Br$_y$:

$$[Br_y] = [BrO] + [Br] + [BrONO_2] + [HBr] + [HOBr] + [BrCl] \qquad (4.72)$$

Several minor species, such as BrONO and Br$_2$, have been neglected in Equation (4.72). The abundance of inorganic bromine Br$_y$, as a function of other long-lived species, is provided by Wamsley *et al.* [130].

Figure 4.29 plots daytime-averaged lifetimes of the various members of Br$_y$ as a function of altitude. Owing to the larger size of bromine atoms compared to chlorine atoms, molecules containing bromine tend to have weaker intramolecular bonds, and are therefore shorter lived than the chlorine-bearing version of the same molecule. For example, the lifetime of HBr in the lower stratosphere is about a day, while the lifetime of HCl in the same region is about a month. In fact, the lifetimes of the Br$_y$ species are so short (a day or less) that the partitioning of Br$_y$ is almost entirely determined by photochemistry, with little contribution from transport.

In analogy to the Cl$_x$, we define Br$_x$ to contain the short-lived components of Br$_y$:

$$[Br_x] = [BrO] + [Br] \qquad (4.73)$$

Like Cl$_x$, Br$_x$ therefore contains the species involved in the catalytic loss cycles that destroy O$_x$ (e.g. the "active" members).

Figure 4.30 shows the interconversion pathways of the components of Br$_x$. BrO is converted to Br in the reactions

$$BrO + h\nu \longrightarrow Br + O \qquad (4.74)$$

$$BrO + NO \longrightarrow Br + NO_2 \qquad (4.75)$$

In the upper stratosphere, the reaction with O atoms becomes important:

$$BrO + O \longrightarrow Br + O_2 \qquad (4.76)$$
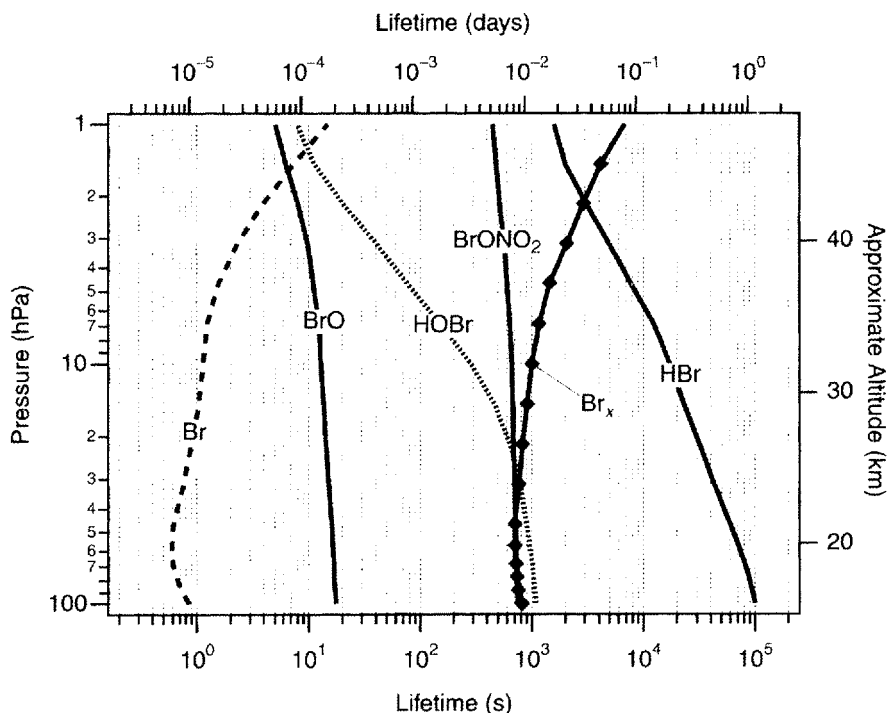
Figure 4.29 Lifetime of the components of Br_y. Calculated for 45°N equinoctial conditions based on daytime-average constituent abundances and photolysis rates: $\tau_{BrO} \sim 1/(J_{BrO} + k_{BrO+O}[O] + k_{BrO+NO}[NO])$, $\tau_{Br} \sim 1/(k_{Br+O_3}[O_3])$, $\tau_{BrONO_2} \sim 1/J_{BrONO_2}$, $\tau_{HBr} \sim 1/(k_{HBr+OH}[OH] + k_{HBr+O}[O])$, $\tau_{HOBr} \sim 1/(J_{HOBr} + k_{HOBr+O}[O])$, $\tau_{Br_y} \sim [Br_x]/(k*_{BrO+NO_2}[BrO][NO_2] + k_{BrO+HO_2}[BrO][HO_2] + k_{Br+HO_2}[Br][HO_2])$.
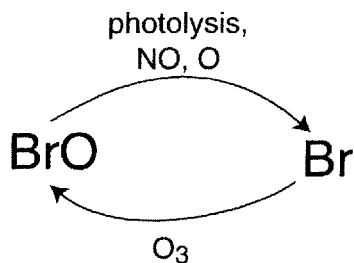
Figure 4.30 Schematic of the partitioning between BrO and Br (the sum of which is Br_x). Each arrow is marked with the reactants that facilitate the conversion indicated by the arrow.

To complete the cycle, Br is converted back to BrO in the reaction

$$Br + O_3 \longrightarrow BrO + O_2 \tag{4.77}$$

Using reactions (4.74)–(4.77) and assuming photochemical steady state, the ratio [Br]/[BrO] can be written as

$$\frac{[Br]}{[BrO]} = \frac{k_{BrO+NO}[NO] + J_{BrO} + k_{BrO+O}[O]}{k_{Br+O_3}[O_3]} \tag{4.78}$$

Figure 4.31 plots the related quantity [BrO]/[Br$_x$], the fraction of Br$_y$ that is in the form of BrO ([BrO]/[Br$_x$] = 1/(1 + [Br]/[BrO])). BrO makes up the vast majority of Br$_x$ in the lower stratosphere, and about 50% in the upper stratosphere. This can be contrasted to the Cl$_x$ family, in which ClO makes up the vast majority of Cl$_x$ throughout the stratosphere.
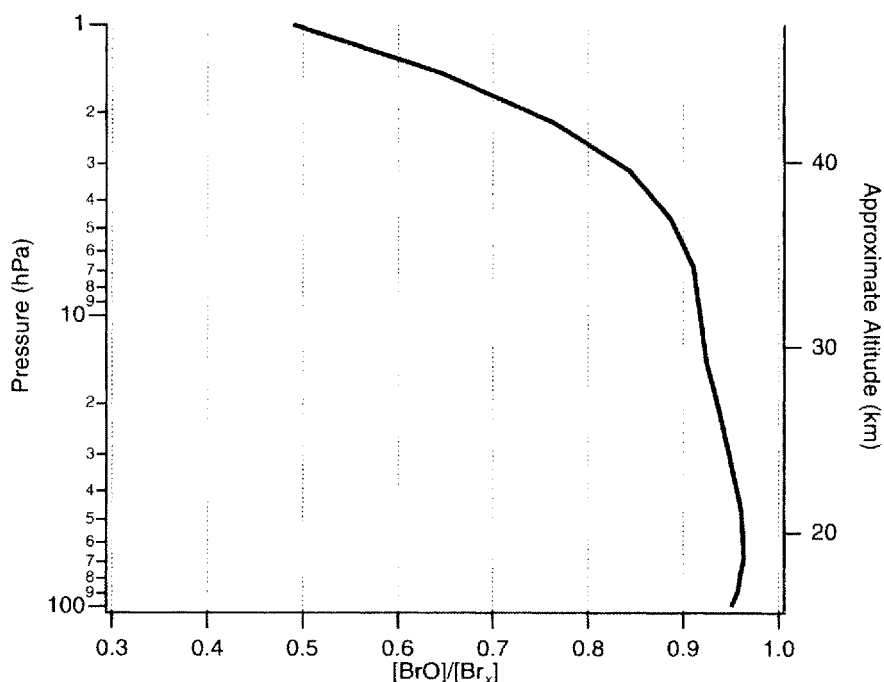
Figure 4.31 Fraction of Br$_y$ in the form of BrO. Calculated for 45°N equinoctal conditions based on daytime-average constituent abundances and photolysis rates.

Figure 4.32 shows a schematic of the partitioning between Br_x and the Br_y reservoir species.

Formation of reservoirs from Br_x   Bromine nitrate, $BrONO_2$, is formed from Br_x in the three-body reaction (4.43):

$$BrO + NO_2 \xrightarrow{\text{M}} BrONO_2$$
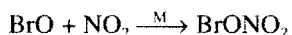
HOBr is formed from Br_x in reaction (4.67):

$$BrO + HO_2 \longrightarrow HOBr + O_2$$

HBr is formed from Br_x primarily in the reactions

$$Br + HO_2 \longrightarrow HBr + O_2 \tag{4.79}$$

$$Br + CH_2O \longrightarrow HBr + HCO \tag{4.80}$$

In the lower stratosphere, both reaction (4.79) and (4.80) can be important. In the upper stratosphere, reaction (4.79) dominates. There is also some speculation of an HBr product channel for the reaction between BrO and HO_2 [131,132]:

$$BrO + HO_2 \longrightarrow HBr + O_3 \tag{4.81}$$

The primary source of BrCl is reaction (3.22a) between BrO and ClO:

$$ClO + BrO \longrightarrow BrCl + O_2$$
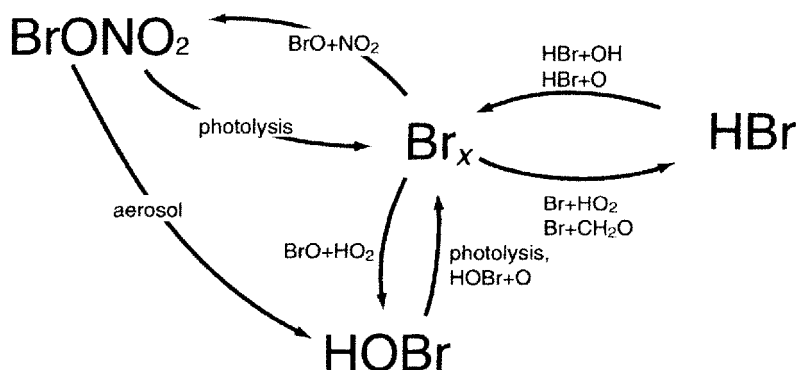
Figure 4.32 Schematic of the Br_y family. Arrows show conversion pathways between species.

Note that BrCl production is just one product channel of the reaction between ClO and BrO; the other products are ClOO + Br and OClO + Br (reactions (3.22b) and (3.22c)).

Formation of Br$_x$ from reservoirs BrONO$_2$ is converted back to Br$_x$ through the photolysis reaction

$$BrONO_2 + h\nu \longrightarrow Br + NO_3$$
$$\longrightarrow BrO + NO_2 \qquad (4.82)$$
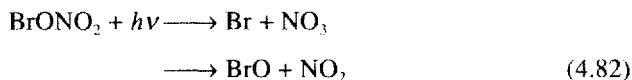
About 29% of the BrONO$_2$ molecules photolyze to produce Br and NO$_3$, with the remaining 71% producing BrO and NO$_2$ (see DeMore *et al.* [5], p. 199). Loss of BrONO$_2$ via oxidation is not important.

HBr is converted back to Br$_x$ in the reaction

$$HBr + OH \longrightarrow Br + H_2O \qquad (4.83)$$

In the upper stratosphere, the reaction between HBr and O atoms becomes important:

$$HBr + O \longrightarrow Br + OH \qquad (4.84)$$

The primary pathway for conversion of HOBr back to Br$_x$ is photolysis below ~25 km,

$$HOBr + h\nu \longrightarrow OH + Br \qquad (4.85)$$

and oxidation by O atoms at higher altitudes,

$$HOBr + O \longrightarrow OH + BrO \qquad (4.86)$$

BrCl is rapidly photolyzed and destroyed by oxidation ($\tau_{BrCl} < 1$ min) [131] to reform Br$_x$. In general, under normal sunlit conditions the abundance of BrCl is negligible. At night in the upper stratosphere, BrCl can become an important Br$_y$ reservoir.

Interconversion among Br$_y$ reservoirs The heterogeneous hydrolysis of BrONO$_2$ on aerosol surfaces,

$$BrONO_2 + H_2O \xrightarrow{aerosol} HOBr + HNO_3 \qquad (4.87)$$
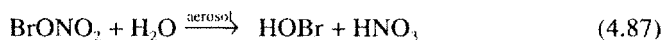
is an important reaction for bromine partitioning in the lower stratosphere [133]. The sticking coefficient γ for this reaction is ~0.8, independent of temperature [102].

There is an analogous hydrolysis reaction involving $ClONO_2$ on sulfate aerosol surfaces. The sticking coefficient γ for this $ClONO_2$ reaction, however, shows a strong temperature dependence, and the reaction turns out to be important only at extremely low temperatures (< 200 K) or at high SADs such as those found after volcanic eruptions. These hydrolysis reactions will be discussed more thoroughly in Chapters 6 and 7.

There are relatively few measurements of bromine species in the stratosphere. Those measurements that exist, however, generally show reasonable agreement with models [132,134]. Figures 4.33–4.36 show cross-sections of Br_y and its important components, Br_x, $BrONO_2$, and HOBr.

Br_y (Figure 4.33) increases rapidly with altitude in the lower and mid-stratosphere, with no increase above ~30 km. This occurs because organic bromine molecules are reasonably weak, and so are destroyed in the lower and mid-stratosphere—by the time an air parcel reaches the mid-stratosphere all of the organic bromine molecules have been destroyed. This can be compared to Cl_y (see Figure 4.7), which increases with altitude throughout the stratosphere owing to the stronger bonds and therefore slower destruction rates of organic chlorine molecules.

Figure 4.34 shows a model simulation of Br_x mixing ratio. As one can see, the abundance of Br_x increases rapidly with altitude due to an increase in both Br_y and in the ratio $[Br_x]/[Br_y]$ with altitude. Figure 4.35 shows a cross-section of the abundance of $BrONO_2$. The distribution of $BrONO_2$ is similar to that of $ClONO_2$: in the lower stratosphere the rapid increase in Br_y with altitude causes the abundance of
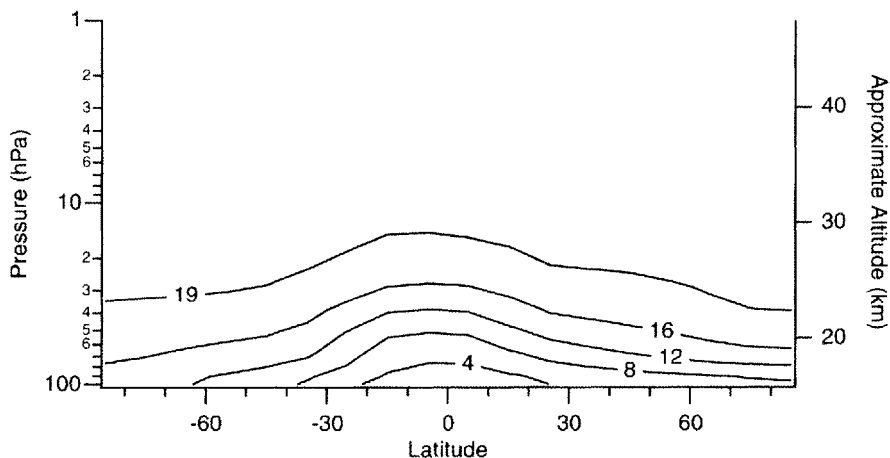

Figure 4.33 Contours of Br_y abundance (pptv) for December. Values are from the Goddard two-dimensional climatological circulation model [73]. Based on a model run to steady state using CFC and halon emission levels for 1990.
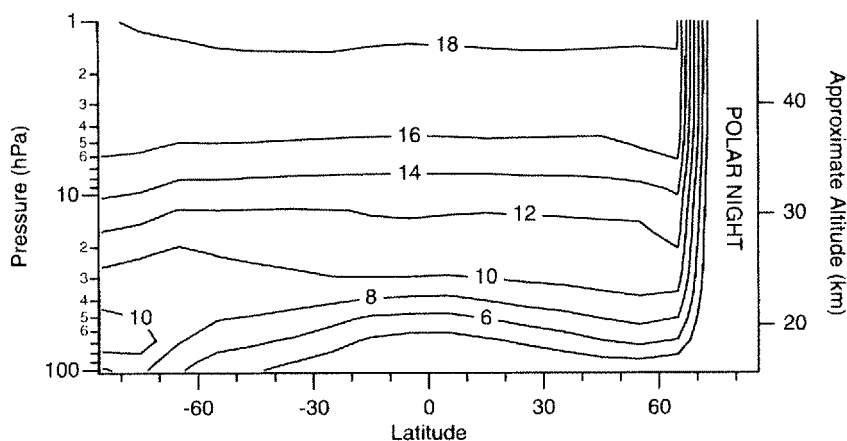
Figure 4.34 Contours of Br$_x$ abundance (pptv) for December. Data from the Goddard two-dimensional climatological circulation model [73]. Based on a model run to steady state using CFC and halon emission levels for 1990.
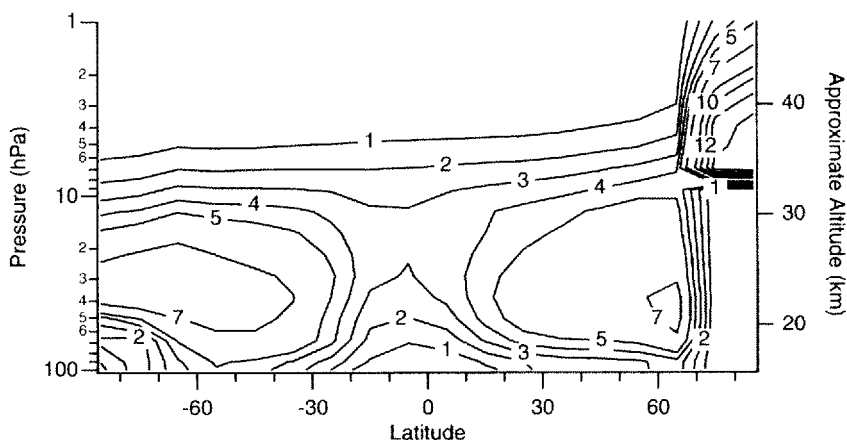
Figure 4.35 Contours of BrONO$_2$ abundance (pptv) for December. Values are from the Goddard two-dimensional climatological circulation model [73]. Based on a model run to steady state using CFC and halon emission levels for 1990.

BrONO$_2$ to increase with altitude. In the upper half of the stratosphere the loss of BrONO$_2$ increases much faster than production, and Br$_y$ is no longer increasing with altitude, so the abundance of BrONO$_2$ decreases with altitude. Figure 4.36 shows a cross-section of the abundance of HOBr. As with BrONO$_2$, the rapid increase in Br$_y$ with altitude causes the abundance of HOBr to increase with altitude. In the mid- and
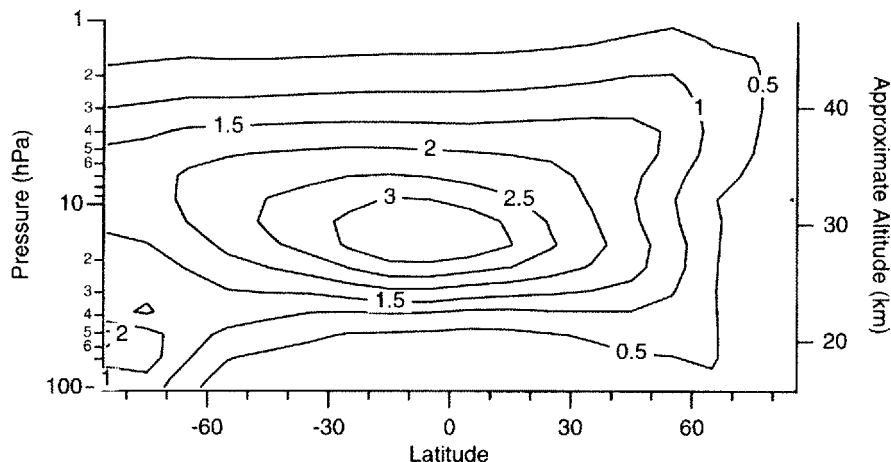
Figure 4.36 Contours of HOBr abundance (pptv) for December. Values are from the Goddard two-dimensional climatological circulation model [73]. Based on a model run to the steady state using CFC and halon emission levels for 1990.

upper stratosphere, the abundance of HOBr decreases as partitioning of the Br_y family shifts toward Br_x.

In the lower-stratospheric polar night region (high northern latitudes in Figs 4.34–4.36), the partitioning of Br_y is in a unique state. Because photolysis rates are approximately zero, the reaction between BrO and NO_2 rapidly depletes Br_x by converting it to $BrONO_2$ (reaction (4.43)). The $BrONO_2$ is subsequently converted to HOBr in a time-scale of a few hours through hydrolysis on aerosol surfaces (reaction (4.87)). When exposed to temperatures below about 210 K (common in the lower-stratospheric wintertime polar regions), the reaction

$$HCl + HOBr \xrightarrow{\text{aerosol}} BrCl + H_2O \qquad (4.88)$$

converts all of the HOBr into BrCl in a few days or less. The net result is that the vast majority of Br_y in the lower stratosphere polar night region is in the form of BrCl.

Figure 4.37 shows typical diurnal cycles for the members of Br_y at mid-latitudes. Br_x declines after sunset, and is zero for most of the night throughout the stratosphere. At sunrise, destruction of $BrONO_2$ through photolysis leads to a rapid decline in $BrONO_2$ and a concomitant increase in Br_x. Much like HOCl, HOBr shows little diurnal variation despite its relatively short photochemical lifetime. BrCl is important in the upper stratosphere, where significant abundances of ClO and BrO survive well after sunset, leading to a buildup of BrCl.
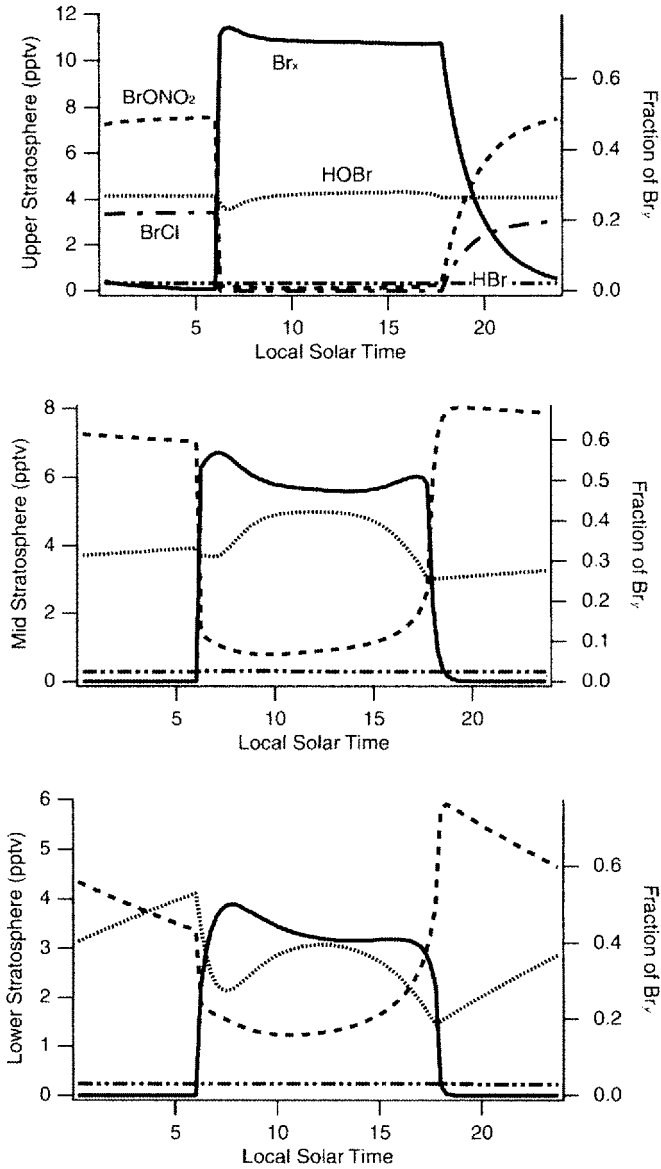
Figure 4.37 Diurnal cycle of the primary components of Br$_y$ derived from a model incorporating the reaction set of JPL 94 [91]. The model run is at 45°N on March 21, 1996 and using background aerosol abundances; "upper stratosphere" is from the 3.16 hPa level of the model, "mid stratosphere" is 14.7 hPa, and "lower stratosphere" is 57.0 hPa. The BrCl trace is only shown on the upper-stratosphere panel.

In the lower stratosphere, the hydrolysis of $BrONO_2$ (reaction (4.87)) causes the abundance of $BrONO_2$ to decrease and HOBr to increase throughout the night (bottom panel of Figure 4.37). As a result, HOBr is an important Br_y night-time reservoir, especially at high aerosol loading, such as after a volcanic eruption. At sunrise, the rapid photolysis of HOBr leads to a burst of HO_x [74,115].

A comparison between the diurnal cycles in Figure 4.37 and the Cl_y cycles plotted in Figure 4.12 shows important differences between these two families. Most importantly, the fraction of the Br_y family in the form of the O_x-destroying BrO radical (which is the rate-limiting reactant of the bromine catalytic cycles) is ~40–50% throughout the stratosphere. In contrast, only a few percent of Cl_y is in the form of ClO in the lower stratosphere, rising to ~10–20% in the upper stratosphere. In addition, the rate constant for the reaction between BrO and HO_2, which rate limits the most important O_x-destroying bromine catalytic cycle, is five to six times greater under stratospheric conditions than the rate constant for the reaction between ClO and HO_2, the rate-limiting step of the comparable chlorine catalytic cycle. As a result, on a per mole basis, bromine atoms released into the stratosphere are 40–50 times more effective at destroying O_x than chlorine atoms [13,135,136]. This suggests that despite the small abundance of Br_y (~15–20 pptv), it can still be an important catalyst for O_x loss.

4.5.3 Loss of Br_y

There are no loss processes for the Br_y family. Instead, the concentration of Br_y in an air parcel increases until all of the bromine-bearing organic molecules have been destroyed.

## 4.6 Other Halogen Families

4.6.1 Fluorine

As their name implies, CFCs generally contain fluorine atoms in addition to the chlorine atoms discussed earlier. Thus, the transport of CFCs into the stratosphere followed by their breakdown serves as a source of F atoms for the stratosphere [137]. The abundance of tropospheric fluorine bound in stable organic molecules—and therefore bound for the stratosphere—was 1.82 ppbv in September 1993 [138].

By analogy to Cl_y and Br_y, we can define the odd fluorine family, F_y, to be the sum of the abundances of HF and other F species such as $FONO_2$, HOF, FO, and F. Further, we expect the FO radical to rate limit catalytic cycles that destroy O_x.

F atoms released in the stratosphere can react with H_2O or CH_4 to form HF. Owing to the small size of the F atom, the HF molecule is extremely stable (compared to

HCl and HBr). In fact, the HF molecule is not photolyzed or oxidized in the stratosphere, and can therefore be considered chemically inert. As a result of this, virtually all F_y is in the form of HF, and very little is in the form of FO. This can be contrasted to the chlorine and bromine families, in which a few percent and a few tens of percent of Cl_y and Br_y, respectively, are in the form of active O_x-destroying radicals. Because of this, fluorine is not expected to contribute to O_x loss in the stratosphere.

Figure 4.38 shows vertical profiles of HF, the major F_y reservoir molecule in the stratosphere. Also shown are profiles of COF_2 and COFCl, two species that are formed from partially decomposed CFCs created during the oxidation of the CFCs. About 70–80% of stratospheric fluorine not attached to an intact CFC is in the form of HF, with the remainder in COF_2 and COFCl.

While fluorine chemistry is unimportant in the stratosphere, the inertness of HF makes it useful as a tracer of atmospheric motion [139].

As with the other halogen families, Cl_y and Br_y, there are no loss processes for inorganic fluorine. Instead, the concentration of HF in an air parcel increases until all of the fluorine-bearing organic molecules have been destroyed.
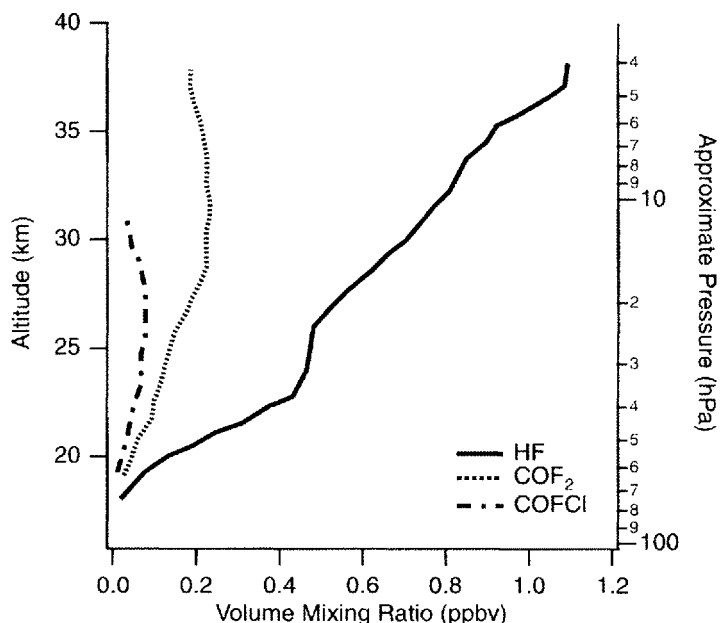
Figure 4.38 Measured mid-latitude profiles of HF and COF_2. COFCl is derived from a model. (After Sen *et al.* [138], Figure 9.)

4.6.2 Iodine

The chemistry of iodine and its implications for stratospheric O_x loss are less well known than those of the other halogens discussed in this chapter (chlorine, bromine, and fluorine). Because the lifetime of iodocarbons, the iodine source gas, is a few days in the troposphere—compared to tropospheric lifetimes of years for CFCs—it has generally been assumed that these molecules do not survive long enough to be transported into the stratosphere. It has been speculated, however, that iodine source molecules, such as methyl iodide (CH_3I), might be transported into the stratosphere in convective events. Should this iodine be released in the stratosphere, catalytic cycles involving iodine could catalyze O_x loss in the stratosphere. (See Solomon *et al.* [140] for a review of the tropospheric sources and stratospheric chemistry of iodine.)

The importance of iodine can be seen in Figure 4.39, which shows what fraction of the chlorine, bromine, and iodine families are in the active O_x-destroying form. As the size of the halogen atom increases, the associated reservoir molecules (HX, $XONO_2$, HOX) become more weakly bound. Attendant with the weakening of the reservoir species, a greater fraction of the family exists in the O_x-destroying forms
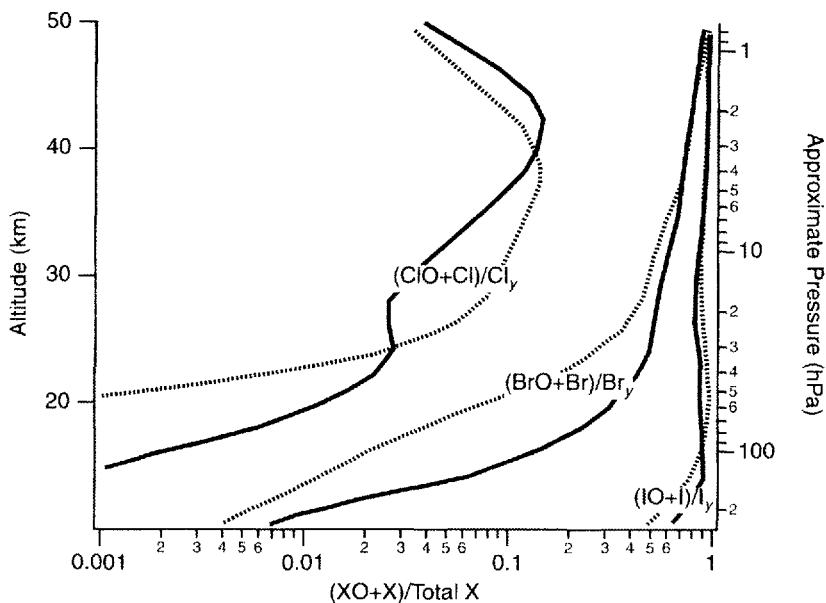
Figure 4.39 Ratio of active members of the chemical family to the total abundance of the chemical family. Values are from a two-dimensional model; solid lines represent the partitioning at 50°N, and the dotted line represents the partitioning at 8°N. (After Solomon *et al.* [140], Figure 1.)

XO and X—making the chemical family more effective at destroying O_x. One can see that virtually all of the inorganic iodine in the stratosphere is in the form of the I and IO radicals. At the other extreme is fluorine, which, owing to the stability of the HF molecule, has an $([FO] + [F])/[total F]$ ratio of approximately zero throughout the stratosphere—and is therefore unimportant for O_x loss.

Ground-based measurements of IO absorption imply total stratospheric iodine abundances of 0.2 (+0.3/–0.2) pptv. This result, combined with recent laboratory measurements of the rate of the reactions of IO with other halogen species, suggests that iodine chemistry is not responsible for the observed reductions in lower stratospheric O_x during the last several decades [141].

An aside: environmental engineering

As evidence mounts that human activity is changing the atmosphere, it is becoming increasingly clear that mankind has the power to intentionally engineer the climate. Is this a good idea?

Leaving aside the legal and ethical questions, imagine that we live on an Earthlike (class M) planet that is a bit too cool, and we want to warm it. We might try releasing CFCs. These molecules are nontoxic, have large infrared cross-sections, and absorb in regions of the spectrum (the "window" region, 8–12 µm) that the atmosphere is largely transparent to. As a result, even in parts per trillion by volume abundances, these species are potent greenhouse gases [142], and their release would be expected to warm the planet.

Up to the mid-1980s, it was generally agreed that this was the end of the story. Since then, however, we have learned much about the atmospheric effects of CFCs. As we have shown, the release of CFCs leads to an increase in stratospheric chlorine and a reduction of O_3 in the lower stratosphere. O_3 however is itself a powerful greenhouse gas. It turns out that the reduction in lower-stratospheric O_3 can offset much if not all of the anticipated warming due to CFCs [143,144]. Thus, it is not clear how much, if any, surface warming would actually result from the release of CFCs.

The lesson here is that any attempt at environmental engineering must be undertaken with care. Our knowledge of the atmosphere is often incomplete and unknown factors might not only cause the desired outcome to not occur: it might cause the opposite outcome to occur!

Problems

1. What is the lifetime of Cl_x with respect to conversion into HCl and $ClONO_2$? Over these lifetimes, how many O_x molecules does a Cl_x molecule destroy? Express your answer in terms of rate constants and concentrations.

2. Imagine that J_{ClONO_2} suddenly increases. Describe qualitatively what would happen to the abundance of HCl in the lower and upper stratosphere?

3. HOCl is generally a minor component of the Cl_y family. Consider the following reactions involving HOCl:

$$ClO + HO_2 \longrightarrow HOCl + O_2 \tag{1}$$

$$HOCl + hv \longrightarrow OH + Cl \tag{2}$$

$$HOCl + OH \longrightarrow H_2O + ClO \tag{3}$$
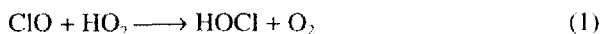
(a) Assume the photochemical steady state. Write an expression for $[Cl_x]/[HOCl]$. Make any assumptions that you make explicitly clear.
(b) The loss lifetime of HOCl ($1/L$) is about an hour. Is this system in the strict photochemical steady state where production equals loss at all times? Explicitly state what time constants you are comparing and their approximate magnitudes.

4. Assume that the NO_y family is in photochemical steady state. Write an expression for $[NO_x]/[HNO_3]$ (in terms of rate constants, photolysis frequencies, and the abundance of other species) assuming gas-phase-only reactions. How does the hydrolysis of N_2O_5 affect the partitioning?

5. Ozone loss from $BrONO_2$ photolysis. Consider the following bromine reactions:

$$BrO + NO_2 \xrightarrow{M} BrONO_2$$

$$Br + O_3 \longrightarrow BrO + O_2$$

$$NO_3 + hv \longrightarrow NO + O_2$$

$$NO + O_3 \longrightarrow NO_2 + O_2$$
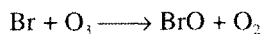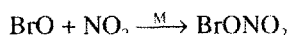
Given these reactions, show that if $BrONO_2$ photolyzes to form Br and NO_3 then this will lead to a catalytic odd-oxygen loss cycle, but if the photolysis products are BrO and NO_2, then no net loss occurs. Feel free to include other reactions discussed in this chapter.

Chapter 5 | Transport

In general, the abundance of a constituent at a fixed point in space is determined by a combination of chemical production, chemical loss, and transport of the constituent. To highlight the effects of transport of O_x on the O_x distribution, we estimate the O_x abundance in the stratosphere in the absence of transport. In this case, the continuity equation for O_x is:

$$\frac{\partial [O_x]}{\partial t} = P_{O_x} - L_{O_x}[O_x] \qquad (5.1)$$

where P_{O_x} is the production rate (molecules cm^{-3} s^{-1}) and L_{O_x} is the loss frequency (1 s^{-1}) of O_x. Using daytime-averaged P_{O_x} and L_{O_x} from a model and assuming that the time rate of change of O_x ($\partial[O_x]/\partial t$) is equal to zero, we can solve for $[O_x]_{ss} = P_{O_x}/L_{O_x}$ and thereby obtain an estimate of the "steady-state" abundance of O_x in the absence of transport of O_x. Figure 5.1 plots annually averaged $[O_x]_{ss}$, which we will call the "no transport" case. It should be noted that only transport of O_x has been neglected; the effects of transport of other species, such as NO_y, Cl_y, and other long-lived species, are included in P_{O_x} and L_{O_x}. In addition, P_{O_x} and L_{O_x} are both functions of the distribution of O_x; Figure 5.1 is calculated using P_{O_x} and L_{O_x} that incorporate realistic background abundances of O_x.

Figure 5.2 shows the annually and zonally averaged "transported" O_x distribution—by "transported" we mean that O_x is subject to the full continuity equation, including transport. This distribution is quite similar to the satellite-derived distribution shown in Figure 1.2a in Chapter 1.

Figure 5.3, a plot of the difference between Figures 5.1 and 5.2, shows the influence of the transport of O_x. Above about 30 km there is virtually no difference between the O_x fields. At these altitudes the rate of transport of O_x is negligible compared to the chemical production and loss rates, and the system is in either diurnal or photochemical steady state. It should be noted that transport is still important insofar as it affects the abundances of Cl_y, NO_y, etc., that regulate the loss rate of O_x.

Below ~30 km (~10 hPa), however, the difference between the "transported" and "no transport" O_x fields is significant, demonstrating the role that transport plays in determining the O_x distribution. There are positive values in the tropical lower and
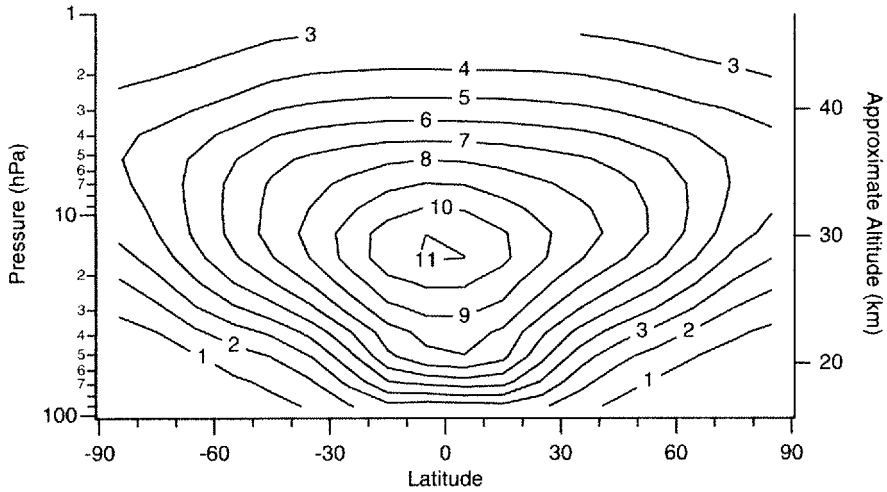
Figure 5.1 Estimate of O_x distribution (ppmv) in the absence of transport of O_x—the "no transport" case. The contours were calculated from annually averaged P_{O_x} and L_{O_x} obtained from the Goddard two-dimensional climatological circulation model [73].
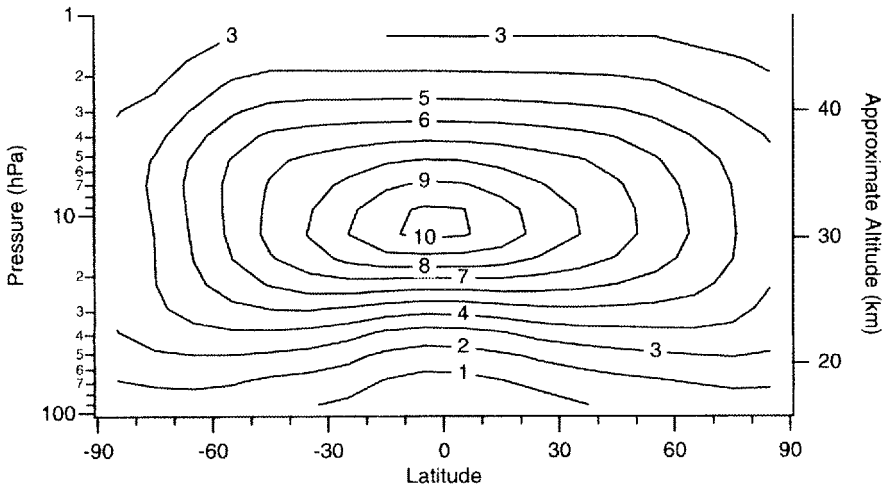
Figure 5.2 Model calculation of the annually averaged O_x field—"transported" O_x—from a calculation including the effects of the transport of O_x. Calculated from the Goddard two-dimensional climatological circulation model [73].
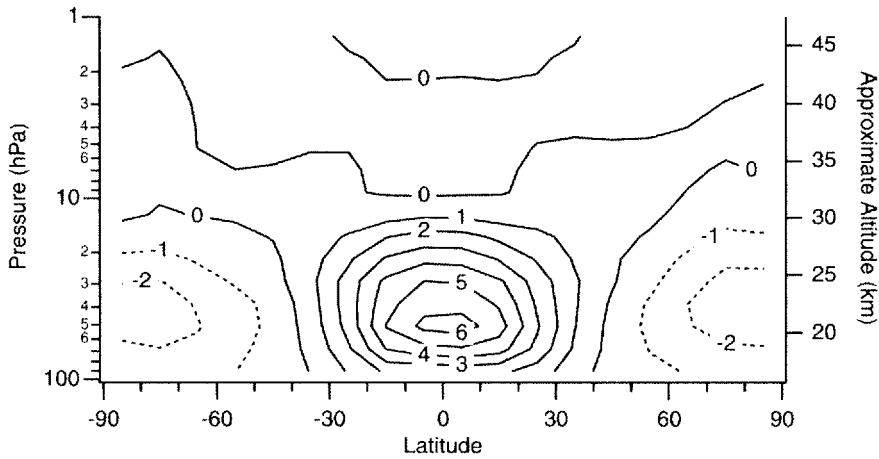
Figure 5.3 Difference (ppmv) between Figures 5.1 and 5.2.

mid-stratosphere, meaning that the transport of O_x lowers the O_x abundance in this region of the atmosphere, i.e. there is a net transport of O_x out of this region. There are negative values at mid- and high latitudes, meaning that the transport of O_x acts to increase the O_x abundance in this region of the atmosphere, i.e. there is a net transport of O_x into this region. In other words, O_x production exceeds loss in the tropics, and O_x loss exceeds production in the mid- and high latitudes. Transport evens out this imbalance by transporting O_x out of the region of excess production into the region of excess loss.

Thus, transport plays an important role in regulating lower- and mid-stratospheric O_x. We present in this chapter a short discussion of the salient features of the stratospheric circulation, with an emphasis on the transport of O_x in the stratosphere. The interested reader can find in-depth treatments of the circulation of the stratosphere elsewhere [56,145,146].

5.1 Transport Into and Out of the Stratosphere

The stratosphere is not a closed system but exchanges mass with its neighbors, the troposphere (below) and mesosphere (above). We will discuss these interactions in this section.

Since the late 1940s, when it was recognized that troposphere-to-stratosphere transport was important for regulating the abundance of water vapor in the stratosphere [147], stratosphere–troposphere exchange (STE) has been a subject of great interest in stratospheric science. Recent research into the loss processes of O_x has

emphasized the need for understanding STE because the vast majority of the precursors of the O_x-destroying radicals (such as chlorofluorocarbons (CFCs) and N_2O) originate in the troposphere and are transported into the stratosphere. STE is also important because it leads to the injection of O_x- and NO_y-rich stratospheric air into the troposphere, affecting the chemistry of that region. Our present understanding of STE is reviewed in detail by Holton *et al.* [148].

Following the nomenclature of Hoskins [149], we divide the atmosphere into three regions: the "overworld," "middleworld," and "underworld" (Figure 5.4). The overworld is defined to be the region above the ~380 K potential temperature surface (about 16 km altitude), and contains surfaces of constant potential temperature (isentropes) that are within the stratosphere at all latitudes. The middleworld is defined to be the region between the ~380 and ~310 K potential temperature surfaces, and contains isentropes that are in the troposphere at low latitudes and in the stratosphere at high latitudes. The stratospheric part of the middleworld is often called the "lowermost stratosphere". The underworld is defined to be the region below the ~310 K potential temperature surface, and it contains isentropes that are within the troposphere at all latitudes.

Mass flux into the stratosphere occurs on some combination of the three paths shown in Figure 5.4. Path A is the mean meridional circulation, often referred to as the Brewer–Dobson circulation [147,150]. It consists of air rising through the tropopause into the stratosphere at low latitudes and descending back into the
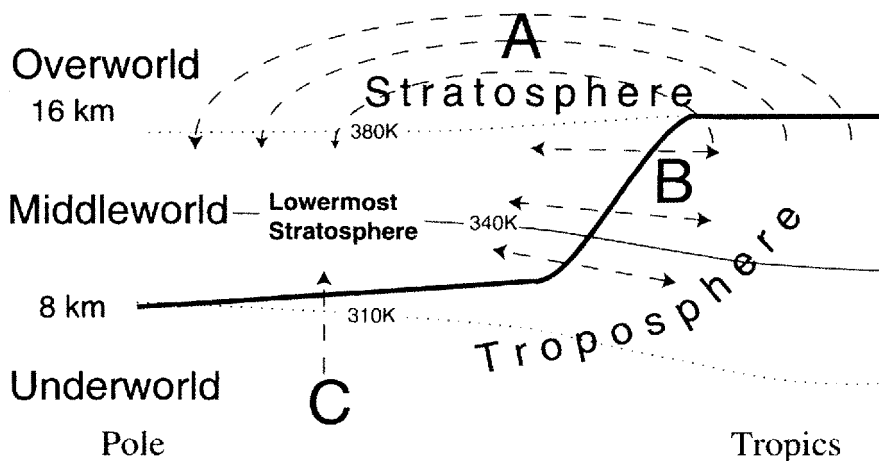
Figure 5.4 Latitude–height schematic cross-section of the atmosphere. The heavy line is the tropopause. Overworld–middleworld and middleworld–underworld boundaries are shown as dotted lines. The middleworld stratosphere is hereafter referred to as the "lowermost stratosphere." See text for details about paths A, B, and C. (After Dessler *et al.* [164], Figure 1.)

troposphere at mid- and high latitudes. Associated with these vertical motions is a poleward mass flux.

Brewer [147] and Dobson [150] envisioned the flux into the stratosphere along path A as slow, large-scale upwelling through the tropical tropopause. It was later argued that the tropical tropopause was generally too warm to explain the extremely dry stratosphere [151]. Based on this, the region where air slowly ascends into the overworld was further narrowed to those regions and times in which the tropical tropopause is much colder than average: in the western tropical Pacific, northern Australia, and Indonesia during the November to March period and over the Bay of Bengal and India during the monsoon. This temporally and spatially limited region has become known as the "stratospheric fountain". Recent measurements of water vapor [152] and CO_2 [153] show that air enters the stratosphere throughout the entire year; this has persuaded many that the temporal restrictions of the "stratospheric fountain" theory are likely wrong. An analysis using improved data sets re-examined the spatial restriction and found that it too did not stand up upon further investigation [154]. At the present time, it is unclear if there are any preferred locations for transferring mass from the troposphere to the overworld.

General objections to the slow-ascent theories of troposphere-to-overworld transport have also been raised. It was argued that large-scale uplift would cause thick cirrus decks to form in the upwelling regions, which is not the case [155]. However, the recent observations of widespread subvisible cirrus clouds near the tropopause [156–158] have lessened this criticism. Another problem is that no theory can definitively explain how air slowly ascending into the overworld can be dehydrated to the very low humidity observed in the stratosphere [159,160].

An alternative to slow ascent is that energetic convection, originating at the surface, overshoots the tropopause and mixes with stratospheric air, thereby transferring mass from the troposphere into the overworld (see Danielson [161], and the STEP collection of papers [162] and the references therein). During the injection process, the air mass is dehydrated to stratospheric abundances. While theories of the dehydration process exist [163], there is currently not enough data to validate these theories with any certainty.

It should be noted that both slow-ascent and direct convective injection are almost certainly both occurring. The real question is the relative importance of these two processes. At the present time the answer to this question is unknown.

Path B is isentropic transport between the troposphere and the lowermost stratosphere. Ordinarily, air parcels are prevented from crossing the tropopause on an isentrope by the large gradient in potential vorticity (PV) at the tropopause [148]. Synoptic-scale waves, however, can transport material from the tropical troposphere to the mid-latitude stratosphere and vice versa by means of wave breaking. Path C is mid- and high-latitude convective transport of air from the troposphere to the lowermost stratosphere.

Much of our understanding of the relative contributions of the different paths is provided by measurements of water vapor. As an air parcel cools below the frost point (the temperature at which the relative humidity with respect to ice is 100%), condensation of water vapor and subsequent sedimentation of particles dehydrates the air mass. If the temperature of the air parcel subsequently rises, the water vapor volume mixing ratio (VMR) remains unchanged, and continues to reflect the previously encountered minimum temperature.

This last fact, combined with the fact that the minimum saturation VMR is most often encountered at the tropopause, makes the water vapor abundance a useful indicator of where air crosses the tropopause. Figure 5.5 shows the distribution of temperature, pressure, and saturation water vapor abundance along the tropopause. Air following path A, which goes through the tropical tropopause, typically encounters temperatures of 195 K or below, and therefore carries only a few parts per million by volume of water into the stratosphere. Paths B and C, however, which transit the extratropical tropopause, encounter far warmer temperatures (~210–225 K) than the tropical tropopause, and can carry tens of parts per million by volume of water vapor into the stratosphere.
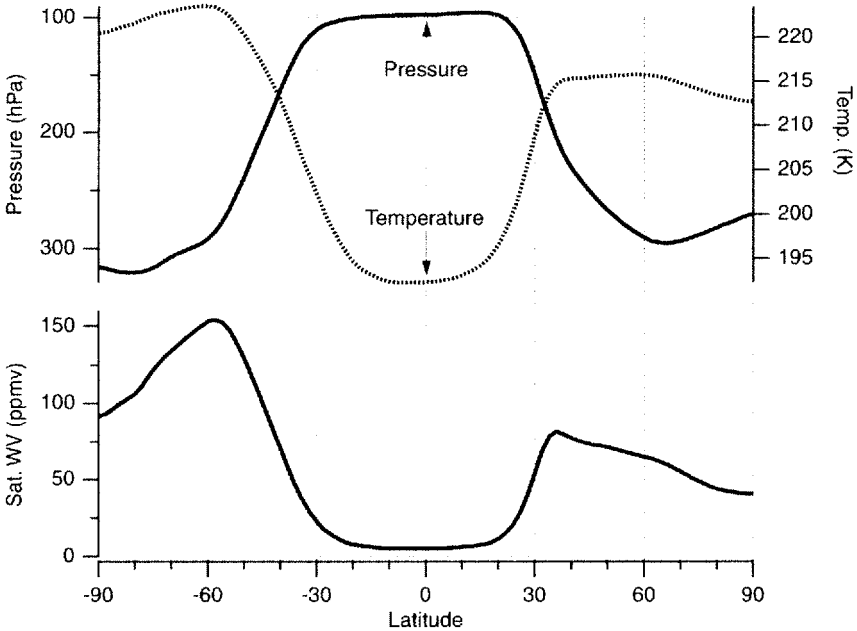
Figure 5.5 Temperature, pressure, and saturation water vapor abundance of the tropopause. Data are zonal and monthly averaged for January 1994.

Figure 5.6 shows several mid-latitude profiles of water vapor covering the region between the upper troposphere and overworld. The abundance of water vapor in the overworld is a few parts per million by volume. Only at the tropical tropopause are the temperatures low enough to dehydrate air to such a low abundance (Figure 5.5). Additional support for the tropical tropopause as the entry point of air into the overworld comes from observations of a correspondence between the seasonal cycle of the abundance of water entering the stratosphere and the seasonal cycle of tropical tropopause layer temperature [152], as well as measurements of other tracers [165]. As a result, it is generally believed that all of the air in the overworld transited the tropical tropopause.

Measurements suggest that, on an annual average, air enters the overworld with ~3.85 ppmv of H_2O [166], 1.7 ppmv of CH_4 [167], and 0.5 ppmv of H_2 [114,168,169]. Once in the stratosphere, the CH_4 and H_2 are slowly oxidized to form
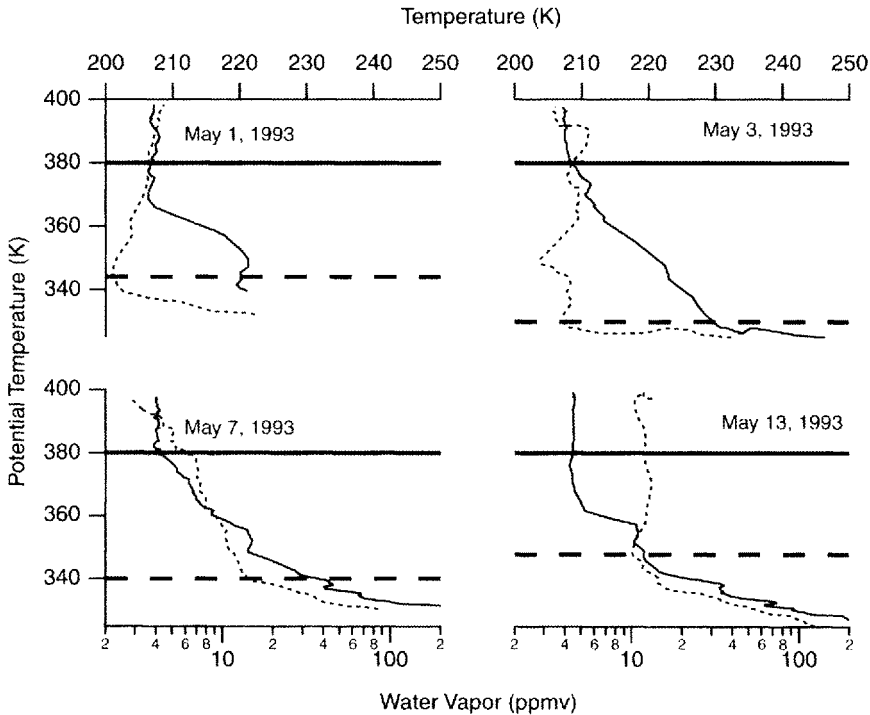
Figure 5.6 Mid-latitude profiles of water vapor (solid line) and temperature (light dashed line) vs. potential temperature (K). The heavy dashed line indicates the location of the tropopause; the heavy solid line indicates the 380 K surface, the boundary between the over-world and lowermost stratosphere. (After Dessler *et al.* [164], Figure 2.)

additional water vapor [110,112-114]. Complete oxidation of CH_4 and H_2 would form an additional $2 \times 1.7 + 0.5 = 3.9$ ppmv of water vapor. In agreement with this simple constraint, stratospheric H_2O abundances greater than 8 ppmv are never observed, with typical observed abundances between 4.5 and 7 ppmv [170].

Figure 5.7 shows typical cross-sections of H_2O and CH_4. As one can see, the decrease in CH_4 (due to oxidation) is mirrored by an increase in H_2O. H_2 is also
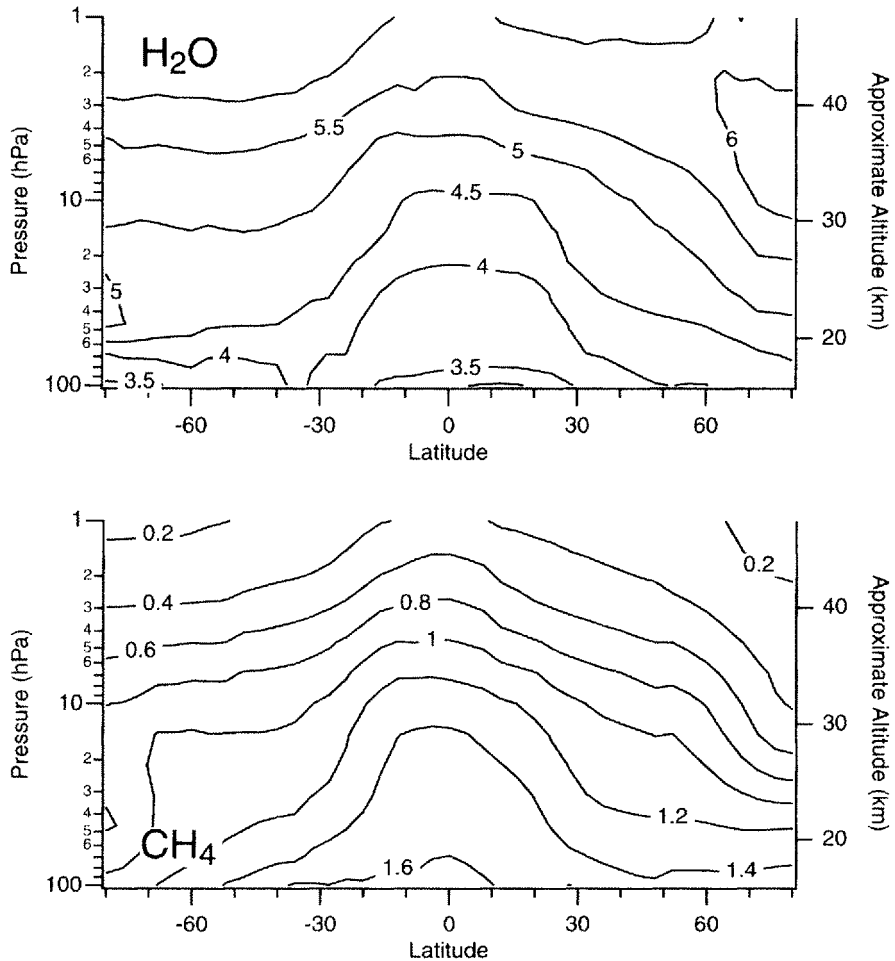
Figure 5.7 Latitude–height cross-sections of H_2O and CH_4 for December 1992. Data were measured by instruments onboard the UARS; in the UARS Reference Atmosphere Project (W. J. Randel, personal communication, 1998). (See Randel *et al.* [174] for details of the plots.)

oxidized to form H_2O, but it is also produced in the stratosphere as a by-product of CH_4 oxidation. These two processes are approximately equal, so the abundance of H_2 remains constant at ~0.5 ppmv throughout the lower and mid-stratosphere, decreasing to lower values in the upper stratosphere [171]. (For more discussion on the hydrogen budget, see Dessler *et al.* [172] and Hurst *et al.* [173].)

Between the mid-latitude tropopause and the overworld lies the lowermost stratosphere. Figure 5.6 shows that in this region the abundance of water vapor is variable but can reach several tens of parts per million by volume. We know that some of the air in this region has descended from the overworld via path A as part of the Brewer–Dobson circulation. This air, however, carries 4–8 ppmv of water vapor, and so cannot be the only source of air for the lowermost stratosphere [164]. It is concluded, therefore, that some of the air must have followed a path that crossed the extratropical tropopause—thereby allowing the air to carry more water vapor into the stratosphere. It is generally agreed that isentropic transport of air into the stratosphere (path B) is responsible for much of this transport [175,176].

While mid- and high-latitude convective transport into the stratosphere (path C) has been shown to occur [177], it is presently unknown how important this path is for the global budget of STE. It should be noted that this pathway likely only transports air into the lowest few kilometers of the lowermost stratosphere [177,178]. Mid- and high-latitude convection is simply not energetic enough to reach overworld potential temperatures.

To summarize, the stratosphere can be thought of as being made up of two separate but related regions. The overworld is the region of the stratosphere above 380 K potential temperature. Air enters this region exclusively through the tropical tropopause, and the water vapor abundance in this region is set by the cold temperatures encountered there. The lowermost stratosphere—the mid- and high-latitude stratosphere between 380 K and the tropopause—is made up of a mix of overworld air that has descended from above and air that has gone through the extratropical tropopause. Air crossing the extratropical tropopause experiences higher temperatures than air crossing the tropical tropopause, allowing higher water vapor in the lowermost stratosphere (tens of parts per million by volume) than in the overworld stratosphere (a few parts per million by volume).

Most of the ozone in the stratosphere resides in the overworld. As a result, the focus of this book is almost exclusively on the overworld, and we use the terms "stratosphere" and "overworld" interchangeably. This loose notation is not problematic, however, because most of the concepts presented also apply to the lowermost stratosphere.

Finally, the stratosphere also exchanges mass with the mesosphere. By almost any measure this exchange of mass is less important than exchange with the troposphere, but there are aspects of it worthy of note. Probably the most important is the transport of NO_y formed in the mesosphere and thermosphere into the stratosphere. This

can be a potentially important source of NO_x for the upper stratosphere, especially following severe solar proton events [97].

5.2 The General Circulation

The existence of winds can be attributed to differential heating of the atmosphere—the fact that the tropics receive more solar energy per unit area, on an annual average, than the poles (see Hartmann [179], Figure 2.7). This differential heating causes a pressure gradient between the pole and equator, which drives a strong zonal flow with typical velocities in the stratosphere of $10–100$ m s^{-1}. Dissipation of planetary waves in the stratosphere and above leads to meridional and vertical flow; this cause-and-effect relationship has become known as the "wave-driven pump" [148]. The meridional flow typically has zonally averaged velocities of tens of centimeters per second, and is therefore weaker than the zonal flow. The vertical flow typically has zonal average velocities of the order of millimeters per second, smaller than both the zonal or meridional velocities.

While flow in the atmosphere is obviously three-dimensional, strong zonal flow means that the stratosphere tends to be well mixed in the zonal direction. Thus, air at different longitudes but the same latitude and altitude tends to be similar. For this reason, we have often relied in this book on plots in which the data from the same latitude and altitude but different longitudes have been averaged together to form a "zonal average" plot. Using this same logic, two-dimensional (2D) models of the stratosphere have been developed that take advantage of this fact and represent the atmosphere in only two dimensions: latitude and height (see WMO [15], Chapter 12).

It should be remembered, however, that important longitudinal asymmetries do exist in the O_x field. As Figure 1.3 shows, column O_3 varies with the synoptic weather pattern (i.e. the pattern of high and low pressure). This occurs because high-pressure systems push up the tropopause. This causes convergence of tropospheric air into the bottom of the column and a divergence of stratospheric air out of the upper parts of the column. Since tropospheric air has a much lower O_x content than stratospheric air, this causes the total column abundance to decrease. Low-pressure systems have the opposite effect.

Despite these longitudinal asymmetries, many of the important facets of the transport of O_x can be understood by examining the 2D circulation of the atmosphere. In the next section we examine this circulation. Then, we will discuss how it affects the distribution of trace gases, especially O_x, in the stratosphere.

5.2.1 The 2D circulation

The 2D circulation of the stratosphere in the meridional plane can be divided into two parts: the Brewer–Dobson circulation, a mean overturning circulation, and

quasi-horizontal meridional eddy transport. The Brewer–Dobson circulation was introduced earlier in this chapter in our discussion on STE. It comprises upwelling in the tropics and downwelling in the extratropics, and is shown schematically as path A in Figure 5.4. Figure 5.8 shows streamlines of the circulation during northern hemisphere winter, while Figures 5.9 and 5.10 show estimates of the horizontal and vertical components of the Brewer–Dobson circulation. Upwelling in the tropics is primarily compensated for by downwelling in the winter hemisphere [180,181]; the meridional circulation in the summer hemisphere is much weaker. Most mass entering the stratosphere rises into the lower stratosphere, is transported poleward, and descends out of the stratosphere, with only a small fraction of the mass rising to high altitudes. Finally, the Brewer–Dobson circulation in the northern hemisphere during its winter is stronger than the circulation in the southern hemisphere during its winter. This arises from differences in the layout of continents and mountain ranges in the two hemispheres [146,148].

The second part of the 2D circulation is the quasi-horizontal transport arising from longitudinally asymmetric processes such as planetary-scale wave breaking. Because there is no longitude coordinate in the 2D zonally averaged framework, these processes must be parameterized in terms of other variables, and how this parameterization is implemented remains a central problem in the implementation of a 2D framework. This class of processes is generally referred to as "eddy transport".

Eddy transport is relatively fast, transporting and mixing material on horizontal
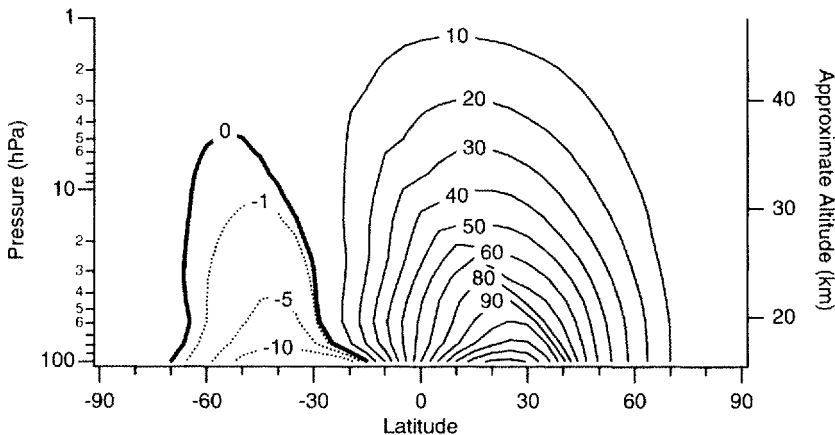
Figure 5.8 Stream function (arbitrary units, but proportional to mass flux) in January, from the Goddard two-dimensional climatological circulation model [73]. The velocity fields used to derive this figure, as well as Figures 5.9 and 5.10, are a "transformed Eulerian mean" circulation, in which the canceling effects of eddy transport have been removed from the mean meridional circulation (see WMO [15], Chapter 12 and Andrews et al. [145], Chapter 3).

surfaces on time-scales of weeks. There are latitude ranges, however, where eddy transport is slow. These regions are referred to as "transport barriers" because horizontal mixing through these regions is slow [59]. This can be seen in Figure 5.11, which shows strong gradients in N_2O located at 20°N and S and at 65°N. Such strong gradients in a constituent with a lifetime of weeks or longer can be maintained only if meridional mixing is slow; otherwise, mixing would wipe out the gradient.
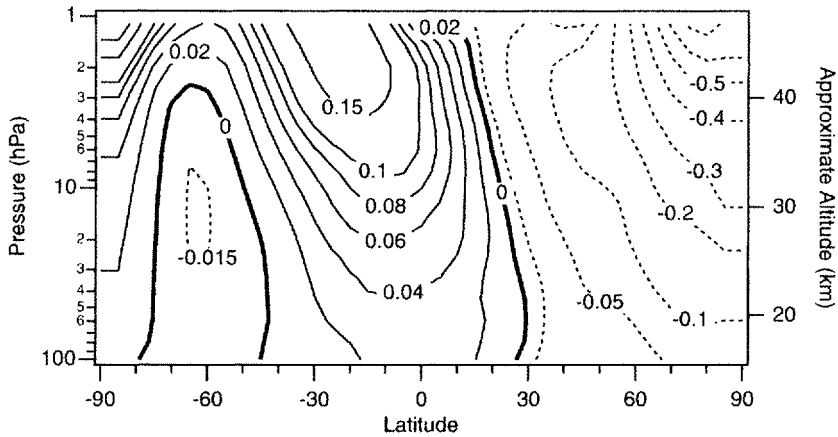
Figure 5.9 Vertical velocity (cm s^{-1}) during January. Positive values correspond to air rising, and negative values correspond to air sinking. (See the caption of Figure 5.8 for more information about this plot.)
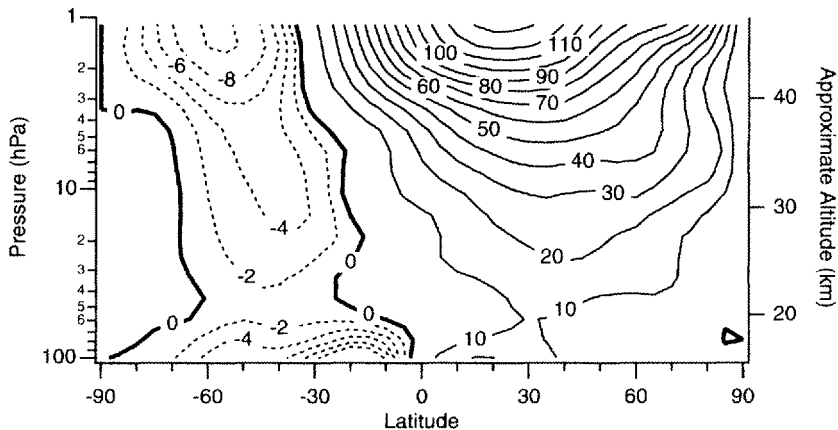
Figure 5.10 Horizontal velocity (cm s^{-1}) during January. Positive values correspond to northward flow, and negative values correspond to southward flow. (See the caption of Figure 5.8 for more information about this plot.)
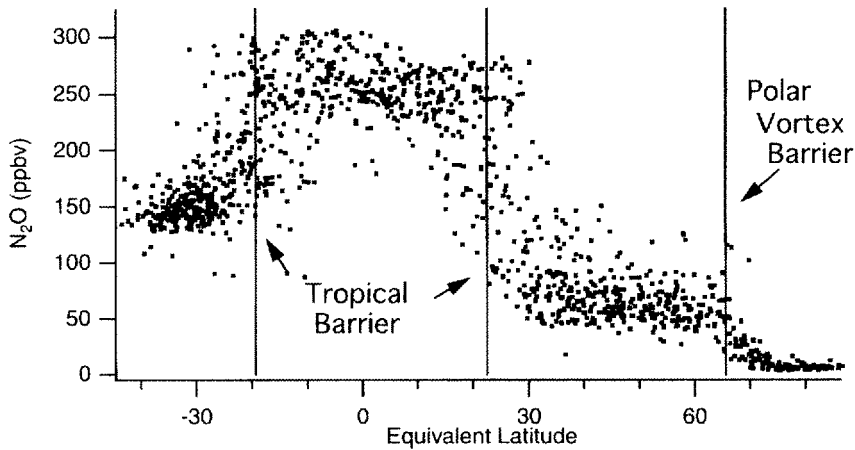
Figure 5.11 N$_2$O abundance on February 20, 1992, at 800 K potential temperature versus equivalent latitude. N$_2$O was measured by the CLAES on the UARS. The equivalent latitude was determined using UKMO meteorological fields from that day.

The barriers at 20°N and S isolate the tropics [152,182–184]. Thus, air ascends in the tropics as part of the Brewer–Dobson circulation in relative isolation from the mid-latitudes—this has become known as the "tropical pipe" [185]. The barrier at 65°N exists only in the northern hemisphere winter. A similar barrier exists in the southern hemisphere during its winter. These polar barriers slow mixing between the mid-latitudes and the polar regions [186,187] and play an import role in the formation and maintenance of the ozone hole (discussed in Chapter 7).

As a result of these transport barriers, air in the tropics, mid-latitudes, and polar region can have very different chemical compositions [185,188]. These transport barriers, therefore, have a profound impact on the distribution of gases in the stratosphere and their subsequent chemistry.

Finally, just as there is a seasonal cycle in the Brewer–Dobson circulation, there is also a seasonal cycle in the eddy transport. In fact, it is now understood that the Brewer–Dobson circulation and the eddy processes are physically related, and that it would be impossible to have one without the other. A thorough discussion of this is outside the scope of this book, but this point is discussed in detail elsewhere [146,148].

It is easy to see how the 2D circulation creates the observed distribution of long-lived trace gases in the stratosphere (Figure 5.12). The Brewer–Dobson circulation lifts the lines of constant mixing ratio (isopleths) of CH$_4$ in the tropics and pushes the isopleths down at mid- and high latitudes (indicated by the solid arrows in Figure 5.12). Thus, as one moves from the tropics to the poles at a constant altitude, the
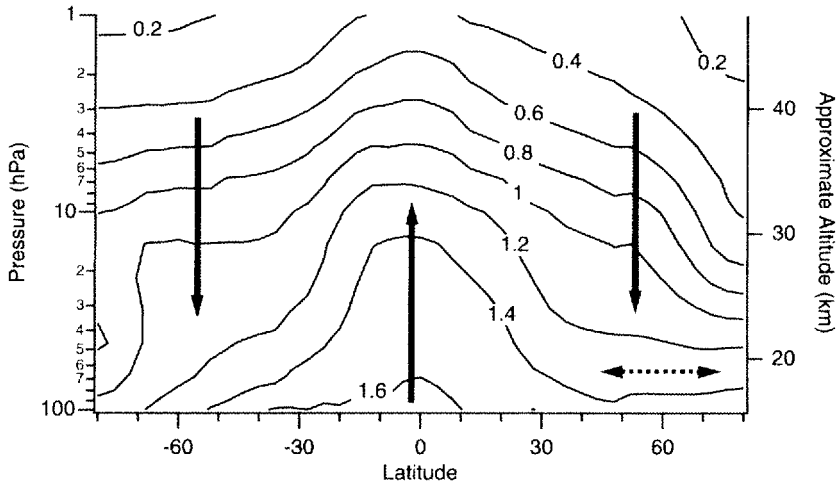
Figure 5.12 Cross-section of CH_4 from Figure 5.7. Solid arrows indicate the effects of the Brewer–Dobson circulation: lifting the isopleths up in the tropics and pushing the isopleths down in the extratropics. Dashed arrows indicate the isopleth-flattening effect of quasi-horizontal eddy transport.

abundance of CH_4 decreases. Eddy processes, on the other hand (dashed arrows in Figure 5.12), transport constituents quasi-horizontally and attempt to remove any horizontal gradients. In other words, eddy processes tend to flatten the isopleths, opposing the isopleth-steepening effects of the Brewer–Dobson circulation. The actual slope of the isopleth observed in the atmosphere is a result of the competition between these two processes.

As we have already said, air enters the stratosphere primarily through the tropical tropopause. By a combination of the Brewer–Dobson circulation and quasi-horizontal eddy transport, the air then moves poleward and eventually exits the stratosphere by descending back across the tropopause at mid- and high latitudes. As the air travels through the stratosphere, the abundances of Cl_y, Br_y, and NO_y build up as the source molecules for these species (CFCs, halons, and N_2O) are photolyzed. The abundance of Cl_y, Br_y, and NO_y in an air parcel is therefore determined by the total exposure of the air parcel to radiation and oxidizing species [146].

The mean age of air in the stratosphere is shown in Figure 5.13, where age is defined as the number of years since the air crossed the tropopause. In general, the air in the stratosphere is a few years old, with the average age increasing with both altitude and latitude in a way that is consistent with the general 2D circulation. "Age of air" is actually a fairly complex subject; it is discussed more thoroughly elsewhere [82,189].
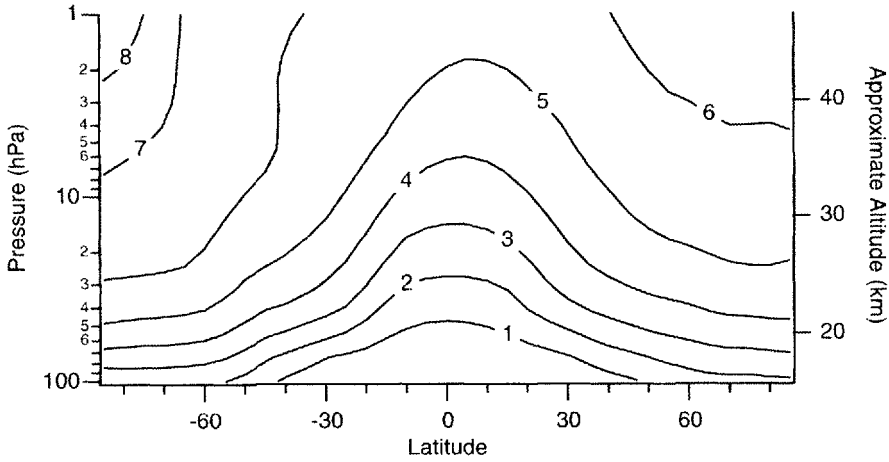
Figure 5.13 Average age of air (years) from a model. (Adapted from Waugh *et al.* [189].)

5.2.2 *Effect of transport on atmospheric constituents*

In this section we discuss the effects of the general circulation of the stratosphere on O_x and long-lived constituents.

Odd oxygen We can derive time constants with respect to transport for O_x using a "replacement time" formalism: $\tau = f_{O_x}/$(transport rate in VMR per second), where f_{O_x} is the VMR of O_x. We further subdivide the total transport lifetime into lifetimes with respect to vertical and horizontal transport [190]:

$$\frac{1}{\tau_{\text{vert}}} = -\frac{1}{f_{O_x}}\left[w\frac{\partial f_{O_x}}{dz} + \frac{\partial}{dz}\left(K_{zz}\frac{\partial f_{O_x}}{dz}\right)\right] \tag{5.2}$$

$$\frac{1}{\tau_{\text{horiz}}} = -\frac{1}{f_{O_x}}\left[v\frac{\partial f_{O_x}}{dy} + \frac{\partial}{dy}\left(K_{yy}\frac{\partial f_{O_x}}{dy}\right)\right] \tag{5.3}$$

where v and w are the horizontal and vertical wind velocities. Eddy transport is often parameterized as a diffusion process (see WMO [15], Chapter 12, for more discussion of this). In Equations (5.2) and (5.3), K_{yy} and K_{zz} represent the diffusion coefficients for horizontal and vertical diffusion, respectively. Note that, in the stratosphere, K_{zz} is generally negligible. Both Equations (5.2) and (5.3) are made up of two terms: the first one (e.g. $v\,\partial f_{O_x}/\partial y$) is the rate of transport due to advection by the Brewer–Dobson circulation, the second one (e.g. $\partial(K_{yy}\,\partial f_{O_x}/\partial y)/\partial y$) is the rate of

transport due to eddy transport. It is important to recognize that the transport time scales defined in Equations (5.2) and (5.3) contain the spatial derivatives of the tracer abundance. As a result, the transport time-scale is a function of the spatial distribution of the tracer, and two tracers that have different spatial gradients will therefore have different transport time-scales.

Figure 5.14 shows profiles of τ_{vert} and τ_{horiz} for O_x at the equator, 30°N, and 60°N (at the equator, $\tau_{horiz} > 1000$ days). Also shown are estimates of the lifetime of O_x with respect to production ($\tau_{prod} \approx [O_x]/P_{O_x}$) and loss ($\tau_{loss} \approx 1/L_{O_x}$). Solid lines represent processes that increase O_x while dashed lines represent processes that decrease O_x. Production always increases O_x, so it is a solid line in all three panels. Loss always decreases O_x, so it is a dashed line in all three panels. Transport can either increase or decrease O_x, depending on the wind field and the spatial gradients of O_x, and therefore appears in Figure 5.14 as both solid and dashed lines.
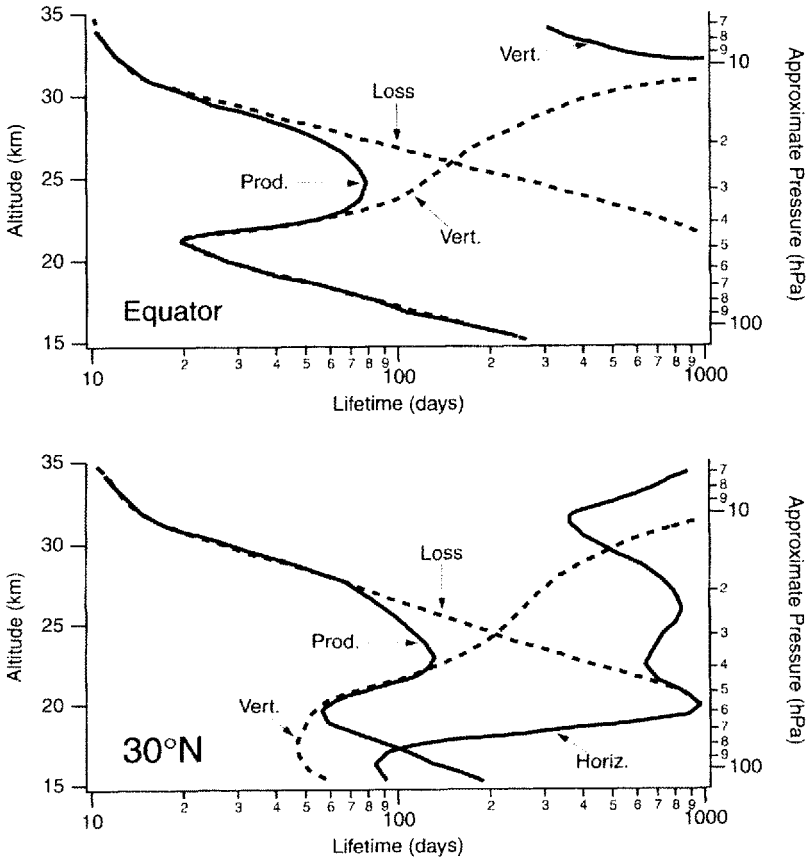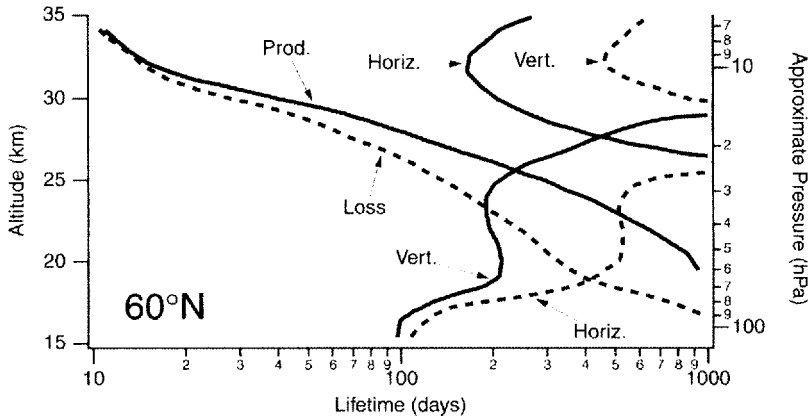
Figure 5.14 Lifetime of O_x with respect to production, loss, and vertical and horizontal transport at the equator, 30°N, and 60°N. Solid lines represent processes that increase O_x; dashed lines represent processes that decrease O_x. (After Ko *et al.* [190], Figure 4.)

At all latitudes, above 30 km the lifetime of O_x with respect to production and loss is very much shorter than the transport lifetimes. As a result, the distribution of O_x is controlled entirely by chemical production and loss. In the lower and mid-stratosphere, the distribution of O_x is controlled by a combination of production, loss, and transport—the exact combination is a function of altitude and latitude. This is consistent with the picture presented in Figure 5.3, where it was shown that transport of O_x had little impact on the O_x distribution above ~30 km but plays an important role below ~30 km.

It must be remembered that the net of production, loss, and transport in the lower stratosphere is not necessarily zero at any instant in time; instead the balance occurs only when these terms are averaged over a sufficiently long time. Because of seasonal and interannual variations, this "sufficiently long time" can be a year or longer.

Long-lived tracers　Of special interest to the stratospheric chemist are the so-called "long-lived tracers": constituents such as nitrous oxide (N_2O), methane (CH_4), and the CFCs that have long lifetimes ($\tau > $ years) in the troposphere and lower stratosphere but are destroyed rapidly in the middle and upper stratosphere. We stated earlier (e.g. see Figure 5.12) that the distribution of these species is heavily influenced by transport.

It has been noted that scatter plots of one long-lived tracer against another often show tight one-to-one relationships between the data—even when the species are completely unrelated chemically. Figure 5.15 shows a good example of this tight correlation.

Because these correlations exist, a knowledge of the abundance of one long-lived
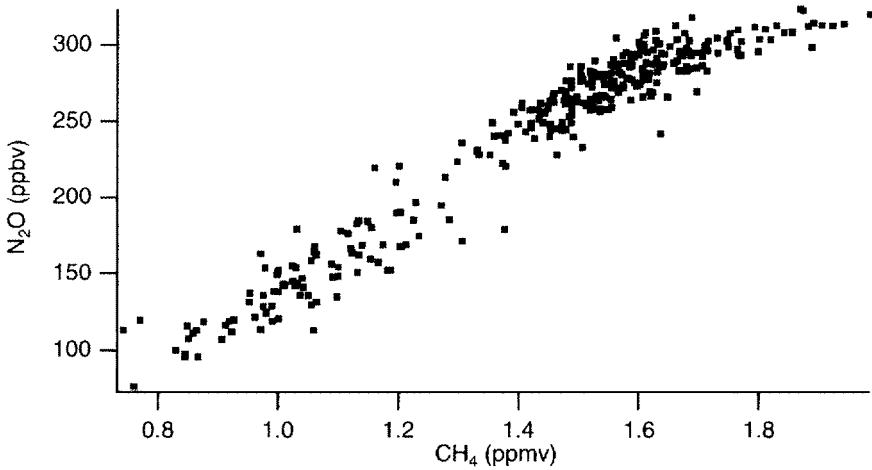
Figure 5.15 N₂O abundance versus CH₄ abundance, measured between 400 and 450 K potential temperature and between 72.4°S and 68.4°N. Data measured by the shuttle-borne ATMOS instrument [191] on the ATLAS 1, 2, and 3 missions.

tracer provides information about other long-lived constituents in an air parcel. This is extremely useful when one does not have measurements of all of the constituents needed for an analysis. For example, if one knows that the N_2O in an air parcel is 175 ppbv, then from Figure 5.15 it can be inferred that the CH_4 abundance is 1.2 ppmv.

To understand why the abundances of long-lived species correlate, one must first understand the concept of slope equilibrium. In regions of the atmosphere where the photochemical lifetime $1/L$ of a constituent is much longer than the time-scale for horizontal eddy transport (a few months), it was shown by Plumb and Ko [192] that the slopes of the isopleths are functions *only* of the circulation of the atmosphere [192]. This situation is known as slope equilibrium.

If two species both obey slope equilibrium, isopleths of the species will therefore be coincident, as is shown in the lower stratosphere of Figure 5.16. How one samples this region of the stratosphere is irrelevant [192]. Concentration A1 will always be associated with concentration B1, A2 with B2, and A3 with B3. A scatter plot of the concentrations will therefore yield a "compact relation": one where the abundance of tracer A is a unique function of the abundance of another tracer B, i.e. [A] = f([B]), with no dependence on other variables such as altitude or latitude. The condition where both constituents obey slope equilibrium is often called the "compact relation regime".

Now, assume that constituent A has a shorter lifetime than constituent B. There is some altitude range in the atmosphere over which constituent A is not in slope equilibrium, but because of its longer lifetime, constituent B is. As a result, the
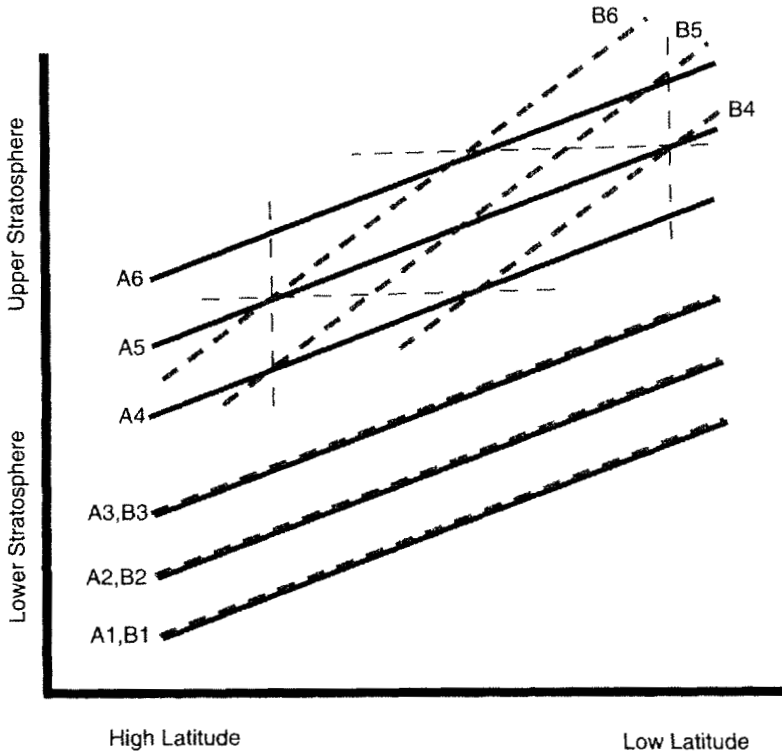
Figure 5.16 Tracer correlation schematic. Solid black lines are isopleths for tracer A, and gray dashed lines are isopleths for tracer B. Thin dashed lines are paths in the atmosphere over which the tracers are sampled.

isopleths of constituent A are shallower than those of constituent B. This situation is shown in the upper stratosphere in Figure 5.16. Because the isopleths are not coincident, there is not a single compact relation between constituents A and B. Instead, the correlation obtained depends on how the atmosphere is sampled. To illustrate this, Figure 5.16 also has four thin dashed lines on it—two vertical and two horizontal. Consider the two vertical lines first and imagine that one is measuring A and B along these two paths. On the equatorward line, one sees that concentration A5 is associated with B4. On the poleward line, A5 is associated with B6. Sampled this way, there appears to be a latitude dependence to the tracer relation [185]. Now consider the two horizontal lines and imagine measuring A and B along these two paths. On the lower altitude line, concentration A4 correlates with B4, and A5 correlates with B6. On the higher altitude line, concentration A5 correlates with B4, and A6 correlates with B6. Sampled this way, there appears to be an altitude dependence to the tracer relation.

Problems

1. Imagine that the Brewer–Dobson circulation and the horizontal eddy transport both speed up.
(a) What will happen to the mean age of air in the stratosphere?
(b) What will happen to the total amount of Cl_y, NO_y, and Br_y in the stratosphere?

2. Water vapor budget of the stratosphere.
(a) What is the mass of the stratosphere?
(b) Assuming a lifetime of stratospheric air of 2 years, what is the mass flow out of the stratosphere (in kg s^{-1})?
(c) The "small comet" hypothesis. Virtually all of the hydrogen in the stratosphere is transported there from the troposphere. However, it was suggested at one point that 20 comets hit the Earth every minute, and that each comet contained 30 tonnes of H_2O. If this water is deposited in the stratosphere (and then well mixed throughout the stratosphere), then how much water vapor in the stratosphere would be attributable to this source?
(d) Tropospheric sources of total hydrogen match the observed stratospheric total hydrogen abundance to within a few percent. How much of a missing source of water vapor can therefore be accommodated? Is the small-comet hypothesis consistent with this uncertainty? How could one modify the small-comet hypothesis to be consistent with these calculations?

3. DIY ("debunk it yourself"). Explain why this is wrong:

A new study reports measurements by a satellite that indicate a localized and natural source of BrO, a known ozone-depleting substance, in the Arctic troposphere, especially over the Hudson Bay area. The measurements show a springtime "plume" of bromine, which destroys ozone in the Arctic troposphere. If this naturally produced chemical mixes into the polar stratosphere it could be the source of the stratospheric "ozone hole", found in polar regions during springtime, instead of man-made refrigerant chemicals (as is currently believed).

4. Help Mark S. calculate column O_3:
(a) Given the O_3 VMR as a function of pressure, derive an expression for the column abundance in Dobson units.
(b) Assuming that the VMR of O_3 is zero in the troposphere and 5 ppmv in the stratosphere, what is the column abundance? Assume the tropopause is at 200 hPa.
(c) Now assume that a weather system causes the tropopause to rise to 150 hPa. What is the column abundance?
(d) Franco asks Mark to explain why the column changes. Help Mark out.

Chapter 6 | Volcano!! Effects of the 1991 Eruption of Mount Pinatubo on the Stratosphere

In Chapters 1–5 we discussed the processes that produce, destroy, and transport O_x. Together, these processes determine the distribution of O_x in the stratosphere. In this chapter we study the effect of a perturbation to the stratosphere—in this case, a large increase in SO_2 abundance following a major volcanic eruption.

The focal point of this discussion is the eruption of Mount Pinatubo in the Phillipines (15°N, 120°E) on June 15, 1991. This eruption injected ~20×10^{12} g (20 Mt) of SO_2 into the tropical stratosphere [22,23]. Figure 1.9 shows that in the years after the eruption, global average column O_3 declined significantly (see also [24–26]). There is now a general consensus that this decrease in O_3 was causally linked to the injection of SO_2 into the stratosphere by Mount Pinatubo. In this chapter, we will discuss the theories about how this injection of SO_2 led to the reduction of stratospheric O_x. This exercise will demonstrate the subtlety and complexity that makes ozone such an interesting constituent.

It should be noted that volcanic perturbations to the stratosphere are not rare events but occur on average every few years [193]. Between 1984 and 1996, for example, there were at least three eruptions besides Mount Pinatubo that perturbed the stratosphere [194]. And just prior to that time frame, in March and April 1982, there was a major eruption of El Chichón (17.3°N), which is also believed to have reduced stratospheric O_3 [195].

6.1 Evolution of the Aerosol Surface Area from 1985 to 1997

As discussed in Chapter 2, a volcanic eruption can significantly increase the stratospheric aerosol surface area density (SAD) of the stratosphere. Figure 6.1 shows two views of the evolution of the lower stratospheric SAD between 1985 and 1997. Between 1985 and mid-1991 the lower-stratospheric SAD gradually decreased from ~3 to ~1 μm^2 cm^{-3} as the aerosol from the eruptions of El Chichón in 1982 and Nevado del Ruiz in November 1985 was flushed from the stratosphere. The eruption of Nevado del Ruiz can be seen in both parts of Figure 6.1 as the increase in the SAD in late 1985 and early 1986 over the equator. In mid-1991, Mount Pinatubo erupted, and the effects on the stratosphere were dramatic [196]. The aerosol SAD
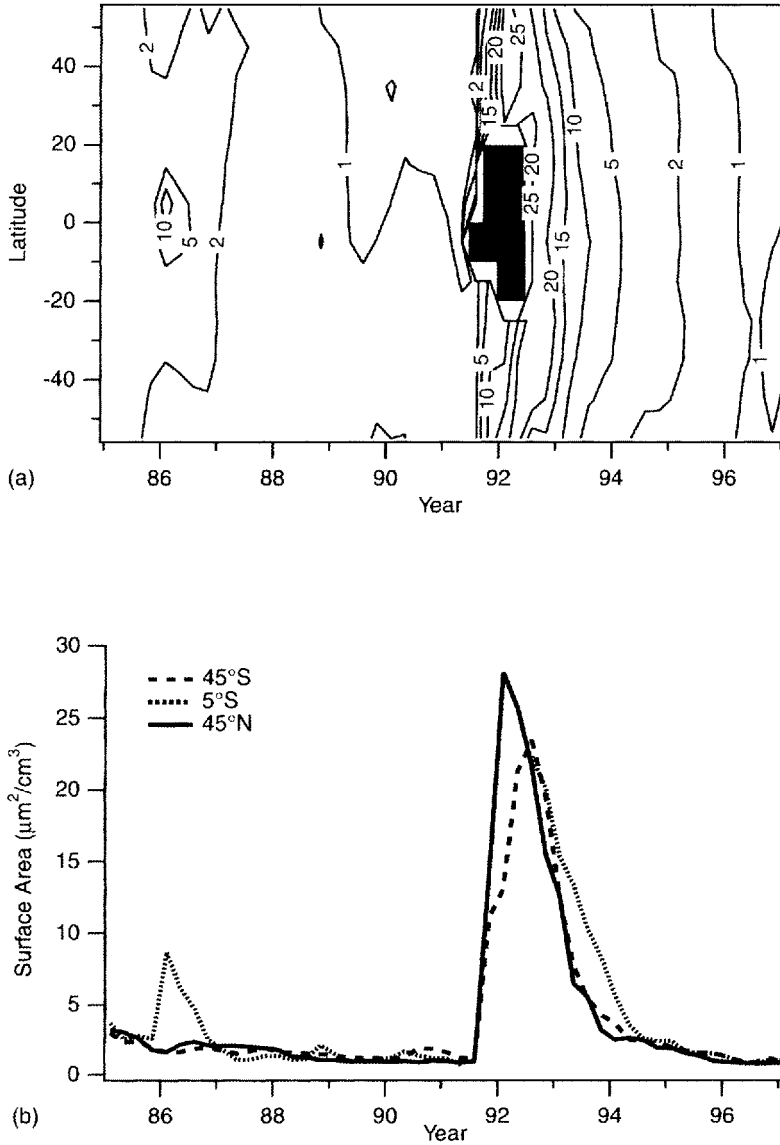
Figure 6.1 (a) Aerosol SAD (μm² cm⁻³) at 19.5 km. The black region in late 1991 and early 1992 indicates regions where aerosols were so thick that there were no measurements. (b) Time series of the aerosol SAD at 19.5 km for three different latitude bands. The data in both top and bottom plots are zonally and seasonally averaged [194]. The tick marks in the plots are January 1 of each year.

increased within months to about 30 times its abundance prior to the eruption [45]. In the years since the eruption, the aerosol SAD has decreased, and, by 1999, the aerosol SAD was nearing the background.

The maximum enhancement of the SAD from a volcanic eruption generally occurs in the lower stratosphere (e.g. see Figure 2.3) because the vast majority of the volcanic effluent is only energetic enough to reach this level of the stratosphere.

In addition to the changes in the aerosol SAD, the size distribution and the related properties of the particles (e.g. effective radius, optical depth) making up the aerosol cloud also varied after the eruption of Mount Pinatubo [48,197]. No other species of importance to stratospheric chemistry, in particular HCl, appear to have been injected into the stratosphere by the eruption [198,199].

6.2 Effect of an Increase in Aerosol Abundance

The increase in the aerosol SAD due to a volcanic eruption affects the chemistry, radiation field, and circulation of the stratosphere. We will discuss each effect in turn.

6.2.1 Chemical effects due to heterogeneous chemistry

As discussed in Chapter 2, the rate constant for the first-order loss of a constituent in a heterogeneous reaction can be written (Equation (2.21)):

$$k^{\text{H}} = \frac{VA\gamma}{4}$$

where V is the thermal velocity of the reactant molecule, A is the aerosol SAD, and γ is the reactive uptake coefficient (the fraction of collisions between X and the particle that result in a reaction).

The increase in the SAD following an eruption leads to an increase in the rate constants of the heterogeneous reactions. As we will show, this in turn leads to changes in the partitioning of the chemical families relative to the nonvolcanic state. If these changes include changes in the abundances of O_x-destroying radicals, then changes in the abundance of O_x may result. Finally, because the increase in SAD due to a volcano occurs primarily in the lower stratosphere, the major impact of heterogeneous chemistry occurs there.

N_2O_5 *hydrolysis*   The most important heterogeneous reaction in the stratosphere is the hydrolysis of N_2O_5. During the night, N_2O_5 is formed in the reaction between

NO_2 and NO_3 (reaction (4.41)). This N_2O_5 is subsequently converted to HNO_3 via hydrolysis (reaction (4.48)) [101]:

$$N_2O_5 + H_2O \xrightarrow{aerosol} 2HNO_3$$
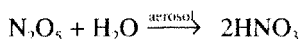
The increase in the aerosol SAD after volcanic eruptions increases the rate constant $k^H_{N_2O_5 + aerosol}$, which, in general, increases the rate at which N_2O_5 is hydrolyzed and HNO_3 is formed. Because the rate at which HNO_3 is converted back to NO_x is unchanged, the abundance of NO_x relative to HNO_3 decreases [116].

Figure 6.2 shows the $[NO_x]/[NO_y]$ ratio in the lower stratosphere as a function of the SAD in three different seasons. Consistent with our previous discussion, this figure shows that an increase in the SAD is generally accompanied by a decrease in the abundance of NO_x. Additionally, the abundance of NO_x (relative to NO_y) increases from winter to equinox to summer. This occurs because of the decreasing length of night (during which NO_x is converted to HNO_3 via N_2O_5 hydrolysis) and increasing photolysis rates of the NO_y reservoirs HNO_3, N_2O_5, and $ClONO_2$ (whose photolysis produces NO_x).

Interestingly, changing the aerosol SAD has the largest effect on the $[NO_x]/[NO_y]$ ratio at low SADs. Above ~5 μm^2 cm^{-3}, changes in the SAD have little effect on the NO_x/NO_y ratio [116,200]. Note that the background SAD in the lower stratosphere, ~1 μm^2 cm^{-3}, is in the region where the $[NO_x]/[NO_y]$ ratio shows a large sensitivity to changes in the SAD.

The small sensitivity to changes in the aerosol SAD seen in Figure 6.2 when the
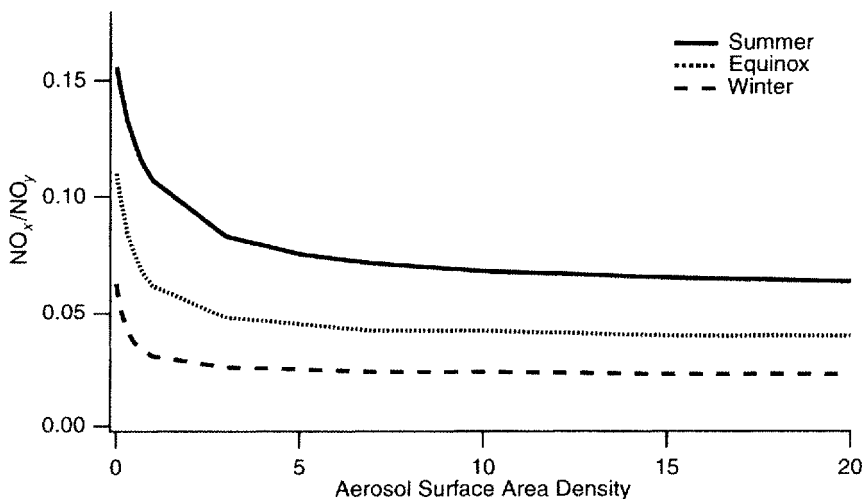
Figure 6.2 Daytime-averaged steady-state lower-stratospheric $[NO_x]/[NO_y]$ ratio versus the aerosol SAD (μm^2 cm^{-3}) from a model. Model run for 45°N, 220 K, and 50 hPa.

surface area is greater than ~5 μm^2 cm^{-3} is often referred to as "saturation"—i.e. the atmosphere is saturated with respect to N_2O_5 hydrolysis, so further increases in surface area have no effect on the NO_x abundance. Saturation occurs when the life-time of N_2O_5 with respect to hydrolysis ($1/H_2Ok^{II}_{N_2O_5+}$) is much shorter than the length of the night. When this is true, every N_2O_5 formed during the night is hydrolyzed to form HNO_3. In this case, the rate at which NO_x is converted to HNO_3 through hydrolysis is limited by the rate at which N_2O_5 is formed, and not by the rate of N_2O_5 hydrolysis. Additional SAD does not increase the rate of N_2O_5 formation, and therefore does not affect the rate of conversion of NO_x to HNO_3.

There is a subtle point here. The addition of aerosol SAD always increases the *rate constant* for the heterogeneous reaction. However, the rate of the reaction is the rate constant times the concentration of the reactant. For N_2O_5 hydrolysis, once sat-uration is reached, further increases in the rate constant are accompanied by decreases in the concentration of N_2O_5, so that the product of these is unchanged.

BrONO$_2$ hydrolysis Another hydrolysis reaction is the hydrolysis of BrONO$_2$ (reaction (4.87)):

$$BrONO_2 + H_2O \xrightarrow{aerosol} HOBr + HNO_3$$
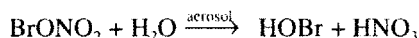
There are two fundamental differences between the hydrolysis of N_2O_5 and that of $BrONO_2$. First, because formation of N_2O_5 occurs only at night, the effectiveness of the hydrolysis of N_2O_5 increases as the length of the night increases. $BrONO_2$, on the other hand, is formed during the day. In air exposed to sunlight, the following cycle converts NO_x and H_2O to HNO_3 and OH:

$$BrONO_2 + H_2O \xrightarrow{aerosol} HOBr + HNO_3$$
$$HOBr + hv \longrightarrow OH + Br$$
$$Br + O_3 \longrightarrow BrO + O_2$$
$$BrO + NO_2 \xrightarrow{M} BrONO_2$$
$$\text{net: } NO_2 + H_2O + O_3 \longrightarrow HNO_3 + OH + O_2 \tag{6.1}$$
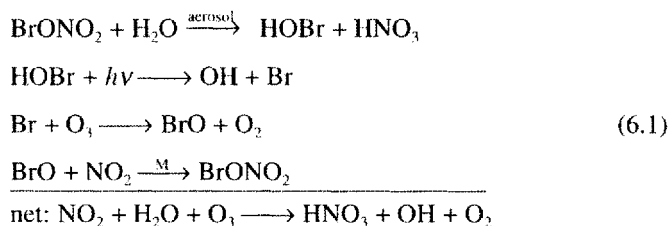
After sunset, photolysis ceases, bringing the cycle to a halt. As a result, the effec-tiveness of this cycle increases with the length of day.

Second, BrONO$_2$ hydrolysis cycle does not saturate with increasing aerosol abun-dance [102]. Assuming that BrONO$_2$ is in the photochemical steady state, we can write its abundance as

$$[BrONO_2] = \frac{k^*_{BrO+NO_2}[BrO][NO_2]}{J_{BrONO_2} + k^{II}_{BrONO_2+H_2O}} \tag{6.2}$$

Multiplying Equation (6.2) by $k^{H}_{BrONO_2+H_2O}$ yields an expression for $k^{H}_{BrONO_2+H_2O}[BrONO_2]$, which is the rate of reaction (4.87), the hydrolysis of $BrONO_2$:

$$k^{H}_{BrONO_2+H_2O}[BrONO_2] = \frac{(k^{*}_{BrONO_2+H_2O})k^{*}_{BrO+NO_2}[BrO][NO_2]}{J_{BrONO_2} + k^{H}_{BrONO_2+H_2O}} \qquad (6.3)$$

Since $J_{BrONO_2} \gg k^{H}_{BrONO_2+H_2O}$, the denominator $J_{BrONO_2} + k^{H}_{BrONO_2+H_2O} \approx J_{BrONO_2}$ and the rate of $BrONO_2$ hydrolysis scale linearly with the rate constant $k^{H}_{BrONO_2+H_2O}$—which, as we discussed previously, is linearly proportional to the aerosol SAD. It should be noted that the condition $J_{BrONO_2} \gg k^{H}_{BrONO_2+H_2O}$ is satisfied even for the high aerosol SAD found after the eruption of Mount Pinatubo [102].

Thus, the importance of the hydrolysis of $BrONO_2$ increases with increasing length of day and with increasing aerosol SAD. This can be contrasted with the hydrolysis of N_2O_5, which becomes less important as the exposure to sunlight by an air mass increases and exhibits a saturation condition where continued addition of aerosol abundance does not increase the rate of N_2O_5 hydrolysis.

Low-temperature heterogeneous reactions The hydrolysis reactions of N_2O_5 and $BrONO_2$ have large, temperature-independent reactive uptake coefficients ($\gamma_{N_2O_5+H_2O} \approx 0.1$, $\gamma_{BrONO_2+H_2O} \approx 0.8$), and therefore can be important under many conditions. There are several other reactions that occur in/on sulfate aerosols, but are important only at cold temperatures:

$$ClONO_2 + H_2O \xrightarrow{\text{aerosol}} HOCl + HNO_3 \qquad (6.4)$$

$$ClONO_2 + HCl \xrightarrow{\text{aerosol}} Cl_2 + HNO_3 \qquad (6.5)$$

$$HOCl + HCl \xrightarrow{\text{aerosol}} Cl_2 + H_2O \qquad (6.6)$$

$$HOBr + HCl \xrightarrow{\text{aerosol}} BrCl + H_2O \qquad (6.7)$$
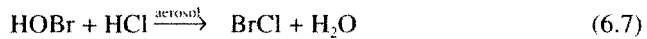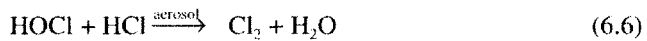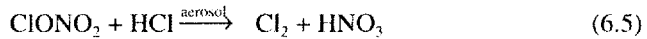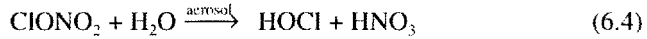
These four reactions convert chlorine from the long-lived reservoir species HCl and $ClONO_2$ to the more labile species Cl_2, HOCl, and BrCl. When exposed to sunlight, Cl_2, HOCl, and BrCl are rapidly photolyzed to produce Cl_x. Thus, all of these reactions increase the abundance of Cl_x at the expense of Cl_y reservoir species. The reactions involving $ClONO_2$ also produce the less labile species HNO_3, which reduces NO_x.

Figure 6.3 shows the reactive uptake coefficients γ for reactions (6.4)–(6.7) as functions of temperature for typical lower stratospheric conditions. In general, the reactive uptake coefficients γ are functions of water vapor abundance, particle radius, ambient pressure, and the abundance of other trace species [29,33]. As one can see, the reactive uptake coefficients for these reactions are strongly temperature-
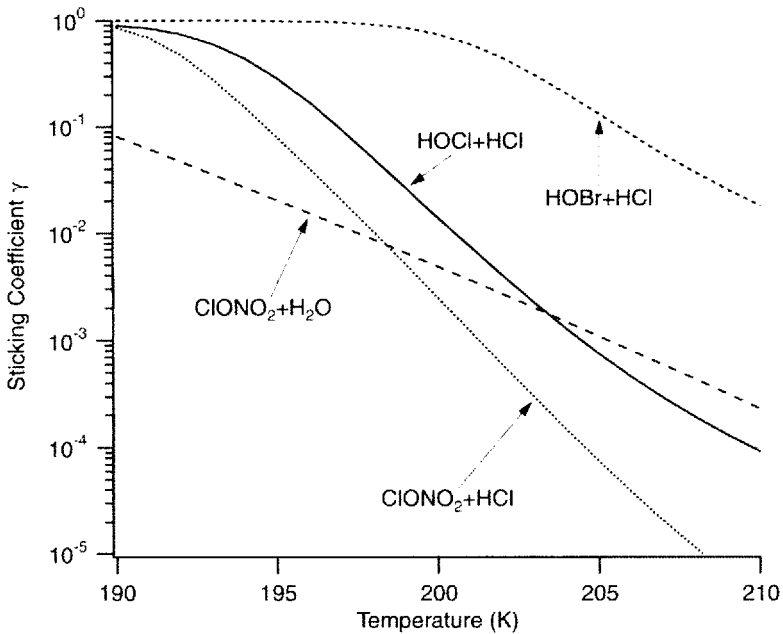
Figure 6.3 Reactive uptake coefficients γ for various reactions of stratospheric importance as a function of temperature. γ is for first-order loss of $ClONO_2$, HOCl, and HOBr. Conditions are typical of the lower stratosphere: 60 hPa, 5 ppmv H_2O, and aerosol radius 0.2 µm. [HCl] is 1.5 ppbv, except for the $ClONO_2+H_2O$ reaction, where [HCl] is zero. The $ClONO_2+HCl$ and $ClONO_2+H_2O$ formulations are from Hanson and Ravishankara [30] and Hanson [201], the HCl+HOCl formulation is from Donaldson *et al.* [202], and the HCl+HOBr formulation is from D. R. Hanson (personal communication, 1998).

dependent. At temperatures typical of the lower stratosphere (> 210–220 K), these reactions have reactive uptake coefficients that are so small that the reactions are negligible. At extremely low temperatures (below ~200 K), such as those found in the lower stratosphere at high latitudes in winter, these reactions have reactive uptake coefficients that are large enough for the reactions to become important. For temperatures between these extremes (200–210 K), the reactive uptake coefficients are such that these reactions are negligible for the background SAD, but potentially important for an enhanced SAD, such as that found immediately after a volcanic eruption.

Net effect of the increase in heterogeneous reaction rates The primary direct result of the eruption of Mount Pinatubo was the decrease in the abundance of NO_x in the lower and mid-stratosphere compared to the pre-eruption atmosphere

[46,106,107,116,200,203]. Because the partitioning of each chemical family generally depends on the partitioning of other chemical families, this direct effect led to changes in the partitioning of the other chemical families.

Let us first investigate the effect of changing NO_x on Cl_y, with all other atmospheric parameters fixed. Cl_y is almost entirely composed of the species $ClONO_2$, HCl, and Cl_x. Because of the short lifetimes of Cl_x and $ClONO_2$ compared to HCl, a change in NO_x initially drives changes in Cl_x and $ClONO_2$, and a new equilibrium between these two species is established within a few hours. Assuming the photochemical steady state, the relative abundance of Cl_x and $ClONO_2$ can be written as

$$\frac{[Cl_x]}{[ClONO_2]} \approx \frac{[ClO]}{[ClONO_2]} = \frac{J_{ClONO_2}}{k^*_{ClO+NO_2}[NO_2]} \tag{6.8}$$

Note that this ratio is proportional to $1/[NO_2]$. Assuming that the reduction in NO_x leads to a reduction in NO_2, Cl_x will increase at the expense of $ClONO_2$. This inverse relationship has been verified by observations [70]. It should be noted that because the abundance of $ClONO_2$ in the lower and mid-stratosphere is 5–20 times the abundance of ClO, large fractional increases—e.g. factors of 2–3—in ClO are accompanied by small fractional changes in the abundance of $ClONO_2$.

On time-scales longer than the lifetime of HCl (weeks in the lower stratosphere), the abundance of HCl adjusts to the reduced abundance of NO_x and the new partitioning between ClO and $ClONO_2$. As discussed in Chapter 4, HCl is produced primarily from the reaction between Cl and CH_4 (reaction (4.11)) and is destroyed by the reaction between HCl and OH (reaction (4.16)). Assuming photochemical steady state, the abundance of HCl is therefore a function of the OH, CH_4, and Cl abundances:

$$[HCl] = \frac{k_{CH_4+Cl}[CH_4][Cl]}{k_{HCl+OH}[OH]} \tag{6.9}$$

Note that the assumption of the photochemical steady state for HCl is not necessarily correct owing to the long lifetime of HCl in the lower stratosphere (weeks). We expect, however, that Equation (6.9) gives an accurate indication of how [HCl] will, on average, change as the abundance of other constituents changes.

According to Equation (6.9), the abundance of HCl is proportional to the abundance of Cl atoms. As discussed above, the abundance of Cl_x is proportional to $1/[NO_2]$, so the decrease in NO_2 causes the abundance of Cl_x to increase. At the same time, however, the decrease in NO_x changes the partitioning between Cl and ClO. Equation (4.9) says that [Cl]/[ClO] is proportional to [NO]; so while Cl_x is increasing, the decrease in NO_x also causes Cl to make up a smaller component of Cl_x. If

the ratio of [NO] to [NO$_2$] remains fixed, then these two effects cancel, and [Cl] remains unchanged.

In the lower and mid-stratosphere the ratio [NO]/[NO$_2$] (Equation (4.39)) can be approximated:

$$\frac{[NO]}{[NO_2]} = \frac{J_{NO_2}}{k_{NO+O_3}[O_3]} \qquad (6.10)$$

If there is no change in O$_3$ or J_{NO_2}, the ratio [NO]/[NO$_2$] will be unchanged by a reduction in NO$_x$. Thus, the abundance of Cl atoms will remain unchanged—despite a significant increase in Cl$_y$. Reiterating, this occurs because the increase in [Cl$_y$] = [ClO] + [Cl] driven by the decrease in NO$_2$ is exactly compensated for by a decrease in the [Cl]/[Cl$_y$] ratio driven by the decrease in NO. Because [Cl] does not change, we expect little change in [HCl] from the direct effect of decreases in NO$_x$.

Thus, a reduction in NO$_x$, holding everything else constant (OH, CH$_4$, and O$_3$, rate constants, photolysis frequencies), increases Cl, at the expense of ClONO$_2$, while leaving HCl unchanged. In reality, of course, the response of Cl$_y$ partitioning will depend on the changes in all of the geophysical parameters. It turns out, however, that the decrease in NO$_x$ is the dominant effect and can explain most of the changes in the partitioning of Cl$_y$.

Observations verify that the eruption of Mount Pinatubo in 1991 did indeed have a dramatic effect on the partitioning of Cl$_y$. Concomitant with the decrease in NO$_x$, ClO (which accurately approximates Cl$_x$) was observed to increase [46,70,116,204], with little change observed in HCl [205]. Models [206–209] estimate that, in the years following the eruption of Mount Pinatubo, Cl$_x$ increased by thirty to several hundred percent, depending on the latitude, time of year, and aerosol abundance.

Next we turn to the HO$_x$ family. We saw in Chapter 4 how the hydrolysis of N$_2$O$_5$ and BrONO$_2$ followed by the photolysis of HNO$_3$ produces HO$_x$ (cycles (4.55) and (4.56)). The increase in the aerosol SAD after a volcanic eruption therefore leads to an increase in the rate of HO$_x$ production, which tends to increase the HO$_x$ abundance. The increase in production rate due to hydrolysis reactions can be significant: at high surface areas, production of HO$_x$ from the hydrolysis of BrONO$_2$ competes with the direct gas phase oxidation of H$_2$O (reaction (4.54)) [102]. Additionally, the decrease in NO$_x$ slows the loss of HO$_x$ due to formation of HNO$_3$ (reaction (4.42)), which further tends to increase HO$_x$. Models [206–208] estimate that, in the years following the eruption of Mount Pinatubo, HO$_x$ increased by 20–100%, depending on the latitude, time of year, and aerosol abundance.

In addition to affecting the total abundance of HO$_x$, NO$_x$ also plays a role in partitioning HO$_x$. Equation (4.66) indicates that the ratio [OH]/[HO$_2$] is proportional to the abundance of NO, so a reduction of NO leads to increased HO$_2$ relative to OH, an effect verified by lower-stratospheric observations of HO$_x$ [74]. This is potentially

important because it is the HO_2 radical that rate limits the most important O_x loss cycles: increasing HO_2 at the expense of OH will increase the loss rate of O_x attributed to HO_x chemistry. It should be noted, however, that because the abundance of HO_2 generally exceeds OH by a factor of 5, significant increases in the ratio are accompanied by modest increases in the absolute abundance of HO_2.

The net effect of heterogeneous chemistry on odd-oxygen abundance   As we have discussed several times, the total loss rate of O_x is twice the sum of the rates of the catalytic cycles. For the NO_x catalytic cycle the rate of O_x loss is proportional to the abundance of NO_x. The increase in the aerosol SAD leads to a reduction in NO_x and therefore a decrease in the loss rate of O_x due to the NO_x cycle. This same reduction in NO_x, however, leads to an increase in the rate of O_x loss due to the Cl_x and HO_x catalytic cycles. These two effects oppose each other, and the sign as well as the magnitude of the net effect depends on which of these changes is largest.

In the case of the eruption of Mount Pinatubo, in the lower stratosphere the increase in the rates of the Cl_x and HO_x catalytic cycles dominated the decrease in the rate of the NO_x catalytic cycle [74]. As a result, the total O_x loss rate increased with decreasing NO_x, leading to a decrease in lower-stratospheric O_x. In the mid-stratosphere, on the other hand, the decrease in NO_x dominated the increase in Cl_x and HO_x. As a result, the total O_x loss rate decreased with decreasing NO_x, leading to an increase in mid-stratospheric O_x [203]. This is shown schematically in Figure 6.4.

Because the abundance of NO_x is very sensitive to changes in the SAD when the
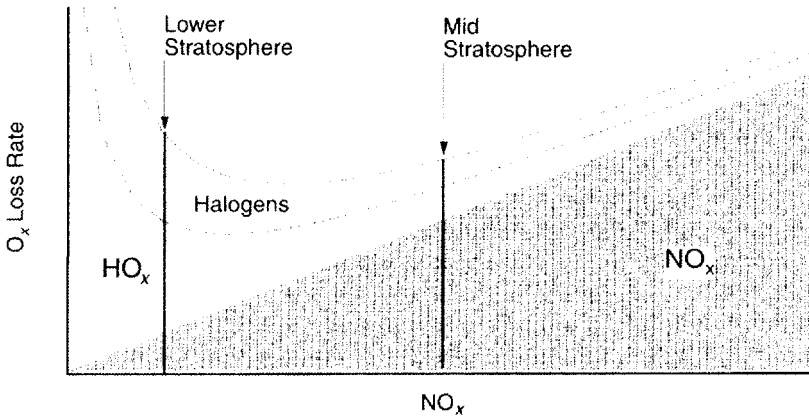
Figure 6.4 Schematic of the contributions of the various catalytic cycles to the rate O_x loss as a function of NO_x abundance. The solid vertical lines represent the situations in the lower and mid-stratosphere. (Modified from Wennberg *et al.* [74], Figure 7.)

SAD is near background amounts, even small increases in the SAD above background can lead to important changes in the chemistry of the stratospheric O_x. As a result, an energetic volcanic eruption like Mount Pinatubo can perturb the heterogeneous chemistry of the stratosphere over almost the entire globe. And the chemistry will remain perturbed until the SAD is back to near background, which takes several years.

Finally, it should be pointed out that the response of the atmosphere to Mount Pinatubo was possibly unique in the history of the Earth. It has been argued that for stratospheric total chlorine abundances consistent with only natural sources—about 0.6 ppbv—the decrease in O_x loss caused by the decrease in NO_x would have dominated increases in HO_x and Cl_x [210]. As a result, O_x would have increased throughout the stratosphere after a Pinatubo-like eruption.

6.2.2 Effects due to changes in photolysis rates

In addition to modifying heterogeneous chemistry, aerosols also absorb and scatter ultraviolet, visible, and infrared radiation. Thus, a change in the number, composition, or sizes of aerosol particles can modify the radiation field of the atmosphere [211,212]. This can lead to changes in the photolysis frequencies of molecules in the stratosphere, leading to changes in the chemical composition of the stratosphere. For Mount Pinatubo, the greatest impact was in the tropics, where the SO_2 was injected, and immediately after the eruption, before the cloud had a chance to disperse. After about a year, the aerosol cloud was sufficiently dispersed that it had a negligible effect on the photolysis frequencies.

In the tropical lower and mid-stratosphere, abundances of NO_x, Cl_x, and Br_y are low. Consequently, the most important photolysis frequencies are J_{O_2} and J_{O_3}, the dissociation frequencies of O_2 (reaction (3.1)) and O_3 (reaction (3.4)), respectively. After the eruption, J_{O_2} decreased by a few tens of percent in the lower stratosphere as a result of direct and diffusive beam attenuation due to the aerosol cloud [213]. This slowed the production of O_x, which tended to decrease the abundance of lower- and mid-stratospheric O_x.

J_{O_3}, the photolysis frequency of O_3, on the other hand, increased by several percent in the lower stratosphere. This increase occurs because the peak O_3 absorption occurs at wavelengths longer than ~250 nm, where multiple scattering plays an important role in distributing the solar radiation. At these wavelengths the increase in scattered radiation due to the aerosol particles dominates the attenuation of the direct beam by the aerosol particles [213]. The increase in J_{O_3} increases the abundance of O atoms, which increases the rate of destruction of O_x. This in turn tends to decrease the abundance of O_x.

Thus, changes in J_{O_2} and J_{O_3} both tend to decrease O_x in the lower and mid-stratosphere.

6.2.3 Changes in the circulation of the atmosphere

Another consequence of the perturbation of the radiation field by aerosols can be seen in Figure 6.5. This figure shows clearly that the aerosols from the Mount Pinatubo and El Chichón eruptions caused a rise in the temperature of the lower stratosphere [214,215] (Figure 6.5). This warming is collocated with the volcanic cloud, so for both El Chichón and Mount Pinatubo most of the warming took place at low latitudes.

This heating resulted in a strengthening of the Brewer–Dobson circulation— enhanced rising motion in the tropics and enhanced downwelling at mid- and high latitudes [209,214–216]. As discussed in the last chapter, the circulation of the stratosphere plays an important role in determining the distribution of stratospheric O_x. Changes in the circulation can therefore be expected to effect the distribution of stratospheric O_x.

In the tropical lower stratosphere, the air has low abundances of NO_y, Cl_y, and Br_y, so chemical loss of O_x is negligible compared to production and transport (see Figure 5.14). Horizontal transport can be neglected because of a combination of weak horizontal mass transport into the tropics [182,184] combined with the small horizontal gradient of O_x. It should be noted that for some species, such as N_2O or F11,
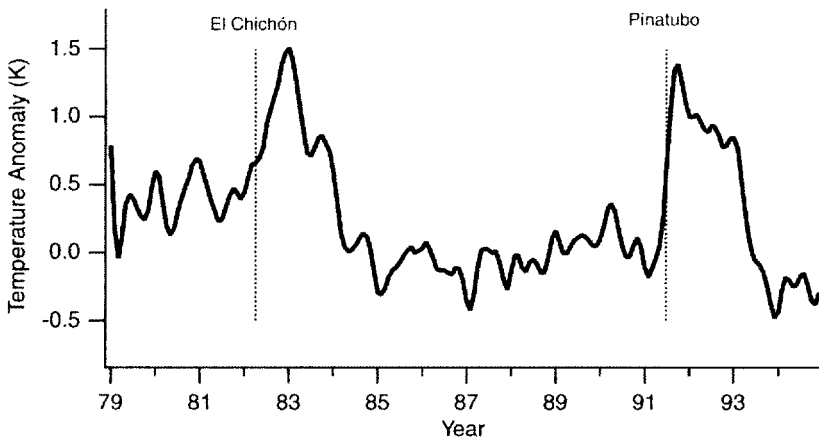
Figure 6.5 Globally integrated (65°S–N) and area-weighted temperature anomaly in the MSU channel 4 data, which provide a measure of the weighted mean temperature in the 150–50 hPa layer. The anomaly is calculated as differences from a seasonally varying pre-Pinatubo average calculated over the 4 years 1987–1990. The dotted lines marked "El Chichón" and "Pinatubo" show the times of the eruptions. Quasi-biennial oscillation effects have been removed. (Adapted from Randel *et al.* [25], Figure 15, but using updated MSU data W. J. Randel, F. Wu, personal communication, 1998.) Tick marks represent January 1 of each year.

the gradient between the tropics and mid-latitudes is large enough that horizontal transport cannot be neglected [182].

Based on this, O_x in the tropical lower stratosphere (below ~24 km altitude) can be modeled simply. We can write the continuity equation for O_x in this region [217] as

$$\frac{\partial[O_x]}{\partial t} = P_{O_x} - w\,\frac{\partial[O_x]}{\partial z} \qquad (6.11)$$

where P_{O_x} is photochemical production rate and w is the vertical velocity. Assuming production is unchanged, at steady state an increase in vertical velocity w will be accompanied by a decrease in the vertical gradient of O_x ($\partial[O_x]/\partial z$). Assuming that $[O_x]$ at the tropopause does not change, a decrease in the vertical gradient means that there is less O_x at each altitude above it [217]. Thus, the strengthening of the Brewer–Dobson circulation decreased column O_3 in the tropics [215,218].

At mid- and high latitudes the O_x abundance is set by the more complicated interplay between production, loss, and transport. Model simulations indicate that the increasing strength of the Brewer–Dobson circulation after the eruption of Mount Pinatubo led to the transport of more O_x into these regions, leading to an increase in column O_3 [207,209,214,216].

6.3 The Net Effect

The net change of O_x following a volcanic eruption is determined by the combination of the three effects discussed in this chapter: the increase in the rate of heterogeneous reactions, changes in the photolysis frequencies, and changes in the circulation of the stratosphere.

The dominant effect is the increase in the rate of heterogeneous reactions. Models [207–209] suggest that this effect by itself led to significant decreases of O_x after the eruption of Mount Pinatubo (as well as after El Chichón [195]). The effect is most pronounced at mid- and high latitudes during the winter and early spring. Here the enhancement of N_2O_5 hydrolysis is most effective because of the long nights found there.

Additionally, in regions of cold temperatures (high latitude, wintertime, lower stratosphere), the heterogeneous chlorine reactions (reactions (6.4) to (6.7)) become important due to the enhanced SAD. These reactions convert the relatively unreactive Cl_y reservoir species HCl and $ClONO_2$ into more easily photolyzed species such as Cl_2 and HOCl, thereby increasing Cl_x.

Models predict that the heterogeneous-chemistry perturbation alone reduced lower stratospheric O_x by 20–40% at mid- and high latitudes during winter and early spring, leading to a ~10% decrease in column O_x. At other times of year,

extratropical column decreases were a few percent. In the tropics, the heterogeneous-chemistry perturbation had little effect, consistent with the general lack of importance of chemical loss for O_x in this region. Predicted changes in tropical column O_x from the heterogeneous-chemistry perturbation were a percent or less throughout the year.

The models predict that the effect from changes in the photolysis frequencies is small. The maximum effect occurs in the tropics, where changes in the photolysis frequencies decreased column O_3 by at most a percent or so.

Finally, the models predict that changes in the strength of the stratospheric circulation reduced column ozone in the tropics by a few Dobson units, i.e. a few percent. This low-latitude decrease is accompanied by an increase in extratropical O_x of about the same magnitude.

Column O_3 measurements do indeed show substantial decreases in column ozone (of the order of 5–10%) over large regions of the globe following the eruption of Mount Pinatubo (Figure 6.6) [25]. The largest losses were observed in northern hemisphere middle and high latitudes during winter–spring of each year (largest in 1992–1993), over southern hemisphere high latitudes in spring 1993, and episodically over the tropics during 1991–1993. In general, these changes are consistent with model simulations of the post-Mount Pinatubo stratosphere.
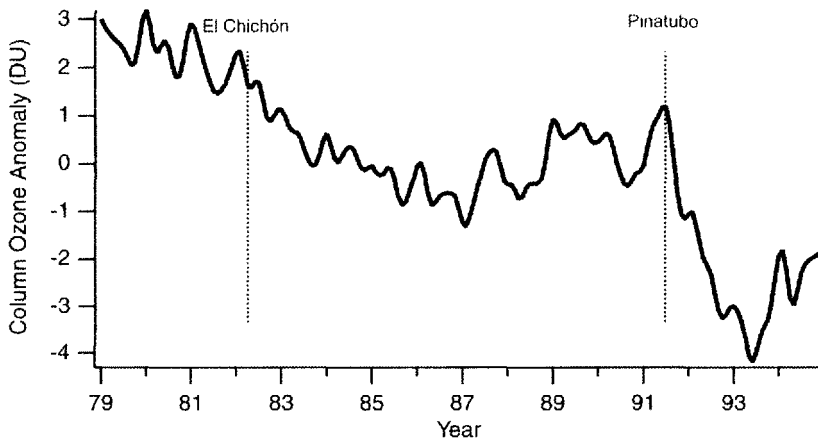
Figure 6.6 Globally integrated (65°S–N) and area-weighted TOMS column ozone anomaly. The anomaly is calculated as differences from a seasonally varying pre-Pinatubo average calculated over the 4 years 1987–1990. The dotted lines marked "El Chichón" and "Pinatubo" show the times of the eruptions. QBO effects have been removed. (After Randel *et al.* [25], Figure 15.)

Problems

1. Would a volcano erupting at high latitude have as significant global effect on stratospheric chemistry as one erupting near the equator?

2. Because $J_{BrONO_2} \gg k^{II}_{BrONO_2 + H_2O}$, the rate of $BrONO_2$ hydrolysis scales linearly with aerosol surface area density. How would it scale if $J_{BrONO_2} \ll k^{II}_{BrONO_2 + H_2O}$?

3. In steady state the abundance of HCl is proportional to the abundance of Cl atoms. Derive the ratio $[Cl]/([Cl_x] + [ClONO_2])$ in terms of rate constants, photolysis frequencies, and the abundances of other trace species. Assume steady state applies. How do you expect HCl to change if NO_x changes (you can assume the ratio $[NO]/[NO_2]$ does not change)?

4. It turns out that the reactive uptake coefficients for reactions (6.4)–(6.7) increase with increasing water vapor abundance. If water vapor were to increase (but other geophysical parameters remained the same), would that make a Pinatubo-like eruption have a greater or lesser impact on stratospheric O_x? Explain your answer.

Chapter 7 | Polar Chemistry

7.1 The Antarctic

The discovery of the Antarctic "ozone hole" by Farman *et al.* [12] was a watershed in atmospheric science. Prior to this discovery, the idea that human activity could affect stratospheric O_3 was theoretical and the effect was expected to be relatively small. In the years after the discovery, it was firmly established that chemical compounds emitted by human activities at the Earth's surface could cause spectacular changes of stratospheric O_3. In this chapter, we will discuss the scientific evidence linking the emission of chlorofluorocarbons (CFCs) at the surface with winter and springtime ozone loss in the high latitudes of both hemispheres.

7.1.1 Observations

The term "Antarctic ozone hole" refers to the annual decrease of column O_3 at high southern latitudes in late winter and early spring. Its formation follows a similar pattern every year. Starting in mid-August, corresponding to the return of sunlight to the polar region, a region of low column O_3 develops, centered approximately over the South Pole. In subsequent weeks, the area and depth of the low column O_3 region increases, reaching a maximum in early to mid-October. Thereafter, column O_3 increases, leading to a reduction in the size of the low-O_3 region. By the beginning of December, column O_3 is approximately back to normal, and the ozone hole is gone until the next year.

Figure 7.1 shows the area of the Antarctic ozone hole as a function of time. In 1980, the area of the ozone hole was small; in fact, it is generally agreed that the Antarctic ozone hole did not exist prior to the late 1970s. By the mid-1990s the ozone hole covered ~25 million km^2, or about 10% of the area of the southern hemisphere. The uncertainty in the data in Figure 7.1 is quite small; year-to-year fluctuations in the area are caused by year-to-year meteorological variability.

One can also measure the "depth" of the ozone hole—how low the column O_3 gets within this region of low O_3. Figure 7.2 shows a time series of October-average Antarctic column O_3. Prior to the mid- to late 1970s, high-latitude column ozone was
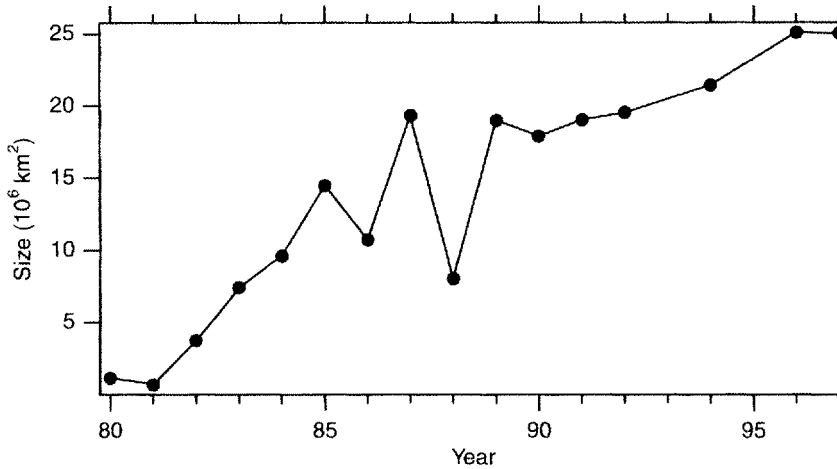
Figure 7.1 Area of the Antarctic ozone hole between October 1 and October 15 of each year versus year. By convention, the size of the ozone hole is defined to be the average area enclosed by the 220 DU contour. Column O_3 data are version 7 TOMS data.

above 300 DU in October. During the 1980s and 1990s, column O_3 decreased rapidly. By the mid-1990s, column O_3 in this region was only about one-third of its 1950–1960s value.

Figure 7.2 also shows that the increases in size and depth of the Antarctic ozone hole correspond well with the growth of the tropospheric abundance of CFC F11 (CCl_3F), which is a primary contributor to stratospheric Cl_y. Farman *et al.* [12] used this correlation to suggest correctly that the ozone hole was the result of the build-up of chlorine in the stratosphere.

Figure 7.3 show the anatomy of the Antarctic ozone hole. The distribution of early spring ozone shows the same overall shape in all years: there is a maximum in column ozone around 55°S (the "subpolar maximum"), with column ozone decreasing toward the pole. This overall distribution, a subpolar maximum surrounding a polar minimum, is caused by the circulation of the southern hemisphere and is not related to O_3 chemistry.

In October 1979, considered representative of the atmosphere prior to the ozone hole, the subpolar maximum in the column O_3 is ~370 DU, while the polar minimum is ~300 DU. By the mid-1990s, the subpolar maximum had decreased little, if any, but the polar minimum had decreased to 150–170 DU, a decrease of nearly 50%. And individual measurements of column ozone of ~100 DU or less were observed [14]. Thus, we see that the Antarctic ozone hole is a deepening of an already existing polar ozone minimum.
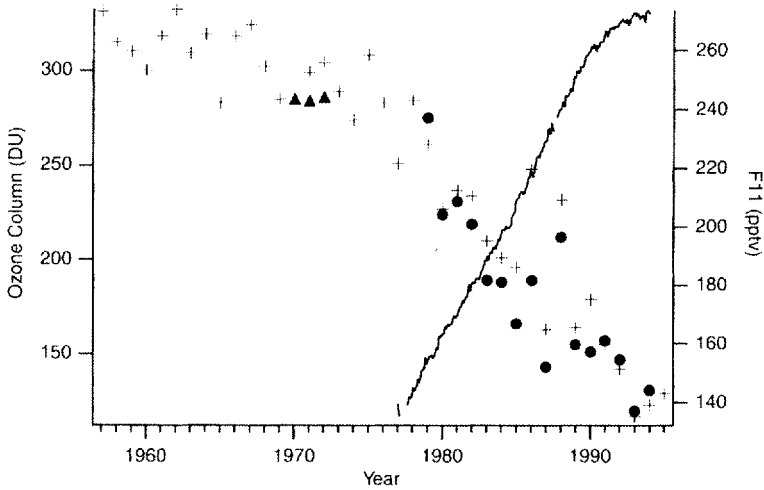
Figure 7.2 High-latitude southern hemisphere column O_3 observed in October versus year. Solid symbols are satellite measurements, and are the value of the minimum grid point of the October monthly average column O_3 fields. Circles are Nimbus 7 and METEOR TOMS; triangles are Nimbus 4/BUV. Crosses are the October averages from the British Antarctic Survey's Dobson instrument at Halley Bay. The solid line is global average tropospheric F11 (CCl_3F) abundance (from NOAA CMDL).
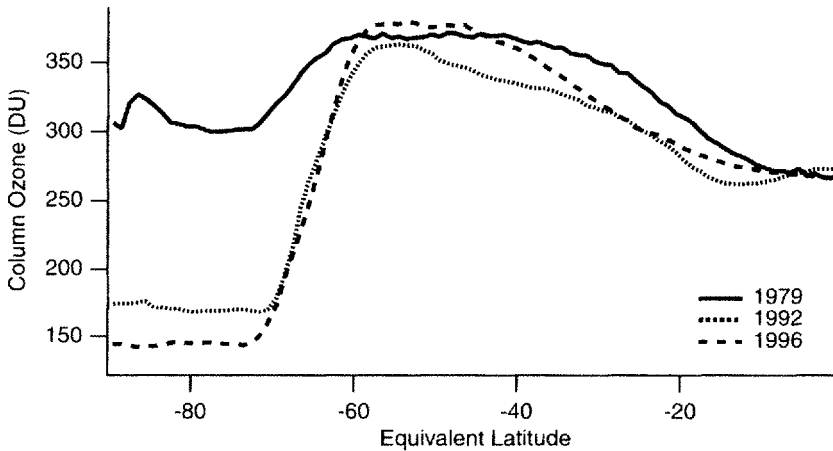
Figure 7.3 Column O_3 versus equivalent latitude averaged over October 1 to 15, 1979, 1992, and 1996. Equivalent latitude is calculated from NCEP balanced winds on the 465 K potential temperature surface. Column O_3 measurements are version 7 Nimbus 7/TOMS data for 1979 and 1992 and EPTOMS data for 1996.

In the rest of this chapter we discuss the physical processes that lead to the formation of the ozone hole. We will initially focus on the Antarctic, and then turn our attention to polar O_3 loss in the Arctic.

7.1.2 The vortex

The first step in the formation of the Antarctic ozone hole is the formation of the polar vortex [187]. During the winter the Antarctic region experiences 24 h of darkness every day. There is no heating by absorption of solar ultraviolet radiation during this time. Emission of thermal radiation, however, continues, causing the Antarctic lower stratosphere to cool (Figure 7.4). The resulting cold polar temperatures coupled with relatively warm temperatures in the mid-latitudes causes a strong pressure gradient to form between the polar and mid-latitude regions. Because of the coriolis force, this north–south pressure gradient creates a zonal (east–west) wind.

Figure 7.5 shows contours of the zonal wind velocity. Note the region of high wind velocities near 60°S. Such a region of high wind velocity is often referred to as a "jet", and the jet near 60°S is known as the "polar night jet". The polar night jet extends vertically from about 100 hPa to the upper stratosphere, reaching a
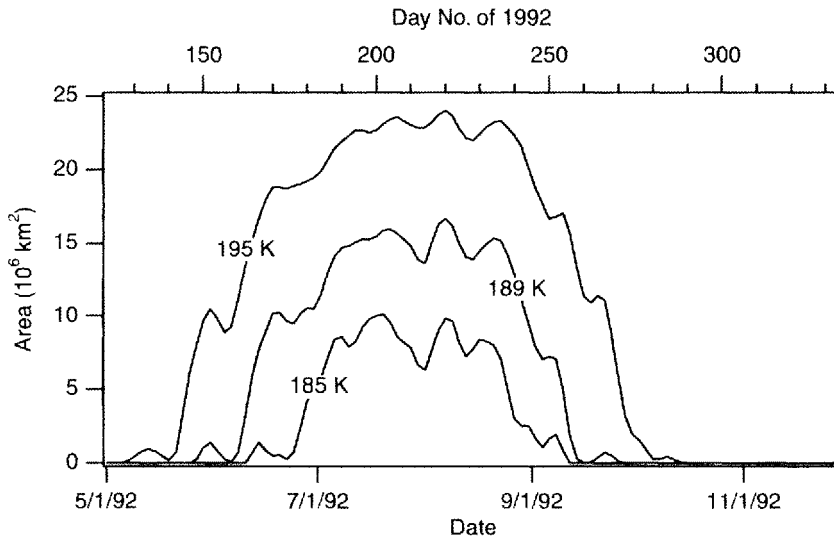
Figure 7.4 Area covered by temperatures less than 195, 189, and 185 K at 465 K potential temperature (~20 km) in the southern hemisphere. Temperatures are from the UKMO assimilation system.
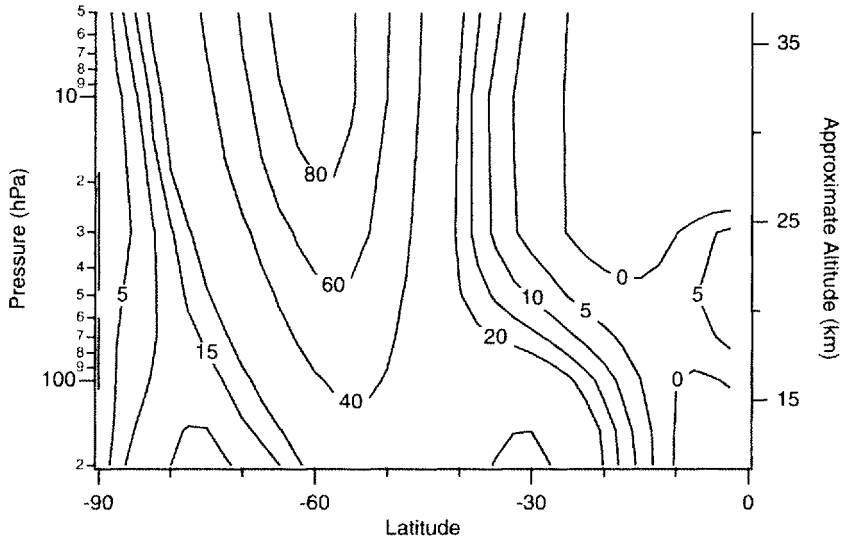
Figure 7.5 Contours of the zonal average of the zonal wind velocity (m s^{-1}) on August 21, 1995. Positive values represent westerly winds. Winds are from the UKMO assimilation system.

maximum velocity of nearly 100 m s^{-1} in the middle stratosphere between 30 and 35 km.

The term "polar vortex" refers to the region poleward of the polar night jet. Scientific analyses of the vortex, however, generally use a definition of the vortex edge based on the maximum gradient in potential vorticity (PV) [219]. This definition is superior to a definition based on maximum wind speed because PV is conserved by atmospheric transport (on time-scales of a month or less) in a manner similar to trace gases. Thus, defining the vortex using PV better captures the effects of vortex isolation on the trace gas distribution. In 1992, the Antarctic polar vortex covered ~35 million km^2, encompassing virtually all of the southern hemisphere poleward of about 60°S. While the vortex is subject to normal meteorological variability, there is no evidence that the overall properties of the Antarctic polar vortex have changed over the last 18 years.

It is important to note that the polar vortex and the Antarctic ozone hole are different entities. The ozone hole is the region covered by low values of column O_3, while the polar vortex is defined by the meteorological conditions. Between 1980 and 1996 the area covered by the polar vortex remained roughly constant. During this same time the size of the Antarctic ozone hole increased dramatically (see Figure 7.1). By the mid-1990s the ozone hole covered about two-thirds of the vortex. As we will discuss, the increase in areal extent of the ozone hole is due almost

entirely to the increase in stratospheric chlorine over this time period, and not to changes in meteorology [220].

The Antarctic polar vortex has two important properties without which the formation of the Antarctic ozone hole would not occur. First, the temperatures in the vortex are cold (see Figure 7.4). This allows the formation of polar stratospheric clouds (PSCs), which play a pivotal role in the chemistry of the ozone hole. We will discuss PSCs in detail in the next section. Second, as mentioned in Chapter 5, the edge of the polar vortex is a mixing barrier that isolates the Antarctic polar stratosphere from the mid-latitudes over the altitude range between ~425 and ~1000 K (~18 and 35 km) [186,188,221,222]. To show the isolation of the vortex, in Figure 7.6 we plot O_3 measured on the 465 K potential temperature surface (~20 km, in the lower stratosphere) as a function of equivalent latitude. There is a strong gradient in ozone collocated with the edge of the polar vortex at 60°S. A strong gradient in a constituent with a lifetime of weeks or longer can be maintained only if mixing is slow; otherwise, mixing would wipe out the gradient.

As we will show, the chemical composition of the polar vortex is very different from the chemical composition of the mid-latitudes. As a result, the isolation of the vortex from mid-latitude air is crucial for the development and maintenance of the Antarctic ozone hole. Without it, mixing of polar vortex and mid-latitude air would short circuit O_3 loss, and prevent the formation of the whole.
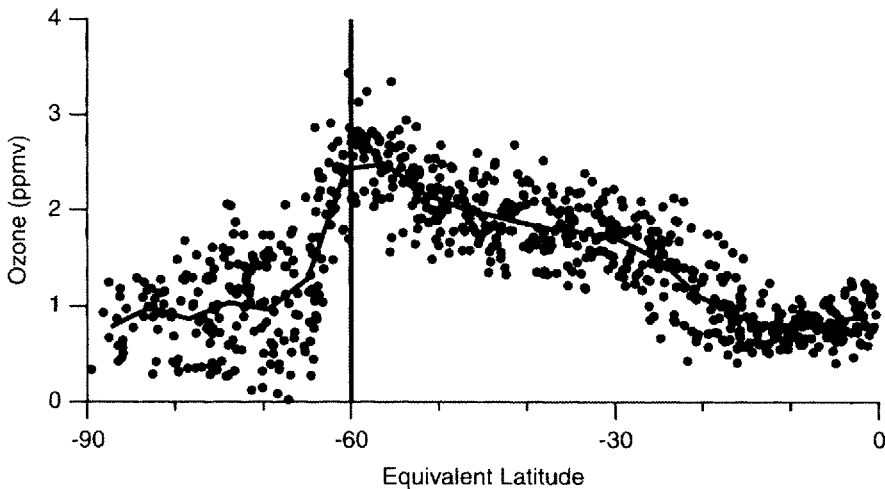
Figure 7.6 Ozone abundance versus equivalent latitude on the 465 K potential temperature surface for September 15, 1992. Dots are individual measurements, and the solid line is an average of the data. Equivalent latitude is derived from UKMO PV. The vertical line denotes the edge of the vortex, as determined by the Nash *et al.* [219] algorithm. Ozone data are from the 205 GHz channel of the UARS MLS (version 4).

While horizontal transport into the Antarctic polar vortex is negligible between ~425 and ~1000 K (18 and 35 km), vertical descent within the vortex does occur [186,221,223,224]. This descent is attributable to the mean overturning circulation of the stratosphere, which features air descending at mid- and high latitudes, as well as the fact that the polar lower stratosphere is cooling, and air occupies a smaller volume as it cools. Figure 7.7 shows a calculation of the descent of air parcels within the Antarctic polar vortex. The calculation shows that air in the Antarctic polar region descends rapidly during the fall, with the rate of descent slowing as the region enters winter. By the middle of winter (late July) the descent in the lower stratosphere has virtually stopped, and the polar vortex is close to radiative equilibrium; in the upper stratosphere, descent is still occurring, but at a greatly reduced rate.

The return of sunlight at the end of winter begins heating the polar vortex, leading to higher temperatures there (see Figure 7.4). This in turn reduces the latitudinal pressure gradient, which in turn reduces wind speeds around the vortex. As the speed of the jet around the vortex is reduced, so too is the stability and isolation of the vortex. The vortex wind system abruptly transitions to the summer wind regime by way of an event called the final stratospheric warming [222,225–226], which typically occurs in late November to late December, depending on altitude. During this final warming the Antarctic vortex breaks into smaller air masses which then mix with mid-latitude air [227]. It is this break-up of the Antarctic polar vortex that marks the end of the Antarctic ozone hole.

Finally, it should be noted that the area covered by, the range of temperatures of, and the longevity of the Antarctic polar vortex exhibit year-to-year variability (see WMO [13], Figure 3.3). As will be shown later, the meteorological variability of the polar vortex has important implications for the size and depth of the ozone hole.

7.1.3 Polar processing

Polar stratospheric clouds   At the cold temperatures found within the polar vortex, water vapor and nitric acid condense to form particles known as PSCs. PSCs are crucial to the chemistry of the polar region because, much like sulfate aerosols, they provide surfaces on which heterogeneous reactions can take place. The exact temperature at which PSCs form is a function of pressure and trace gas abundances, but a canonical formation temperature, valid near 20 km for typical lower stratospheric conditions, is ~196 K. Because of the requirement for such low temperatures, PSCs exist only in the winter and early spring polar regions from the tropopause to altitudes as high as ~26 km (see WMO [13], Figure 3.10).

PSCs are subdivided into two classes, designated imaginatively as type 1 and type II. Type I PSCs form at temperatures several degrees above the frost point (where water vapor condenses into ice). Because of this, it was suggested that type I PSCs were composed of a mixture of water and nitric acid [228–230]. Laboratory work
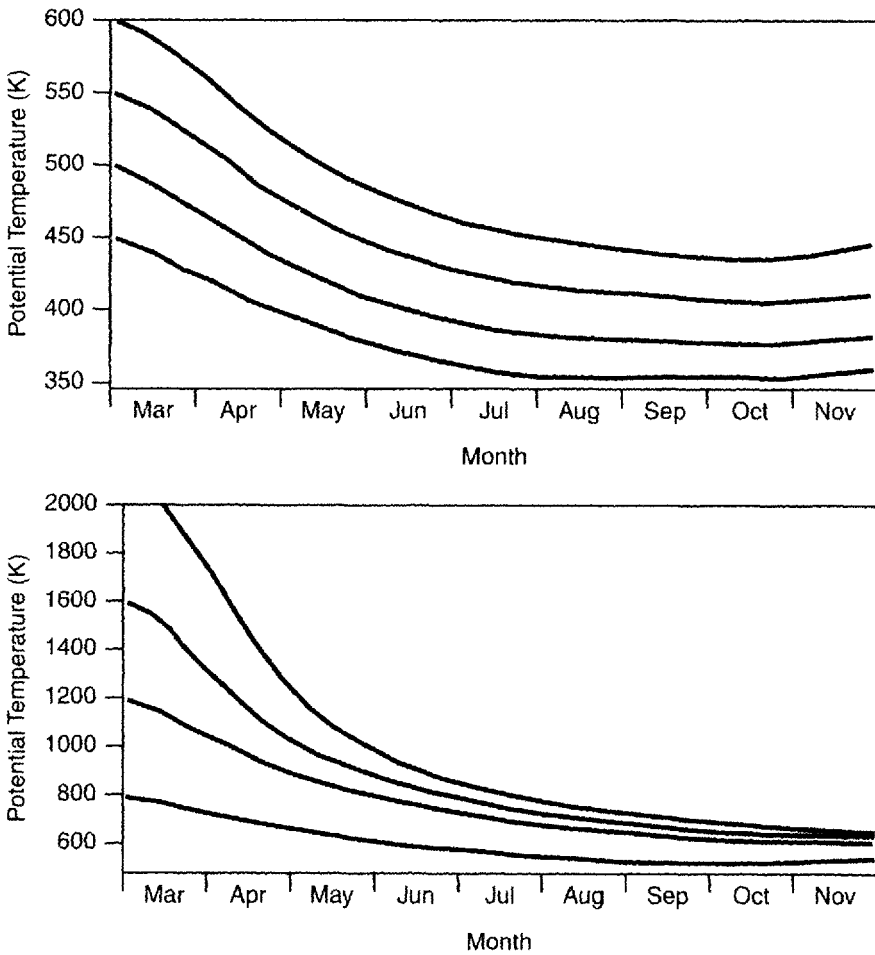
Figure 7.7 Potential temperature versus time for air parcels initialized at various potential temperatures in the Antarctic polar vortex in 1987. The lines show the evolution of potential temperature of individual parcels. (After Rosenfield *et al.* [224].)

showed that crystalline $HNO_3 \cdot 3H_2O$ (nitric acid trihydrate or NAT) was thermodynamically stable for stratospheric conditions below ~196 K [231]. This work, combined with *in situ* observations [232], led the field initially to identify NAT as the composition of type I PSCs.

Subsequent atmospheric observations, however, could not be reconciled with the NAT composition. By the mid-1990s it became apparent that the real situation is more complex. Other compositions, such as liquid $H_2O/HNO_3/H_2SO_4$ aerosol [36],

also known as supercooled ternary solution or STS, or crystalline $HNO_3 \cdot 2H_2O$ (nitric acid dihydrate or NAD) [233], are now thought likely to play a role [234–239].

Further, measurements have identified two classes of type I PSC, designated as type Ia and type Ib. Type Ia particles are crystalline, likely NAT or NAD, while type Ib particles are liquid, likely STS [240,241]. These particles have typical characteristic radii of 0.5–1 μm.

Type II PSCs form at temperatures below the frost point, which, for typical stratospheric values, is ~189 K. For this reason, they are believed to be ice crystals. Type II PSCs are predicted to have characteristic radii of 5–20 μm [242,243].

Chlorine activation   As discussed in Chapter 4, normally ~95% of total inorganic chlorine, Cl_y, in the lower stratosphere during the day is in the form of HCl and $ClONO_2$, with HCl the slightly more abundant reservoir. ClO typically makes up most of the rest. However, it has been observed that there are regions in the Antarctic lower stratosphere where nearly all of the Cl_y is in the form of ClO and ClOOCl [244,245]. As we will show, ClOOCl is involved in catalytic destruction of O_x, so we include it in our definition of Cl_x:

$$[Cl_x] = [ClO] + [Cl] + 2[ClOOCl] \approx [ClO] + 2[ClOOCl] \qquad (7.1)$$

Thus, observations suggest that virtually all of the Cl_y has been converted to Cl_x. Our present understanding of polar chemistry suggests that this repartitioning occurs because the following reactions occur on the surfaces of PSCs:

$$ClONO_2 + HCl \xrightarrow{\text{PSC}} Cl_2 + HNO_3 \qquad (7.2)$$

$$ClONO_2 + H_2O \xrightarrow{\text{PSC}} HOCl + HNO_3 \qquad (7.3)$$

$$HOCl + HCl \xrightarrow{\text{PSC}} H_2O + Cl_2 \qquad (7.4)$$

$$HOBr + HCl \xrightarrow{\text{PSC}} BrCl + H_2O \qquad (7.5)$$
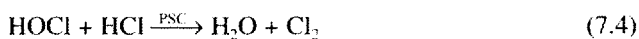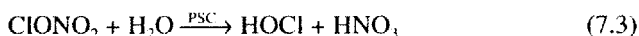
In the parlance of atmospheric chemistry, the conversion of chlorine reservoirs HCl and $ClONO_2$ into Cl_x is known as "chlorine activation".

Reactive uptake coefficient γ for the various reactions on NAT (type Ia), STS (type Ib), and ice PSCs (type II) are listed in Table 7.1. Reactions on NAD have not been studied as thoroughly as those on NAT; what laboratory measurements have been made suggest that the rates on NAD are comparable to those on NAT [246,247].

Extinction measurements suggest that PSCs exist only briefly (hours to days), and air masses are only occasionally exposed. The reactive uptake coefficients, however, are generally so large that even intermittent exposure to PSCs can cause significant

repartitioning of the Cl_y family. In many cases, even a brief exposure to a PSC causes reactions (7.2)–(7.5) to run to completion—i.e. run until one reactant is depleted.

Table 7.1 Reactive uptake coefficients on PSCs

Reaction	γ on NAT	γ on STS	γ on Ice
$ClONO_2+HCl$	0.1	0.08	0.3
$HOCl+HCl$	0.1	0.3	0.3
$ClONO_2+H_2O$	0.001	0.02	0.3
$HOBr + HCl$	Not measured	1	0.3

γ for reactions on NAT and Ice from Table 64 of DeMore *et al.* [5]; γ for reactions on STS are assumed to occur at 195 K; the values are obtained from Figure 6.3. Reactive uptake coefficients are for the first-order loss of $ClONO_2$, $HOCl$, or $HOBr$.

All of these PSC reactions convert relatively long-lived reservoir chlorine species (HCl and $ClONO_2$) into Cl_2 and $HOCl$, labile forms of chlorine that are easily photolyzed. Upon exposure to sunlight, Cl_2 and $HOCl$ are photolyzed within several hours to Cl atoms. Cl_x is in photochemical steady state, so these Cl atoms are rapidly converted to ClO or ClOOCl molecules in order to maintain steady-state partitioning of Cl_x.

Figure 7.8 shows the effect of PSC reactions. Above ~196 K about 50% of the Cl_y is in the form of HCl, with only a few percent present as Cl_x (we expect most of the rest is $ClONO_2$). Below ~196 K, at temperatures where PSCs are expected to occur, we see chlorine activation: reduced abundances of HCl and enhanced abundances of Cl_x.

It is presently unknown whether NAT, NAD, or STS is the dominant form of type I PSC. There is a body of evidence emerging, however, that STS might be the most important [237,248]. It should be noted, however, that while some details of the microphysics are incompletely understood, the net effects of PSCs on Cl_y are well defined. There is abundant empirical evidence that *any time* an air parcel is exposed to temperatures in the mid-190s Kelvin and below, chlorine reservoirs in the air mass are converted to Cl_x [249,250].

It should be pointed out that temperatures below ~196 K are common throughout the Antarctic lower stratosphere in the winter and early spring (see Figure 7.4). As a result, a significant fraction of Cl_y in this region in the winter and spring is in the form of Cl_x.

The ClO dimer   ClOOCl (also called "the ClO dimer" or simply "the dimer") plays a crucial role in the formation of the ozone hole. ClOOCl is formed in the three-body reaction of ClO with itself:

$$ClO + ClO \xrightarrow{M} ClOOCl \qquad (7.6)$$
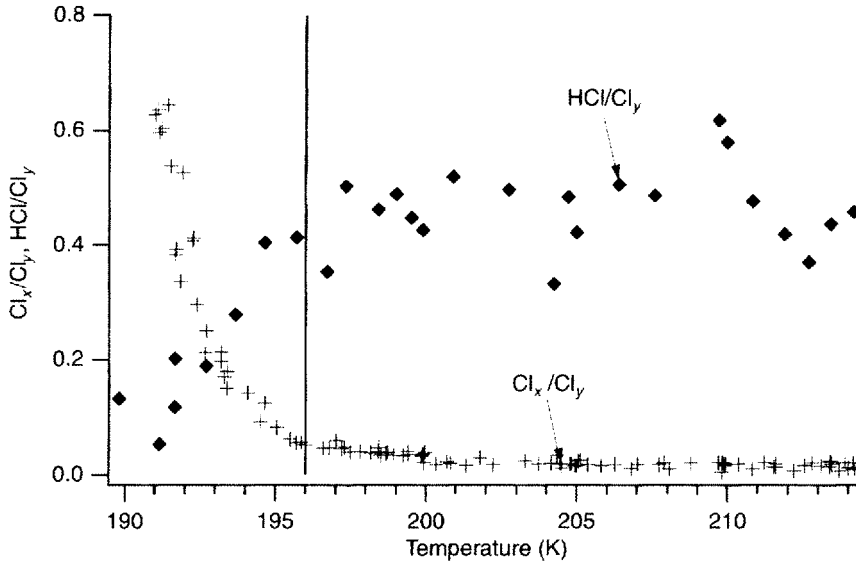
Figure 7.8 Measured Cl_x/Cl_y and HCl/Cl_y ratios versus simultaneously measured temperature. The data were obtained at high southern latitudes in the lower stratosphere (potential temperatures around 450 K, about 20 km altitude). On this flight, the measured temperature was the minimum temperature the air had encountered within the previous 10 days. (After Kawa *et al.* [248], Figure 1.)

At ClO abundances of 1–2 ppbv the time-scale to convert all of the ClO to dimer is tens of minutes to several hours. The ClO dimer is lost through photolysis with a lifetime ranging from tens of minutes to several hours at solar zenith angles (SZAs) typical of the early spring polar lower stratosphere:

$$ClOOCl + h\nu \longrightarrow ClOO + Cl \tag{7.7}$$
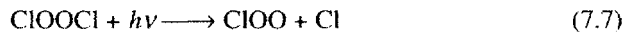
Thermal decomposition of the dimer is also an important loss pathway at temperatures above ~200 K:

$$ClOOCl \xrightarrow{M} ClO + ClO \tag{7.8}$$

Figure 7.9 plots the fraction of Cl_x in the form of the dimer as a function of temperature. The solid lines in Figure 7.9 are for 3 ppbv of Cl_x. At a SZA of 95°, the air parcel line is in darkness, and formation of ClOOCl (reaction (7.6)) is balanced by thermal decomposition (reaction (7.8)). Below about 200 K, virtually all of the Cl_x is in the form of dimer. As the temperature rises, thermal decomposition becomes
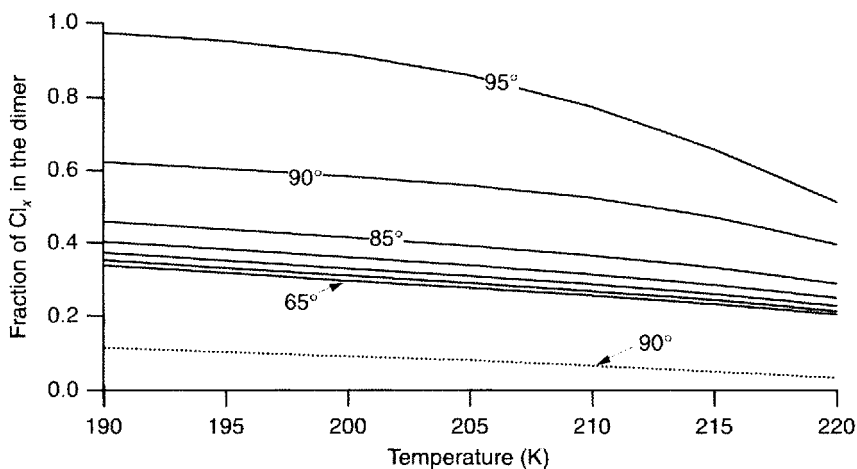
Figure 7.9 Fraction of active chlorine Cl_x ($ClO + 2 \times ClOOCl$) in the form $ClOOCl$ determined from a steady-state calculation. Pressure and [M] are held fixed at 46.4 hPa and 1.67×10^{18} molecules cm^{-3}, respectively; the temperature variation affects only the values of the rate constants. Lines are labeled with the SZA of calculation (unlabeled lines are 5° increments from surrounding lines). Solid lines are for 3 ppbv of Cl_x, and the dotted line is for 100 pptv of Cl_x. Rate constants are from DeMore *et al.* [5]; photolysis calculations are from the photolysis routine from the Goddard three-dimensional chemical transport model [28].

increasingly important, and $[ClOOCl]/[Cl_x]$ decreases. Under sunlight conditions (SZAs less than or equal to about 90°), formation of $ClOOCl$ (reaction (7.6)) is balanced by the combination of photolysis (reaction (7.7)) and thermal decomposition (reaction (7.8)). As the sun moves higher in the sky (i.e. to lower SZAs) the rate of photolysis increases rapidly and in general dominates thermal decomposition, except when temperatures are warm (> 220 K). For typical high-Cl_x polar sunlit conditions the dimer makes up 40–60% of Cl_x.

The rate of formation of the ClO dimer is $k^*[ClO][ClO]$, which is proportional to the square of the ClO abundance. This causes the formation rate of the dimer to drop off rapidly with decreasing ClO concentrations. As a result, the dimer is an unimportant component of Cl_x at typical mid-latitude Cl_x abundances. The dotted line in Figure 7.9 is a calculation at 90° SZA for 100 pptv of Cl_x, typical of the mid-latitude lower stratosphere. A comparison between this line and the 90° line calculated for 3 ppbv of Cl_x (solid line) demonstrates the effect of the quadratic dependence of the rate of ClO dimer formation. At the low Cl_x abundance the dimer makes up only a few percent of Cl_x, even at the very low stratospheric temperature of 190 K.

Thus, in the polar regions Cl_x comprises Cl, ClO, and ClOOCl, with Cl being a negligible component of Cl_x. Together, ClO and ClOOCl make up the vast majority

of Cl_x, with their relative abundances set by the temperature, SZA, and total abundance of Cl_x.

Denitrification and dehydration   PSCs are composed of HNO_3 and H_2O, so their formation and growth leads to the removal of these species from the gas phase, a process known as "denitrification" and "dehydration", respectively. How much of each of these species is removed depends on the composition of the PSC particles. Type I PSCs contain HNO_3 and H_2O in approximately comparable abundances. Because gas phase H_2O is initially about 10^3 times more abundant than HNO_3, the growth of type I PSCs can deplete HNO_3 while leaving H_2O essentially unchanged. And because almost all of the NO_y in the lower stratospheric polar vortex is in the form of HNO_3 [244], removal of HNO_3 is tantamount to removal of NO_y. Thus, formation and growth of type I PSCs leads to denitrification without accompanying dehydration.

Type II PSCs are composed of H_2O ice, and formation of these particles depletes gas phase H_2O. Additionally, it is thought that type II PSCs also incorporate NO_y [251]—and therefore remove the NO_y from an air mass. Thus, formation and growth of type II PSCs lead to both dehydration and denitrification.

Measurements of type I PSCs reveal characteristic radii of ~1 μm [241]. Such small particles have small settling velocities, and therefore sedimentation of these particles is negligible. When the air parcel warms up, the HNO_3 in the particle is released back into the gas phase. In this case, the denitrification is only temporary. It is possible, however, that growth of a much smaller number of type I PSC will result in larger particles and subsequent sedimentation of type I PSCs [243]. In this case the HNO_3 is physically removed from the air mass, and the denitrification is irreversible. Irreversible denitrification by type I PSCs is consistent with the observation of air masses that have experienced significant irreversible denitrification but not dehydration [252]. Type II PSCs are predicted to have characteristic radii of 5–20 μm or so [242,243], and so can experience significant sedimentation during their lifetimes. For example, at 20 km altitude, a particle with radius of 10 μm falls about a kilometer in a day [253]. As these type II particles sediment, they carry H_2O and NO_y to lower altitudes, leading to both irreversible denitrification and irreversible dehydration of the region where the particles were formed [252,254].

Eventually, the sedimenting PSC particles fall into warmer air and sublimate, forming to layers of enhanced water vapor and oxides of nitrogen [255]. *In situ* measurements of the lower stratosphere from the NASA ER-2 aircraft show that as much as 90% of the NO_y and 50–70% of the H_2O has been removed from the Antarctic lower stratosphere [252,256]. Satellite measurements [254,257] are consistent with these results, and show that this denitrification covers virtually the entire vortex.

Figure 7.10 shows a time series of lower stratospheric HNO_3 abundance, the dominant component of NO_y in the lower stratosphere. HNO_3 begins in late May at between 7 and 13 ppbv, with higher values at higher latitudes. At 60°S, HNO_3
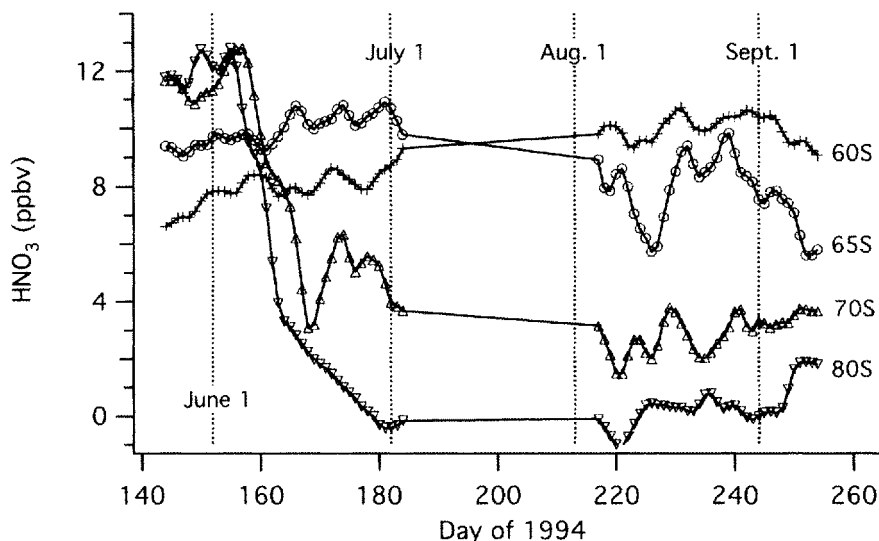
Figure 7.10 Time series of HNO₃ abundance at several equivalent latitudes in the high southern latitudes. MLS HNO₃ measurements (version 4) at 465 K in a ±1° equivalent latitude (derived from UKMO PV) band are averaged to produce an average HNO₃ abundance for each day. The time series has been smoothed to reduce the day-to-day variability.

increases throughout the winter; i.e. there is no hint of denitrification at this latitude. At 65°S, HNO₃ decreases by about 20% between May and September, suggesting slight denitrification. At higher latitudes there is a pronounced drop in HNO₃ starting in the first few days of June. At 70°S, about two-thirds of the HNO₃ has been removed by the end of June. At 80°S, virtually all of the HNO₃ has removed from the gas phase by the end of June. There is little change in August and September. Particle extinction measurements as well as *in situ* data [252] indicate that the NO_y is not simply sequestered in particles but has been irreversibly removed from the lower stratosphere. Also, note that air in the polar vortex is descending during the late fall and early winter (see Figure 7.7). Because the abundance of HNO₃ (and NO_y) increases with altitude in the polar lower stratosphere, such descent brings down air with higher values of HNO₃. This explains, for example, the increase in HNO₃ seen at 60°S. Descent cannot therefore explain the rapid decrease in HNO₃ shown in Figure 7.10.

Why is denitrification important? It turns out that NO_y can reverse chlorine activation. If HNO₃ is present, then reactions (4.46) and (4.47),

$$HNO_3 + h\nu \longrightarrow OH + NO_2$$

$$HNO_3 + OH \longrightarrow NO_3 + H_2O$$

produce NO_x, which can then react with ClO (reaction (4.10)),
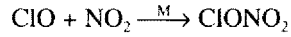
$$ClO + NO_2 \xrightarrow{\text{M}} ClONO_2$$

leading to conversion of Cl_x into $ClONO_2$. However, the removal of NO_y from the air mass through sedimentation of NO_y-rich PSCs shuts off this deactivation pathway and allows Cl_x abundances to remain high for a longer period than without denitrification.

The net result of PSC processing and denitrification is enhanced Cl_x abundances inside the vortex (Figure 7.11) for a sustained length of time. At 465 K (~20 km), ClO in the chemically perturbed regions of the vortex averages about 1700 pptv,
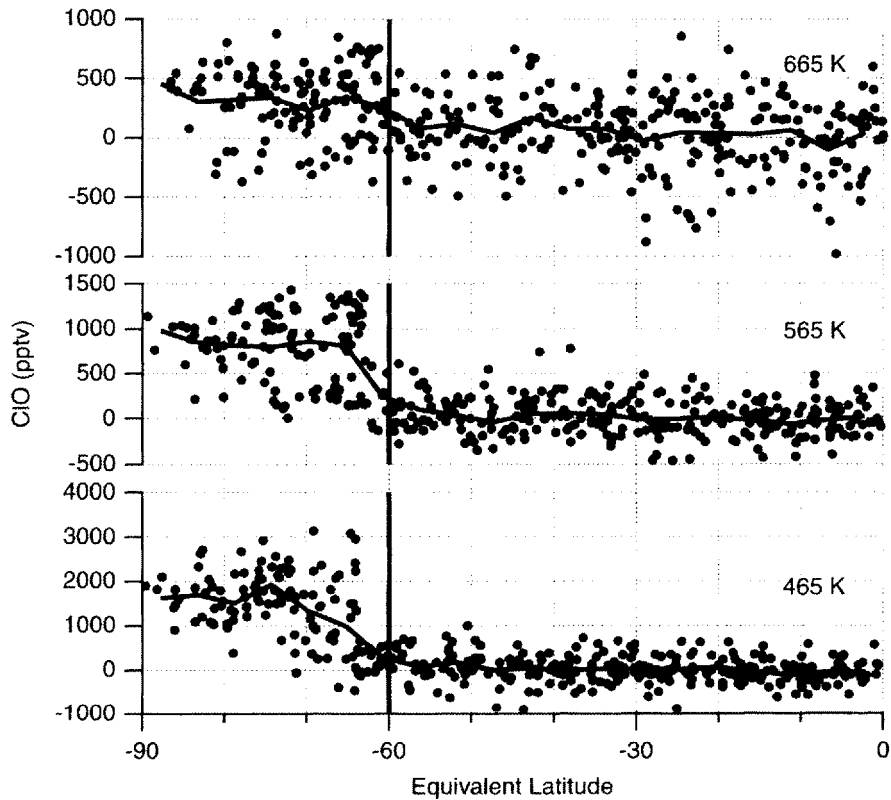
Figure 7.11 ClO abundance versus equivalent latitude on the 465, 565, and 665 K potential temperature surface on September 15, 1992. Dots are individual daytime measurements of ClO by the UARS MLS (version 4), interpolated to theta surfaces using UKMO temperatures [259]. The equivalent latitude and vortex edge are derived from UKMO PV. The vertical line denotes the edge of the vortex. Much of the scatter in the data, and especially the negative values of ClO, are due to precision uncertainty in the MLS ClO measurements [260,261].

while ClO near the edge and outside of the vortex is tens of pptv. If the ClO dimer makes up ~50–60% of Cl_x, then the total reactive chlorine Cl_x abundance in the vortex is ~2800–3400 pptv. In other words, ~80–100% of the Cl_y has been converted to Cl_x in the chemically perturbed regions of the vortex. At 565 K (~24 km), vortex ClO abundances are lower. Noting that the ClO dimer should also make a smaller contribution at this level, we conclude that less Cl_y has been converted to Cl_x. This is consistent with warmer temperatures (less PSC processing and denitrification) and higher photolysis rates (faster NO_x production rates) with increasing altitude. At 665 K (27 km), there is evidence of only a slight enhancement of Cl_x inside the vortex compared to mid-latitudes. Aircraft measurements indicate that ClO is also enhanced below 465 K [258].

It can be seen in Figure 7.11 that the edge of the high-ClO region is not coincident with the edge of the vortex. This should not be surprising: the vortex is defined by the meteorological field [219], while the region of high ClO is determined by cold temperatures. While these two geophysical parameters are physically related, there is no reason that the vortex, as defined by PV, will exactly overlap the region containing PSC-processed high-Cl_x air. Because of this, researchers will sometimes define a chemically perturbed region to be that region of the vortex containing PSC-processed air.

As will be discussed later, the late winter and early spring is the critical time period for the formation of the ozone hole. Figure 7.12 shows a time series of vortex-averaged lower-stratospheric Cl_x abundance in the Antarctic vortex during this
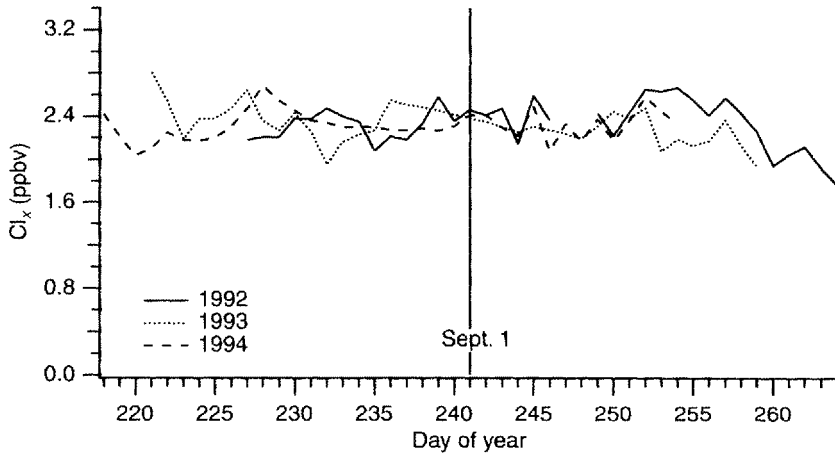
Figure 7.12 Time series of average Cl_x abundance at 465 K potential temperature for 1992, 1993, and 1994 in the Antarctic polar vortex. Cl_x is derived from daytime UARS MLS ClO data (version 4) assuming photochemical steady state. (After Wu and Dessler [262].)

time. Averaging over the entire vortex, Cl_x is ~2.4 ppbv, with little variation throughout this time.

It should be noted that even in June and early July, ClO measurements show that PSC processing has activated a significant faction of Cl_x. While Cl_x is elevated at this time, little of the vortex is exposed to sunlight at this time of the year, so chemical loss of O_x is negligible.

There are few measurements of bromine species in the Antarctic polar vortex. Taking measurements from the Arctic [263] as a guide, it is likely that BrO is ~10 pptv throughout the sunlit Antarctic polar vortex.

An aside: can Mount Erebus be supplying chlorine to the Antarctic stratosphere?

Mount Erebus is an active volcano on Ross Island in Antarctica. In 1991 the volcano pumped 13.3 Gg of HCl into the Antarctic troposphere [264]. It has been speculated that chlorine from Mount Erebus might be a significant contributor to stratospheric chlorine. Could chlorine from Mount Erebus be making it into the Antarctic stratosphere, where it could be contributing to the formation of the ozone hole?

Almost certainly not. First, the budget of stratospheric chlorine is well balanced: the formation of inorganic chlorine closely matches the destruction of CFCs and methyl chloride. Any additional source of stratospheric Cl_y would have to be small (less than a few percent of Cl_y). Second, the mean overturning circulation features air rising over the tropics and descending at high latitudes. Air descends from the stratosphere to the troposphere over Antarctica; air in the Antarctic troposphere is not ascending into the stratosphere.

It should be noted that Mount Erebus' effluents remain in the troposphere because the eruption is not energetic. Energetic eruptions, such as that of Mount Pinatubo in 1991, can inject their effluents well into the mid-stratosphere. Such eruptions can significantly perturb the chemistry of the stratosphere (e.g. see Chapter 6).

7.1.4 Odd Oxygen loss

Under the high-Cl_x conditions of the Antarctic polar vortex, O_x is destroyed through two catalytic cycles. The most important one is based on the ClO-dimer molecule [265]:

$$ClO + ClO \xrightarrow{\text{M}} ClOOCl$$
$$ClOOCl + h\nu \longrightarrow ClOO + Cl$$
$$ClOO \xrightarrow{\text{M}} Cl + O_2 \qquad\qquad (7.9)$$
$$\underline{2 \times (Cl + O_3 \longrightarrow ClO + O_2)}$$
$$\text{net: } O_3 + O_3 \longrightarrow O_2 + O_2 + O_2$$
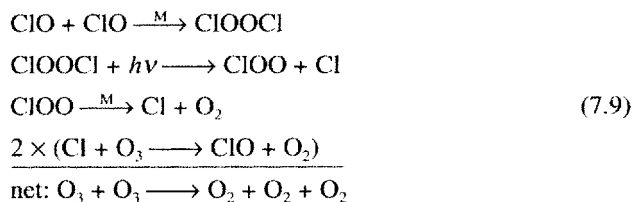
The rate-limiting step of this cycle is the photolysis of the ClO dimer. Thus, the rate of O_x loss from this cycle is $2J_{ClOOCl}[ClOOCl]$. As we mentioned earlier, thermal decomposition of ClOOCl is negligible at the cold temperatures found in the Antarctic polar vortex. As a result, the formation rate of the dimer (the self-reaction of ClO, reaction (7.6)) is equal to the photolysis rate of the dimer (reaction (7.7)). One can therefore approximate the rate of O_x loss due to this cycle as twice the rate of formation of the dimer ($2k^*_{ClO+ClO}[ClO]^2$). In the warmer Arctic, thermal decomposition can be important, and therefore this approximation is less valid.

The second important catalytic cycle is the ClO–BrO cycle discussed in Chapter 3 (cycles (3.23) and (3.24)). Finally, the ClO–O cycle (cycle (3.16)) also contributes.

It is crucial to recognize that all three of these catalytic cycles require sunlight to destroy O_x. For the ClO–dimer cycle (7.9), it is obvious why it does not run in darkness: one of the steps in the cycle is the photolysis of ClOOCl, which ceases without sunlight. The ClO–BrO cycles (cycles (3.23) and (3.24)) cease because ClO is greatly reduced at night because most of Cl_x is tied up in ClOOCl, and BrO is depleted through reaction with any remaining ClO to form BrCl, which is stable at night. Finally, the ClO–O cycle (cycle (3.16)) does not run because, at night, the abundance of ClO is low and the abundance of O is zero.

Figure 7.13 shows the O_x loss per day in the lower stratosphere during the last month of winter. The O_x loss per day is relatively small in the middle of August,
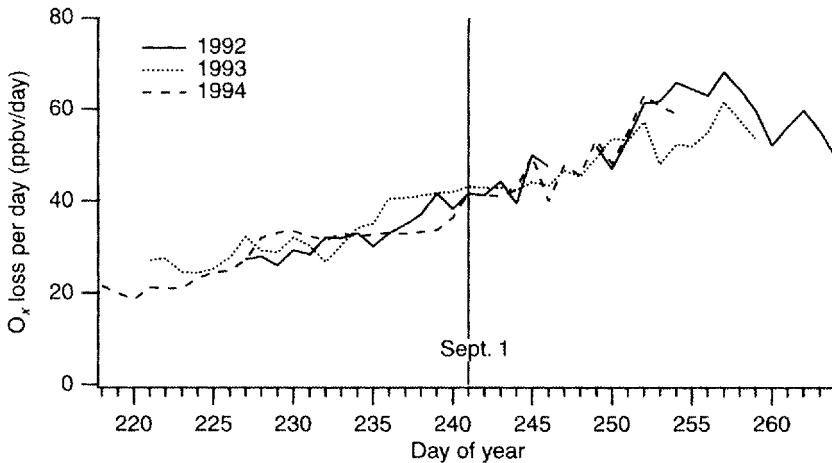
Figure 7.13 Antarctic vortex-averaged daily O_x loss per day versus day of the year. Calculated as the sum of the rates of the ClO–ClO and ClO–BrO catalytic cycles, using UARS MLS ClO measurements (version 4) and assuming [BrO] = 12 pptv. This sum is adjusted upward by 5% to account for other cycles, such as ClO + O. (Adapted from Wu and Dessler [262].)

increasing rapidly through the end of August and the first half of September. From Figure 7.12 we see that daytime average Cl_x is approximately constant during this time, so changes in Cl_x abundance cannot explain the increase in O_x loss per day during this time. Instead, it is the rapidly rising number of hours of sunlight per day during this time period, from about 5 h of sunlight per day in mid-August to nearly 12 h in mid-September (Figure 7.14) that causes the increase. As previously mentioned, the catalytic cycles that destroy polar O_x require sunlight to operate, so we expect the O_x loss per day to be proportional to the number of hours of sunlight per day.

At the same time that the days are lengthening the average SZA is also decreasing (Figure 7.14), leading to increased photolysis frequencies. The increased photolysis frequencies drive the photochemistry faster, again leading to enhanced O_x loss. This effect is, however, less important than the increasing length of day.

Because of the rapid increase in the O_x loss per day during the last month of winter and first month of spring, most of the O_x destroyed in the formation of the ozone hole is destroyed between mid-September and early October. Therefore, in order to destroy enough O_x to form an ozone hole, Cl_x must remain enhanced well into the first few weeks of spring. This occurs in the Antarctic, but as we will discuss later in this chapter, Cl_x in the Arctic is generally not activated past the end of winter and, as a result, total O_x loss is much smaller.

The ClO–dimer cycle destroys about two-thirds of the O_x lost in the Antarctic. The ClO–BrO cycle destroys most of the remainder, with the ClO–O cycle contributing a few percent of the loss.
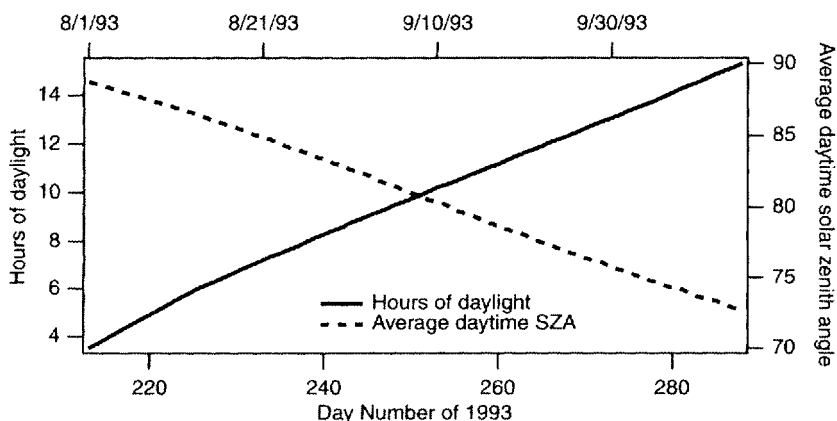
Figure 7.14 Hours of daylight per day (defined as hours per day with SZA < 90°) and average daytime SZA (daytime is defined as SZA < 90°) versus day number. Calculated for a parcel located at 70°S, which is typical of the Antarctic polar vortex.

In Figure 7.15, we plot vortex-average O_3 at several levels in the lower and mid-stratosphere. The vast majority of O_x loss occurs between mid-August and mid-September, the time period featuring both high Cl_x (see Figure 7.12) and long periods of sunlight (see Figure 7.14). At 465 K, about two-thirds of the O_x in the vortex is lost during the last month of winter. At higher altitudes the loss becomes progressively smaller, consistent with lower values of Cl_x (see Figure 7.11). The increase in O_x between the end of September and the beginning of November is likely due to the weakening of the polar vortex by rising polar temperatures, followed by horizontal transport of ozone-rich air from mid-latitudes to the high latitudes.

Another dramatic view of the decrease of Antarctic O_x is shown in Figure 7.16. During the month of September virtually all of the O_3 between 14 and 22 km is destroyed. O_3 above ~23 km, where the ClO abundance is much lower, is unaffected. It has been verified that models using realistic values of chlorine and bromine can accurately reproduce such rapid loss [262].

It is important to point out that the observed changes in lower stratospheric polar O_x cannot be caused by the transport into that region of low-O_x air. First, as we mentioned before, calculations [224] suggest that vertical motion of air in the vortex
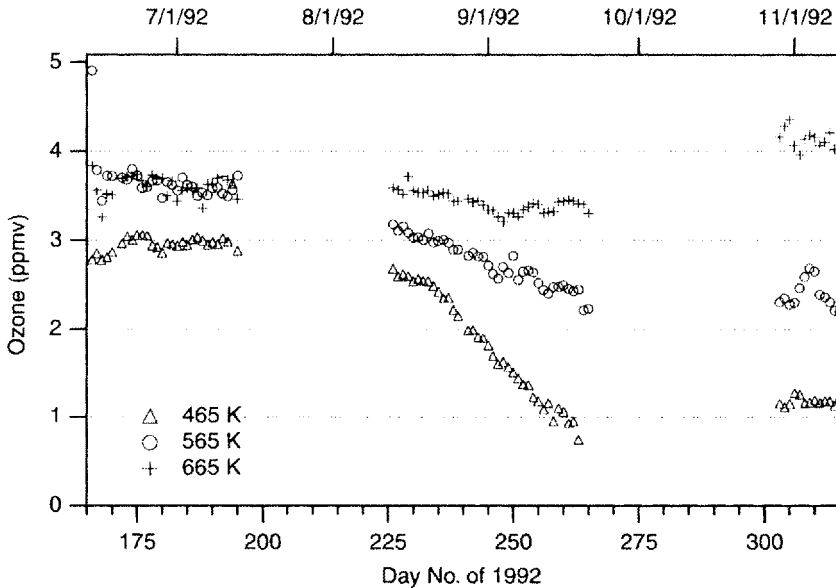
Figure 7.15 Time series of O_3 abundance on three potential temperature surfaces. Each point is one day of UARS MLS O_3 data (version 4, 205 GHz) averaged over the Antarctic polar vortex, defined using the Nash *et al.* [219] algorithm and PV from the UKMO assimilation system.
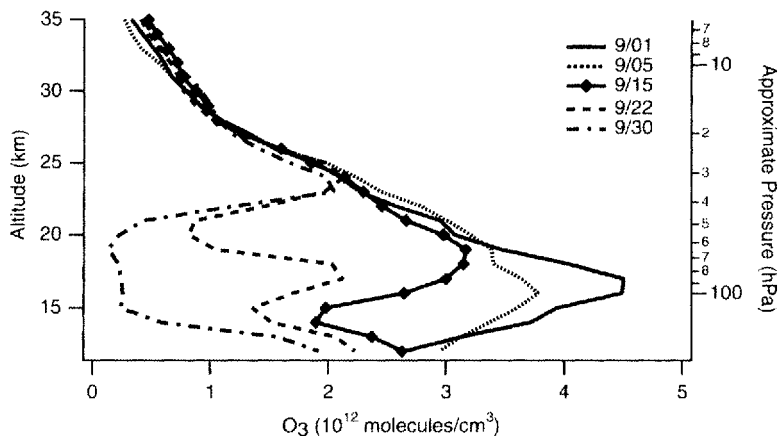
Figure 7.16 O_3 profiles measured in the Antarctic vortex during September 1998 by the POAM III instrument. (J. D. Lumpe, personal communication, 1999.)

has essentially stopped by the late winter/early spring period (see Figure 7.7), so vertical transport is negligible. And other analyses suggest that horizontal transport into and out of the vortex is strongly suppressed by the polar night jet [187,222,266]. As a result, it is generally agreed that changes in the abundance of O_x in the Antarctic polar vortex during the formation of the ozone hole arise almost entirely from chemical loss.

Finally, for completeness we note that production of O_x is extremely slow in this region. While the photolysis of O_2 can occur by the absorption of photons with wavelengths as long as 242 nm, most of the photolysis occurs from absorption of photons with wavelengths of 200 nm or less. This flux of these photons falls off rapidly as the Sun moves to higher SZAs, and as a result J_{O_2} is negligible in the polar lower stratosphere during the period of rapid O_x loss.

7.15 Deactivation

At the same time that O_x is being destroyed by Cl_x- and Br_x-mediated catalytic cycles, Cl_x is also being converted back into Cl_y reservoir species in a process known as deactivation. Deactivation occurs primarily through two processes. As NO_2 is produced from destruction of HNO_3 (reactions (4.46) and (4.47)), it reacts to reform $ClONO_2$ (reaction (4.10)):
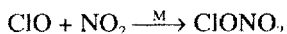
$$ClO + NO_2 \xrightarrow{M} ClONO_2$$

Second, the reaction between Cl and CH_4 forms HCl (reaction (4.11)):

$$Cl + CH_4 \longrightarrow HCl + CH_3$$
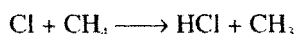
Under nonpolar conditions, formation of NO_x from HNO_3 destruction and the subsequent formation of $ClONO_2$ would rapidly deplete Cl_x on a time-scale of a week or so—much faster than formation of HCl would. Equilibration between $ClONO_2$ and HCl would then be re-established on time-scales of several weeks.

In the low-NO_y, low-O_x environment of the Antarctic lower stratosphere, however, production of HCl from Cl_x is much faster than under nonpolar conditions for two reasons. First, the conversion of Cl to ClO through reaction with O_3 (reaction (4.8)) is slowed due to low O_x abundances. Second, the reaction scheme

$$ClO + ClO \xrightarrow{M} ClOOCl$$

$$ClOOCl + h\nu \longrightarrow ClOO + Cl$$

$$\underline{ClOO \xrightarrow{M} Cl + O_2}$$

$$\text{net: } ClO + ClO \longrightarrow Cl + Cl + O_2$$

(7.10)
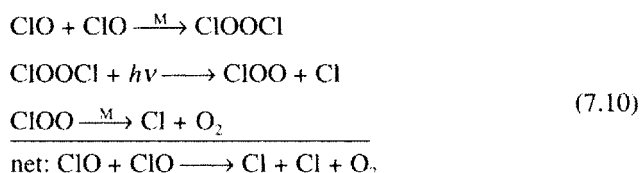
provides an efficient mechanism to convert ClO to Cl. The result is a high $[Cl]/[Cl_x]$ ratio, and consequently a conversion of Cl_x to HCl at a rate of several tenths of a part per billion by volume per day [267,268]. Other research has pointed out that the reaction between OH and ClO to produce HCl (reaction (4.13)) might also be important [269]. Combined with the slow formation of $ClONO_2$ due to the low abundance of NO_y (and therefore the slow formation rate of NO_2), the formation of HCl dominates the formation of $ClONO_2$.

It should be noted that deactivation is going on continuously throughout the winter and spring. However, during the Antarctic winter and early spring the temperatures are sufficiently cold that PSC processing recurs frequently enough to reverse any deactivation and prevent a significant build-up of the reservoirs of HCl and $ClONO_2$. As a result, a high $[Cl_x]/[Cl_y]$ ratio is maintained in the polar lower stratosphere. At some point during the spring, however, the Antarctic polar vortex has warmed sufficiently that PSC formation ceases. Thereafter, Cl_x decreases as it is converted back to the Cl_y reservoir species. As the polar vortex breaks up and HNO_3 mixes into the region, its photolysis produces NO_x and the equilibrium between HCl and $ClONO_2$ is re-established on a time-scale of weeks. The decline in Cl_x and the reformation of HCl and $ClONO_2$ signals the end of O_x loss due to polar chemistry.

The timing of the deactivation of Cl_x is a crucial factor in determining how much polar O_x is destroyed by chlorine chemistry. As discussed previously, the amount of O_x destroyed during a day is a function of both the Cl_x abundance and the amount of sunlight the vortex is exposed to. Deactivation of Cl_x in the late winter, after the

vortex has been exposed to relatively little sunlight, would result in comparatively little O_x loss there. In the Antarctic, however, Cl_x remains high for several weeks into the spring, so the high-Cl_x air experiences many hours of sunlight every day. This allows the destruction of virtually all of the O_x in the polar lower stratosphere and the formation of an ozone hole.

Meteorological variability means that the Antarctic vortex is warmer in some years than others (e.g. see WMO [13], Figure 3.3), and exactly how far into the spring PSCs occur shows interannual variability. For example, Figures 7.1 and 7.2 show that ozone hole during the relatively warm year 1988 was both smaller and had higher minimum ozone than the ozone holes of the colder years 1987 and 1989.

7.2 The Arctic

To a good approximation the Earth is symmetric about the Equator. One might therefore expect the mechanisms that create the Antarctic ozone hole to create an analogous Arctic ozone hole. Figure 7.17 shows average March high-latitude northern hemisphere column O_3. While there is a clear downward trend, with 1997 column ozone ~30% less than 1971–1972, a comparison between Figures 7.2 and 7.17 shows that the ozone loss in the north is less severe than in the southern hemisphere (note that different quantities are plotted in these figures). It should also be pointed
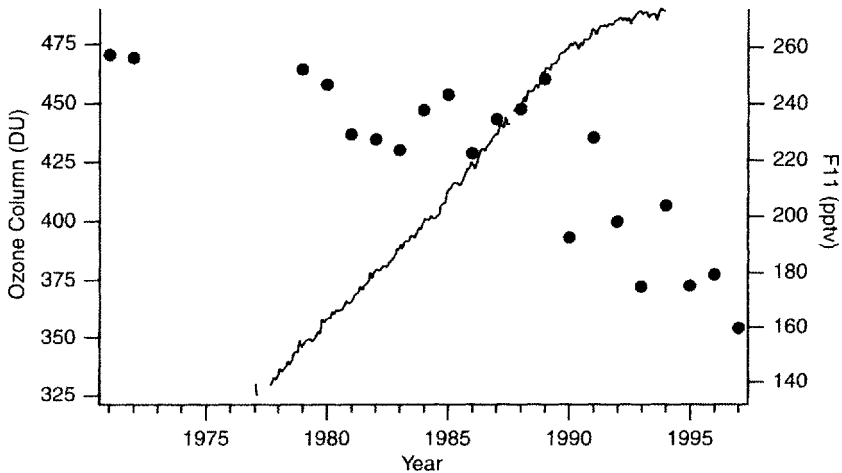
Figure 7.17 Column ozone averaged between 63°N and 90°N observed in March versus year. (After Newman *et al.* [270]. Figure 1.) The solid line is global average tropospheric F11 (CCl_3F) abundance (pptv) (from NOAA CMDL).

out that there are significantly higher values of column O_3 in the northern hemisphere in March than in the southern hemisphere in October. Figure 7.2 shows that in the 1960s and early 1970s, before the formation of the Antarctic ozone hole, typical high-latitude southern hemisphere column O_3 was 300–350 DU, while comparable northern hemisphere values were 450–500 DU.

The annual loss of O_x in the late winter and early spring in the Arctic is due to the same mechanisms that create the Antarctic ozone hole. There are, however, important differences between the two hemispheres, and it is these differences that are responsible for less severe O_x loss in the northern hemisphere.

7.2.1 The vortex

The cooling of the lower and mid-stratosphere during the polar night causes a northern hemisphere polar vortex to be set up just as one is set up in the southern hemisphere [186,271]. However, as mentioned in Chapter 5, there are important differences in the circulation of the hemispheres due to differences in the placement of the continents in the two hemispheres. A result of these differences is that the polar vortex in the northern hemisphere is smaller and warmer than its counterpart in the southern hemisphere. Figure 7.18 shows the area covered by the 195 and 189 K contours in the northern polar vortex during the 1992–1993 winter (area
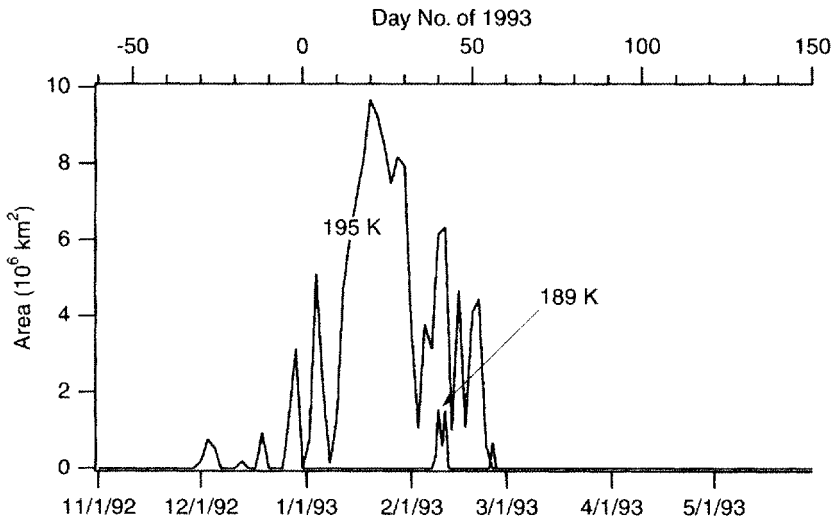
Figure 7.18 Area covered by temperatures less than 195 and 189 K at 465 K potential temperature (~20 km) in the northern hemisphere. Temperatures are from the UKMO assimilation system.

covered by the 185 K contour is negligible). Comparison with Figure 7.4 shows that the chlorine activation (~195 K) and ice–water frost point (~189 K) thresholds cover a far smaller area in the northern than in the southern hemisphere.

Additionally, meteorological conditions of the Arctic exhibit significant year-to-year variability [272–274]. This variability is far greater in most vortex metrics—size, temperature, wind speed at vortex edge, etc.—than is seen in the southern hemisphere.

The descent of air in the northern polar vortex is plotted in Figure 7.19. Comparison with Figure 7.7 shows that total descent during the winter and early
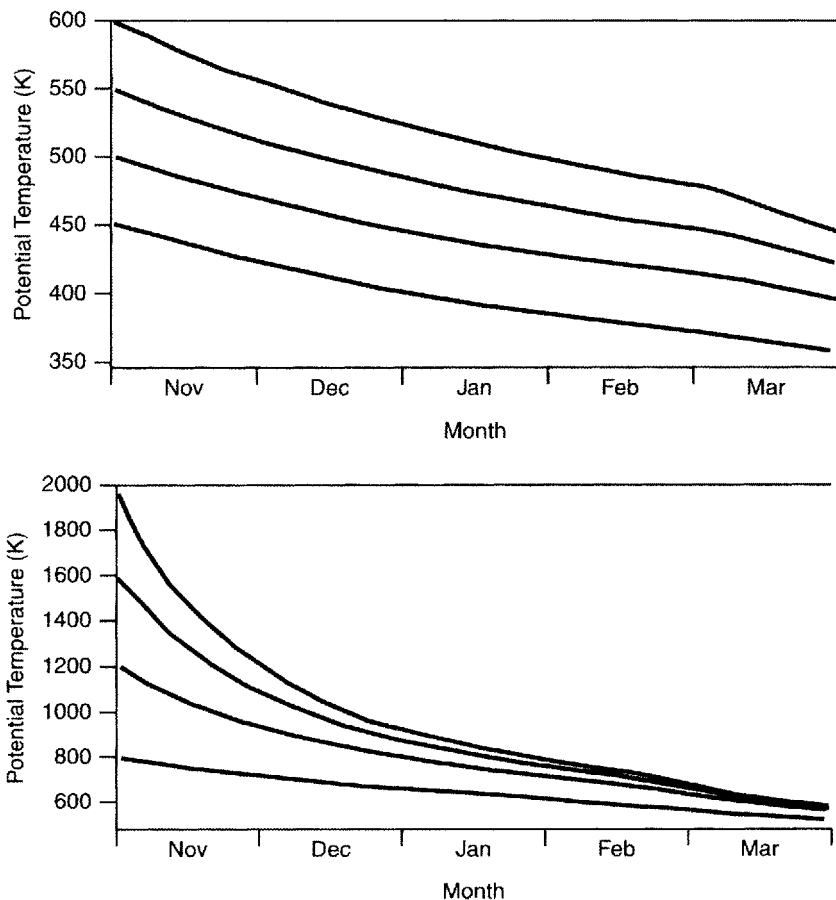
Figure 7.19 Potential temperature versus time for air parcels initialized at various potential temperatures in the Arctic polar vortex in 1988–1989. The lines show the evolution of potential temperature of individual parcels. (After Rosenfield *et al.* [224].)

spring is much greater in the northern polar vortex than in the southern polar vortex. This is consistent with higher vortex temperatures and therefore higher rates of radiative cooling in the north. Of special interest is the fact that descent in the vortex occurs throughout the northern hemisphere winter and into spring. In the southern hemisphere, descent has essentially stopped by mid-winter. As we will discuss later in this chapter, this makes it much more difficult to quantify O_x loss in the northern polar vortex.

7.2.2 Polar processing

Polar stratospheric clouds   Temperatures below the 196 K chlorine activation threshold occur every year in the Arctic, leading to chlorine activation throughout the polar vortex [249,275]. The time period over which these temperatures exist, however, is generally shorter than in the southern hemisphere (compare Figures 7.18 and 7.4).

Denitrification   The cold temperatures of the wintertime northern polar vortex lead to denitrification [252,255], just as they do in the southern hemisphere. However, the warmer temperatures of the northern hemisphere vortex result in far less denitrification than in the southern hemisphere. Figure 7.20 shows a time series of HNO_3
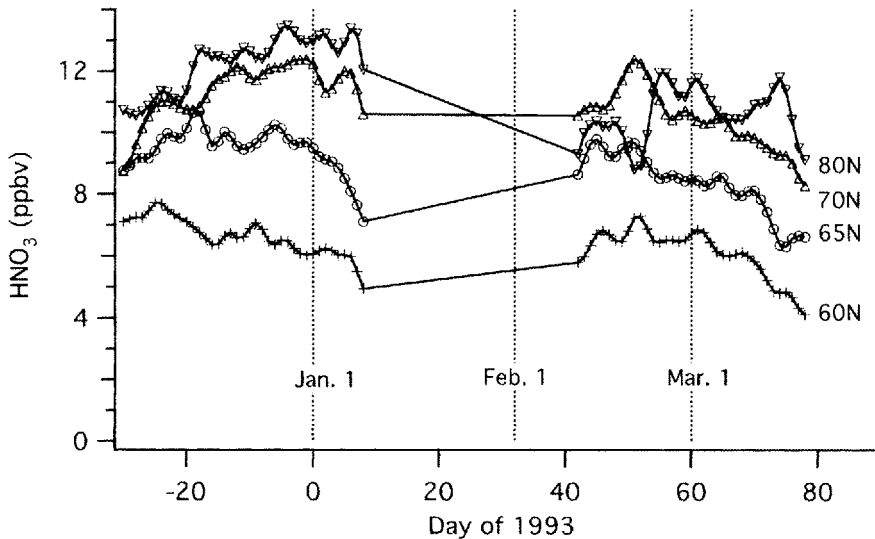
Figure 7.20 Time series of HNO_3 abundance at several equivalent latitudes in the high northern latitudes. MLS HNO_3 measurements (version 4) at 465 K in a $\pm 1°$ equivalent latitude (derived from UKMO PV) band are averaged to produce an average HNO_3 abundance for each day. The time series has been smoothed to reduce the day-to-day variability.

abundance, the dominant component of NO_y in the lower stratosphere. There is little change of lower-stratospheric HNO_3 through the winter. Comparison with Figure 7.10, the comparable plot for the southern hemisphere, shows the dramatic difference between the hemispheres.

7.2.3 Chlorine activation in the Arctic

The presence of temperatures below the chlorine activation threshold (~196 K, see Figure 7.18) suggests that Cl_x in the Arctic should be enhanced; in other words, the abundance of Cl_x should be much higher than its normal abundance of a few tens of parts per trillion by volume. Figure 7.21 shows that this is indeed the case.

Also shown in Figure 7.21 is Cl_x in the Antarctic polar vortex. As one can see, Cl_x in the Antarctic is generally higher throughout this time period. The difference between the two hemispheres can be attributed to two factors, both related to the warmer temperatures in the Arctic polar vortex. First, warmer temperatures mean that there is less irreversible denitrification in the Arctic. As a result, abundances of HNO_3 are higher in the Arctic, and this in turn leads to a proportionately higher production rate of NO_x from HNO_3 destruction. This NO_x reacts with ClO to form $ClONO_2$. In concert with production of HCl, this leads to a much faster deactivation of Cl_x in the Arctic than in the Antarctic [267,269]. Second, the warmer temperatures
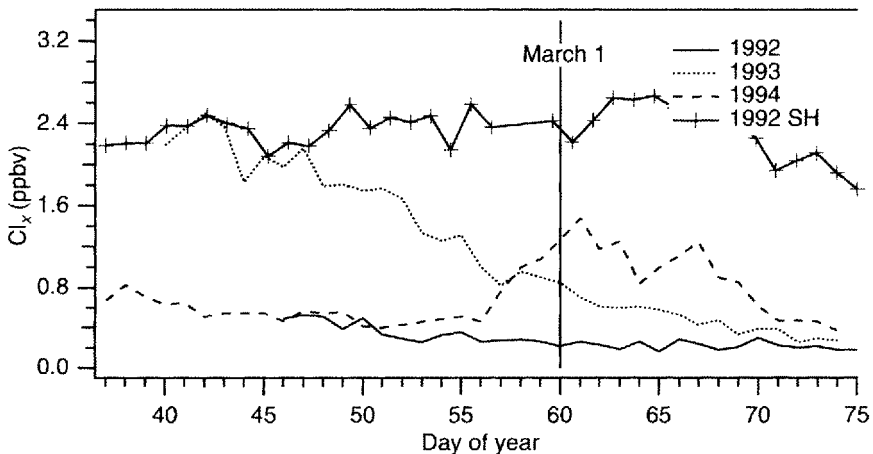
Figure 7.21 Time series of average Cl_x abundance at 465 K potential temperature for 1992, 1993, and 1994 in the Arctic polar vortex, and for 1992 in the Antarctic vortex (day of the year is shifted by 6 months). Cl_x is derived from daytime UARS MLS ClO data (version 4) assuming photochemical steady-state. (After Wu and Dessler [262].)

in the Arctic mean that less frequent PSC processing, and therefore less chlorine activation, occurs during the Arctic winter, and stops earlier in the year, than in the Antarctic.

The upshot of this is that, in the Arctic, the rate of chlorine activation is lower and the rate of chlorine deactivation is higher than in the Antarctic. This leads to generally lower abundances of Cl_x in the northern hemisphere, as shown in Figure 7.21.

It is also noteworthy that the interannual variability of Cl_x abundance is higher in the north than in the south. In the Antarctic the temperatures are so far below the PSC-processing threshold temperature of 196 K that interannual variability in the Antarctic vortex temperatures has little effect on the amount of PSC processing and, therefore, on the abundance of Cl_x. Consequently, Cl_x shows little year-to-year variability (see Figure 7.12). In the Arctic, however, the temperatures are much closer to the PSC-processing threshold. As a result, a variability of a few degrees can have a dramatic effect on the amount of air exposed to temperatures below ~196 K. This leads to significant year-to-year variability in the abundance of Cl_x in the Arctic (Figure 7.21). As we will see, this year-to-year variability in the abundance of Cl_x leads to significant year-to-year variability in the loss of O_x [276].

7.2.4 Odd Oxygen loss

Figure 7.22 shows O_x loss per day calculated for the northern hemisphere vortex during the last month of winter. Comparison with Figure 7.13 reveals much lower O_x loss rates in the Arctic than the Antarctic. The amount of sunlight the polar regions receive is comparable, so the difference in O_x loss rates can be almost fully attributed to differences in Cl_x.

The rate of the ClO–dimer loss cycle scales approximately as $[ClO]^2$, while the rate of the ClO–BrO loss cycle is linear in $[ClO]$. Thus, at the lower Cl_x abundances of the Arctic the ClO dimer cycle makes up about half of the total loss, compared to about two-thirds in the Antarctic. In both hemispheres the ClO–BrO cycle makes up most of the remainder, with the ClO–O cycle making up a few percent.

In Figure 7.23 we plot vortex-average O_x on several potential temperature surfaces in the lower and mid-stratosphere. Unlike the Antarctic (see Figure 7.15), Arctic O_x shows little change during the late winter and early spring. This might seem puzzling because we have shown that O_x is being lost during this period. The answer is that significant transport of O_x-rich air into the vortex is also occurring, and the net result of these two processes is that there was little change in vortex O_x in this year.

To demonstrate the importance of this transport, in Figure 7.24 we plot a calculation of the evolution of vortex-averaged lower stratospheric O_x in the absence of chemical O_x loss. In this case, all changes in O_x in the lower stratosphere are due to transport (solid line)—e.g. if O_x behaved like a passive tracer. This calculation shows
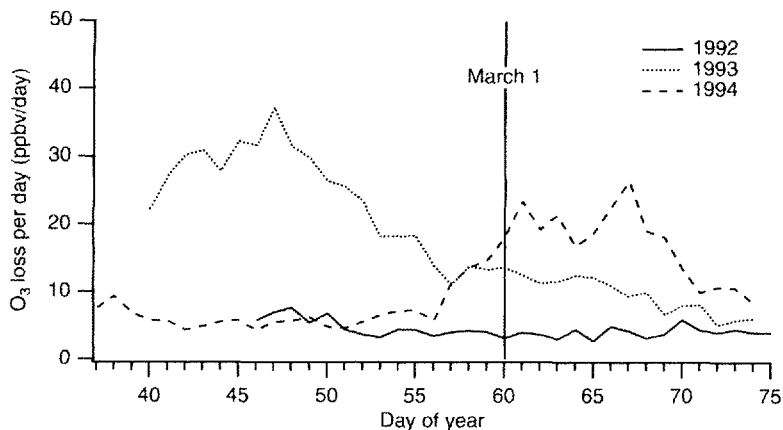
Figure 7.22 Arctic vortex-averaged daily O$_x$ loss per day versus day of the year. Values were calculated as the sums of the rates of the ClO–ClO and ClO–BrO catalytic cycles, using UARS MLS ClO measurements (version 4) and assuming [BrO] = 12 pptv. This sum is adjusted upward by 5% to account for other cycles, such as ClO + O. (Adapted from Wu and Dessler [262].)
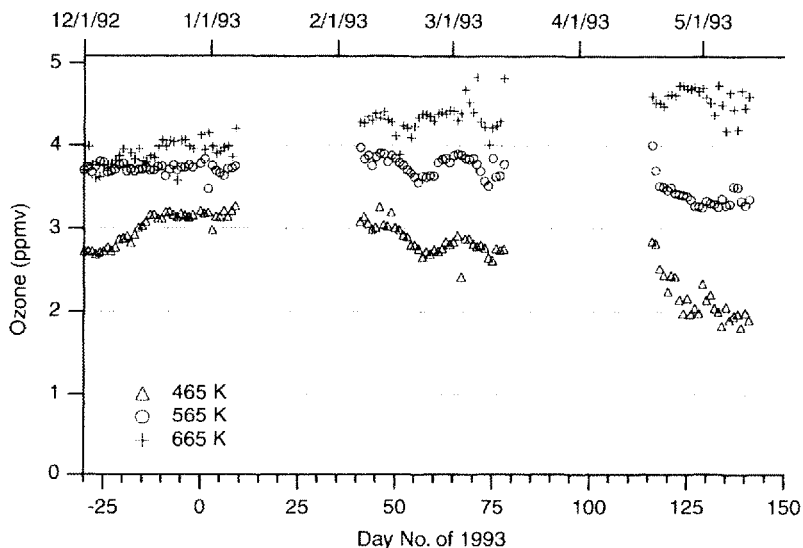
Figure 7.23 Time series of O$_x$ abundance on three potential temperature surfaces. Each point is one day of UARS MLS O$_3$ data (version 4, 205 GHz) averaged over the Arctic polar vortex. The boundary of the Antarctic polar vortex is determined from the method of Nash *et al.* [219] using UKMO PV.
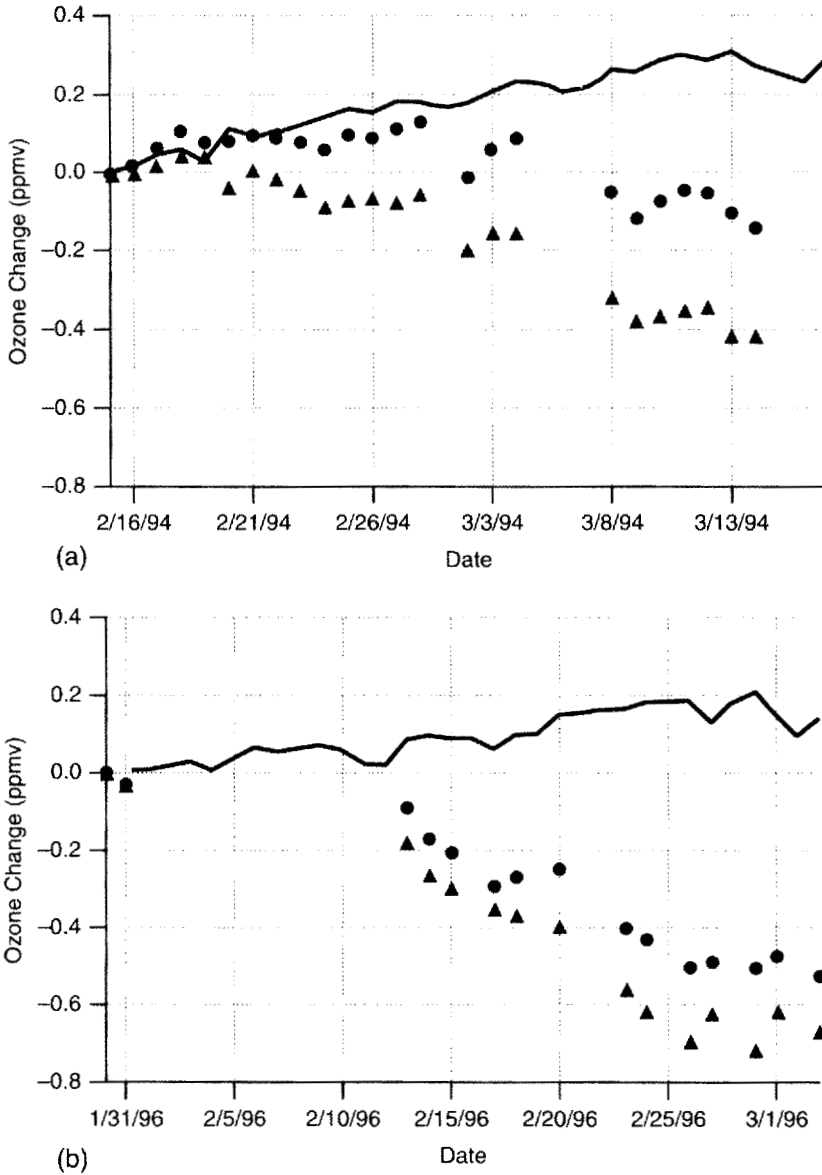
Figure 7.24 Vortex-averaged chemical O_x loss (triangles) estimated as the difference between the observed ozone (black circles) and the ozone calculated using transport alone (line), for 30 day periods in February and March of the (a) 1993–1994 and (b) 1995–1996 Arctic winters. Observations and calculations performed at 465 K (~20 km). (Adapted from Manney et al. [276,277].)

O_x increasing over this time period primarily because descent of air in the polar vortex brings air with higher O_x abundances downward. Also plotted (circles) are the observed O_x changes over the same period. The difference between the passive-tracer calculation and the observed O_x is an estimate of chemical loss of O_x (diamonds). In 1994 (Figure 7.24a), descent of O_x-rich air cancels most of the total chemical O_x loss. The net result is that vortex-averaged lower-stratospheric ozone remains fairly constant despite estimated chemical loss of ~0.4 ppmv of O_x. In contrast, in 1996 (Figure 7.24b) there was less transport of O_x-rich air from above as well as significantly greater chemical loss. The net result is a large decrease in lower-stratospheric O_x. Chemical loss and transport of O_x in the Arctic generally fall between these two extreme cases.

It turns out that the two processes that can control O_x in the northern hemisphere lower stratosphere—chemistry and transport—are not independent. As air descends, it is warmed through compressional heating. Thus, years with significant vertical descent in the polar vortex—and hence significant vertical transport of O_x—are associated with a warmer polar lower stratosphere. Warmer temperatures mean less PSC processing and therefore less O_x loss than in a colder vortex. The strong vertical descent is also associated with enhanced horizontal transport of air into the lower stratosphere from mid-latitudes. The strong descent case is exemplified in 1994 (Figure 7.24a), a year in which there was little chemical loss of O_x and significant transport of O_x from above. The net result was only small changes in observed O_3.

Weak descent, on the other hand, is associated with little compressional warming and therefore colder temperatures in the polar lower stratosphere. These cold temperatures support enhanced PSC processing and more O_x loss. The weak descent also implies a small amount of transport of O_x-rich air into the lower stratosphere from above. The weak-descent case is exemplified in 1996 (Figure 7.24b), a year in which there was significant chemical loss of O_x and little transport of O_x from above. The Antarctic polar vortex can be considered the extreme limit of the weak descent case: during the maximum ozone loss period in the Antarctic, vertical descent has essentially stopped and temperatures are nearly at radiative equilibrium. PSC activity is consequently widespread and the O_3-loss rate is high.

As suggested by this last discussion, the meteorological conditions of the Arctic exhibit significant year-to-year variability [272–274]. This variability is significantly greater in most vortex metrics—size, temperature, wind speed at vortex edge, etc.—than is seen in the southern hemisphere. Additionally, the temperatures in the northern hemisphere polar lower stratosphere tend to be near the 196 K chlorine activation temperature threshold. Thus, normal variations in temperature of just a few degrees can significantly change the amount of the vortex that is exposed to temperatures below the chlorine activation threshold. This leads to significant interannual variability in the amount of O_x lost (as shown, for example, in Figure 7.24 and by Manney *et al.* [276]).

Problems

1. Calculate the abundance of:
(a) ClOOCl given a fixed amount of Cl_x. Assume steady-state partitioning between ClO and ClOOCl and that the only important reactions are ClO+ClO $\longrightarrow$ ClOOCl and photolysis of ClOOCl. Calculate the solution in terms of $k^*_{ClO+ClO}$, J_{ClOOCl}, and $[Cl_x]$.
(b) Cl atoms for this same case. Assume steady-state partitioning among Cl_x species and that the only important reactions are photolysis of ClOOCl to produce two Cl atoms and $Cl+O_3$ to produce ClO. Calculate the solution in terms of $[ClOOCl]$, $[O_3]$, and k_{Cl+O_3}.
Combine your answer from part (a) to:
(c) determine $[Cl]$ as a function of $[Cl_x]$.

2. Even under favorable conditions the rate of loss of $ClONO_2$ in heterogeneous reactions is not much faster than the rate at which $ClONO_2$ is destroyed in photolysis. Why, then, does heterogeneous loss activate chlorine, while photolysis does not?

3. Polar processing.
(a) If the photolysis rate of HNO_3 is $1/(30$ days$)$ and there are no sources of HNO_3, write an expression for the abundance of HNO_3 as a function of time. Assume the initial abundance of HNO_3 is 10 ppbv.
(b) If all of the NO_x produced in HNO_3 photolysis combines with ClO to form $ClONO_2$, use the answer to part (a) to write an expression for $d[Cl_x]/dt$.
(c) Integrate this equation to determine Cl_x as a function of time. Assume the Cl_x abundance at $t = 0$ is 3 ppbv.
(d) Assume that this air mass encounters PSCs every 5 days. When the air mass hits a PSC, Cl_x and HNO_3 abundances return to their initial values of 3 and 10 ppbv, respectively. What is the average value of Cl_x?
(e) Now assume the air is denitrified, so the initial abundance of HNO_3 is 1 ppbv. In this case, what is the average value of Cl_x abundance?
(f) Explain how this helps explain the differing amounts of O_x lost in the northern and southern hemispheres.

4. The O_x continuity equation.
(a) Write the full continuity equation for O_x.
(b) Which terms are important during August and September in the Antarctic polar vortex?
(c) Which terms are important during February and March in the Arctic polar vortex?
(d) Is it possible for O_x loss to be occurring in the southern hemisphere polar vortex but for the O_x abundance to not be decreasing? And in the northern hemisphere? Explain why.

Appendix | Terms and Definitions

activation   See *chlorine activation.*

activation energy   The minimum kinetic energy possessed by the reactants in a bimolecular reaction in order for a collision to result in a reaction. See Equation (2.10) and accompanying discussion.

adiabatic   A thermodynamic process occurring at constant entropy and thus without gain or loss of heat. In the atmosphere such a process conserves potential temperature and potential vorticity.

aerosols   See *sulfate aerosols.*

association reaction   A reaction that involves the association of two atoms or molecules to form a single reaction. Sometimes called a termolecular reaction.

CFC   See *chlorofluorocarbons.*

chemically perturbed region   That region of the polar vortex containing air which has been exposed to PSCs and, in general, contains high abundances of Cl_x.

chlorofluorocarbons (CFCs)   A class of organic molecules containing chlorine and fluorine. This term generally applies to man-made chemicals.

CLAES   The Cryogenic Limb Array Etalon Spectrometer, an instrument onboard the UARS. See Roche *et al.* [278] for more details.

chlorine activation   When reactions on PSCs lead to the conversion of the chlorine reservoir species HCl and $ClONO_2$ into Cl_x.

Cl_x $Cl + ClO + 2 \times ClOOCl$. Cl_x is the sum of the chlorine species that are involved in the catalytic cycles that destroy odd oxygen. Cl_x is also known as "reactive chlorine".

Cl_y $HCl + ClONO_2 + HOCl + ClO + Cl + 2 \times ClOOCl$. Cl_y is total inorganic chlorine. It is the sum of all of the chlorine that has been released from CFCs and other chlorine-bearing organic molecules.

CCl_y   The concentration of chlorine atoms in an air mass that are bound into long-lived organic molecules such as CFCs. The sum of Cl_y and CCl_y is a conserved quantity and is equal to the total amount of chlorine that entered the stratosphere in the air mass.

deactivation   The opposite of chlorine activation: the net conversion of enhanced amounts of Cl_x back into the chlorine reservoir species HCl and $ClONO_2$.

denitrification   The removal of NO_y from the gas phase by incorporation into solid

184

or liquid particles. If the particles formed are large enough, they will sediment out of the stratosphere and the denitrification is irreversible. If the particles formed are small, then they do not sediment and when the air warms, the particles release the NO_y back into the gas phase. In this case, the denitrification is temporary.

diurnal cycle   A cycle over 24 h.

diurnal steady-state   Photochemical production is equal to photochemical loss when averaged over 24 h.

diabatic   A thermodynamic process in which heat is gained or lost and entropy therefore changes. In the atmosphere such a process does not conserve potential temperature or potential vorticity.

Dobson unit (DU)   The unit of measure for column O_3. If you were to take all the O_3 in a column of air stretching from the surface of the Earth to space, and bring it to standard temperature (273 K) and pressure (1013 mb), the O_3 would be 0.25–0.50 cm thick (except in the Antarctic "ozone hole"). The "Dobson unit" is defined to be this thickness in milli-centimeters, so 0.25–0.50 cm corresponds to 250–500 DU. Alternatively, 1 DU = 2.69×10^{16} molecules cm^{-2}.

DU   see *Dobson Unit.*

***e*-folding time**   The time for some geophysical parameter to decrease by a factor $1/e = 0.368$. Often referred to as the lifetime or time scale of the parameter/process.

easterly   Coming from the east.

equivalent latitude   The equivalent latitude of a point in the atmosphere is the latitude circle that encloses the same area as the PV contour that runs through that point.

first-order reaction   A reaction in which a reactant is transformed into one or more products. Examples of this include photolysis, thermal dissociation, radioactive decay, and isomerization.

free radical   See *radical.*

HCFC   A CFC that contains a hydrogen atom. This shortens the lifetime of the molecule. As a result the molecule is destroyed lower in the atmosphere, where its chlorine and bromine will have less of an effect on stratospheric O_x.

hectopascal (hPa)   A unit of pressure, equal to 1 mb or 100 N m^{-2}. Surface pressure is generally taken to be 1013 hPa, and the stratosphere runs from ~300–100 hPa to ~1 hPa.

F10 CCl_4.

F11 CCl_3F.

F12 CCl_2F_2.

global lifetime   Total amount of a molecule in the atmosphere divided by the loss rate of the molecule integrated over the entire atmosphere.

hPa   See *hectopascal.*

Junge layer   The region of the atmosphere—generally speaking between 16 and 20 km—that contains most of the stratosphere's burden of sulfate aerosol.

local lifetime   The reciprocal of the chemical loss frequency ($1/L$).

local solar time (lst)   The time based on the position of the Sun. Noon LST occurs each day when the Sun is at its highest point in sky.

loss rate   The rate of loss of a chemical constituent, with units of amount/unit time (most often molecules cm^{-3} s^{-1} or VMR s^{-1}). It is generally the product of a loss frequency L and the abundance of the species in question.

lowermost stratosphere   That part of the stratosphere located between the ~380 K potential temperature surface and the tropopause; it exists only in mid- and high latitudes.

isentrope   A line or surface of constant potential temperature (and therefore constant entropy).

isopleth   A line or surface of constant mixing ratio of a constituent.

M   In a chemical reaction, M refers to "any molecule"; in practice, it refers to N_2 or O_2. [M] is the number density of all molecules in a volume. A useful shortcut to calculating total number density is: [M] (in molecules cm^{-3}) = $7.22 \times 10^{18} P/T$, where pressure P is in hectopascals (hPa) and temperature T is in Kelvin (K). The VMR of M is, of course, 1.

meridional   North–south, toward or away from the pole or equator.

meridional plane   The latitude–height plane. It can be obtained by zonally averaging a three-dimensional field.

millibar (mb)   Also known as the hectopascal (hPa).

mixing ratio   The mixing ratio of a constituent is defined to be the ratio of the density of a trace constituent divided by the density of air. If the number density is used, then volume mixing ratio is obtained; if the mass density is used, then mass mixing ratio is obtained. Throughout the literature on the stratosphere, volume mixing ratio is by far the more common form. Because volume mixing ratio is generally a very small number, it is typically expressed in parts per million by volume (ppmv), parts per billion by volume (ppbv), or parts per trillion by volume (pptv). Mixing ratio is always a unitless quantity.

MLS   The Microwave Limb Sounder is an instrument on UARS which measures O_3, ClO, H_2O, HNO_3, and SO_2. For more information see Barath *et al.* [279].

National Meteorological Center (NMC)   See *NCEP*.

NCEP   National Center for Environmental Prediction.

number density   The number density of some constituent χ, usually denoted [χ], is the number of molecules of constituent χ per unit volume. Number density typically has units of molecules per cubic centimeter (molecules cm^{-3}).

overworld   That part of the stratosphere located above the ~380 K potential temperature surface.

photochemical steady state   Photochemical production is equal to photochemical loss at each instant in time.

photolysis   Chemical decomposition of a molecule after absorption of a photon of radiation (usually visible or ultraviolet).

POAM   Polar Ozone and Aerosol Measurement (POAM) [280].

polar night   That period during the winter when the high latitudes experience 24 h of darkness every day.

polar stratospheric clouds (PSCs)   These clouds form in the cold temperatures of the lower stratosphere of the winter and early spring polar vortex. Type I PSCs form from the co-condensation of H_2O and HNO_3, while type II PSCs form from the condensation of water vapor. Chemistry necessary for the formation of the ozone hole occurs on the surfaces of these clouds.

polar vortex   The air mass that is located poleward of the polar night jet. This region is cold (so allows the formation of PSCs) and isolated from mid-latitudes by the strong zonal winds of the polar night jet.

potential temperature (theta)   The temperature that the parcel would have if it were moved adiabatically to a reference pressure, usually the surface pressure (1000 hPa).

potential vorticity (PV)   PV may be thought of as a fluid dynamical analog of spin angular momentum. PV is normally positive in the northern hemisphere and negative in the southern hemisphere, consistent with the sense of the Earth's rotation, and increases in absolute value with latitude on isentropic surfaces. PV is conserved on time-scales similar to the time-scale over which potential temperature is conserved (see Figure 2.5). There are several definitions of potential vorticity: Ertel's potential vorticity (EPV), quasigeostrophic potential vorticity, and modified potential vorticity (MPV). See Lait [57] for a discussion of PV.

ppbv   Parts per billion by volume.

ppmv   Parts per million by volume.

pptv   Parts per trillion by volume.

PV   See *potential vorticity*.

radical   A radical is a molecule with an unpaired electron. Such molecules are very reactive.

rate constant   The product of the rate constant of a reaction and the abundance of the reactants yields the rate of the reaction.

reactive chlorine   See Cl_x.

reactive uptake coefficient (γ)   The fraction of collisions between a molecule and a particle that results in a reaction. γ is dimensionless and always between 0 and 1.

reservoir species   A member of a chemical family that does not participate in the catalytic cycles that destroy O_x. Destruction of these species will often lead to the production of O_x-destroying radicals. Examples of reservoir species include $ClONO_2$ and HNO_3.

SAD   See *surface area density*.

surface area density (SAD)   The particle surface area per unit volume, usually expressed in square centimeters per cubic centimeter ($cm^2\ cm^{-3}$) or square micrometers per cubic centimeter ($\mu m^2\ cm^{-3}$).

second-order reaction   A reaction between two reactants that produces two or more products: $X + Y \longrightarrow C + D$.

solar zenith angle (SZA)   This is the angle between the Sun and the point located directly over the observers head (the zenith). Thus, a SZA of $0°$ means that the Sun is directly overhead, while a SZA of $90°$ means that the sun is at the horizon. SZAs $>$ ~$90°$ correspond to night-time.

steady state   See *photochemical steady state* and *diurnal steady state*.

stratopause   The boundary between the stratosphere and mesosphere. It is located at ~1 hPa (2000 K potential temperature).

sulfate aerosols   Liquid particles composed primarily of H_2O and H_2SO_4, and at temperatures below about 200 K, HNO_3. The particles have typical radii of a few tenths of a micron.

SZA   See *solar zenith angle*.

theta   See *potential temperature*.

time-scale   The characteristic length of time over which some process occurs.

TOMS   Total Ozone Mapping Spectrometer. This instrument measures ultraviolet light that has been back-scattered off the atmosphere, and infers the column O_3 from this. See McPeters and Labow [281] and McPeters *et al.* [282] for more information.

total inorganic chlorine   See Cl_y.

tropopause   The boundary between the troposphere and stratosphere. It ranges from ~300 hPa (310 K potential temperature) at high latitudes to 100 hPa (380 K potential temperature) over the equator.

UARS   Upper Atmosphere Research Satellite [283].

UKMO   United Kingdom Meteorological Office. It produces a set of meteorological fields that are widely used in stratospheric analyses. See Swinbank and O'Neill [259] for more information about these fields.

ultraviolet (UV) radiation   Radiation with a wavelength less than ~300 nm.

VMR   Volume mixing ratio. See *mixing ratio*.

westerly   Coming from the west.

zonal   East–west, along a line of constant latitude.

zonal average   All of the data taken at a single latitude and altitude, but covering all longitudes, are averaged to produce a single data value for that latitude and altitude. This is based on the assumption that the atmosphere is well mixed in the zonal direction.

References

1. Chamberlain, J.W. and D.M. Hunten, 1987: *Theory of Planetary Atmospheres*. Academic Press, San Diego.
2. Nachtwey, D.S. and R.D. Rundel, 1982: Ozone change: Biological effects. In *Stratospheric Ozone and Man*, F.A. Bower and R.B. Ward, eds. CRC Press, Boca Raton, 81–121.
3. Smith, R.C., B.B. Prézelin, K.S. Baker, R.R. Bidigare, N.P. Boucher, T. Coley, D. Karentz, S. MacIntyre, H.A. Matlick, D. Menzies, M. Ondrusek, Z. Wan and K.J. Waters, 1992: Ozone depletion: ultraviolet radiation and phytoplankton biology in Antarctic waters. *Science*, **255**, 952–959.
4. Slaper, H., G.J.M. Velders, J.S. Daniel, F.R. de Gruijl and J.C. van der Leun, 1996: Estimates of ozone depletion and skin cancer incidence to examine the Vienna Convention achievements. *Nature*, **384**, 256–258.
5. DeMore, W.B., S.P. Sander, D.M. Golden, R.F. Hampson, M.J. Kurylo, C.J. Howard, A.R. Ravishankara, C.E. Kolb and M.J. Molina, 1997: *Chemical Kinetics and Photochemical Data for Use in Stratospheric Modeling*, JPL Pub. 97-4. Jet Propulsion Laboratory, Pasadena.
6. Dobson, G.M.B., 1968: Forty years' research on atmospheric ozone at Oxford: a history. *Appl. Opt.*, **7**, 387–405.
7. Nicolet, M., 1979: *The First Years of the Study of Atmospheric Ozone*. US Dept of Transportation, Report No. 1979.
8. Goody, R.M. and Y.L. Yung, 1989: *Atmospheric Radiation: Theoretical Basis*. Oxford University, New York.
9. Ramanathan, V. and R.E. Dickinson, 1979: The role of stratospheric ozone in the zonal and seasonal radiative energy balance of the Earth–troposphere system. *J. Atmos. Sci.*, **36**, 1084.
10. Forster, P.M.D. and K.P. Shine, 1997: Radiative forcing and temperature trends from stratospheric ozone changes. *J. Geophys. Res.*, **102**, 10,841–10,855.
11. Lacis, A.A., D.J. Wuebbles and J.A. Logan, 1990: Radiative forcing of climate by changes in the vertical distribution of ozone. *J. Geophys. Res.*, **95**, 9971–9981.
12. Farman, J.C., B.G. Gardiner and J.D. Shanklin, 1985: Large losses of total ozone in Antarctica reveal seasonal ClO_x/NO_x interaction. *Nature*, **315**, 207–210.
13. WMO, 1995: *Scientific Assessment of Ozone Depletion: 1994, Global Ozone Research and Monitoring Project*. World Meteorological Organization, Geneva, 1995.
14. Hofmann, D.J., S.J. Oltmans, J.A. Lathrop, J.M. Harris and H. Vömel, 1994: Record low ozone at the South Pole in the spring of 1993. *Geophys. Res. Lett.*, **21**, 421–424.

15. WMO, 1986: *Atmospheric ozone 1985: Assessment of our understanding of the processes controlling its present distribution and change. Global Ozone Research and Monitoring Project.* World Meteorological Organization, Geneva.

16. Stolarski, R.S., P. Bloomfield, R.D. McPeters and J.R. Herman, 1991: Total ozone trends deduced from Nimbus 7 TOMS data. *Geophys. Res. Lett.,* **18**, 1015–1018.

17. Hood, L.L. and J.P. McCormack, 1992: Components of interannual ozone change based on Nimbus 7 TOMS data. *Geophys. Res. Lett.,* **19**, 2309–2312.

18. McPeters, R.D., S.M. Hollandsworth, L.E. Flynn, J.R. Herman and C.J. Seftor, 1996: Long-term ozone trends derived from the 16-year combined Nimbus 7/Meteor 3 TOMS Version 7 record. *Geophys. Res. Lett.,* **23**, 3699–3702.

19. Hood, L.L., R.D. McPeters, J.P. McCormack, L.E. Flynn, S.M. Hollandsworth and J.F. Gleason, 1993: Altitude dependence of stratospheric ozone trends based on Nimbus 7 SBUV data. *Geophys. Res. Lett.,* **20**, 2667–2670.

20. Randel, W.J., R.S. Stolarski, D.M. Cunnold, J.A. Logan, M.J. Newchurch and J.M. Zawodny, 1999: Trends in the vertical distribution of ozone. *Science,* **285**, 1689–1692.

21. WMO, 1998: *SPARC, Assessment of Trends in the Vertical Distribution of Ozone. Ozone Research and Monitoring Project Report 43.* N. Harris, R. Hudson and C. Phillips, eds. World Meterological Organization, Geneva.

22. Bluth, G.J.S., S.D. Doiron, C.C. Schnetzler, A.J. Krueger and L.S. Walter, 1992: Global tracking of the SO_2 clouds from the June, 1991 Mount Pinatubo eruptions. *Geophys. Res. Lett.,* **19**, 151–154.

23. McCormick, M.P. and R.E. Veiga, 1992: SAGE II measurements of early Pinatubo aerosols. *Geophys. Res. Lett.,* **19**, 155–158.

24. Gleason, J.F., P.K. Bhartia, J.R. Herman, R. McPeters, P. Newman, R.S. Stolarski, L. Flynn, G. Labow, D. Larko, C. Seftor, C. Wellemeyer, W.D. Komhyr, A.J. Miller and W. Planet, 1993: Record low global ozone in 1992. *Science,* **260**, 523–526.

25. Randel, W.J., F. Wu, J.M. Russell, III, J.W. Waters and L. Froidevaux, 1995: Ozone and temperature changes in the stratosphere following the eruption of Mount Pinatubo. *J. Geophys. Res.,* **100**, 16,753–16,764.

26. Herman, J.R. and D. Larko, 1994: Low ozone amounts during 1992–1993 from Nimbus 7 and Meteor 3 Total Ozone Mapping Spectrometers. *J. Geophys. Res.,* **99**, 3483–3496.

27. Brasseur, G. and S. Solomon, 1986: *Aeronomy of the Middle Atmosphere.* Reidel, Norwell.

28. Kawa, S.R., J.B. Kumer, A.R. Douglass, A.E. Roche, S.E. Smith, F.W. Taylor and D.J. Allen, 1995: Missing chemistry of reactive nitrogen in the upper stratospheric polar winter. *Geophys. Res. Lett.,* **22**, 2629–2632.

29. Hanson, D.R., A.R. Ravishankara and S. Solomon, 1994: Heterogeneous reactions in sulfuric acid aerosols: a framework for model calculations. *J. Geophys. Res.,* **99**, 3615–3629.

30. Hanson, D.R. and A.R. Ravishankara, 1994: Reactive uptake of $ClONO_2$ onto sulfuric acid due to reaction with HCl and H_2O. *J. Phys. Chem.,* **98**, 5728–5735.

31. Peter, T., 1997: Microphysics and heterogeneous chemistry of polar stratospheric clouds. *Annu. Rev. Phys. Chem.,* **48**, 785–822.

32. Kolb, C.E., D.R. Worsnop, M.S. Zahniser, P. Davidovits, L.F. Keyser, M.-T. Leu, M.J. Molina, D.R. Hanson, A.R. Ravishankara, L.R. Williams and M.A. Tolbert, 1995:

Laboratory studies of atmospheric heterogeneous chemistry. In *Progress and Problems in Atmospheric Chemistry*, J.R. Barker, ed. World Scientific, New Jersey, pp. 771–875.

33. Robinson, G.N., D.R. Worsnop, J.T. Jayne, C.E. Kolb and P. Davidovits, 1997: Heterogeneous uptake of $ClONO_2$ and N_2O_5 by sulfuric acid solutions. *J. Geophys. Res.*, **102**, 3583–3601.

34. Junge, C.E., C.W. Chagnon and J.E. Manson, 1961: Stratospheric aerosols. *J. Meteor.*, **18**, 81–108.

35. Tabazadeh, A., R.P. Turco, K. Drdla, M.Z. Jacobson and O.B. Toon, 1994: A study of type I polar stratospheric cloud formation. *Geophys. Res. Lett.*, **21**, 1619–1622.

36. Carslaw, K.S., B.P. Luo, S.L. Clegg, T. Peter, P. Brimblecombe and P.J. Crutzen, 1994: Stratospheric aerosol growth and HNO_3 gas phase depletion from coupled HNO_3 and water uptake by liquid particles. *Geophys. Res. Lett.*, **21**, 2479–2482.

37. Carslaw, K.S., T. Peter and S.L. Clegg, 1997: Modeling the composition of liquid stratospheric aerosols. *Rev. Geophys.*, **35**, 125–154.

38. Brock, C.A., P. Hamill, J.C. Wilson, H.H. Jonsson and K.R. Chan, 1995: Particle formation in the upper tropical troposphere: a source of nuclei for the stratospheric aerosol. *Science*, **270**, 1650–1653.

39. Hamill, P., E.J. Jensen, P.B. Russell and J.J. Bauman, 1997: The life cycle of stratospheric aerosol particles. *Bull. Am. Meteorol. Soc.*, **78**, 1395–1410.

40. McCormick, M.P., L.W. Thomason and C.R. Trepte, 1995: Atmospheric effects of the Mt Pinatubo eruption. *Nature*, **373**, 399–404.

41. Turco, R.P., P. Hamill, O.B. Toon, R.C. Whitten and C.S. Kiang, 1979: A one-dimensional model describing aerosol formation and evolution in the stratosphere: I. Physical processes and mathematical analogs. *J. Atmos. Sci.*, **36**, 699–717.

42. McKeen, S.A., S.C. Liu and C.S. Kiang, 1984: On the chemistry of stratospheric SO_2 from volcanic eruptions, *J. Geophys. Res.*, **89**, 4873–4881.

43. Yue, G.K., L.R. Poole, P.-H. Wang and E.W. Chiou, 1994: Stratospheric aerosol acidity, density and refractive index deduced from SAGE II and NMC temperature data. *J. Geophys. Res.*, **99**, 3727–3738.

44. Hoff, R.M., 1992: Differential SO_2 column measurements of the Mt. Pinatubo volcanic plume. *Geophys. Res. Lett.*, **19**, 175–178.

45. Wilson, J.C., H.H. Jonsson, C.A. Brock, D.W. Toohey, L.M. Avallone, D. Baumgardner, J.E. Dye, L.R. Poole, D.C. Woods, R.J. DeCoursey, M. Osborn, M.C. Pitts, K.K. Kelly, K.R. Chan, G.V. Ferry, M. Loewenstein, J.R. Podolske and A. Weaver, 1993: *In situ* observations of aerosol and chlorine monoxide after the 1991 eruption of Mount Pinatubo: effect of reactions on sulfate aerosol. *Science*, **261**, 1140–1143.

46. Dessler, A.E., R.M. Stimpfle, B.C. Daube, R.J. Salawitch, E.M. Weinstock, D.M. Judah, J.D. Burley, J.W. Munger, S.C. Wofsy, J.G. Anderson, M.P. McCormick and W.P. Chu, 1993: Balloon-borne measurements of ClO, NO and O_3 in a volcanic cloud: an analysis of heterogeneous chemistry between 20 and 30 km. *Geophys. Res. Lett.*, **20**, 2527–2530.

47. Pinnick, R.G., J.M. Rosen and D.J. Hofmann, 1976: Stratospheric aerosol measurements III: optical model calculations. *J. Atmos. Sci.*, **33**, 304–314.

48. Russell, P.B., J.M. Livingston, R.F. Pueschel, J.J. Bauman, J.B. Pollack, S.L. Brooks, P. Hamill, L.W. Thomason, L.L. Stowe, T. Deshler, E.G. Dutton and R.W. Bergstrom, 1996: Global to microscale evolution of the Pinatubo volcanic aerosol derived from diverse measurements and analyses. *J. Geophys. Res.*, **101**, 18,745–18,763.

49. Deshler, T., B.J. Johnson and W.R. Rozier, 1993: Balloonborne measurements of Pinatubo aerosol during 1991 and 1992 at 41°N: Vertical profiles, size distribution and volatility. *Geophys. Res. Lett.*, **24**, 1435–1438.

50. Hervig, M.E., T. Deshler and J.M. Russell, III, 1998: Aerosol size distribution obtained from HALOE spectral extinction measurements. *J. Geophys. Res.*, **103**, 1573–1583.

51. Volk, C.M., J.W. Elkins, D.W. Fahey, G.S. Dutton, J.M. Gilligan, M. Loewenstein, J.R. Podolske and K.R. Chan, 1997: Evaluation of source gas lifetimes from stratospheric observations. *J. Geophys. Res.*, **102**, 25,543–25,564.

52. Houghton, J.T., 1986: *The Physics of Atmospheres*, Cambridge University, New York.

53. Schoeberl, M.R. and L.C. Sparling, 1995: Trajectory modelling. In *Diagnostic Tools in Atmospheric Physics, Proceedings of the International School of Physics*, G. Fiocco and G. Visconti, eds. IOS Press, Amsterdam, pp. 289–305.

54. Kiehl, J.T. and S. Solomon, 1986: On the radiative balance of the stratosphere. *J. Atmos. Sci.*, **43**, 1525–1534.

55. Newman, P.A. and J.E. Rosenfield, 1997: Stratospheric thermal damping times. *Geophys. Res. Lett.*, **24**, 433–436.

56. Holton, J.R., 1979: *An Introduction to Dynamic Meteorology.* Academic Press, San Diego.

57. Lait, L.R., 1994: An alternative form for potential vorticity. *J. Atmos. Sci.*, **51**, 1754–1759.

58. Schoeberl, M.R., L.R. Lait, P.A. Newman, R.L. Martin, M.H. Proffitt, D.L. Hartmann, M. Loewenstein, J. Podolske, S.E. Strahan, J. Anderson, K.R. Chan and B. Gary, 1989: Reconstruction of the constituent distribution and trends in the Antarctic polar vortex from ER-2 flight observations. *J. Geophys. Res.*, **94**, 16,815–16,845.

59. Nakamura, N. and J. Ma, 1997: Modified Lagrangian-mean diagnostics of the stratospheric polar vortices. 2. Nitrous oxide and seasonal barrier migration in the Cryogenic Limb Array Etalon Spectrometer and SKYHI general circulation model. *J. Geophys. Res.*, **102**, 25,721–25,735.

60. Nakamura, N., J. Ma and J.J. Modi, 1998: Deciphering Lagrangian-mean transport and chemistry from the stratospheric trace constituents data. In *Recent Advances in Stratospheric Processes*, T. Nathan and E. Cordero, eds. Research Signpost, Trivandrum, India, 49–76.

61. Randel, W.J., J.C. Gille, A.E. Roche, J.B. Kumer, J.L. Mergenthaler, J.W. Waters, E.F. Fishbein and W.A. Lahoz, 1993: Stratospheric transport from the tropics to middle latitudes by planetary-wave mixing. *Nature*, **365**, 533–535.

62. Morris, G.A., M.R. Schoeberl, L. Sparling, P.A. Newman, L.R. Lait, L. Elson, J. Waters, R.A. Suttie, A. Roche, J. Kumer and J.M. Russell, III, 1995: Trajectory mapping and applications to data from the Upper Atmosphere Research Satellite. *J. Geophys. Res.*, **100**, 16,491–16,505.

63. Chapman, S., 1930: A theory of upper-atmospheric ozone. *Mem. R. Meteorol. Soc.*, **3**, 103–125.

64. Minschwaner, K., R.J. Salawitch and M.B. McElroy, 1993: Absorption of solar radiation by O_2: implications for O_3 and lifetimes of N_2O, $CFCl_3$ and CF_2Cl_2. *J. Geophys. Res.*, **98**, 10,543–10,561.

65. Michelsen, H.A., R.J. Salawitch, P.O. Wennberg and J.G. Anderson, 1994: Production of $O(^1D)$ from photolysis of O_3. *Geophys. Res. Lett.*, **21**, 2227–2230.

66. Press, W.H., B.P. Flannery, S.A. Teukolsky and W.T. Vetterling, 1988: *Numerical Recipes in C*. Cambridge University Press, Cambridge.

67. Johnston, H.S. and J. Podolske, 1978: Interpretations of stratospheric photochemistry. *Rev. Geophys.*, **16**, 491–519.

68. Stolarski, R.S. and R.J. Cicerone, 1974: Stratospheric chlorine: a possible sink for ozone. *Can. J. Chem.*, **52**, 1610–1615.

69. Dessler, A.E., S.R. Kawa, A.R. Douglass, D.B. Considine, J.B. Kumer, A.E. Roche, J.W. Waters, J.M. Russell, III and J.C. Gille, 1996: A test of the partitioning between ClO and $ClONO_2$ using simultaneous UARS measurements of ClO, NO_2 and $ClONO_2$. *J. Geophys. Res.*, **101**, 12,515–12,521.

70. Stimpfle, R.M., J.P. Koplow, R.C. Cohen, D.W. Kohn, P.O. Wennberg, D.M. Judah, D.W. Toohey, L.M. Avallone, J.G. Anderson, R.J. Salawitch, E.L. Woodbridge, C.R. Webster, R.D. May, M.H. Proffitt, K. Aiken, J. Margitan, M. Loewenstein, J.R. Podolske, L. Pfister and K.R. Chan, 1994: The response of ClO radical concentrations to variations in NO_2 radical concentrations in the lower stratosphere. *Geophys. Res. Lett.*, **21**, 2543–2546.

71. Dessler, A.E., S.R. Kawa, D.B. Considine, J.W. Waters, L. Froidevaux and J.B. Kumer, 1996: UARS measurements of ClO and NO_2 at 40 and 46 km and implications for the model "ozone deficit". *Geophys. Res. Lett.*, **23**, 339–342.

72. Crutzen, P.J., 1970: The influence of nitrogen oxides on the atmospheric ozone content. *Q. J. R. Meteorol. Soc.*, **96**, 320–325.

73. Jackman, C.H., E.L. Fleming, S. Chandra, D.B. Considine and J.E. Rosenfield, 1996: Past, present and future modeled ozone trends with comparisons to observed trends. *J. Geophys. Res.*, **101**, 28,753–28,767.

74. Wennberg, P.O., R.C. Cohen, R.M. Stimpfle, J.P. Koplow, J.G. Anderson, R.J. Salawitch, D.W. Fahey, E.L. Woodbridge, E.R. Keim, R.S. Gao, C.R. Webster, R.D. May, D.W. Toohey, L.M. Avallone, M.H. Proffitt, M. Loewenstein, J.R. Podolske, K.R. Chan and S.C. Wofsy, 1994: Removal of stratospheric O_3 by radicals: *in situ* measurements of OH, HO_2, NO, NO_2, ClO and BrO. *Science*, **266**, 398–404.

75. Osterman, G.B., R.J. Salawitch, B. Sen, G.C. Toon, R.A. Stachnik, H.M. Pickett, J.J. Margitan, J.-F. Blavier and D.B. Peterson, 1997: Balloon-borne measurements of stratospheric radicals and their precursors: Implications for the production and loss of ozone. *Geophys. Res. Lett.*, **24**, 1107–1110.

76. Eluszkiewicz, J. and M. Allen, 1993: A global analysis of the ozone deficit in the upper stratosphere and lower mesosphere. *J. Geophys. Res.*, **98**, 1069–1082.

77. Lovelock, J.E., R.J. Maggs and R.J. Wade, 1973: Halogenated hydrocarbons in and over the Atlantic. *Nature*, **241**, 194–196.

78. Molina, M.J. and F.S. Rowland, 1974: Stratospheric sink for chlorofluoromethanes: Chlorine atom-catalysed destruction of ozone. *Nature*, **249**, 810–812.

79. Tabazadeh, A. and R.P. Turco, 1993: Stratospheric chlorine injection by volcanic eruptions: HCl scavenging and implications for ozone. *Science*, **260**, 1082–1086.

80. Montzka, S.A., J.H. Butler, R.C. Myers, T.M. Thompson, T.H. Swanson, A.D. Clarke, L.T. Lock and J.W. Elkins, 1996: Decline in the tropospheric abundance of halogen from halocarbons: Implications for stratospheric ozone depletion. *Science*, **272**, 1318–1322.

81. Pollock, W.H., L.E. Heidt, R.A. Lueb, J.F. Vedder, M.J. Mills and S. Solomon, 1992: On

the age of stratospheric air and ozone depletion potentials in polar regions. *J. Geophys. Res.*, **97**, 12,993–12,999.

82. Hall, T.M. and R.A. Plumb, 1994: Age as a diagnostic of stratospheric transport. *J. Geophys. Res.*, **99**, 1059–1070.

83. Boering, K.A., S.C. Wofsy, B.C. Daube, H.R. Schneider, M. Loewenstein, J.R. Podolske and T.J. Conway, 1996: Stratospheric mean ages and transport rates from observations of carbon dioxide and nitrous oxide. *Science*, **274**, 1340–1343.

84. Russell, J.M., III, M. Luo, R.J. Cicerone and L.E. Deaver, 1996: Satellite confirmation of the dominance of chlorofluorocarbons in the global stratospheric chlorine budget. *Nature*, **379**, 526–529.

85. Lipson, J.B., M.J. Elrod, T.W. Beiderhase, L.T. Molina and M.J. Molina, 1997: Temperature dependence of the rate constant and branching ratio for the OH + ClO reaction. *J. Chem. Soc. Faraday Trans.*, **93**, 2665–2673.

86. McElroy, M.B. and R.J. Salawitch, 1989: Changing composition of the global stratosphere. *Science*, **243**, 763–770.

87. Michelsen, H.A., R.J. Salawitch, M.R. Gunson, C. Aellig, N. Kämpfer, M.M. Abbas, M.C. Abrams, T.L. Brown, A.Y. Chang, A. Goldman, F.W. Irion, M.J. Newchurch, C.P. Rinsland, G.P. Stiller and R. Zander, 1996: Stratospheric chlorine partitioning: Constraints from shuttle-borne measurements of [HCl], [ClNO$_3$] and [ClO]. *Geophys. Res. Lett.*, **23**, 2361–2364.

88. Solomon, S., R.W. Portmann, R.R. Garcia, W. Randel, F. Wu, R. Nagatani, J. Gleason, L. Thomason, L.R. Poole and M.P. McCormick, 1998: Ozone depletion at mid-latitudes: coupling of volcanic aerosols and temperature variability to anthropogenic chlorine. *Geophys. Res. Lett.*, **25**, 1871–1874.

89. Zander, R., E. Mahieu, M.R. Gunson, M.C. Abrams, A.Y. Chang, M. Abbas, C. Aellig, A. Engel, A. Goldman, F.W. Irion, N. Kämpfer, H.A. Michelsen, M.J. Newchurch, C.P. Rinsland, R.J. Salawitch, G.P. Stiller and G.C. Toon, 1996: The 1994 northern midlatitude budget of stratospheric chlorine derived from ATMOS/ATLAS-3 observations. *Geophys. Res. Lett.*, **23**, 2357–2360.

90. Dessler, A.E., D.B. Considine, G.A. Morris, M.R. Schoeberl, A.E. Roche, J.L. Mergenthaler, J.M. Russell, J.W. Waters, J.C. Gille and G.K. Yue, 1995: Correlated observations of HCl and ClONO$_2$ from UARS and implications for stratospheric chlorine partitioning. *Geophys. Res. Lett.*, **22**, 1721–1724.

91. DeMore, W.B., S.P. Sander, D.M. Golden, R.F. Hampson, M.J. Kurylo, C.J. Howard, A.R. Ravishankara, C.E. Kolb and M.J. Molina, 1994: *Chemical Kinetics and Photochemical Data for Use in Stratospheric Modeling*, JPL Pub. 94-26, Jet Propulsion Laboratory, Pasadena.

92. Johnson, D.G., W.A. Traub, K.V. Chance, K.W. Jucks and R.A. Stachnik, 1995: Estimating the abundance of ClO from simultaneous remote sensing measurements of HO$_2$, OH and HOCl. *Geophys. Res. Lett.*, **22**, 1869–1871.

93. Woodbridge, E.L., J.W. Elkins, D.W. Fahey, L.E. Heidt, S. Solomon, T.J. Baring, T.M. Gilpin, W.H. Pollock, S.M. Schauffler, E.L. Atlas, M. Loewenstein, J.R. Podolske, C.R. Webster, R.D. May, J.M. Gilligan, S.A. Montzka, K.A. Boering and R.J. Salawitch, 1995: Estimates of total organic and inorganic chlorine in the lower stratosphere from *in situ* and flask measurements during AASE II. *J. Geophys. Res.*, **100**, 3057–3064.

94. Khalil, M.A.K. and R.A. Rasmussen, 1992: The global sources of nitrous oxide. *J. Geophys. Res.*, **97**, 14,651–14,660.

95. Greenblatt, G.D. and A.R. Ravishankara, 1990: Laboratory studies on the stratospheric NO$_x$ production rate. *J. Geophys. Res.*, **95**, 3539–3547.

96. Vitt, F.M. and C.H. Jackman, 1996: A comparison of sources of odd nitrogen production from 1974 through 1993 in the Earth's middle atmosphere as calculated using a two-dimensional model. *J. Geophys. Res.*, **101**, 6729–6739.

97. Siskind, D.E., J.T. Bacmeister, M.E. Summers and J.M. Russell, 1997: Two-dimensional model calculations of nitric oxide transport in the middle atmosphere and comparison with Halogen Occultation Experiment data. *J. Geophys. Res.*, **102**, 3527–3545.

98. Kondo, Y., A. Iwata, P. Aimedieu, W.A. Matthews, W.R. Sheldon and J.R. Benbrook, 1989: Profiles of nitric oxide in the upper stratosphere. *Geophys. Res. Lett.*, **16**, 1379–1382.

99. Webster, C.R., R.D. May, R. Toumi and J.A. Pyle, 1990: Active nitrogen partitioning and the nighttime formation of N$_2$O$_5$ in the stratosphere: simultaneous *in situ* measurements of NO, NO$_2$, HNO$_3$, O$_3$ and N$_2$O using the BLISS diode laser spectrometer. *J. Geophys. Res.*, **95**, 13,851–13,866.

100. Kondo, Y., P. Aimedieu, M. Pirre, W.A. Matthews, R. Ramaroson, W.R. Sheldon, J.R. Benbrook and A. Iwata, 1990: Diurnal variation of nitric oxide in the upper stratosphere. *J. Geophys. Res.*, **95**, 22,513–22,522.

101. Cadle, R.D., P. Crutzen and D. Ehhalt, 1975: Heterogeneous chemical reactions in the stratosphere. *J. Geophys. Res.*, **80**, 3381–3385.

102. Hanson, D.R., A.R. Ravishankara and E.R. Lovejoy, 1996: Reaction of BrONO$_2$ with H$_2$O on submicron sulfuric acid aerosol and the implications for the lower stratosphere. *J. Geophys. Res.*, **101**, 9063–9069.

103. Sen, B., G.C. Toon, G.B. Osterman, J.F. Blavier, J.J. Margitan, R.J. Salawitch and G.K. Yue, 1998: Measurements of reactive nitrogen in the stratosphere. *J. Geophys. Res.*, **103**, 3571–3585.

104. Nevison, C.D., S. Solomon and R.R. Garcia, 1997: Model overestimates of NO$_x$ in the upper stratosphere. *Geophys. Res. Lett.*, **24**, 803–806.

105. Nevison, C.D., S. Solomon and J.M. Russell, III, 1996: Nighttime formation of N$_2$O$_5$ inferred from the Halogen Occultation Experiment sunset/sunrise NO$_x$ ratios. *J. Geophys. Res.*, **101**, 6741–6748.

106. Morris, G.A., D.B. Considine, A.E. Dessler, S.R. Kawa, J.B. Kumer, J.L. Mergenthaler, A.E. Roche and J.M. Russell, III, 1997: Nitrogen partitioning in the middle stratosphere as observed by the Upper Atmosphere Research Satellite. *J. Geophys. Res.*, **102**, 8955–8965.

107. Randeniya, L.K., P.F. Vohralik, I.C. Plumb and K.R. Ryan, 1997: Heterogeneous BrONO$_2$ hydrolysis: effect on NO$_2$ columns and ozone at high latitudes in summer. *J. Geophys. Res.*, **102**, 23,543–23,557.

108. Logan, J.A., M.J. Prather, S.C. Wofsy and M.B. McElroy, 1978: Atmospheric chemistry: response to human influence. *Phil. Trans. R. Soc. BA*, **290**, 170–172.

109. Wofsy, S.C., 1976: Interactions of CH$_4$ and CO in the Earth's Atmosphere. *Annu. Rev. Earth Planet. Sci.*, **4**, 441–469.

110. Wofsy, S.C., J.C. McConnell and M.B. McElroy, 1972: Atmospheric CH$_4$, CO and CO$_2$. *J. Geophys. Res.*, **77**, 4477–4493.

111. Pressman, J. and P. Warneck, 1970: The stratosphere as a chemical sink for carbon monoxide. *J. Geophys. Res.*, **27**, 155–163.

112. Penner, J.E., M.B. McElroy and S.C. Wofsy, 1977: Sources and sinks for atmospheric H_2: a current analysis with projections for the influence of anthropogenic activity. *Planet. Space Sci.*, **25**, 521–540.

113. Ehhalt, D.H. and A. Tönnissen, 1979: Hydrogen and carbon compounds in the stratosphere. In *Proceedings of the NATO Advanced Study Institute on Atmospheric Ozone: Its Variations and Human Influences*, A.C. Aikin, ed. Algarve, Portugal, pp. 129–151.

114. Schmidt, U., G. Kulessa and E.P. Röth, 1979: The atmospheric H_2 cycle. In *Proceedings of the NATO Advanced Study Institute on Atmospheric Ozone: Its Variations and Human Influences*, A.C. Aikin, ed. Algarve, Portugal, pp. 307–322.

115. Wennberg, P.O., R.J. Salawitch, D.J. Donaldson, T.F. Hanisco, E.J. Lanzendorf, K.K. Perkins, S.A. Lloyd, V. Vaida, R.S. Gao, E.J. Hintsa, R.C. Cohen, W.H. Swartz, T.L. Kusterer and D.E. Anderson, 1999: Twilight observations suggest unknown sources of HO_x. *Geophys. Res. Lett.*, **26**, 1373–1376.

116. Fahey, D.W., S.R. Kawa, E.L. Woodbridge, P. Tin, J.C. Wilson, H.H. Jonsson, J.E. Dye, D. Baumgardner, S. Borrmann, D.W. Toohey, L.M. Avallone, M.H. Proffitt, J. Margitan, M. Loewenstein, J.R. Podolske, R.J. Salawitch, S.C. Wofsy, M.K.W. Ko, D.E. Anderson, M.R. Schoeberl and K.R. Chan, 1993: *In situ* measurements constraining the role of sulphate aerosols in mid-latitude ozone depletion. *Nature*, **363**, 509–514.

117. Cohen, R.C., P.O. Wennberg, R.M. Stimpfle, J. Koplow, J.G. Anderson, D.W. Fahey, E.L. Woodbridge, E.R. Keim, R. Gao, M.H. Proffitt, M. Loewenstein and K.R. Chan, 1994: Are models of catalytic removal of O_3 by HO_x accurate? Constraints from *in situ* measurements of the OH to HO_2 ratio. *Geophys. Res. Lett.*, **21**, 2539–2542.

118. Jucks, K.W., D.G. Johnson, K.V. Chance, W.A. Traub, R.J. Salawitch and R.A. Stachnik, 1996: Ozone production and loss rate measurements in the middle stratosphere. *J. Geophys. Res.*, **101**, 28,785–28,792.

119. Chance, K., W.A. Traub, D.G. Johnson, K.W. Jucks, P. Ciarpallini, R.A. Stachnik, R.J. Salawitch and H.A. Michelsen, 1996: Simultaneous measurements of stratospheric HO_x, NO_x and Cl_x: comparison with a photochemical model. *J. Geophys. Res.*, **101**, 9031–9043.

120. Stimpfle, R.M., P.O. Wennberg, L.B. Lapson and J.G. Anderson, 1990: Simultaneous, *in situ* measurements of OH and HO_2 in the stratosphere. *Geophys. Res. Lett.*, **17**, 1905–1908.

121. Wennberg, P.O., R.M. Stimpfle, E.M. Weinstock, A.E. Dessler, S.A. Lloyd, L.B. Lapson, J.J. Schwab and J.G. Anderson, 1990: A test of modeled stratospheric HO_x chemistry: simultaneous measurements of OH, HO_2, O_3 and H_2O. *Geophys. Res. Lett.*, **17**, 1909–1912.

122. Stachnik, R.A., J.C. Hardy, J.A. Tarsala, J.W. Waters and N.R. Erickson, 1992: Submillimeterwave heterodyne measurements of stratospheric ClO, HCl, O_3 and HO_2: first results. *Geophys. Res. Lett.*, **19**, 1931–1934.

123. Jucks, K.W., D.G. Johnson, K.V. Chance, W.A. Traub, J.J. Margitan, G.B. Osterman, R.J. Salawitch and Y. Sasano, 1998: Observations of OH, HO_2, H_2O and O_3 in the upper stratosphere: implications for HO_x photochemistry. *Geophys. Res. Lett.*, **25**, 3935–3938.

124. Salawitch, R.J., S.C. Wofsy, P.O. Wennberg, R.C. Cohen, J.G. Anderson, D.W. Fahey, R.S. Gao, E.R. Keim, E.L. Woodbridge, R.M. Stimpfle, J.P. Koplow, D.W. Kohn, C.R. Webster,

R.D. May, L. Pfister, E.W. Gottlieb, H.A. Michelsen, G.K. Yue, J.C. Wilson, C.A. Brock, H.H. Jonsson, J.E. Dye, D. Baumgardner, M.H. Proffitt, M. Loewenstein, J.R. Podolske, J.W. Elkins, G.S. Dutton, E.J. Hintsa, A.E. Dessler, E.M. Weinstock, K.K. Kelly, K.A. Boering, B.C. Daube, K.R. Chan and S.W. Bowen, 1994: The distribution of hydrogen, nitrogen and chlorine radicals in the lower stratosphere: Implications for changes in O_3 due to emission of NO_x from supersonic aircraft. *Geophys. Res. Lett.*, **21**, 2547–2550.

125. Jaeglé, L., D.J. Jacob, P.O. Wennberg, C.M. Spivakovsky, T.F. Hanisco, E.J. Lanzendorf, E.J. Hintsa, D.W. Fahey, E.R. Keim, M.H. Proffitt, E.L. Atlas, F. Flocke, S. Schauffler, C.T. McElroy, C. Midwinter, L. Pfister and J.C. Wilson, 1997: Observed OH and HO_2 in the upper troposphere suggest a major source from convective injection of peroxides. *Geophys. Res. Lett.*, **24**, 3181–3184.

126. Wennberg, P.O., R.C. Cohen, N.L. Hazen, L.B. Lapson, N.T. Allen, T.F. Hanisco, J.F. Oliver, N.W. Lanham, J.N. Demusz and J.G. Anderson, 1994: An aircraft-borne, laser-induced fluorescence instrument for the *in situ* detection of hydroxyl and hydroperoxyl radical. *Rev. Sci. Instrum.*, **65**, 1858–1876.

127. Khalil, M.A.K., R.A. Rasmussen and A.R. Gunawarden, 1993: Atmospheric methyl-bromide: trends and global mass balance. *J. Geophys. Res.*, **98**, 2887–2896.

128. Butler, J.H., S.A. Montzka, A.D. Clarke, J.M. Lobert and J.W. Elkins, 1998: Growth and distribution of halons in the atmosphere. *J. Geophys. Res.*, **103**, 1503–1511.

129. Schauffler, S.M., E.L. Atlas, F. Flocke, R.A. Lueb, V. Stroud and W. Travnicek, 1998: Measurements of bromine containing organic compounds at the tropical tropopause. *Geophys. Res. Lett.*, **25**, 317–320.

130. Wamsley, P.R., J.W. Elkins, D.W. Fahey, G.S. Dutton, C.M. Volk, R.C. Myers, S.A. Montzka, J.H. Butler, A.D. Clarke, P.J. Fraser, L.P. Steele, M.P. Lucarelli, E.L. Atlas, S.M. Schauffler, D.R. Blake, F.S. Rowland, W.T. Sturges, J.M. Lee, S.A. Penkett, A. Engel, R.M. Stimpfle, K.R. Chan, D.K. Weisenstein, M.K.W. Ko and R.J. Salawitch, 1998: Distribution of halon-1211 in the upper troposphere and lower stratosphere and the 1994 total bromine budget. *J. Geophys. Res.*, **103**, 1513–1526.

131. Lary, D.J., 1996: Gas phase atmospheric bromine photochemistry. *J. Geophys. Res.*, **101**, 1505–1516.

132. Johnson, D.G., W.A. Traub, K.V. Chance and K.W. Jucks, 1995: Detection of HBr and upper limit for HOBr: bromine partitioning in the stratosphere. *Geophys. Res. Lett.*, **22**, 1373–1376.

133. Lary, D.J., M.P. Chipperfield, R. Toumi and T. Lenton, 1996: Heterogeneous atmospheric bromine chemistry. *J. Geophys. Res.*, **101**, 1489–1504.

134. Avallone, L.M., D.W. Toohey, S.M. Schauffler, W.H. Pollock, L.E. Heidt, E.L. Atlas and K.R. Chan, 1995: *In situ* measurements of BrO during AASE II. *Geophys. Res. Lett.*, **22**, 831–834.

135. Daniel, J.S., S. Solomon, R.W. Portmann and R.R. Garcia, 1999: Stratospheric ozone destruction: the importance of bromine relative to chlorine. *J. Geophys. Res.*, **104**, 23,871–23,880.

136. Solomon, S., M. Mills, L.E. Heidt, W.H. Pollock and A.F. Tuck, 1992: On the evaluation of ozone depletion potentials. *J. Geophys. Res.*, **97**, 825–842.

137. Kaye, J.A., A.R. Douglass, C.H. Jackman, R.S. Stolarski, R. Zander and G. Roland, 1991: Two-dimensional model calculation of fluorine-containing reservoir species in the stratosphere. *J. Geophys. Res.*, **96**, 12,865–12,881.

138. Sen, B., G.C. Toon, J.-F. Blavier, E.L. Fleming and C.H. Jackman, 1996: Balloon-borne observations of midlatitude fluorine abundance. *J. Geophys. Res.*, **101**, 9045–9054.

139. Chipperfield, M.P., M. Burton, W. Bell, C.P. Walsh, T. Blumenstock, M.T. Coffey, J.W. Hannigan, W.G. Mankin, B. Galle, J. Mellqvist, E. Mahieu, R. Zander, J. Notholt, B. Sen and G.C. Toon, 1997: On the use of HF as a reference for the comparison of stratospheric observations and models. *J. Geophys. Res.*, **102**, 12,901–12,919.

140. Solomon, S., R.R. Garcia and A.R. Ravishankara, 1994: On the role of iodine in ozone depletion. *J. Geophys. Res.*, **99**, 20,491–20,499.

141. Wennberg, P.O., J.W. Brault, T.F. Hanisco, R.J. Salawitch and G.H. Mount, 1997: The atmospheric abundance of IO: implications for stratospheric ozone. *J. Geophys. Res.*, **102**, 8887–8898.

142. Hansen, J., A. Lacis and M. Prather, 1989: Greenhouse effect of chlorofluorocarbons and other trace gases. *J. Geophys. Res.*, **94**, 16,417–16,421.

143. Ramaswamy, V., M.D. Schwarzkopf and K.P. Shine, 1992: Radiative forcing of climate from halocarbon-induced global stratospheric ozone loss. *Nature*, **355**, 810–812.

144. Wang, W.-C., Y.-C. Zhuang and R.D. Bojkov, 1993: Climate implications of observed changes in ozone vertical distributions at middle and high latitudes of the northern hemisphere. *Geophys. Res. Lett.*, **20**, 1567–1570.

145. Andrews, D.G., J.R. Holton and C.B. Leovy, 1987: *Middle Atmosphere Dynamics*. Academic Press, Orlando.

146. McIntyre, M.E., 1992: Atmospheric dynamics: some fundamentals, with observational implications. In *The Use of EOS for Studies of Atmospheric Physics*, J.C. Gille and G. Visconti, eds. Varenna on Lake Como, pp. 313–386.

147. Brewer, A.W., 1949: Evidence for a world circulation provided by the measurements of helium and water vapour distribution in the stratosphere. *Q. J. R. Meteorol. Soc.*, **75**, 351–363.

148. Holton, J.R., P.H. Haynes, M.E. McIntyre, A.R. Douglass, R.B. Rood and L. Pfister, 1995: Stratosphere-troposphere exchange. *Rev. Geophys.*, **33**, 403–439.

149. Hoskins, B.J., 1991: Towards a PV-θ view of the general circulation. *Tellus*, **43AB**, 27–35.

150. Dobson, G.M.B., 1956: Origin and distribution of the polyatomic molecules in the atmosphere. *Proc. R. Soc. Lond.*, **A236**, 187–193.

151. Newell, R.E. and S. Gould-Stewart, 1981: A stratospheric fountain? *J. Atmos. Sci.*, **38**, 2789–2796.

152. Mote, P.W., K.H. Rosenlof, M.E. McIntyre, E.S. Carr, J.C. Gille, J.R. Holton, J.S. Kinnersley, H.C. Pumphrey, J.M. Russell, III and J.W. Waters, 1996: An atmospheric tape recorder: the imprint of tropical tropopause temperatures on stratospheric water vapor. *J. Geophys. Res.*, **101**, 3989–4006.

153. Boering, K.A., E.J. Hintsa, S.C. Wofsy, J.G. Anderson, B.C. Daube, Jr., A.E. Dessler, M. Loewenstein, M.P. McCormick, J.R. Podolske, E.M. Weinstock and G.K. Yue, 1995: Measurements of stratospheric carbon dioxide and water vapor at northern midlatitudes: implications for troposphere-to-stratosphere transport. *Geophys. Res. Lett.*, **22**, 2737–2740.

154. Dessler, A.E., 1998: A reexamination of the "stratospheric fountain" hypothesis. *Geophys. Res. Lett.*, **25**, 4165–4168.

155. Robinson, G.D., 1980: The transport of minor atmospheric constituents between troposphere and stratosphere. *Q. J. R. Meteorol. Soc.*, **106**, 227–253.

156. Prabhakara, C., D.P. Kratz, J.-M. Yoo, G. Dalu and A. Vernekar, 1993: Optically thin cirrus clouds: radiative impact on the warm pool. *J. Quant. Spectrosc. Radiat. Transfer*, **49**, 467–483.

157. Wang, P.-H., M.P. McCormick, L.R. Poole, W.P. Chu, G.K. Yue, G.S. Kent and K.M. Skeens, 1994: Tropical high cloud characteristics derived from SAGE II extinction measurements. *Atmos. Res.*, **34**, 53–83.

158. Jensen, E.J., O.B. Toon, H.B. Selkirk, J.D. Spinhirne and M.R. Schoeberl, 1996: On the formation and persistence of subvisible cirrus clouds near the tropical tropopause. *J. Geophys. Res.*, **101**, 21,361–21,375.

159. Jensen, E.J., O.B. Toon, L. Pfister and H.B. Selkirk, 1996: Dehydration of the upper troposphere and lower stratosphere by subvisible cirrus clouds near the tropical tropopause. *Geophys. Res. Lett.*, **23**, 825–828.

160. Potter, B.E. and J.R. Holton, 1995: The role of monsoon convection in the dehydration of the lower tropical stratosphere. *J. Atmos. Sci.*, **52**, 1034–1050.

161. Danielsen, E.F., 1993: *In situ* evidence of rapid, vertical, irreversible transport of lower tropospheric air into the lower tropical stratosphere by convective cloud turrets and by larger-scale upwelling in tropical cyclones. *J. Geophys. Res.*, **98**, 8665–8681.

162. *STEP Tropical Special Issue*, 1993.

163. Danielsen, E.F., 1982: A dehydration mechanism for the stratosphere. *Geophys. Res. Lett.*, **9**, 605–608.

164. Dessler, A.E., E.J. Hintsa, E.M. Weinstock, J.G. Anderson and K.R. Chan, 1995: Mechanisms controlling water vapor in the lower stratosphere: "a tale of two stratospheres". *J. Geophys. Res.*, **100**, 23,167–23,172.

165. Boering, K.A., B.C. Daube, Jr., S.C. Wofsy, M. Loewenstein, J.R. Podolske and E.R. Keim, 1994: Tracer–tracer relationships and lower stratospheric dynamics: CO_2 and N_2O correlations during SPADE. *Geophys. Res. Lett.*, **21**, 2567–2570.

166. Dessler, A.E. and H. Kim, 1999: Determination of the amount of water vapor entering the stratosphere based on HALOE data. *J. Geophys. Res.*, **104**, 30,605–30,607.

167. Khalil, M.A.K., R.A. Rasmussen and F. Moraes, 1993: Atmospheric methane at Cape Meares: analysis of a high-resolution data base and its environmental implications. *J. Geophys. Res.*, **98**, 14,753–14,770.

168. Pollock, W., L.E. Heidt, R. Lueb and D.H. Ehhalt, 1980: Measurement of stratospheric water vapor by cryogenic collection. *J. Geophys. Res.*, **85**, 5555–5568.

169. Fabian, P., R. Borchers, G. Flentje, W.A. Matthews, W. Seiler, H. Giehl, K. Bunse, F. Müller, U. Schmidt, A. Volz, A. Khedim and F.J. Johnen, 1981: The vertical distribution of stable trace gases at mid-latitudes. *J. Geophys. Res.*, **86**, 5179–5184.

170. Hintsa, E.J., E.M. Weinstock, A.E. Dessler, J.G. Anderson, M. Loewenstein and J.R. Podolske, 1994: SPADE H_2O measurements and the seasonal cycle of stratospheric water vapor. *Geophys. Res. Lett.*, **21**, 2559–2562.

171. Abbas, M.M., M.R. Gunson, M.J. Newchurch, H.A. Michelsen, R.J. Salawitch, M. Allen, M.C. Abrams, A.Y. Chang, A. Goldman, F.W. Irion, E.J. Moyer, R. Nagaraju, C.P. Rinsland, G.P. Stiller and R. Zander, 1996: The hydrogen budget of the stratosphere inferred from ATMOS measurements of H_2O and CH_4. *Geophys. Res. Lett.*, **23**, 2405–2408.

172. Dessler, A.E., E.M. Weinstock, E.J. Hintsa, J.G. Anderson, C.R. Webster, R.D. May, J.W. Elkins and G.S. Dutton, 1994: An examination of the total hydrogen budget of the lower stratosphere. *Geophys. Res. Lett.*, **21**, 2563–2566.

173. Hurst, D.F., G.S. Dutton, P.A. Romashkin, P.R. Wamsley, F.L. Moore, J.W. Elkins, E.J.

Hintsa, E.M. Weinstock, R.L. Herman, E.J. Moyer, D.C. Scott, R.D. May and C.R. Webster, 1999: Closure of the total hydrogen budget of the northern extratropical lower stratosphere. *J. Geophys. Res.*, **104**, 8191–8200.

174. Randel, W.J., W. Fei, J.M. Russell, III, A. Roche and J.W. Waters, 1998: Seasonal cycles and QBO variations in stratospheric CH_4 and H_2O observed in UARS HALOE data. *J. Atmos. Sci.*, **55**, 163–185.

175. Folkins, I. and C. Appenzeller, 1996: Ozone and potential vorticity at the subtropical tropopause break. *J. Geophys. Res.*, **101**, 18,787–18,792.

176. Chen, P., 1995: Isentropic cross-tropopause mass exchange in the extratropics. *J. Geophys. Res.*, **100**, 16,661–16,673.

177. Poulida, O., R.R. Dickerson and A. Heymsfield, 1996: Stratosphere–troposphere exchange in a midlatitude mesoscale convective complex, 1. Observations. *J. Geophys. Res.*, **101**, 6823–6836.

178. Hintsa, E.J., K.A. Boering, E.M. Weinstock, J.G. Anderson, B.L. Gary, L. Pfister, B.C. Daube, S.C. Wofsy, M. Loewenstein, J.R. Podolske, J.J. Margitan and T.P. Bui, 1998: Troposphere-to-stratosphere transport in the lowermost stratosphere from measurements of H_2O, CO_2, N_2O and O_3. *Geophys. Res. Lett.*, **25**, 2655–2658.

179. Hartmann, D.L., 1994: *Global Physical Climatology*. Academic Press, San Diego.

180. Eluszkiewicz, J., 1996: A three-dimensional view of the stratosphere-to-troposphere exchange in the GFDL SKYHI model. *Geophys. Res. Lett.*, **23**, 2489–2492.

181. Rosenlof, K.H. and J.R. Holton, 1993: Estimates of the stratospheric residual circulation using the downward control principle. *J. Geophys. Res.*, **98**, 10,465–10,479.

182. Minschwaner, K., A.E. Dessler, J.W. Elkins, C.M. Volk, D.W. Fahey, M. Loewenstein, J.R. Podolske, A.E. Roche and K.R. Chan, 1996: Bulk properties of isentropic mixing into the tropics in the lower stratosphere. *J. Geophys. Res.*, **101**, 9433–9439.

183. Avallone, L.M. and M.J. Prather, 1996: Photochemical evolution of ozone in the lower tropical stratosphere. *J. Geophys. Res.*, **101**, 1457–1461.

184. Volk, C.M., J.W. Elkins, D.W. Fahey, R.J. Salawitch, G.S. Dutton, J.M. Gilligan, M.H. Proffitt, M. Loewenstein, J.R. Podolske, K. Minschwaner, J.J. Margitan and K.R. Chan, 1996: Quantifying transport between the tropical and mid-latitude lower stratosphere. *Science*, **272**, 1763–1768.

185. Plumb, R.A., 1996: A "tropical pipe" model of stratospheric transport. *J. Geophys. Res.*, **101**, 3957–3972.

186. Schoeberl, M.R., L.R. Lait, P.A. Newman and J.E. Rosenfield, 1992: The structure of the polar vortex. *J. Geophys. Res.*, **97**, 7859–7882.

187. Schoeberl, M.R. and D.L. Hartmann, 1991: The dynamics of the stratospheric polar vortex and its relation to springtime ozone depletions. *Science*, **251**, 46–52.

188. Bowman, K.P., 1993: Large-scale isentropic mixing properties of the Antarctic polar vortex from analyzed winds. *J. Geophys. Res.*, **98**, 23,013–23,027.

189. Waugh, D.W., T.M. Hall, W.J. Randel, P.J. Rasch, B.A. Boville, K.A. Boering, S.C. Wofsy, B.C. Daube, J.W. Elkins, D.W. Fahey, G.S. Dutton, C.M. Volk and P.F. Vohralik, 1997: Three-dimensional simulations of long-lived tracers using winds from MACCM2. *J. Geophys. Res.*, **102**, 21,493–21,513.

190. Ko, M.K.W., N.-D. Sze and D.K. Weisenstein, 1989: The roles of dynamical and chemical processes in determining the stratospheric concentrations of ozone in one-dimensional and two-dimensional models. *J. Geophys. Res.*, **94**, 9889–9896.

191. Gunson, M.R., M.M. Abbas, M.C. Abrams, M. Allen, L.R. Brown, T.L. Brown, A.Y. Chang, A. Goldman, F.W. Irion, L.L. Lowes, E. Mahieu, G.L. Manney, H.A. Michelsen, M.J. Newchurch, C.P. Rinsland, R.J. Salawitch, G.P. Stiller, G.C. Toon, Y.L. Yung and R. Zander, 1996: The Atmospheric Trace Molecule Spectroscopy (ATMOS) experiment: deployment on the ATLAS Space Shuttle missions. *Geophys. Res. Lett.*, **23**, 2333–2336.
192. Plumb, R.A. and M.K.W. Ko, 1992: Interrelationships between mixing ratios of long-lived stratospheric constituents. *J. Geophys. Res.*, **97**, 10,145–10,156.
193. Coffey, M.T., 1996: Observations of the impact of volcanic activity on stratospheric chemistry. *J. Geophys. Res.*, **101**, 6767–6780.
194. Thomason, L.W., L.R. Poole and T. Deshler, 1997: A global climatology of stratospheric aerosol surface area density deduced from Stratospheric Aerosol and Gas Experiment II measurements: 1984–1994. *J. Geophys. Res.*, **102**, 8967–8976.
195. Hofmann, D.J. and S. Solomon, 1989: Ozone destruction through heterogeneous chemistry following the eruption of El Chichón. *J. Geophys. Res.*, **94**, 5029–5041.
196. *Mt. Pinatubo Eruption Special Issue*, 1992: *Geophys. Res. Lett.*, **19**, 149–218.
197. Lambert, A., R.G. Grainger, C.D. Rodgers, F.W. Taylor, J.L. Mergenthaler, J.B. Kumer and S.T. Massie, 1997: Global evolution of the Mt Pinatubo volcanic aerosols observed by the infrared limb-sounding instruments CLAES and ISAMS on the Upper Atmosphere Research Satellite. *J. Geophys. Res.*, **102**, 1495–1512.
198. Wallace, L. and W. Livingston, 1992: The effect of the Pinatubo cloud on hydrogen chloride and hydrogen fluoride. *Geophys. Res. Lett.*, **19**, 1209.
199. Mankin, W.G., M.T. Coffey and A. Goldman, 1992: Airborne observations of SO_2, HCl and O_3 in the stratospheric plume of the Pinatubo volcano in July 1991. *Geophys. Res. Lett.*, **19**, 179–182.
200. Kondo, Y., T. Sugita, R.J. Salawitch, M. Koike and T. Deshler, 1997: Effect of Pinatubo aerosols on stratospheric NO. *J. Geophys. Res.*, **102**, 1205–1213.
201. Hanson, D.R., 1998: Reaction of $ClONO_2$ with H_2O and HCl in sulfuric acid and $HNO_3/H_2SO_4/H_2O$ mixtures. *J. Phys. Chem. A*, **102**, 4794–4807.
202. Donaldson, D.J., A.R. Ravishankara and D.R. Hanson, 1997: Detailed study of HOCl + HCl⟶Cl-2 + H_2O in sulfuric acid. *J. Phys. Chem.*, **101**, 4717–4725.
203. Mickley, L.J., J.P.D. Abbatt, J.E. Frederick and J.M. Russell, III, 1997: Response of summertime odd nitrogen and ozone at 17 mbar to Mount Pinatubo aerosol over the southern midlatitudes: observations from the Halogen Occultation Experiment. *J. Geophys. Res.*, **102**, 23,573–23,582.
204. Avallone, L.M., D.W. Toohey, M.H. Proffitt, J.J. Margitan, K.R. Chan and J.G. Anderson, 1993: *In situ* measurements of ClO at mid-latitudes: is there an effect from Mt. Pinatubo? *Geophys. Res. Lett.*, **20**, 2519–2522.
205. Dessler, A.E., D.B. Considine, J.E. Rosenfield, S.R. Kawa, A.R. Douglass and J.M. Russell, III, 1997: Lower stratospheric chlorine partitioning during the decay of the Mt. Pinatubo aerosol cloud. *Geophys. Res. Lett.*, **24**, 1623–1626.
206. Kinnison, D.E., K.E. Grant, P.S. Connell, D.A. Rotman and D.J. Wuebbles, 1994: The chemical and radiative effects of the Mount Pinatubo eruption. *J. Geophys. Res.*, **99**, 25,705–25,732.
207. Rosenfield, J.E., D.B. Considine, P.E. Meade, J.T. Bacmeister, C.H. Jackman and M.R. Schoeberl, 1997: Stratospheric effects of Mount Pinatubo aerosol studied with a coupled two-dimensional model. *J. Geophys. Res.*, **102**, 3649–3670.

208. Pitari, G. and V. Rizi, 1993: An estimate of the chemical and radiative perturbation of stratospheric ozone following the eruption of Mt. Pinatubo. *J. Atmos. Sci.*, **50**, 3260–3276.

209. Tie, X.X., G.P. Brasseur, B. Briegleb and C. Granier, 1994: Two-dimensional simulation of Pinatubo aerosol and its effect on stratospheric ozone. *J. Geophys. Res.*, **99**, 20,545–20,562.

210. Tie, X.X. and G. Brasseur, 1995: The response of stratospheric ozone to volcanic eruptions—sensitivity to atmospheric chlorine loading. *Geophys. Res. Lett.*, **22**, 3035–3038.

211. Michelangeli, D.V., M. Allen, Y.L. Yung, R.L. Shia, D. Crisp and J. Eluszkiewicz, 1992: Enhancement of atmospheric radiation by an aerosol layer. *J. Geophys. Res.*, **97**, 865–874.

212. Anderson, D.E., R. DeMajistre, S.A. Lloyd and P.K. Swaminathan, 1995: Impact of aerosols and clouds on the troposphere and stratosphere radiation field with application to twilight photochemistry. *J. Geophys. Res.*, **100**, 7135–7145.

213. Huang, T.Y.W. and S.T. Massie, 1997: Effect of volcanic particles on the O_2 and O_3 photolysis rates and their impact on ozone in the tropical stratosphere. *J. Geophys. Res.*, **102**, 1239–1249.

214. Eluszkiewicz, J., D. Crisp, R.G. Grainger, A. Lambert, A.E. Roche, J.B. Kumer and J.L. Mergenthaler, 1997: Sensitivity of the residual circulation diagnosed from the UARS data to the uncertainties in the input fields and to the inclusion of aerosols. *J. Atmos. Sci.*, **54**, 1739–1757.

215. Kinne, S., O.B. Toon and M.J. Prather, 1992: Buffering of stratospheric circulation by changing amounts of tropical ozone: a Pinatubo case study. *Geophys. Res. Lett.*, **19**, 1927–1930.

216. Pitari, G., 1993: A numerical study of the possible perturbation of stratospheric dynamics due to Pinatubo aerosols: implications for tracer transport. *J. Atmos. Sci.*, **50**, 2443–2461.

217. Dessler, A.E., K. Minschwaner, E.M. Weinstock, E.J. Hintsa, J.G. Anderson and J.M. Russell, III, 1996: The effects of tropical cirrus clouds on the abundance of lower stratospheric ozone. *J. Atmos. Chem.*, **23**, 209–220.

218. Schoeberl, M.R., P.K. Bhartia, E. Hilsenrath and O. Torres, 1993: Tropical ozone loss following the eruption of Mt. Pinatubo. *Geophys. Res. Lett.*, **20**, 29–32.

219. Nash, E.R., P.A. Newman, J.E. Rosenfield and M.R. Schoeberl, 1996: An objective determination of the polar vortex using Ertel's potential vorticity. *J. Geophys. Res.*, **101**, 9471–9478.

220. Schoeberl, M.R., A.R. Douglass, S.R. Kawa, A.E. Dessler, P.A. Newman and R.S. Stolarski, 1996: The development of the Antarctic ozone hole. *J. Geophys. Res.*, **101**, 20,909–20,924.

221. Schoeberl, M.R., M. Luo and J.E. Rosenfield, 1995: An analysis of the Antarctic Halogen Occultation Experiment trace gas observations. *J. Geophys. Res.*, **100**, 5159–5172.

222. Manney, G.L., R.W. Zurek, A. O'Neill and R. Swinbank, 1994: On the motion of air through the stratospheric polar vortex. *J. Atmos. Sci.*, **51**, 2973–2994.

223. Fisher, M., A. O'Neill and R. Sutton, 1993: Rapid descent of mesospheric air into the stratospheric polar vortex. *Geophys. Res. Lett.*, **20**, 1267–1270.

224. Rosenfield, J.E., P.A. Newman and M.R. Schoeberl, 1994: Computations of diabatic descent in the stratospheric polar vortex. *J. Geophys. Res.*, **99**, 16,677–16,689.

225. Hess, P.G., 1991: Mixing processes following the final stratospheric warming. *J. Atmos. Sci.*, **48**, 1625–1641.

226. Schoeberl, M.R., 1978: Stratospheric warmings: observations and theory. *Rev. Geophys.*, **16**, 521–538.

227. Atkinson, R.J. and R.A. Plumb, 1997: Three-dimensional ozone transport during the ozone hole breakup in December 1987. *J. Geophys. Res.*, **102**, 1451–1466.

228. Toon, O.B., P. Hamill, R.P. Turco and J. Pinto, 1986: Condensation of HNO_3 and HCl in the winter polar stratospheres. *Geophys. Res. Lett.*, **13**, 1284–1287.

229. Crutzen, P.J. and F. Arnold, 1986: Nitric acid cloud formation in the cold Antarctic stratosphere: a major cause for the springtime 'ozone hole'. *Nature*, **324**, 651–655.

230. McElroy, M.B., R.J. Salawitch and S.C. Wofsy, 1986: Antarctic O_x: chemical mechanisms for the spring decrease. *Geophys. Res. Lett.*, **13**, 1296–1299.

231. Hanson, D. and K. Mauersberger, 1988: Laboratory studies of the nitric acid trihydrate: Implications for the south polar stratosphere. *Geophys. Res. Lett.*, **15**, 855–858.

232. Fahey, D.W., K.K. Kelly, G.V. Ferry, L.R. Poole, J.C. Wilson, D.M. Murphy, M. Loewenstein and K.R. Chan, 1989: *In situ* measurements of total reactive nitrogen, total water and aerosol in a polar stratospheric cloud in the Antarctic. *J. Geophys. Res.*, **94**, 11,299–11,315.

233. Worsnop, D.R., L.E. Fox, M.S. Zahniser and S.C. Wofsy, 1993: Vapor pressures of solid hydrates of nitric acid: Implications for polar stratospheric clouds. *Science*, **259**, 71–74.

234. Drdla, K., A. Tabazadeh, R.P. Turco, M.Z. Jacobson, J.E. Dye, C. Twohy and D. Baumgardner, 1994: Analysis of the physical state of one Arctic polar stratospheric cloud based on observations. *Geophys. Res. Lett.*, **21**, 2475–2478.

235. Toon, O.B. and M.A. Tolbert, 1995: Spectroscopic evidence against nitric acid trihydrate in polar stratospheric clouds. *Nature*, **375**, 218–221.

236. Dye, J.E., D. Baumgardner, B.W. Gandrud, K. Drdla, K. Barr, D.W. Fahey, L.A. Delnegro, A. Tabazadeh, H.H. Jonsson, J.C. Wilson, M. Loewenstein, J.R. Podolske and K.R. Chan, 1996: *In-situ* observations of an Antarctic polar stratospheric cloud: Similarities with Arctic observations. *Geophys. Res. Lett.*, **23**, 1913–1916.

237. Dessler, A.E., J. Wu, M.L. Santee and M.R. Schoeberl, 1999: Satellite observations of temporary and irreversible denitrification. *J. Geophys. Res.*, **104**, 13,993–14,002.

238. Santee, M.L., A. Tabazadeh, G.L. Manney, R.J. Salawitch, L. Froidevaux, W.G. Read and J.W. Waters, 1998: UARS MLS HNO_3 observations: implications for Antarctic PSCs. *J. Geophys. Res.*, **103**, 13,285–13,313.

239. Massie, S.T., J.E. Dye, D. Baumgardner, W.J. Randel, F. Wu, X.X. Tie, L. Pan, F. Figarol, G.P. Brasseur, M.L. Santee, W.G. Read, R.G. Grainger, A. Lambert, J.L. Mergenthaler and A. Tabazadeh, 1997: Simultaneous observations of polar stratospheric clouds and HNO_3 over Scandinavia in January, 1992. *Geophys. Res. Lett.*, **24**, 595–598.

240. Browell, E.V., C.F. Butler, S. Ismail, P.A. Robinette, A.F. Carter, N.S. Higdon, O.B. Toon, M.R. Schoeberl and A.F. Tuck, 1990: Airborne LIDAR observations in the wintertime Arctic stratosphere: polar stratospheric clouds. *Geophys. Res. Lett.*, **17**, 385–388.

241. Toon, O.B., E.V. Browell, S. Kinne and J. Jordan, 1990: An analysis of LIDAR observations of polar stratospheric clouds. *Geophys. Res. Lett.*, **17**, 393–396.

242. Panegrossi, G., D. Fuà and G. Fiocco, 1996: A 1-D model of the formation and evolution of polar stratospheric clouds. *J. Atmos. Chem.*, **23**, 5–35.

243. Drdla, K. and R.P. Turco, 1991: Denitrification through PSC formation: a 1-D model incorporating temperature oscillations. *J. Atmos. Chem.*, **12**, 319–366.

244. Kawa, S.R., D.W. Fahey, L.E. Heidt, W.H. Pollock, S. Solomon, D.E. Anderson, M. Loewenstein, M.H. Proffitt, J.J. Margitan and K.R. Chan, 1992: Photochemical partitioning of the reactive nitrogen and chlorine reservoirs in the high-latitude stratosphere. *J. Geophys. Res.*, **97**, 7905–7923.

245. Webster, C.R., R. D. May, D.W. Toohey, L.M. Avallone, J.G. Anderson, P. Newman, L. Lait, M.R. Schoeberl, J.W. Elkins and K.R. Chan, 1993: Chlorine chemistry on polar stratospheric cloud particles in the Arctic winter. *Science*, **261**, 1130–1134.

246. Barone, S.B., M.A. Zondlo and M.A. Tolbert, 1997: A kinetic and product study of the hydrolysis of $ClONO_2$ on type Ia polar stratospheric cloud materials at 185 K. *J. Phys. Chem. A*, **101**, 8643–8652.

247. Hanson, D.R. and A.R. Ravishankara, 1993: Reaction of $ClONO_2$ with HCl on NAT, NAD and frozen sulfuric acid and hydrolysis of N_2O_5 and $ClONO_2$ on frozen sulfuric acid. *J. Geophys. Res.*, **98**, 22,931–22,936.

248. Kawa, S.R., P.A. Newman, L.R. Lait, M.R. Schoeberl, R.M. Stimpfle, D.W. Kohn, C.R. Webster, R.D. May, D. Baumgardner, J.E. Dye, J.C. Wilson, K.R. Chan and M. Loewenstein, 1997: Activation of chlorine in sulfate aerosol as inferred from aircraft observations. *J. Geophys. Res.*, **102**, 3921–3933.

249. Toohey, D.W., L.M. Avallone, L.R. Lait, P.A. Newman, M.R. Schoeberl, D.W. Fahey, E.L. Woodbridge and J.G. Anderson, 1993: The seasonal evolution of reactive chlorine in the northern hemisphere stratosphere. *Science*, **261**, 1134–1136.

250. Schoeberl, M.R., A.R. Douglass, R.S. Stolarski, P.A. Newman, L.R. Lait, D. Toohey, L. Avallone, J.G. Anderson, W. Brune, D.W. Fahey and K. Kelly, 1993: The evolution of ClO and NO along air parcel trajectories. *Geophys. Res. Lett.*, **20**, 2511–2514.

251. Kawa, S.R., D.W. Fahey, K.K. Kelly, J.E. Dye, D. Baumgardner, B.W. Gandrud, M. Loewenstein, G.V. Ferry and K.R. Chan, 1992: The Arctic polar stratospheric cloud aerosol: aircraft measurements of reactive nitrogen, total water and particles. *J. Geophys. Res.*, **97**, 7925–7938.

252. Fahey, D.W., K.K. Kelly, S.R. Kawa, A.F. Tuck, M. Loewenstein, K.R. Chan and L.E. Heidt, 1990: Observations of denitrification and dehydration in the winter polar stratospheres. *Nature*, **344**, 321–324.

253. Kasten, F., 1968: Falling speed of aerosol particles. *J. Appl. Meteor.*, **7**, 944–947.

254. Rinsland, C.P., M.R. Gunson, R.J. Salawitch, M.J. Newchurch, R. Zander, M.M. Abbas, M.C. Abrams, G.L. Manney, H.A. Michelsen, A.Y. Chang and A. Goldman, 1996: ATMOS measurements of $H_2O + 2CH_4$ and total reactive nitrogen in the November 1994 Antarctic stratosphere: dehydration and denitrification in the vortex. *Geophys. Res. Lett.*, **23**, 2397–2400.

255. Hintsa, E.J., P.A. Newman, H.H. Jonsson, C.R. Webster, R.D. May, R.L. Herman, L.R. Lait, M.R. Schoeberl, J.W. Elkins, P.R. Wamsley, G.S. Dutton, T.P. Bui, D.W. Kohn and J.G. Anderson, 1998: Dehydration and denitrification in the Arctic polar vortex during the 1995–1996 winter. *Geophys. Res. Lett.*, **25**, 501–504.

256. Kelly, K.K., A.F. Tuck, D.M. Murphy, M.H. Proffitt, D.W. Fahey, R.L. Jones, D.S. McKenna, M. Loewenstein, J. R. Podolske, S.E. Strahan, G.V. Ferry, K.R. Chan, J.F. Vedder, G.L. Gregory, W.D. Hypes, M.P. McCormick, E.V. Browell and L.E. Heidt, 1989: Dehydration in the lower Antarctic stratosphere during late winter and early spring, 1987. *J. Geophys. Res.*, **94**, 11,317–11,357.

257. Santee, M.L., W.G. Read, J.W. Waters, L. Froidevaux, G.L. Manney, D.A. Flower, R.F. Jarnot, R.S. Harwood and G.E. Peckham, 1995: Interhemispheric differences in polar stratospheric HNO₃, H₂O, ClO and O₃. *Science*, **267**, 849–852.

258. Brune, W.H., J.G. Anderson and K.R. Chan, 1989: *In situ* observations of ClO over Antarctica: ER-2 aircraft results from 54°S to 72°S latitude. *J. Geophys. Res.*, **94**, 16,649–16,663.

259. Swinbank, R. and A. O'Neill, 1994: A stratosphere-troposphere data assimilation system. *Mon. Weather Rev.*, **122**, 686–702.

260. Waters, J.W., W.G. Read, L. Froidevaux, T.A. Lungu, V.S. Perun, R.A. Stachnik, R.F. Jarnot, R.E. Cofield, E.F. Fishbein, D.A. Flower, J.R. Burke, J.C. Hardy, L.L. Nakamura, B.P. Ridenoure, Z. Shippony, R.P. Thurstans, L.M. Avallone, D.W. Toohey, R.L. deZafra and D.T. Shindell, 1996: Validation of UARS MLS ClO measurements. *J. Geophys. Res.*, **101**, 10,091–10,127.

261. Schoeberl, M.R., R.S. Stolarski, A.R. Douglass, P.A. Newman, L.R. Lait, J.W. Waters, L. Froidevaux and W.G. Read, 1993: MLS ClO observations and Arctic polar vortex temperatures. *Geophys. Res. Lett.*, **20**, 2861–2864.

262. Wu, J. and A.E. Dessler, 2000: Comparisons between modeled and measured polar ozone loss. *J. Geophys. Res.*, submitted.

263. McKinney, K.A., J.M. Pierson and D.W. Toohey, 1997: A wintertime *in situ* profile of BrO between 17 and 27 km in the Arctic vortex. *Geophys. Res. Lett.*, **24**, 853–856.

264. Zreda-Gostynska, G., P.R. Kyle and D.L. Finnegan, 1993: Chlorine, fluorine and sulfur emissions from Mount Erebus, Antarctica and estimated contributions to the Antarctic atmosphere. *Geophys. Res. Lett.*, **20**, 1959–1962.

265. Molina, L.T. and M.J. Molina, 1987: Production of Cl₂O₂ from the self-reaction of the ClO radical. *J. Phys. Chem.*, **91**, 433–436.

266. Chen, P., 1994: The permeability of the Antarctic vortex edge. *J. Geophys. Res.*, **99**, 20,563–20,571.

267. Douglass, A.R., M.R. Schoeberl, R.S. Stolarski, J.W. Waters, J.M. Russell, III, A.E. Roche and S.T. Massie, 1995: Interhemispheric differences in springtime production of HCl and ClONO₂ in the polar vortices. *J. Geophys. Res.*, **100**, 13,967–13,978.

268. Grooss, J.-U., R.B. Pierce, P.J. Crutzen, W.L. Grose and J.M. Russell, III, 1997: Reformation of chlorine reservoirs in southern hemisphere polar spring. *J. Geophys. Res.*, **102**, 13,141–13,152.

269. Santee, M.L., L. Froidevaux, G.L. Manney, W.G. Read, J.W. Waters, M.P. Chipperfield, A.E. Roche, J.B. Kumer, J.L. Mergenthaler and J.M. Russell, III, 1996: Chlorine deactivation in the lower stratospheric polar regions during late winter: results from UARS. *J. Geophys. Res.*, **101**, 18,835–18,859.

270. Newman, P.A., J.F. Gleason, R.D. McPeters and R.S. Stolarski, 1997: Anomalously low ozone over the Arctic. *Geophys. Res. Lett.*, **24**, 2689–2692.

271. Manney, G.L., L. Froidevaux, J.W. Waters, R.W. Zurek, W.G. Read, L.S. Elson, J.B. Kumer, J.L. Mergenthaler, A.E. Roche, A. O'Neill, R.S. Harwood, I. MacKenzie and R. Swinbank, 1994: Chemical depletion of ozone in the Arctic lower stratosphere during winter 1992–93. *Nature*, **370**, 429–434.

272. Nagatani, R.M., A.J. Miller, M.E. Gelman and P.A. Newman, 1990: A comparison of Arctic lower stratospheric winter temperatures for 1988–89 with temperatures since 1964. *Geophys. Res. Lett.*, **17**, 333–336.

273. Coy, L., E.R. Nash and P.A. Newman, 1997: Meteorology of the polar vortex: spring 1997. *Geophys. Res. Lett.*, **24**, 2693–2696.

274. Zurek, R.W., G.L. Manney, A.J. Miller, M.E. Gelman and R.M. Nagatani, 1996: Interannual variability of the north polar vortex in the lower stratosphere during the UARS mission. *Geophys. Res. Lett.*, **23**, 289–292.

275. Waters, J.W., G.L. Manney, W.G. Read, L. Froidevaux, D.A. Flower and R.F. Jarnot, 1995: UARS MLS observations of lower stratospheric ClO in the 1992–93 and 1993–94 Arctic winter vortices. *Geophys. Res. Lett.*, **22**, 823–826.

276. Manney, G.L., R.W. Zurek, L. Froidevaux, J. W. Waters, A. O'Neill and R. Swinbank, 1995: Evidence for Arctic ozone depletion in late February and early March 1994. *Geophys. Res. Lett.*, **22**, 2941–2944.

277. Manney, G.L., M.L. Santee, L. Froidevaux, J.W. Waters and R.W. Zurek, 1996: Polar vortex conditions during the 1995–96 Arctic winter: Meteorology and MLS ozone. *Geophys. Res. Lett.*, **23**, 3203–3206.

278. Roche, A.E., J.B. Kumer, J.L. Mergenthaler, G.A. Ely, W.G. Uplinger, J.F. Potter, T.C. James and L.W. Sterritt, 1993: The Cryogenic Limb Array Etalon Spectrometer (CLAES) on UARS: experiment description and performance. *J. Geophys. Res.*, **98**, 10,763–10,775.

279. Barath, F.T., M.C. Chavez, R.E. Cofield, D.A. Flower, M.A. Frerking, M.B. Gram, W.M. Harris, J.R. Holden, R.F. Jarnot, W.G. Kloezeman, G. J. Klose, G. K. Lau, M.S. Loo, B.J. Maddison, R.J. Mattauch, R.P. McKinney, G.E. Peckham, H.M. Pickett, G. Siebes, F.S. Soltis, R.A. Suttie, J.A. Tarsala, J.W. Waters and W.J. Wilson, 1993: The Upper Atmosphere Research Satellite Microwave Limb Sounder instrument. *J. Geophys. Res.*, **98**, 10,751–10,762.

280. Bevilacqua, R.M., C.P. Aellig, D.J. Debrestian, M.D. Fromm, K. Hoppel, J.D. Lumpe, E.P. Shettle, J.S. Hornstein, C.E. Randall, D.W. Rusch and J.E. Rosenfield, 1997: POAM II ozone observations in the Antarctic ozone hole in 1994, 1995 and 1996. *J. Geophys. Res.*, **102**, 23,643–23,657.

281. McPeters, R.D. and G.J. Labow, 1996: An assessment of the accuracy of 14.5 years of Nimbus 7 TOMS Version 7 ozone data by comparison with the Dobson network. *Geophys. Res. Lett.*, **23**, 3695–3698.

282. McPeters, R.D., P.K. Bhartia, A.J. Krueger, J.R. Herman, B.M. Schlesinger, C.G. Wellemeyer, C.J. Seftor, G. Jaross, S.L. Taylor, T. Swissler, O. Torres, G. Labow, W. Byerly and R.P. Cebula, 1996: *Nimbus-7 Total Ozone Mapping Spectrometer (TOMS) Data Product User's Guide*, NASA Ref. Pub. 1384. NASA, Washington, DC.

283. Dessler, A.E., M.D. Burrage, J.-U. Grooss, J.R. Holton, J.L. Lean, S.T. Massie, M.R. Schoeberl, A.R. Douglass and C.H. Jackman, 1998: Selected science highlights from the first five years of the Upper Atmosphere Research Satellite (UARS) program. *Rev. Geophys.*, **36**, 183–210.

Index

This Page Intentionally Left Blank

International Geophysics Series

EDITED BY

RENATA DMOWSKA
Division of Engineering and Applied Science
Harvard University
Cambridge, MA 02138

JAMES R. HOLTON
Department of Atmospheric Sciences
University of Washington
Seattle, Washington

H. THOMAS ROSSBY
University of Rhode Island
Kingston, Rhode Island

* Out of Print

* Out of Print

* Out of Print

* Out of Print